

Advances in Nanotechnology and the Environment

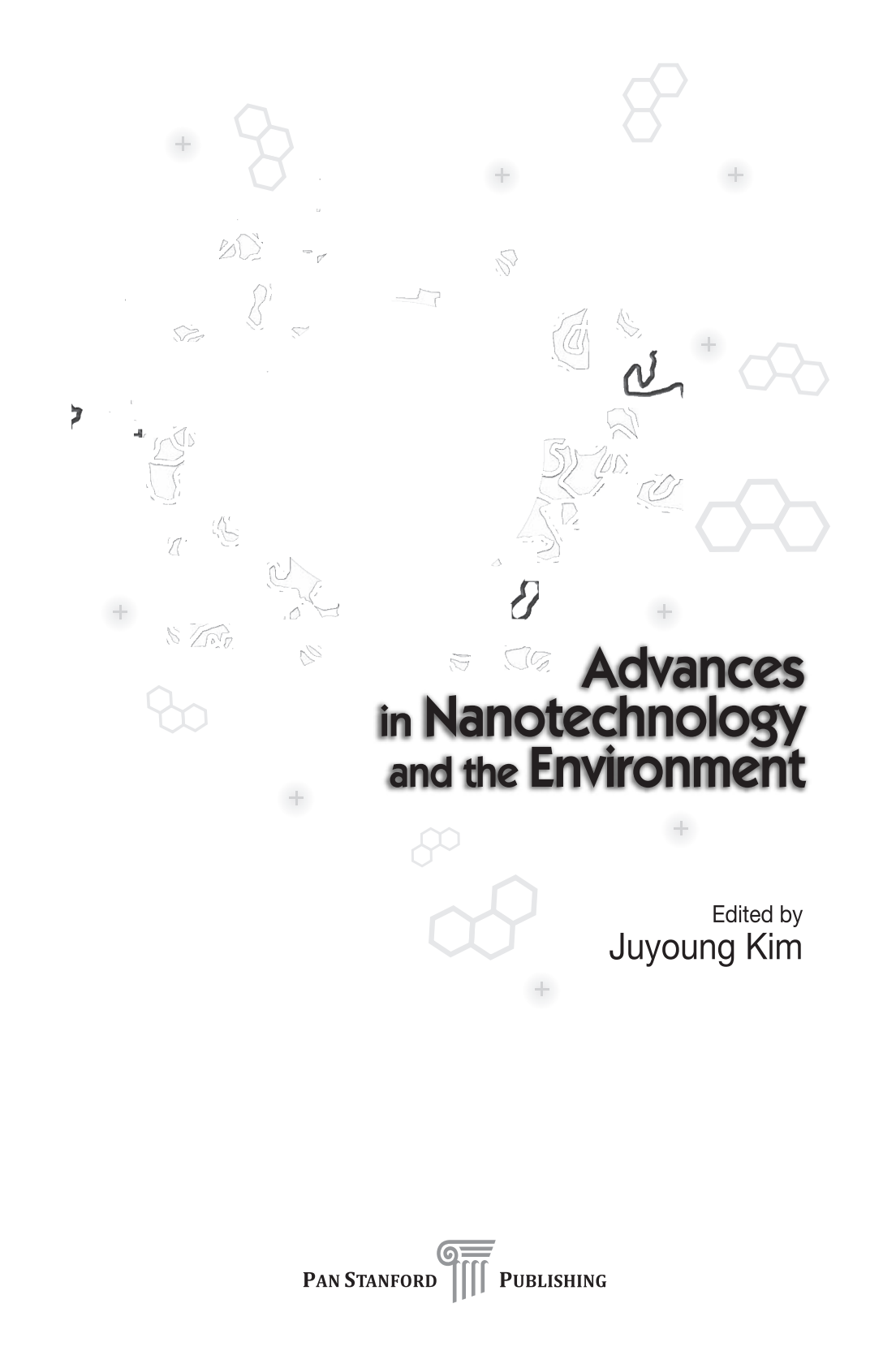
Edited by
Juyoung Kim





Advances in Nanotechnology and the Environment

This page intentionally left blank



Advances in Nanotechnology and the Environment

Edited by
Juyoung Kim

CRC Press
Taylor & Francis Group
6000 Broken Sound Parkway NW, Suite 300
Boca Raton, FL 33487-2742

© 2012 by Taylor & Francis Group, LLC
CRC Press is an imprint of Taylor & Francis Group, an Informa business

No claim to original U.S. Government works
Version Date: 20111012

International Standard Book Number-13: 978-9-81426-760-1 (eBook - PDF)

This book contains information obtained from authentic and highly regarded sources. Reasonable efforts have been made to publish reliable data and information, but the author and publisher cannot assume responsibility for the validity of all materials or the consequences of their use. The authors and publishers have attempted to trace the copyright holders of all material reproduced in this publication and apologize to copyright holders if permission to publish in this form has not been obtained. If any copyright material has not been acknowledged please write and let us know so we may rectify in any future reprint.

Except as permitted under U.S. Copyright Law, no part of this book may be reprinted, reproduced, transmitted, or utilized in any form by any electronic, mechanical, or other means, now known or hereafter invented, including photocopying, microfilming, and recording, or in any information storage or retrieval system, without written permission from the publishers.

For permission to photocopy or use material electronically from this work, please access www.copyright.com (<http://www.copyright.com/>) or contact the Copyright Clearance Center, Inc. (CCC), 222 Rosewood Drive, Danvers, MA 01923, 978-750-8400. CCC is a not-for-profit organization that provides licenses and registration for a variety of users. For organizations that have been granted a photocopy license by the CCC, a separate system of payment has been arranged.

Trademark Notice: Product or corporate names may be trademarks or registered trademarks, and are used only for identification and explanation without intent to infringe.

Visit the Taylor & Francis Web site at
<http://www.taylorandfrancis.com>

and the CRC Press Web site at
<http://www.crcpress.com>

Contents

<i>Preface</i>	vii
Chapter 1 Amphiphilic Organic Nanoparticles as Nano-Absorbent for Pollutants <i>Juyoung Kim</i>	1
Chapter 2 Use of Amphiphilic Cross-Linked Polymer Nanoparticles Containing Anionic Hydrophilic Segments for Enhanced Desorption of Polyaromatic Hydrocarbons (PAHs) From Aquifer Soil <i>Juyoung Kim</i>	17
Chapter 3 Use of Amphiphilic Nonionic Polymer Nanoparticles for Removal of Hydrophobic Pollutants from Soil <i>Juyoung Kim</i>	45
Chapter 4 Adsorption and Concentration of Organic Contaminants by Carbon Nanotubes from Environmental Samples <i>Hongyun Niu and Yaqi Cai</i>	79
Chapter 5 Efficient Removal of Organic Pollutants and Metal Ions Using Amphiphilic Polymer Nanoparticle <i>Jin Kie Shim</i>	137
Chapter 6 Nanoparticles for Fuel Cell Applications <i>Chang Hyun Lee</i>	159
Chapter 7 The Occurrence, Behavior, and Effects of Engineered Nanomaterials in the Environment <i>Bernd Nowack</i>	183

This page intentionally left blank

Preface

Compared with conventional technologies and sciences, the development of nanoscience and nanotechnology dealing with the synthesis and characterization of nanostructure materials has been quite rapid and intensive, while also unprecedented. Now the technologies based on nanoscience and nanotechnology are exerting a profound and strong impact on every field of conventional technology and science.

Science and technology in the 21st century are evolving in four major directions: environmental technology, information technology, biotechnology, and nanotechnology. Technologies created and advanced by these four disciplines have continuously had an impact on daily life. Drug delivery systems, vaccines, animal cloning, genetically modified organisms, fuel cells, solar cells, electroluminescence devices, flexible displays, wireless telecommunications, World Wide Web, and so on, were created and brought to us by these technologies. There is no doubt that because of these four pillars of technology, humankind will experience an unprecedented technology-based life.

The role of nanotechnology in advanced modern technologies is to provide materials as breakthrough and to materialize technology, and these materials have been considered the unique and sole solution to the limitations of other technologies and a means of widening their applications. Therefore, nanoparticles and nano-sized materials—such as nano-imprinting materials, nano-lithography materials, nano-sized sensors, as well as nano-sized detectors for biomolecules in DNA assay, immunoassay, and cell bio-imaging—have been widely used in biotechnology and information technology. However, little has been reported about the application of nanoparticles in environmental technology and about their influence on the environment. Most of the environmental applications of nanoparticles have been limited to the fabrication of nano-sensors for VOC detection and nano-sized catalysts for air purification systems. The use of nanoparticles for the direct removal of pollutants from the contaminated soil and wastewater has been

seldom reported. Environmental processes for soil remediation, wastewater treatment, and air purification strongly need innovative new materials to improve their performance and efficiency. Hence, the demand for materials created by nanotechnology in environmental technology is ever stronger than before.

This book presents the possible applications of nano-sized materials in environmental processes. It is by far the most reliable guideline for the selection of nanomaterials to improve the efficiency of environmental processes and for designing nanomaterials for specific environmental processes and pollutants. The impact of nanomaterials on the environment has also been discussed in the book to help avoid causing secondary contamination by use of nanomaterials and to provide proper information about nanomaterials to potential users who wish to use and apply them in environmental technology.

Chapter 1

AMPHIPHILIC ORGANIC NANOPARTICLES AS NANO- ABSORBENTS FOR POLLUTANTS

Juyoung Kim

*Department of Advanced Materials Engineering,
Kangwon National University, Samcheok, Kangwon 245-711,
South Korea*
juyoungk@kangwon.ac.kr

Environmental engineers have invented very large numbers of processes and devices for removal of pollutants from various water phases and soils. Recently, material engineers and environmental engineers have begun fusing their technologies to improve efficiency of environmental process. Material engineers found new applications of their materials, at the same time environmental engineers could enhance performance of their processes by just adding materials without big modification in the process (technically no modification). Users and engineers keep trying to find magical materials that can improve the efficiency and reduce the cost of their environmental engineering process by just adding small amount of magical materials. That is, antifouling agent, coagulants (aluminum sulphate, ferrous sulphate, ferric chloride, polyelectrolyte), sedimentation, activated carbon, surfactants, microorganism, etc., have been used for enhancing efficiency of environmental process, which is running in real field [1-3].

Advances in Nanotechnology and the Environment

Edited by Juyoung Kim

Copyright © 2012 by Pan Stanford Publishing Pte. Ltd.

www.panstanford.com

However, environmental engineers keep demanding an innovative material for enhancing performance of conventional environmental process. As presented at Fig. 1.1, if nano-sized absorbent dispersed in water, which can solubilize or absorb various hydrophobic pollutants and metals, would be added in contaminated sites (soil or wastewater), performance of conventional environmental process could be innovatively improved without changing environmental process.

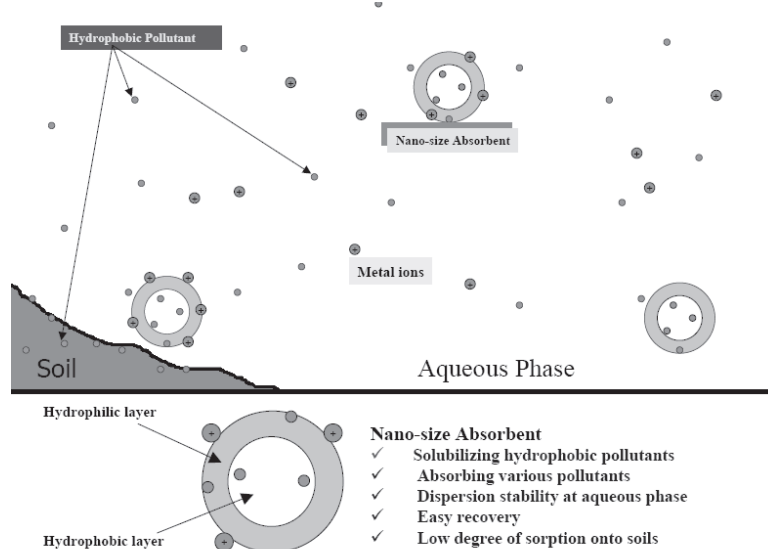


Figure 1.1 Schematic illustration of nano-sized absorbent for enhancing the performance of environmental process.

During the last decade, various kinds of nanomaterials have been created and applied at various fields of engineering because these materials have very unique properties that are different from the property of their atoms as well as the property of their bulk materials [4–12]. And physical and chemical properties of the nanomaterials can be significantly changed not by the composition but by their size and morphology. Recently, environmental engineers have begun to use nanomaterials to improve the performance of their devices and processes. Fused technology between nanotechnology and environmental technology can be divided into three broad categories:

- (1) Nanomaterials for monitoring environmental pollutions
- (2) Nanomaterials for improving the performance of environmental-friendly energy system such as solar cell, fuel cell, secondary battery, etc.
- (3) Nanomaterials for direct removal of environmental pollutants

Sensors fabricated using SnO₂ nanoparticles can detect 3 ppm of CO₂, 15 ppb of NO₂, and O₃, and 50 ppb of NO gas. Sensors incorporated with WO₃ nanoparticles can also monitor concentration changes in few ppm of H₂S, N₂O, and CO gas. Recently, carbon nanotubes have been used for fabrication of nano-sized sensor [13–17].

Unlike conventional solar cell system containing organic or inorganic pigments, brand-new solar cell system has been fabricated using CdS, CdSe nanoparticles, whose efficiency is much higher than those of conventional solar cell system [6–7]. Clay minerals and silica nanoparticles have also been used as nano-sized filler for improving chemical and thermal stability of secondary battery [18–20]. There have been many reports on improving chemical stability and reducing methanol permeability of proton exchange membranes in fuel cell system [21–27]. In these technology and engineering, nanomaterials were just used for detecting pollutants and enhancing the performance of environmental-friendly devices. Metal, metal oxide, and metal sulfide nanoparticles, which disperse on inorganic supports having high surface area (silica or alumina), can directly remove environmental pollutants such VOC, NO_x, and carbon monoxide through several catalysis reactions. These nanomaterials can remove environmental pollutants such VOC, NO_x, and CO through several catalyze reactions. It has also been reported that zero-valent iron nanoparticles could remove pesticides and herbicides in wastewater and drinking water by oxidative degradation reaction [28]. However, there were fewer reports on the use of nanomaterials as a nano-sized absorbent for removal of pollutants from water and soil.

Among conventional additives for enhancing the performance of environmental engineering, surfactant has been recognized as the most useful material for this purpose. Surfactants are amphiphilic molecule having hydrophilic (lipophobic) and hydrophobic (lipophilic) at the same backbone, so these molecules can be located at the interface between two immiscible phases (e.g., water–oil). This peculiar behavior, that is, the interfacial activity can reduce in interfacial tension, increases the miscibility of two immiscible phases.

Owing to the interfacial activity of surfactant molecules, they have been widely used in various industrial and academic fields as detergent, wetting and foaming agents, dispersant, emulsifier, adhesives, de-emulsifiers, etc. [29–30]. When surfactants are applied in the environmental engineering process, surfactant molecules can enhance the efficiency of soil washing and remediation, and wastewater purification. Surfactant-enhanced environmental engineering process is called as surfactant-enhanced soil remediation (SESR) [31–35] and micellar-enhanced ultrafiltration (MEUF) process [36–39], which have been known as the most effective environmental process for the removal of pollutants from soil and water (Figs. 1.2 and 1.3). In both the processes, nano-sized aggregates of surfactant molecules (micelles) absorb and solubilize pollutants from soil and aqueous phase, which move through soil pores or separate from aqueous phase through separation membranes, resulting in improvement of washing and separation efficiency of conventional soil washing and filtration process. So, it can be thought that micelle is the first application of nano-sized absorbent in the environmental engineering process. In other words, the first fused technology between NT and ET is SESR and MEUF process.

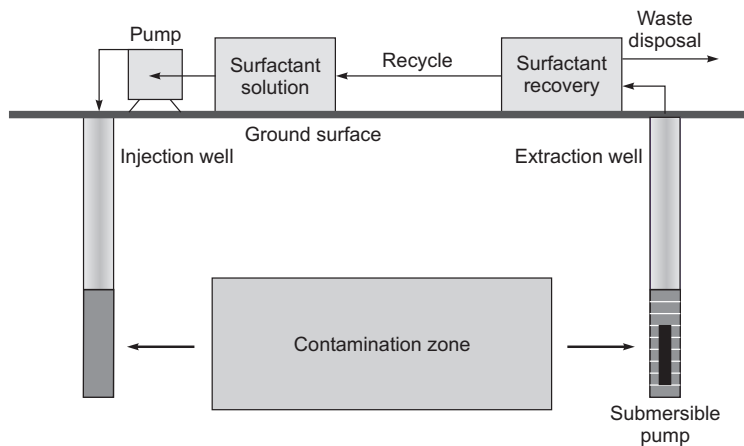


Figure 1.2 Schematic illustration of surfactant-enhanced soil remediation. Adapted from Ref. [35].

During the past two decades, large number of reports related to SESR and MEUF process have been published, and some of them have been already applied and used in real field. However, the real-field application of these processes was still limited by the fatal

drawbacks of MEUF and SESR process: very easy breakage and too small size of surfactant micelles, and strong sorption of surfactant to soil and membrane cause secondary contamination. So, it has been strongly demanded to develop a new type of micelle-like nanoparticles to overcome these drawbacks and highly improve the efficiency of SESR and MEUF process.

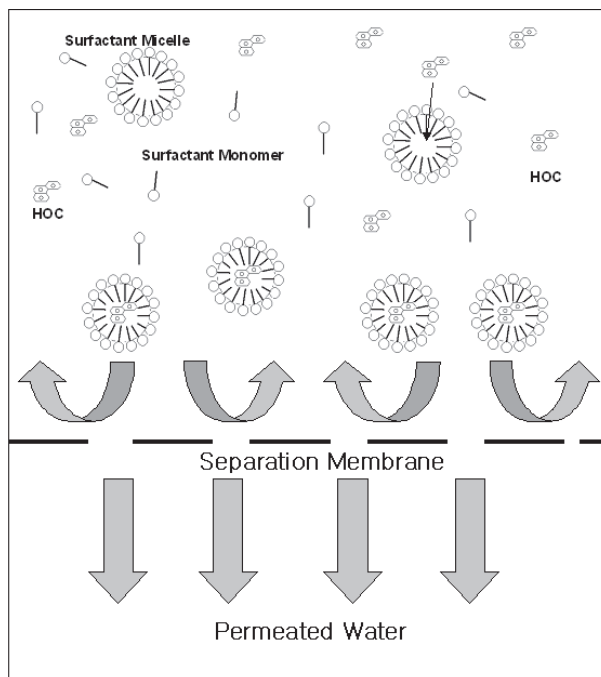


Figure 1.3 Schematic illustration of micellar-enhanced ultrafiltration process.

1.1 AMPHIPHILIC POLYMERS AND AMPHIPHILIC OLIGOMERS

Amphiphilic polymers can be classified into amphiphilic homopolymer, random copolymer, and block copolymer. Amphiphilic homopolymers and random copolymers have hydrophilic or hydrophobic components as side groups or pendant groups along the backbone. Poly(2-hydroxyalkyl methacrylate), poly(oxybutylene), poly(4-vinyl-2-pyrrolidone), poly(4-vinyl

pyridine), poly(butadiene-co-maleic acid), poly(styrene-co-styrene sulfonic acid), poly(styrene-co-4-(carboxy)styrene), poly(styrene-co-methacrylic acid), poly(*N*-vinyl-2-pyrrolidone-co-acrylic acid), etc., belong to these amphiphilic polymers [40–55]. Most of the amphiphilic polymers are water-soluble but they can stabilize metals, polymer particles, and inorganic particles in polar and nonpolar solvents. Recently, these polymers have been used as stabilizer or template for the synthesis of inorganic nanoparticles or nano-colloids [42–54]. Hydrophilic components of these polymers can dissociate metal salts or make a complex with metal precursors; at the same time hydrophobic components provide stabilizing and protecting function for synthesis of nanoparticles and nano-colloids via several stabilization mechanisms such as steric stabilization, depletion stabilization, electrostatic stabilization, etc.

Amphiphilic block copolymers are a unique kind of polymers containing two immiscible hydrophobic and hydrophilic components or segments at the same backbone. During the past two decades, several kinds of amphiphilic polymers have been synthesized with various synthetic processes, such as anionic polymerization (polystyrene-polyethylene oxide, polystyrene-poly(2-vinylpyridine), polystyrene-polybutadiene-polystyrene (Kraton), and PPO-PEO (Pluronics) triblock copolymers), cationic polymerization, group-transfer polymerization, ring-opening metathesis polymerization, living radical polymerization, etc. [55–58]. Like surfactants, low-molecular weight amphiphilic molecules, amphiphilic block copolymers can be located at the interface between immiscible phases and form several kinds of aggregates in solvents such as micelle, body-centered cubic packed sphere, hexagonally ordered cylinder, gyroid, lamellae, cylindrical micelles and spherical micelle in solvents dissolving one of the components or segments Fig. 1.4 [40, 44, 46, 54]. In most of the cases, amphiphilic polymers form spherical micelles in water at relatively low concentration. These polymers can form micelle-like nanoparticles at extremely low concentration in aqueous phase and maintain stable dispersion even at extremely high dilution, and their nanoparticles are much more stable compared to surfactant micelles. Amphiphilic block copolymers have been used for compatibilizer, dispersant, emulsifier, drug delivery carriers, nano-sized template (or reactor) for nanoparticle synthesis, etc., because they have interfacial activity and solubilization performance, and can form various nano-sized morphologies with external conditions. It has been reported that among amphiphilic polymers, block copolymers have

a better performance for controlling the morphology of inorganic nanoparticles and stabilizing the synthesized nanoparticles compared to homo- and random amphiphilic polymers [40, 44–47, 49–51].

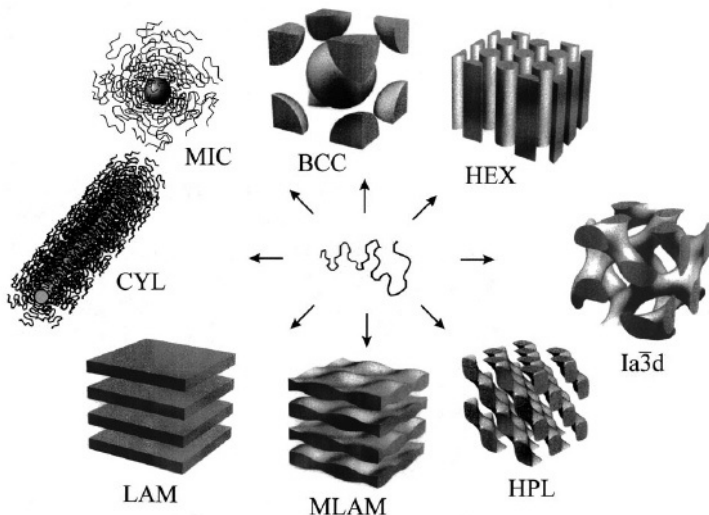


Figure 1.4 Common morphology of microphase-separated block copolymers: body-centered cubic (bcc) packed spheres (BCC), hexagonally ordered cylinders (HEX), gyroid ($Ia\bar{3}d$), hexagonally perforated layers (HPL), modulated lamellae (MLAM), lamellae (LAM), cylindrical micelles (CYL), and spherical micelles (MIC). Reprinted with permission from Ref. [56].

Amphiphilic homo- and random copolymers are usually water-soluble and can form aggregates in polar and nonpolar solvents. But, it has not been reported that their aggregates are micelle-like and can take up hydrophobic molecules in water. So, in most of the cases, solubilization of hydrophobic molecules in amphiphilic polymers has been studied for amphiphilic block copolymers. Their micelles can take up hydrophobic molecules within their hydrophobic cores, resulting in the increase of solubility of hydrophobic molecules in water (solubilization) [59–61]. Unlike extremely short lifetime of surfactant micelles, aggregates of amphiphilic polymers (micelles) can maintain their structure for hours, due to their much higher molecular weight compared to surfactants. Owing to relatively higher inter- and intramolecular interaction (e.g., hydrophobic interaction) of amphiphilic polymers compared to surfactant molecules,

concentration for the formation of micelle of amphiphilic polymers is much lower than that of surfactant molecules, so that micelles can be formed and maintained at extremely low concentration.

It has been reported by several research groups that micelles of amphiphilic block copolymer can solubilize several kinds of hydrophobic molecules such as polycyclic aromatic compounds, aliphatic and aromatic hydrocarbons, alcohols, aldehydes, and fluorescent dyes [55–56, 60–61]. In addition, these nano-aggregates have longer lifetime, more stable structure, and much lower concentration for the formation of nano-aggregate. These advantages make amphiphilic block polymers a potential alternative material for surfactant micelles. However, there were few reports on the use of amphiphilic polymers for enhancing the efficiency and performance of filtration process (e.g., ultrafiltration) and soil remediation processes. PPO-PEO block copolymers were employed at ultrafiltration process and soil remediation process as nano-sized absorbents. However, amphiphilic block copolymers are costlier than other kinds of amphiphilic polymers and commercialized surfactants because of their complicated synthetic process, which limit widening of their applications. Even though many research groups have tried to develop more simple synthetic routes, and some of them can be efficiently produced in large scale (Pluronic and Kraton), their price is still high enough to make engineers and industrialists refrain from using them. Practically, the environmental engineering process cannot employ these very expensive amphiphilic block copolymers for remediation and treatment of extremely large volumes of water and soil.

1.2 AMPHIPHILIC CROSS-LINKED POLYMER NANOPARTICLES

As amphiphilic block copolymers are very expensive and can be obtained only by extremely difficult synthetic processes, their practical applications are limited in spite of their highly versatile functionality. If amphiphilic nanoparticles having the same performance of surfactant micelles could be created using a cheaper amphiphilic molecule synthesized by easy and simple process, amphiphilic nanoparticles would be applied at various engineering fields and replace surfactant molecules. Also, the above-mentioned drawbacks of SESR and MEUF processes could be solved by these nanoparticles, as a consequence, a new NT-ET fused technology for

direct removal of pollutants from water and soil could be developed.

As a most promising alternative material for amphiphilic block copolymers, amphiphilic reactive oligomers could be suggested. These oligomers correspond to amphiphilic precursor chains that can be polymerized to form amphiphilic polymer. Representative examples of amphiphilic reactive oligomers are photo-curable water-dispersible coating materials such water-dispersible epoxy acrylate, urethane acrylate, polyester acrylate, etc. [64–73]. That is, epoxy acrylate and urethane acrylate chains are originally hydrophobic, but by introducing hydrophilic components at their backbone, these chains can be dispersible in water. These chains can also be polymerized by radical-initiated reaction between their acrylate groups. Compared with amphiphilic block copolymers, these reactive oligomers are much cheaper and can be synthesized using much simpler process. As these oligomers can be applied at various substrates and their viscosity can be easily controlled using environment-friendly solvent (water), they have been widely used at paint and coating industries to replace the conventional organic solvent-based coatings and paints.

Amphiphilic reactive oligomers can also be classified into anionic, cationic, nonionic amphiphilic oligomers with type of hydrophilic component [63–68]. That is, the oligomer having carboxylic acid or sulfonic acid as hydrophilic side group or in the backbone is called anionic amphiphilic oligomers. One of representative amphiphilic reactive oligomer is amphiphilic urethane acrylate that can be nano-dispersed in water without using external surfactants. Various amphiphilic urethane acrylate can be synthesized with type of hydrophobic polyol (e.g., polytetramethylene glycol, polypropylene glycol, etc.), diisocyanate (e.g., toluene diisocyanate, methylene diphenyl diisocyanate, hexamethylene diisocyanate, etc.), and hydrophilic monomers such as dimethyl propionic acid, dimethyl butdimethanol amine, etc. [69–73].

On contacting with water, amphiphilic urethane acrylate oligomers form nano-sized aggregates, which are formed by microphase separation between hydrophilic and hydrophobic segments just like the formation of surfactant micelles or amphiphilic block copolymer micelles. Even though these aggregates are micelle-like oligomer nanoparticles, these nanoparticles can be easily converted into amphiphilic polymer nanoparticles through conventional polymerization process. So, micelle-like amphiphilic polymer nanoparticles dispersed in water can be obtained not by amphiphilic block copolymers but by amphiphilic oligomers, which can be synthesized by an easier and simple process.

In the subsequent chapters, synthesis of amphiphilic polymer nanoparticles using amphiphilic urethane acrylates will be presented. These oligomers have hydrophobic polypropylene or polytetramethylene oxide segment and hydrophilic carboxylic groups or polyethylene oxide segment at the same chain. In addition, these oligomers have reactive vinyl groups that make them polymerized by various radical initiation methods. These chains formed nano-sized oligomer particles dispersed in water without the use of any dispersant. That is, on mixing with water, their hydrophobic segments were aggregated with each other to form hydrophobic interior while their hydrophilic groups and segments were reacted with water and oriented toward outer water phase, resulting in the formation of micelle-like amphiphilic oligomer nanoparticles dispersed in water. Through radical-initiated polymerization process, amphiphilic oligomer nanoparticles were converted into amphiphilic cross-linked polymer (ACP) nanoparticles and their individual morphology and functionality were maintained. Our amphiphilic oligomers could be synthesized using relatively simple and easy process with much lower price. In addition to this, these oligomers could form micelle-like amphiphilic polymer nanoparticles in water. So, it could be highly expected that ACP nanoparticles prepared using our amphiphilic oligomers could have better performance and be more competitive compared to surfactants and ABCs.

References

- [1] Metcalf and Eddy (1972) *Wastewater Engineering: Collection, Treatment, Disposal*, McGraw-Hill, New York.
- [2] Henze, M. (2002) *Wastewater Treatment: Biological and Chemical Processes*, 3rd edn, Springer, Berlin, New York.
- [3] Jain, R. K., Aurelle, Y., Cabassud, C., Roustan, M., and Shelton, S. P. (1997) *Environmental Technologies and Trends: International and Policy Perspectives*, Springer-Verlag, Berlin, Heidelberg, New York.
- [4] Parak, W. J., Manna, L., Simmel, F. C., Gerion, D., and Alivisatos, P. (2004) *Nanoparticles* (ed. Schmid, G.), Wiley-VCH Verlag GmbH & Co. KGaA, Weinheim, Germany, pp. 4–358.
- [5] Moser, W. R., Find, J., Emersom, S. C., and Krausz, I. M. (2001) *Nanostructured Materials* (ed. Ying, J. Y.), Academic Press, London, UK, pp. 2–121.
- [6] Wang, Z. L., Liu, Y., and Zhang, Z. (eds) (2003) *Handbook of Nanophase and Nanostructured Materials: Vol. 3, Materials System and Application (I)*, Kluwer Academic/Plenum Publishers, New York.

- [7] Wang, Z. L., Liu, Y., and Zhang, Z. (eds) (2003) *Handbook of Nanophase and Nanostructured Materials: Vol. 4, Materials System and Application (II)*, Kluwer Academic/Plenum Publishers, New York.
- [8] Nicolais L., and Carotenuto, G. (eds) (2005) *Metal-Polymer Nanocomposites*, Wiley Interscience, Hoboken, NJ.
- [9] Adachi, M., and Lockwood, D. J. (eds) (2006) *Self-Organized Nanoscale Materials*, Springer, New York.
- [10] Ventra, M. D., Evoy, S., and Heflin, J. R. (eds) (2004) *Introduction to Nanoscale Science and Technology*, Kluwer Academic Publishers, Norwell, MA.
- [11] Klabunde, K. J. (ed.) (2001) *Nanoscale Materials in Chemistry*, John Wiley & Sons, New York.
- [12] Karn, B., Masciagioli, T., Zhang, W. X., Colvin, V., and Alivisatos, P. (2005) *Nanotechnology and the Environment: Applications and Implications*, ACS Symposium Series 890, American Chemical Society, Washington DC.
- [13] Heol, A., Reyes, L. F., Heszler, P., Lantto, V., and Granqvist, C. G. (2004) Nanomaterials for environmental applications: novel WO₃-based gas sensors made by advanced gas deposition, *Curr. Appl. Phys.*, **4**, 547–553.
- [14] Kong, J., Franklin, N. R., Zhou, C., Chapline, M. G., Peng, S., Cho, K., and Dai, H. (2000) Nanotube molecular wires as chemical sensors, *Science*, **287**, 622.
- [15] Murray, B. J., Walter, E. C., and Penner, R. M. (2004) Amine vapor sensing with silver mesowires, *Nano Lett.*, **4**, 665.
- [16] Chiou, C. Y., and Chou, T. C. (1996) Amperometric sulfur dioxide sensors using the gold deposited gas-diffusion electrode, *Electroanalysis*, **8**, 1179.
- [17] Riu, J., Maroto, A., and Rius, F. X. (2006) Nanosensors in environmental analysis, *Talanta*, **69**, 288–301.
- [18] Okamoto, M., Morita, S., and Kotaka, T. (2001) Dispersed structure and ionic conductivity of smectic clay/polymer nanocomposite, *Polymer*, **42**, 2685–2688.
- [19] Chen, H. W., Lin, T. P., and Chang, F. C. (2002) Ionic conductivity enhancement of the plasticized PMMA/LiClO₄ polymer nanocomposites electrolyte containing clay, *Polymer*, **43**, 5281–5288.
- [20] Kim, J. Y., Han, K. H., Suh, K. D., and Ihn, K. J. (2007) Synthesis of microphase-separated solvent-free solid polymer electrolytes nanocomposites films using amphiphilic urethane acrylate precursors, *J. Appl. Polym. Sci.*, **106**, 1359–1367.

- [21] Kim, D. W., Choi, H. S., Lee, C. J., Blumstein, A., and Kang, Y. K. (2004) Investigation on methanol permeability of Nafion modified by self assembled clay-nanocomposite multilayers, *Electrochim. Acta*, **50**, 659–662.
- [22] Chang, J. H., Park, J. H., Park, G. G., Kim, C. H., and Park, O. O. (2003) Proton-conducting composite membranes derived from sulfonated hydrocarbon and inorganic materials, *J. Power Sources*, **124**, 18–25.
- [23] Kim, D. S., Park, H. B., Rhim, J. W., and Lee, Y. M. (2005) Proton conductivity and methanol transport behavior of cross-linked PVA/PAA/silica hybrid membranes, *Solid State Ionics*, **176**, 117–126.
- [24] Kim, D. S., Park, H. B., Rhim, J. W., and Lee Y. M. (2004) Preparation and characterization of crosslinked PVA/SiO₂ hybrid membranes containing sulfonic acid groups for direct methanol fuel cell applications, *J. Membr. Sci.*, **240**, 37–48.
- [25] Aparicio, M., Castro, Y., and Duran, A. (2005) Synthesis and characterisation of proton conducting styrene-co-methacrylate-Silica sol-gel membranes containing tungstophosphoric acid, *Solid State Ionics*, **176**, 333–340.
- [26] Lassegues, J. C., Grondin, J., Hernandez, M., and Maree, B. (2001) Proton conducting polymer blends and hybrid organic inorganic materials, *Solid State Ionics*, **145**, 37–45.
- [27] Xu, W., Lu, T., Liu, C., and Xing, W. (2005) Low methanol permeable composite Nafion/Silica/PWA membranes for low temperature direct methanol fuel cells, *Electrochim. Acta*, **50**, 3280–3285.
- [28] Cumbal, L., Greenleaf, J., Leun, D., and SenGupta, A. K. (2003) Polymer supported inorganic nanoparticles: characterization and environmental applications, *React. Funct. Polym.*, **54**, 167–180.
- [29] Myers, D. (1988) *Surfactant Science and Technology*, Wiley-VCH, New York.
- [30] Rosen, M. J. (2004) *Surfactants and Interfacial Phenomena*, Wiley-Interscience, Hoboken, NJ.
- [31] Scamehorn, J. F., and Harwell, J. H. (2000) *Surfactant-Based Separations: Science and Technology*, American Chemical Society, Washington, DC.
- [32] Sabatini, D. A., Knox, R. C., and Harwell, J. H. (eds) (1995) *Surfactant-Enhanced Subsurface Remediation: Emerging Technologies*, American Chemical Society, Washington, DC.
- [33] Mulligan, C. N., Yong, R. N., and Gibbs, B. F. (2001) Surfactant-enhanced remediation of contaminated soil: a review, *Eng. Geol.*, **60**, 371–380.
- [34] Paria, S. (2008) Surfactant-enhanced remediation of organic contaminated soil and water, *Adv. Colloid Interface Sci.*, **138**, 24–58.

- [35] Cheng, H., and Sabatini, D. A. (2007) Separation of organic compounds from surfactant solutions: a review, *Sep. Sci. Technol.*, **42**, 453–475.
- [36] Choi, Y. K., Lee, S. B., Lee, D. J., Ishigami, Y., and Kajiuchi, T. (1998) Micellar enhanced ultrafiltration using PEO-PPO-PEO block copolymers, *J. Membr. Sci.*, **148**, 185–194.
- [37] Dunn, R. O., Jr., Scamehorn, J. F., and Christian, S. D. (1985) Use of micellar-enhanced ultrafiltration to remove dissolved organics from aqueous stream, *Sep. Sci. Technol.*, **20**, 257–284.
- [38] Kandori, K., and Schechter, R. S. (1990) Selection of surfactants for micellar-enhanced ultrafiltration, *Sep. Sci. Technol.*, **25**, 83–108.
- [39] Fillipi, B. R., Brant, L. W., Scamehorn, J. F., and Christian, S. D. (1999) Use of micellar-enhanced ultrafiltration at low surfactant concentrations and with anionic-nonionic surfactant mixtures, *J. Colloid Interface Sci.*, **213**, 68–80.
- [40] Förster, S., and Antonietti, M. (1998) Amphiphilic block copolymers in structure-controlled nanomaterials hybrids, *Adv. Mater.*, **10**, 195–217.
- [41] Mayer, A. B. (2001) Colloidal metal nanoparticles dispersed in amphiphilic polymers, *Polym. Adv. Technol.*, 96–106.
- [42] Zhu, J., and Jiang, W. (2007) Fabrication of conductive metallized nanostructures from self-assembled amphiphilic triblock copolymer templates: nanospheres, nanowires, nanorings, *Mater. Chem. Phys.*, **101**, 56.
- [43] Ho, R. M., Tseng, W. H., Fan, H. W., Chiang, Y. W., Lin, C. C., Ko, B. T., and Huang, B. H. (2005) Solvent-induced microdomains orientation in polystyrene-b-poly(L-lactide) diblock copolymer thin films for nanopatterning, *Polymer*, **46**, 9362.
- [44] Spatz, J. P., Roescher, A., and Möller, M. (1996) Gold nanoparticles in micellar Poly(styrene)-b-Poly(ethylene oxide) films – size and interparticle distance control in monoparticulate films, *Adv. Mater.*, **8**, 337–340.
- [45] Antonietti, M., Wenz, E., Bronstein, L., and Seregina, M. (1995) Synthesis and characterization of nobel metal colloids in block copolymer micelles, *Adv. Mater.*, **7**, 1000–1005.
- [46] Antonietti, M., Förster, S., Hartmann J., and Oestreich, S. (1996) Novel amphiphilic block copolymers by polymer reactions and their use for solubilization of metal salts and metal colloids, *Macromolecules*, **29**, 3800–3806.
- [47] Dresco, P., Zaitsev, V. S., Gambino, R. J., and Chu, B. (1999) Preparation and properties of magnetite and polymer magnetite nanoparticles, *Langmuir*, **15**, 1945–1951.

- [48] Sohn, B. H., and Cohen, R. E. (1997) Processible optically transparent block copolymer films containing superparamagnetic iron oxide nanoclusters, *Chem. Mater.*, **9**, 264–269.
- [49] Moffitt, M., and Eisenberg, A. (1995) Size control of nanoparticles in semiconductor-polymer composites. 1. Control via multiplet aggregation numbers in styrene-based random ionomers, *Chem. Mater.*, **7**, 1178–1184.
- [50] Moffitt, M., McMahon, L., Pessel, V., and Eisenberg, A. (1995) Size control of nanoparticles in semiconductor-polymer composites. 2. Control via size of spherical ionic microdomains in styrene-based Diblock ionomers, *Chem. Mater.*, **7**, 1185–1192.
- [51] Kane, R. S., Cohen, R. E., and Silbey, R. (1996) Synthesis of PbS nanoclusters within block copolymer nanoreactors, *Chem. Mater.*, **8**, 1919–1924.
- [52] Wang, S., and Yang, S. (2000) Preparation and characterization of oriented PbS crystalline nanorods in polymer films, *Langmuir*, **16**, 389–397.
- [53] Mayer, A. B. R., and Mark, J. E. (2000) Poly(2-hydroxyalkyl methacrylates) as stabilizers for colloidal noble metal nanoparticles, *Polymer*, **41**, 1627–1631.
- [54] Carotenuto, G. (2001) Synthesis and characterization of poly(*N*-vinylpyrrolidone) filled by monodispersed silver clusters with controlled size, *Appl. Organomet. Chem.*, **15**, 344–351.
- [55] Nagarajan, R., Barry, M., and Ruckenstein, E. (1986) Unusual selectivity in solubilization by block copolymer micelles, *Langmuir*, **2**, 210–215.
- [56] Forster, S., and Antonietti, M. (1998) Amphiphilic block copolymers in structure-controlled nanomaterial hybrids, *Adv. Mater.*, **10**, 195–217.
- [57] Abetz, V., and Simon, P. F. W. (eds) (2005) *Phase Behaviour and Morphologies of Block Copolymers*, Springer-Verlag, Berlin, Heidelberg.
- [58] Hadjichristidis, N., Pitsikalis, M., and Latrou, H. (eds) (2005) *Synthesis of Block Copolymers*, Springer-Verlag, Berlin, Heidelberg.
- [59] Gohy, J. -F. (ed.) (2005) *Block Copolymer Micelles*, Springer-Verlag, Berlin, Heidelberg.
- [60] Hurter, P. N., and Hatton, T. A. (1992) Solubilization of polycyclic aromatic hydrocarbons by poly(ethylene oxide-propylene oxide) block copolymer micelles: effects of polymer structure, *Langmuir*, **8**, 1291–1299.
- [61] Nagarajan, R. (2001) Solubilization of guest molecules into polymeric aggregates, *Polym. Adv. Technol.*, **12**, 23–43.

- [62] Nivaggioli, T., Tsao, B., Alexandridis, P., and Hatton, T. A. (1995) Microviscosity in pluronic and tetronic poly(ethylene oxide)-poly (propylene oxide) block copolymer micelles, *Langmuir*, **11**, 119–126.
- [63] Kabanov, A. V., Nazarova, I. R., Astafieva, I. V., Batrakova, E. V., Alakhov, V. Y., Yaroslavov, A. A., and Kabanov, V. A. (1995) Micelle formation an solubilization of fluorescent probes in poly(oxyethylene-b-oxypropylene-b -oxyethylene) solutions, *Macromolecules*, **28**, 2303–2314.
- [64] Glass, J. E. (1997) *Technology for Waterborne Coatings*, ACS Symposium Series 663, American Chemical Society, Washington DC.
- [65] Suh, K. -D., Kim, J. -W., and Kim, J. -Y. (1999) Novel waterborne coating materials and their film properties, *J. Adhes. Soc. Jpn.*, **35**(5), 210.
- [66] Suh, K. -D., Kim, J. -W., and Kim, J. -Y. (1999) Synthesis and properties of UV-curable urethane acrylate, *Poly. Sci. Technol.*, **10**(5), 629.
- [67] Park, N. -H., Suh, K. -D., Kim, J. -Y. (1997) Preparation of UV-curable PEG-modified urethane acrylate emulsions and their coating properties II. Effect of chain length of polyoxyethylene groups, *J. Appl. Poly. Sci.*, **64**, 2657.
- [68] Song, M. -E., Kim, J. -Y., and Suh, K. -D. (1996) Preparation of UV-curable emulsions using PEG-modified urethane acrylates: the effect of nonionic and anionic groups, *J. Appl. Poly. Sci.*, **62**, 1775.
- [69] Ghosh, S., and Krishnamurti, N. (2001) Preparation and properties of UV-curable polyurethane methacrylate cationomers and their use as adhesives, *Polym. Plast. Technol. Eng.*, **40**(4), 539–559.
- [70] Ryu, J. -H., Kim, J. -W., Suh, K. -D. (1999) Synthesis of water-soluble urethane acrylate cationomers and their ultraviolet coating properties, *J. Macromol. Sci.*, Part 1-Pure and Applied Chemistry.
- [71] Kim, H. -D., and Kim, T. -W. (1998) Preparation and properties of UV-curable polyurethane acrylate ionomers, *J. Appl. Polym. Sci.*, **67**, 2153–2162.
- [72] Lee, K. H., and Kim, B. K. (1996) Structure-property relationships of polyurethane anionomer acrylates, *Polymer*, **37**, 2251–2257.
- [73] Kim, J. -Y., Kim, C. -H., Yoo, D. -J., and Suh, K. -D. (2000) Hydrophobic and hydrophilic aggregation of tailor-made urethane acrylate anionomers in various solvents and their network structures, *J. Polym. Sci., Part B: Polym. Phys.*, **38**, 1903–1916.

This page intentionally left blank

Chapter 2

USE OF AMPHIPHILIC CROSS-LINKED POLYMER NANOPARTICLES CONTAINING ANIONIC HYDROPHILIC SEGMENTS FOR ENHANCED DESORPTION OF POLYAROMATIC HYDROCARBONS (PAHs) FROM AQUIFER SOIL

Juyoung Kim

*Department of Advanced Materials Engineering,
Kangwon National University, Samcheok, Kangwon 245-711,
South Korea
juyoungk@kangwon.ac.kr*

Contamination of soil and groundwater by hydrophobic organic carbons (HOCS) is caused by leak, spill from storage tanks, improper disposal of wastes and pesticides, transportation, combustion, and geological phenomena [1–5]. Once soils are contaminated by HOCS, they act as a long-term source of contamination for soil and groundwater, because of low water solubility, adsorption onto the soil matrix, very limited biodegradability. Among HOCS, pesticides, polyaromatic hydrocarbons (PAHs), and chlorinated solvents are of special interest. These organic compounds are known as carcinogenic and mutagenic compounds, but they cannot be easily removed by conventional soil remediation process such as a pump-and-treat process, which has been a tough challenge to scientists and engineers [6–10].

Advances in Nanotechnology and the Environment

Edited by Juyoung Kim

Copyright © 2012 by Pan Stanford Publishing Pte. Ltd.

www.panstanford.com

Especially, PAHs are a class of organic compounds consisting of over 100 individual moieties composed of more than two aromatic rings. PAHs are a kind of ubiquitous compound and have been found widely distributed in atmospheric particulates, freshwater, various sediments, soils, and leachates. Also, soil contamination by PAHs can occur through various sources such as incomplete combustion of organic matter, oil spill and leak from storage tank, and improper disposal of fuel or oil products. Because of their highly hydrophobic nature, and hence their strong adsorption onto the soil, these sorbed contaminants cannot be completely removed by conventional soil-washing process such as pump-and-treatment process and act as a long-term source of groundwater contamination even after the removal of large volumes of the source of PAHs from contaminated sites.

It has been reported that surfactants are the most effective material for removal of highly hydrophobic organic contaminants from soils. Soil washing using surfactant was originally used for oil recovery process because surfactant can decrease interfacial tensions of oils with water and increase apparent solubility of oils in water [3–5]. Later surfactants were first used for removal of nonaqueous phase liquids (NAPLs) such as coal tar, creosote, and petroleum liquids from soil. Surfactant molecules consist of hydrophobic and hydrophilic moieties, so they can locate at oil–water interface to reduce interfacial tension and form nano-aggregates (micelle) above a certain concentration in water (critical micelle concentration, CMC) [11–23]. By applying surfactant aqueous solutions into contaminated soils, mobility of NAPLs in soil matrix is highly increased by reducing the interfacial tensions with water (mobilization), and solubility in NAPLs in water is increased by solubilizing them within surfactant micelles (micellar solubilization). It has also been reported that PAHs strongly sorbed onto soils could be desorbed by mobilization and micellar solubilization performance of surfactant molecules. So, surfactant-enhanced soil remediation (SESR) processes have been extensively studied and applied at various contaminated soil sites for removal of PAHs [24–42]. Efficiency of SESR process strongly depends on the type of surfactant, which is characteristic of soil. Especially, sorption of surfactant on soils is the most decisive factor for determining the performance of SESR process because sorption of surfactant onto soils can alter the nature of soil and CMC of the surfactant. That is, sorbed surfactants onto soil decrease the actual amount of surfactant available for solubilizing and mobilizing contaminants and make contaminants re-adsorbed onto soils. In addition, sorbed surfactant molecules also have toxicity for soil

bacteria and even for human. This strong sorption of surfactant onto soils highly decreases the efficiency of SESR process and increases the surfactant dose required for soil remediation. So, biosurfactants and specially designed surfactants such as twin-head surfactant and polymeric surfactant have been studied to reduce surfactant sorption and minimize the adverse effect of surfactant sorption.

Sorption of surfactant molecules is mainly due to their physical structure. Below CMC, surfactants exist as dissolved single molecules, and above CMC surfactants are self-assembled to form nano-sized aggregates (micelles) in water or oil phase. As micelles are formed by physical association, these nano-sized aggregates are so fragile that they are easily broke down. Even at concentration higher than CMC, micelles and dissolved monomeric surfactant molecules co-exist in the medium, and micelle easily break down and return to monomeric molecules, which result in high degree of surfactant sorption onto soil. So, to highly reduce sorption of surfactant-like molecules, their self-assembled structure should be strong enough on contacting with soil and even in aqueous phase. In previous section, amphiphilic polymer nanoparticles were suggested as the most possible alternative materials for surfactant micelles. Amphiphilic cross-linked polymer (ACP) nanoparticles having surfactant micelle-like structure are formed by self-assembling in aqueous phase but their structures are permanently locked-in by chemical reaction, so ACP nanoparticles can maintain their microstructure on containing with soil and oil phase. In the following sections, performance of surfactant micelles and ACP nanoparticles for removal of phenanthrene is compared and represented.

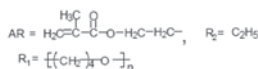
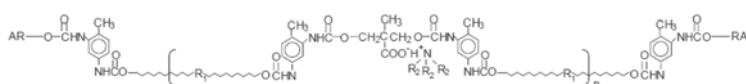
2.1 SYNTHESIS OF REACTIVE AMPHIPHILIC OLIGOMER

As discussed earlier, ACP nanoparticles having micelle-like structures in aqueous phase could be prepared using reactive amphiphilic oligomers such as urethane acrylate anionomer, cationomer, and non-ionomer. These oligomers consist of hydrophilic and hydrophobic segments and have reactive vinyl groups at the same backbone. As hydrophilic and hydrophobic segments in the oligomers chains are chemically connected with each other via urethane linkages and acrylate groups are introduced at hydrophobic segments or end groups, these oligomers were named as amphiphilic urethane acrylate or water-dispersible urethane acrylate. According to the

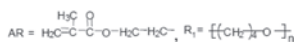
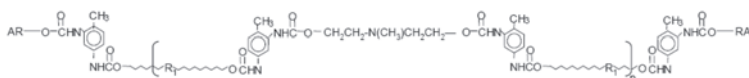
type of hydrophilic segment, urethane acrylate can be classified as urethane acrylate anionomer (UAA), urethane acrylate cationomer (UAC), and urethane acrylate nonionomer (UAN). For example, urethane acrylate anionomer is an amphiphilic urethane acrylate containing anionic hydrophilic segments such as carboxylic acid and sulfonic acid groups.

UAA chains can be synthesized with various processes using various chemicals. One of the representative processes is using dimethylol propionic acid (DMPA) as a hydrophilic anionic monomer. As DMPA has two hydroxyl groups and a carboxylic acid group at the same backbone, hydrophilic carboxylic groups can be introduced at the precursor backbone by the reaction of two hydroxyl groups with isocyanate groups [43–47]. In this chapter, UAA chains synthesized using DMPA were used for the preparation of anionic ACP nanoparticles. For the synthesis of UAA chains, poly(tetramethylene glycol) (PTMG, Mw = 1000) was first mixed with DMPA at various molar ratios and dissolved in *N*-methyl-2-pyrrolidone (NMP). Then, 2,4-toluene diisocyanate (TDI) was added to the mixture of PTMG and DMPA to form NCO-terminated urethane precursor containing carboxylic acid groups at the backbone. As a final step, 2-hydroxyethyl methacrylate (2-HEMA) was reacted with NCO groups of this urethane precursor to introduce reactive vinyl groups at the precursor chains. After completion of the three-step reaction, polytetramethylene oxide (PTMO)-based hydrophobic segments and hydrophilic carboxylic acid groups are randomly connected with each other via urethane linkage. In addition, this amphiphilic precursor has reactive vinyl groups at the both ends of hydrophobic segments.

The hydrophobic/hydrophilic balance of UAA chains could be varied by changing the molar ratio of PTMG/DMPA in the synthesis. As molar ratio of DMPA to PTMG in the synthesis composition is increased, the number of carboxylic groups introduced at UAA chain is increased, resulting in increase of hydrophilicity of UAA chain. Symbol UAA64 represents UAA precursor chain synthesized at 6/4 molar ratio of PTMG/DMPA. The hydrophilicity of UAA chains increases in the order of UAA64, UAA55, and UAA28. The proposed chemical structure of UAA and the recipe for synthesis of UAA chains are shown in Fig. 2.1 and Table 2.1, respectively. The polystyrene equivalent molecular weight of synthesized UAN chains is a 3750–6,700 g/mol weight average molecular weight with a polydispersity of 1.93–2.01.



UAC



UAA

Figure 2.1 Schematic presentation of chemical structure of UAC and UAA. Reprinted with permission from Ref. [48].

Table 2.1 Recipe for the synthesis of UAA chains and their molecular weight

Molar ratio of PTMG/DMPA/TDI/2-HEMA				Symbol	Mn (g/mol)
0.6	0.4	1.5	1	UAA64	6700
0.5	0.5	1.5	1	UAA55	5670
0.2	0.8	1.5	1	UAA28	3750

2.2 SYNTHESIS OF ANIONIC ACP NANOPARTICLES

By just mixing with water, UAA chains can be dispersed as micelle-like nanoparticles. That is, UAA chains can make nano-sized aggregates in water, which is caused by microphase separation between hydrophilic segments (carboxylic anion groups) and the hydrophobic segments within the chains. In the absence of a solvent, hydrophilic and hydrophobic segments in UAA chains are miscible with each other. In some solvents such as toluene, acetone, dimethyl acetamide, and dimethyl sulfoxide, both segments dissolve and do not make an aggregate in these solvents [43–47]. As water reacts

only with hydrophilic carboxylic anion groups of UAA chains, the carboxylic anion groups are microphase-separated from hydrophobic backbone and orient toward the water phase to the anionic exterior of nanoparticles, at the same time hydrophobic backbones are associated with each other through hydrophobic interaction or association and form hydrophobic interior of nanoparticles.

UAA nanoparticles dispersed in water are formed by physical association of oligomer chains with the same mechanism of formation of surfactant and amphiphilic block copolymer micelles. So, like micelles of surfactants and amphiphilic block copolymers are transient and weak microstructure, UAA nanoparticles are physically and chemically vulnerable. Physical and chemical strengths of UAA nanoparticles can be highly improved by chemical cross-linking reactions between vinyl groups located at hydrophobic backbone of UAA chains. Through radical-initiated cross-linking polymerization, UAA chains are chemically connected and cross-linked with each other, as a consequence, amphiphilic oligomer and UAA chains are converted into amphiphilic cross-linked polymers, which have unlimited molecular weight. When this cross-linking polymerization takes place in UAA nanoparticles dispersed in water, micelle-like structure of UAA nanoparticles is permanently locked-in and amphiphilic oligomer nanoparticles are converted into amphiphilic cross-linked polymer (ACP) nanoparticles dispersed in water.

Cross-linking polymerization of UAA nanoparticles dispersed in water can be carried out using conventional emulsion polymerization process. Water-soluble initiator, potassium persulfate (KPS) dissolved in UAA aqueous colloid solution, forms radicals in aqueous phase, and then radicals penetrate into UAA nanoparticles to initiate radical cross-linking polymerization. After the completion of the cross-linking reaction, micelle-like nanostructure of UAA was permanently locked-in by the cross-linking reaction between vinyl end groups in the hydrophobic interior, and then oligomeric UAA nanoparticles were converted into anionic ACP nanoparticles dispersed in aqueous phase. The postulated microstructure of anionic ACP nanoparticles is represented in Fig. 2.2. Anionic ACP nanoparticle synthesized with UAA 64, UAA55, and UAA28 chain is named as ACP 64, ACP 55, and ACP 28 nanoparticle, respectively. The sizes of anionic ACP measured using dynamic light scattering were in the range 32–61 nm.

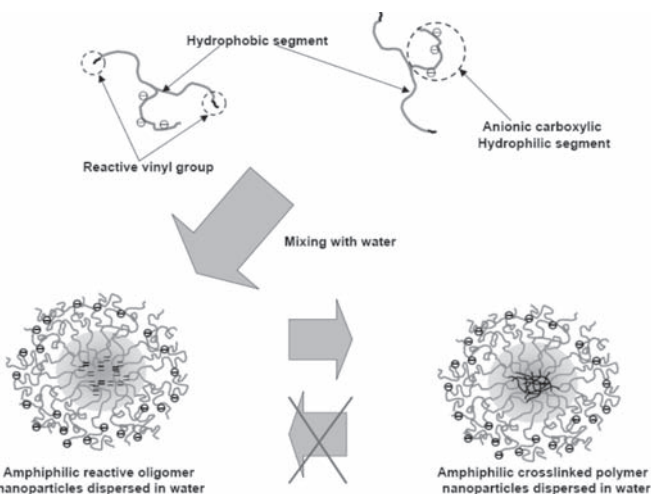


Figure 2.2 The postulated microstructure of anionic ACP nanoparticles.

2.3 INTERFACIAL ACTIVITY OF ANIONIC ACP NANOPARTICLES

The most interesting property of surfactant molecules is that surfactant molecule can locate at two immiscible phases such as water–oil interface, resulting in reducing their interfacial tension. This characteristic property of surfactant is called as interfacial activity, which makes it possible to increase the mobility of HOCs in soil matrix and to solubilize HOCs within surfactant micelles. So, the interfacial activity of anionic ACP nanoparticles was measured and compared with anionic surfactant sodium dodecyl sulfate (SDS). Surface tensions of anionic ACP nanoparticle and SDS aqueous solution at various concentrations were determined using a Model 20 surface tensiometer (Fisher Scientific). This instrument operates on the du Nöuy principle, in which a platinum ring is suspended from a torsion balance.

As shown in Fig. 2.3, surface tension of SDS and ACP aqueous solution decreased with the increase of its concentration in water, indicating that like SDS, ACP nanoparticles can locate at water–air interface. The interesting phenomenon is that the surface tension of SDS aqueous solution sharply decreased and remained

constant at concentration 141–200 mg/L, whereas ACP aqueous solutions showed continuous decrease in surface tensions without the abrupt decrease of surface tension at a specific concentration indicating formation of micelles. This indicates that SDS molecules have a specific concentration for formation of their micelles (CMC), whereas ACP nanoparticles aqueous solutions do not. This result can be interpreted in terms of difference in microstructure between ACP and SDS molecules.

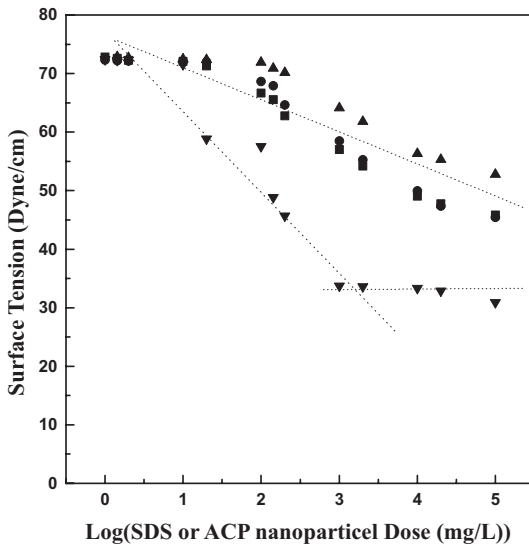


Figure 2.3 Surface tension for SDS and ACP nanoparticle solutions: - ■ - ACP64, - ● - ACP 55, - ▲ - ACP 28, and - ▼ - SDS. Reprinted with permission from Ref. [48].

At concentration lower than CMC, SDS molecules exist as dissolved monomeric molecules in aqueous phase. At concentration equal to or greater than CMC, nano-aggregate (micelle) and dissolved monomeric molecule of SDS co-exists at the aqueous phase. As surfactant molecules can solubilize and mobilize hydrophobic pollutants only at concentration greater than CMC, dose of SDS for removal of hydrophobic pollutants should be greater than 141–200 mg/L. However, ACP nanoparticles do not have a critical concentration for formation of nano-aggregates, that is, UAC chains can form nano-aggregates (micelle) at extremely low concentration in aqueous phase. Schematic illustration of aqueous phase of SDS and ACP nanoparticles is presented in Fig. 2.4.

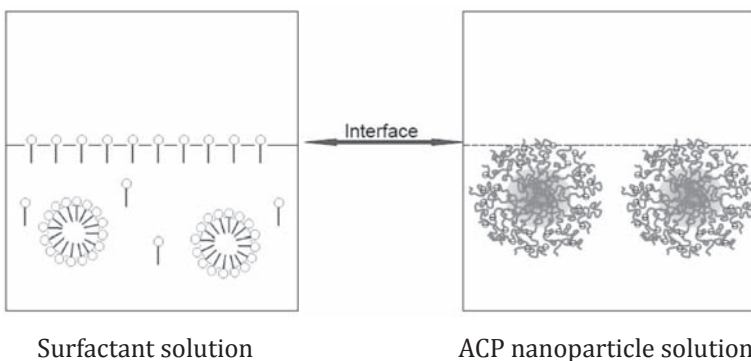


Figure 2.4 Schematic illustration of aqueous phase of SDS and ACP nanoparticles.

2.4 SOLUBILIZATION PERFORMANCE OF ANIONIC ACP NANOPARTICLES

Amphiphilic molecules and surfactant can increase the solubility of HOC molecules in water phase because the hydrophobic core of surfactant micelles can accommodate a certain amount of lipophilic organic compound as a solubilizate. This solubilization capability of surfactant makes itself useful materials for soil-washing process. So, the enhanced solubility of a certain HOC by a surfactant can be used as an index for evaluating a surfactant for soil-washing process and wastewater treatment process of sorbed and solubilized HOC. Solubilization capability of a surfactant is generally described as molar solubilization ratio (MSR) or weight solubilization ratio (WSR) [25–26, 30, 33, 35], but molecular weight of ACP nanoparticles used in this study cannot be calculated because those particles formed by cross-linking polymerization of urethane acrylate anionomer (UAA) have unlimited molecular weight. In polymer chemistry field, molecular weight of cross-linked polymer has been being considered as unlimited molecular weight. So, solubilization capability of ACP nanoparticles has to be presented as enhanced solubility of phenanthrene in water that is ratio of C/C_0 , where C is the concentration of phenanthrene in aqueous solution containing ACP nanoparticles or SDS and C_0 is the concentration of phenanthrene in pure water phase.

As shown in Fig. 2.5, enhanced solubility of HOC in a given surfactant or amphiphilic molecules can be examined by measuring the concentration of HOC in aqueous solution containing surfactant

or amphiphilic molecules and comparing it with the concentration of HOC in pure water. For example, enhanced solubility of phenanthrene in surfactant or ACP nanoparticle solutions can be easily obtained using radio-labeled phenanthrene. That is, concentrated radio-labeled phenanthrene-methylene chloride solutions (35 g/L) were first prepared. Two milliliters of phenanthrene solution was added into 25 mL glass scintillation vial equipped with open-top screw caps and Teflon-backed septa. After evaporation of methylene chloride, SDS or ACP aqueous solutions (10 mL) of various concentrations were added into the vials. As the amount of phenanthrene remaining in the vials was much greater than the solubility of phenanthrene in water, the loss of phenanthrene due to evaporation was inconsequential [32, 49–50].

The vials were sealed and gently agitated with a rotary tumbler for 1 day. After completion of mixing, 5 mL of supernatant was withdrawn and centrifuged at an acceleration $15000 \times g$. One milliliter of the sample was transferred into scintillation vials (Poly-Q vial P/N 566740, Beckman Coulter, U.S.A) containing 10 mL of Ecolume cocktail (Ready Safe P/N 141349, Beckman Coulter, U.S.A), and the concentration of ^{14}C -phenanthrene in the aqueous phase was measured using a liquid scintillation counter (LSC) (see Fig. 2.5).

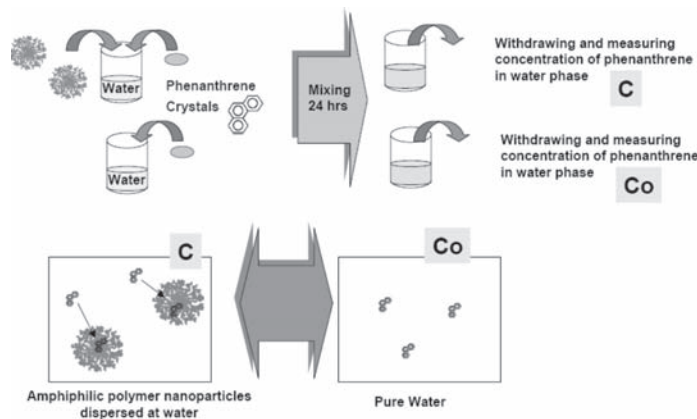


Figure 2.5 Procedure for measuring enhanced solubility of HOC in aqueous solutions containing amphiphilic molecules.

Enhanced solubility (C/C_0) of phenanthrene at various concentrations of SDS or ACP nanoparticles in aqueous solutions is shown in Fig. 2.6. C/C_0 increased with the increase of ACP

nanoparticles, indicating that ACP nanoparticles can solubilize phenanthrene within their hydrophobic interiors just like surfactant micelles solubilize phenanthrene within their hydrophobic core. At higher concentration, SDS micelles and ACP nanoparticles increased the solubility to 55 times and 2–8 times as much as the phenanthrene concentration that an equal amount of pure water can solubilize. This indicates that solubilization capability of SDS is much better than that of ACP nanoparticles.

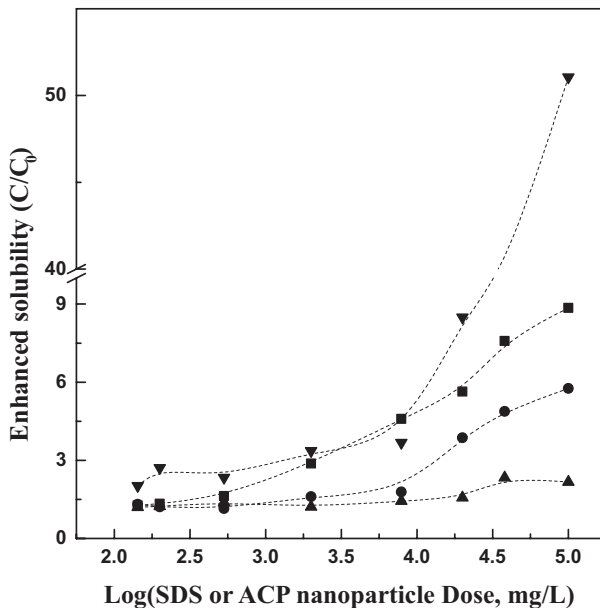


Figure 2.6 Enhanced solubility of phenanthrene in aqueous phase in the presence of SDS or ACP nanoparticles: - ■ - ACP64, - ● - ACP 55, - ▲ - ACP 28, and - ▼ - SDS. Reprinted with permission from Ref. [48].

As illustrated in Fig. 2.6, the lower solubilization efficiency of ACP nanoparticles can be interpreted in terms of microstructural difference between ACP solution and SDS solution. For SDS solution, monomeric SDS molecules can easily contact with crystalline phenanthrene to solubilize phenanthrene and form micelles having phenanthrene within their hydrophobic interior. And SDS micelles can also be broken up to become monomeric SDS molecules and carry out solubilization of phenanthrene. However, for ACP nanoparticles, their micelle-like microstructure is permanently locked-in by cross-

linking polymerization, so solubilization of crystalline phenanthrene by ACP nanoparticles is more difficult compared to SDS molecules.

ACP 64 nanoparticles show a better enhanced solubilization performance (eight times) than ACP 55 (six times) and ACP 28 (two times) nanoparticles. This difference may be due to the difference of hydrophilicity or hydrophobicity among these nanoparticles. For the synthesis of UAA chains, DMPA molecules were reacted with isocyanate compounds to introduce hydrophilic carboxylic groups to hydrophobic PTMG-based backbone, which makes urethane acrylate chains water-dispersible and form nanoparticles in water. As the molar ratio of DMPA to PTMG increases in the synthesis of UAA chains, the hydrophilicity of UAA chains increases, resulting in the formation of smaller ACP nanoparticles in aqueous phase. So, ACP 64 nanoparticles based on UAA 64 chains, which are synthesized at the highest molar ratio of PTMG/DMPA, have the highest hydrophobicity, resulting in the highest solubilization performance among ACP nanoparticles.

2.5 EQUILIBRIUM DISTRIBUTION OF PHENANTHRENE BETWEEN AQUEOUS PHASE AND AQUIFER SAND

Distribution of hydrophobic organic compounds (HOC) between aqueous phase and soil is largely changed with the addition of surfactant, because surfactant molecules enhance the apparent solubility of HOC in aqueous phase through micellar solubilization and mobilization performance of surfactant molecules [41, 51-52]. That is, desorption of HOC from soil can be increased by the surfactant molecules existing in aqueous phase, resulting in change of distribution of HOC between aqueous phase and soil. So, this distribution of compounds can be used as an index for evaluating soil-washing performance of a surfactant and estimated as:

$$K_d = [\text{HOC}]_s / ([\text{HOC}]_w + [\text{HOC}]_{\text{mic}}) = (\text{mol of HOC sorbed/g of solid}) / (\text{mol of HOC in aqueous and micellar solution/L})$$

where K_d is the partition coefficient of HOC between solid and aqueous pseudophase, $[\text{HOC}]_s$ is the moles of HOC sorbed per gram of solid (mole/g), $[\text{HOC}]_w$ is the moles of HOC in water per liter of solution (mole/L), and $[\text{HOC}]_{\text{mic}}$ is the moles of HOC in micelles per liter of solution (mole/L).

As ACP nanoparticles have interfacial activity and solubilization capability, the distribution of HOC molecules between aqueous phase and soil surfactant can be changed by adding ACP nanoparticles into the mixture of aqueous solution and soil where distribution of HOC molecules is equilibrated between the two phases. When ACP nanoparticles dispersed in aqueous phase contact with soil matrix, they extract HOC molecules adsorbed in soil matrix and absorb it within their hydrophobic interior, resulting in increase of distribution of HOC in aqueous phase. So, the degree of increase in the distribution of HOC molecules in the presence of ACP nanoparticles can also be used as an index of desorption capability of ACP nanoparticles for adsorbed HOC molecules.

Change in distribution of HOC between aqueous phase and soil matrix in the presence of amphiphilic molecules can be measured using an artificial contaminated soil matrix. That is, a given soil is mixed with an HOC compound to have HOC molecules adsorbed onto soil. Then, this mixture is mixed with pure water and aqueous solution containing amphiphilic molecules. After reaching equilibrium, the concentration of the HOC compound in pure water and aqueous solution containing amphiphilic molecules is measured and compared with each other. As the solubility of HOC molecules in water is generally low, most of the HOC molecules are within soil, and their concentration in aqueous phase is very low. In the presence of amphiphilic molecules in aqueous phase, these molecules extract or solubilize HOC molecules adsorbed onto soil, causing increasing distribution of HOC molecules in aqueous phase. So, increase in the distribution of HOC in aqueous phase can be considered as desorption capability of amphiphilic molecules for HOC molecules adsorbed onto a soil.

Concentration of an HOC molecule in aqueous phase before and after mixing with aqueous solution containing amphiphilic molecules can be measured using various procedures. In this chapter, change in the concentration of phenanthrene in aqueous phase was measured using the following process:

¹⁴C-phenanthrene aqueous solution (1 mL) was added into the scintillation glass vial containing 1 g of aquifer sand and agitated with a rotary tumbler for 2 days. After completion of mixing, 9 mL of SDS solution or ACP aqueous solutions of various concentrations were added into the vials, and re-agitated with a rotary tumbler for 2 days, at which point they were then centrifuged ($15000 \times g$) to separate

the soil from the aqueous solution. One milliliter of supernatant was withdrawn was transferred into scintillation vials containing 10 mL of Ecolume cocktail, and the concentrations of ^{14}C -phenanthrene in the aqueous phase was measured using an LSC.

The results of the experiments are plotted in Fig. 2.7 as a function of the concentration of ACP nanoparticles or SDS. The K_{d} values of phenanthrene decrease with an increase of ACP or SDS concentration, indicating that adsorbed phenanthrene on the soil was extracted by ACP nanoparticles or SDS molecules.

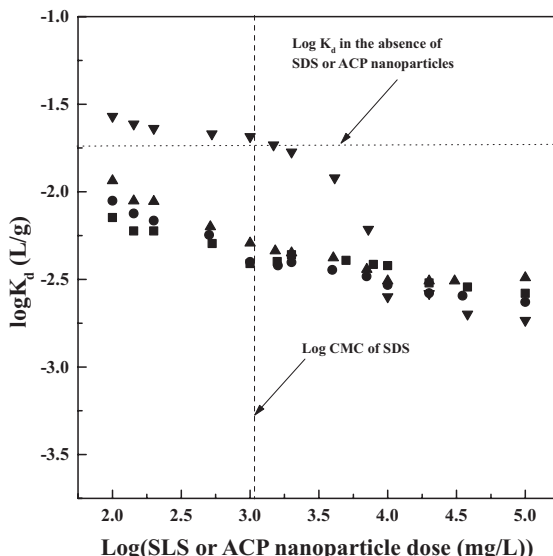


Figure 2.7 Distribution of phenanthrene between soil and aqueous pseudophase containing SDS or ACPU nanoparticles: - ■ - ACP64, - ● - ACP 55, - ▲ - ACP 28, and - ▼ - SDS. Reprinted with permission from Ref. [48].

This desorption behavior of sorbed phenanthrene can be divided into two regions. In the low concentration region (100–2100 mg/L), when one adds SDS to water/aquifer material absorbing phenanthrene, the logarithms of K_{d} are either increased or slightly decreased compared to the K_{d} value in pure water. This result indicates that in this concentration region, SDS molecules do not extract sorbed phenanthrene. Rather they cause an increase of the sorption of phenanthrene from aqueous phase to aquifer sand. However, ACP nanoparticles exhibited decreased K_{d} value even at this low concentration region, indicating that ACP nanoparticles can

extract adsorbed phenanthrene in this concentration region. In higher concentration regions (4000–100,000 mg/L), ACP and SDS solutions exhibited almost the same K_d values, indicating that ACP nanoparticles and SDS have the same extraction efficiency, even though SDS has a stronger affinity for phenanthrene than ACP nanoparticles.

Desorption of adsorbed phenanthrene as function of SDS or ACP particle dose is re-plotted as extraction efficiency (%) and illustrated in Fig. 2.8. Extraction efficiency is calculated as (desorbed amount of phenanthrene)/(adsorbed amount of phenanthrene on aquifer sand) $\times 100$ (%). At higher concentrations (10,000–100,000 mg/L), SDS (79.8%) showed slightly better extraction efficiency than ACP nanoparticles (73.58%). However, at low concentrations (100–7000 mg/L), SDS solutions extract adsorbed phenanthrene less than 20%, whereas ACP nanoparticle solutions extracted 60% of adsorbed phenanthrene.

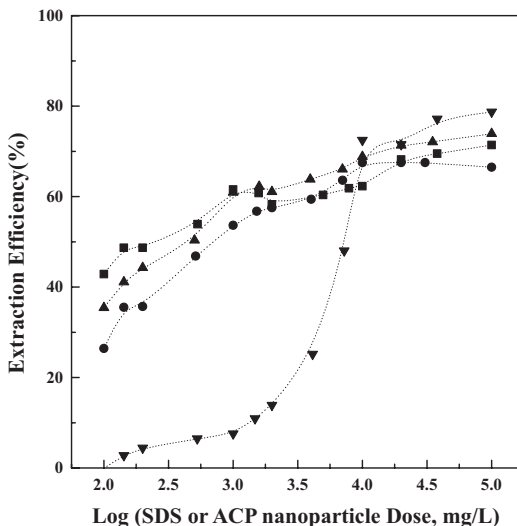


Figure 2.8 Extraction efficiency of ACPU nanoparticle solutions and SDS solution: - ■ - ACP64, - ● - ACP 55, - ▲ - ACP 28, and - ▼ - SDS. Reprinted with permission from Ref. [48].

As mentioned earlier, ACP nanoparticles and SDS molecules have very different microstructure in aqueous phase. As illustrated in Fig. 2.9, on contact with soil matrix, dissolved SDS molecules are easily adsorbed onto soil, and SDS micelles formed by physical association are also breakdown and adsorbed onto soil matrix as a

single molecule. At low concentration of SDS in aqueous phase, most of the SDS molecules are adsorbed onto soil matrix, so SDS molecules cannot extract adsorbed phenanthrene from soil matrix. In addition, SDS molecules adsorbed onto soil matrix absorb phenanthrene in aqueous phase, resulting in increase of phenanthrene distribution onto soil matrix. At higher concentration, SDS micelles can extract adsorbed phenanthrene from soil matrix, but these micelles are also easily adsorbed onto soil matrix due to their vulnerable structure.

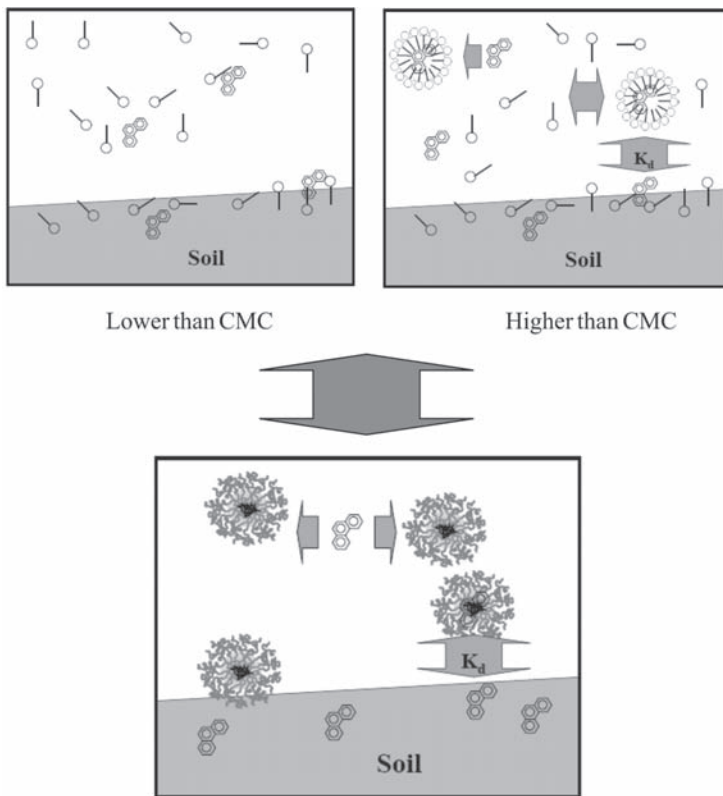


Figure 2.9 Distribution of HOC between soil and aqueous phase in the presence of surfactant and ACP nanoparticles.

Even though ACP nanoparticles were formed by physical association, like surfactant molecules form micelles in water, their microstructure is permanently locked-in by chemical cross-linking. Also, whole UAA chains do not dissolve in water, so UAA chains cannot

exist as dissolved single molecule in aqueous phase even at extremely low concentration. Thus, even at low concentration, desorption and extraction of phenanthrene from soil matrix have to be done not by dissolved UAA molecules but by ACP nanoparticles. On contacting with soil-adsorbing phenanthrene, ACP nanoparticles can maintain their microstructure, which make ACP nanoparticles more efficient material for extraction of adsorbed phenanthrene from soil matrix even though SDS molecules have a better solubilization capability for phenanthrene. Degree of sorption of SDS and ACP onto soil will be discussed in the following chapter.

2.6 *IN SITU EXTRACTION OF ADSORBED PHENANTHRENE*

In situ extraction efficiency of washing materials has been being evaluated as lab scale using a soil column experiment. In general, an aqueous washing solution is pumped into or poured into all glass column packed with soil containing HOC compounds, and then the concentration of HOC molecules in soil and effluent sample is monitored at various conditions. In this section, *in situ* extraction capability of ACP nanoparticles and SDS molecules will be presented using a soil column packed with aquifer sandy soil artificially contaminated by phenanthrene, which can be prepared by the following procedure: To prepare contaminated soil, 10 mL of ^{14}C -phenanthrene solution was mixed with 10 g of aquifer sand for 24 hours in a rotary tumbler. The glass column was then packed with the wet contaminated soil. The amount of ^{14}C -phenanthrene in the column was calculated from a material balance on the original phenanthrene used in the sand mixture and the small amount that eluted out of the column during its preparation, which was based on the procedure described in previous reports [32, 53–54]. All connecting tubes, fittings, and stopcocks were made of Teflon to prevent adsorption of phenanthrene. The feed solutions, SDS aqueous solution or ACP aqueous solutions, were directed downwards using a peristaltic pump through columns. One-milliliter samples of effluent were transferred into scintillation vials containing 10 mL of Ecolume cocktail, and the concentration of phenanthrene was measured by LSC, which is schematically presented in Fig. 2.10.

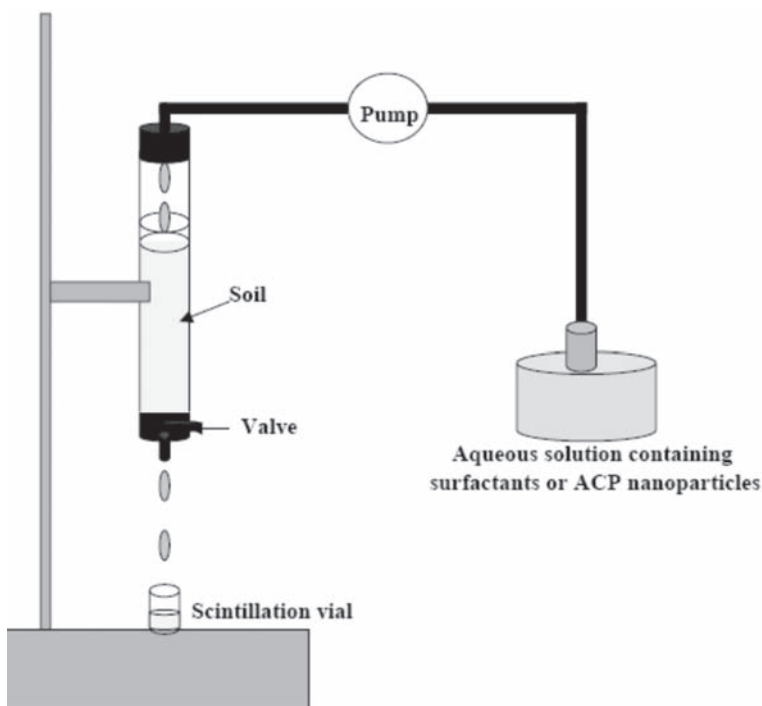


Figure 2.10 Schematic diagram of apparatus for measuring *in situ* soil-washing experiments.

Soil used for the preparation of soil column is aquifer sand obtained from a quarry in New Field, NY. The organic content of the sand was reported to be $0.049 \pm 0.012\%$. And, 47.2% and 47.5% of the particles are in the fine (0.1–0.25 mm) and medium (0.25–0.5 mm) size range, respectively. The remaining constituents included very fine sand (0.05–0.1 mm) at 3.7%, coarse sand (>0.5 mm) at 0.2%, and silt and clay at 1.2%.

Figures 2.11 and 2.12 show the percent mass of phenanthrene remaining in the contaminated soil column versus the number of pore volume of ACP nanoparticle and SDS solution eluted from the column. Flow rate of ACP and SDS solution in the column was regulated at 0.315 mL/min using a peristaltic pump. One pore volume means the total volume of soil pores in the soil-packed column.

In this soil column, a soil column prepared using 10 g of aquifer sand has 4.27 mL of pore volume. For application of 200 mg/L of ACP 64 and 55 nanoparticle solutions, 50% and 30% of the phenanthrene

were removed from the soil column after eight pore volumes, respectively. However, SDS solution (200 mg/L) extracted only 7% of the phenanthrene from soil column after eight pore volumes of washing. At higher concentration (10,000 mg/L) (Fig. 2.11), ACP 64 and 55 nanoparticle solutions also exhibited better *in situ* extraction performance compared to SDS solution.

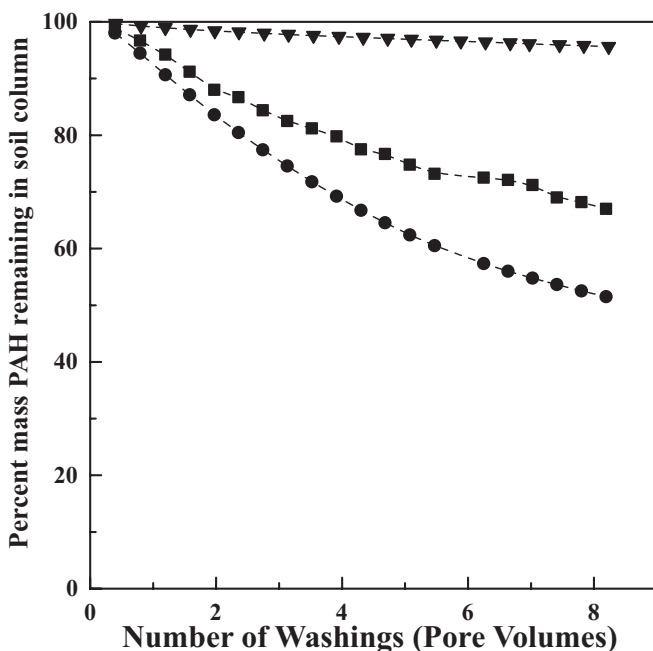


Figure 2.11 Extraction of sorbed phenanthrene from soil column using ACP nanoparticle and SDS solutions at high flow rate: -■- ACP64, -●- ACP 55, and -▼-SDS. Reprinted with permission from Ref. [48].

ACP 64 nanoparticles could extract 97% of adsorbed phenanthrene from soil column, whereas SDS solution removed only 20% of adsorbed phenanthrene with the same number of washings.

As ACP nanoparticles have a better desorption performance in batch experiment, they showed much better soil-washing performance compared with SDS, even though SDS had greater affinity for phenanthrene and higher interfacial activity than ACP nanoparticles. This is because of the lower degree of ACP sorption onto the soil placed at the column. That is, the degree of sorption

onto the soil also played an important role in *in situ* extraction of the adsorbed phenanthrene.

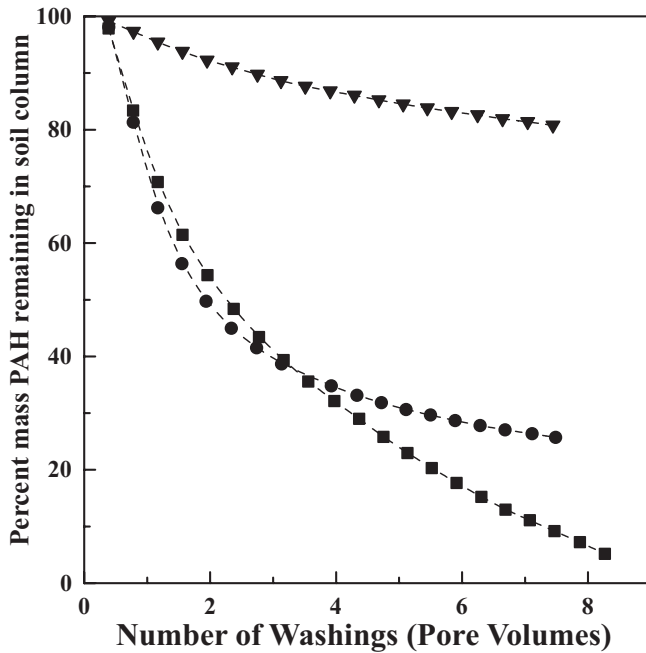


Figure 2.12 Extraction of sorbed phenanthrene from soil column using ACP nanoparticle and SDS solutions at low flow rate: -■- ACP64, -●- ACP 55, and -▼-SDS. Reprinted with permission from Ref. [48].

2.7 SORPTION OF ACP NANOPARTICLES AND SDS ONTO THE AQUIFER SAND

Figure 2.13 shows the sorption of ACP nanoparticles and SDS molecules onto the aquifer sand at various concentrations. In the low concentration region (100–2100 mg/L), the sorption of SDS onto aquifer sand is much higher than that of ACP nanoparticles, i.e., 20–40% of SDS molecules are sorbed, whereas less than 10% of ACP nanoparticles are sorbed onto aquifer materials. At higher concentrations (>7000 mg/L), the sorption of SDS is also greater than that of ACP nanoparticles. This result can be interpreted as due to the difference of aqueous pseudophase between SDS and ACP nanoparticles.

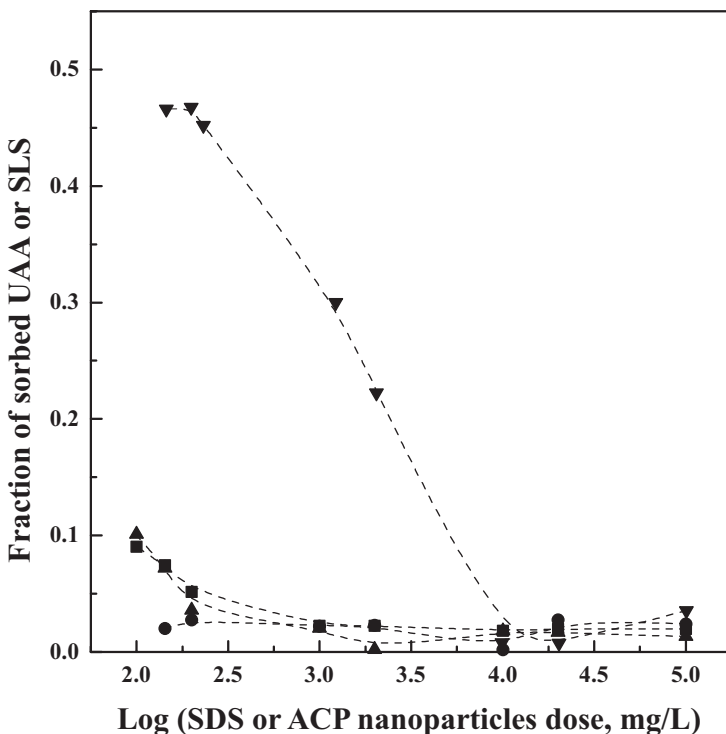


Figure 2.13 Sorption of SDS and ACP nanoparticles onto aquifer sand as a function of SDS or ACP nanoparticle dose: - ■ - ACP64, - ● - ACP 55, - ▲ - ACP 28, and - ▼ - SDS. Reprinted with permission from Ref. [48].

At concentration equal to and less than CMC, surfactant completely dissolves in water, so that SDS aqueous solution consists of monomeric molecules existing as dissolved monomeric molecules. These monomeric molecules are easily sorbed onto the soil because of hydrophobic moiety of surfactant.

Consequently, at concentration less than CMC of SDS (2100 mg/L), large amounts of SDS are sorbed onto the aquifer sand. Unlike SDS molecules that completely dissolve in water below its CMC, UAA chains cannot be dissolved in water but are just dispersed in water to form nano-aggregates (ACP nanoparticles) even at extremely low concentrations, because the whole UAA chains are insoluble in water.

As illustrated in Fig. 2.2, UAA chains have hydrophobic polytetramethylene (PTMO) oxide-based segment and hydrophilic carboxylate anion groups at the same chain. Water is a good solvent for carboxylate anions in UAA chains but is not a solvent for

hydrophobic backbones. On contacting with water, water-soluble carboxylate anion groups in UAA chains are microphase-separated from hydrophobic segment and oriented toward water phase to form outer layer. Hydrophobic PTMO-based segments are associated with each other to form hydrophobic interior, leading to form nano-sized aggregates of UAA chains. Finally, this aggregated structure of UAN chains is permanently locked-in by chemical cross-linking reaction, resulting in the formation of micelle-like ACP nanoparticles. So, much lower degree of sorption of ACP nanoparticles onto the aquifer sand can be interpreted as due to their extremely low concentration for the formation of aggregates and chemically cross-linked structure.

At concentration greater than CMC of SDS (2100–100,000 mg/L), SDS exhibits greater sorption onto the aquifer material than ACP nanoparticles, even though SDS can form aggregates (micelles) in aqueous phase in this concentration region. This result can be also explained by the chemically cross-linked microstructure of ACP nanoparticles. Surfactant micelles formed by physical association of monomeric molecules tend to break up on contacting with a soil or solid. However, ACP nanoparticles, nano-aggregates of UAA chains, cannot be easily destroyed because this aggregated structure is permanently locked-in by chemical cross-linking reaction.

At surfactant concentrations little greater or less than CMC, surfactant monomers can extract sorbed HOC but most of the surfactant monomers are easily sorbed onto the soil. These sorbed surfactants on a soil increase the soil's organic carbon content and solubilize HOCs as well, resulting in an enhanced sorption of HOC onto the soil [31–32, 52]. So, the surfactant can effectively extract sorbed hydrophobic pollutant only at concentrations greater than its CMC. Consequently, at low concentrations (100–2100 mg/L), greater extraction efficiency of ACP nanoparticles than SDS can be interpreted as due to much smaller sorption of ACP nanoparticles onto the aquifer sand compared to SDS.

As illustrated in Fig. 2.3, as the concentration of the SDS increases in the aqueous solution, the surface tension of the solution is abruptly changed and remains constant with the concentration. This result indicates that SDS molecules have a concentration for the formation of micelles. However, surface tension of ACP solutions decreases linearly with the increase of concentration without abrupt change in surface tension. This result also indicates that unlike SDS, UAA chains can form nano-aggregates (ACP nanoparticles) at extremely low concentration.

At concentration much greater than CMC of SDS (4000–100,000 mg/L), SDS and ACP nanoparticles exhibited the little difference of degree of sorption onto the aquifer sand. However, ACP nanoparticles and SDS showed the same extraction effectiveness at this concentration region, even though SDS molecules have greater interfacial activity and affinity for phenanthrene. This can be interpreted as due to stronger interaction between SDS molecules and phenanthrene. If the same amounts of SDS molecules and ACPU nanoparticles are sorbed onto the aquifer sand, SDS molecules having stronger interaction with phenanthrene can absorb the larger amount of phenanthrene, leading to sorption of larger amount of phenanthrene onto the soil.

2.8 CONCLUSIONS

In the case of distribution between amphiphilic nano-aggregates (surfactant micelles or ACP nanoparticles) and aqueous phase, HOC molecules showed higher partitioning into surfactant micelles compared with their partitioning into ACP nanoparticles. This means surfactant molecules have a stronger affinity for HOC compounds and better solubilizing performance than APU nanoparticles. However, for partitioning of HOC into surfactant micelles or ACP nanoparticles in the presence of soil, larger amount of HOC molecules was extracted and moved into aqueous phase by ACP nanoparticles. This indicates that soil-washing performance of amphiphilic molecules strongly depends on their microstructural strength. That is, chemically locked-in microstructure of ACP nanoparticles makes them more favorable materials for extraction of HOC adsorbed onto soil.

References

- [1] Canter, L. W., and Knox, R. C. (1986) *Ground Water Pollution Control*, Lewis Publishers Inc., Chelsea, MI, p. 349.
- [2] Haley, J. L., Hanson, B., Enfield, C., and Glass, J. (1991) Evaluating the effectiveness of groundwater extraction systems, *Ground Water Monit. Rev.*, 119–124.
- [3] Harwell, J. H. (1992) *Transport and remediation of subsurface contaminants* (eds Sabatini, D. A., and Know, R. C.), ACS Symposium Series 491, ACS, Washington, DC, pp. 124–132.
- [4] Mackay, D. M., and Cherry, J. A. (1989) Groundwater contamination: pump-and-treat-remediation, *Environ. Sci. Technol.*, **23**(6), 630–636.

- [5] McCarthy, J. F., and Zachara, J. M. (1989) Subsurface transport of contaminants, *Environ. Sci. Technol.*, **23**(5), 496–502.
- [6] Park, S. -K., and Bielefeldt, A. R. (2003) Aqueous chemistry and interactive effects of non-ionic surfactant and pentachlorophenol sorption to soil, *Water Res.*, **37**, 4663–4672.
- [7] Smith, J. A., Tuck, D. M., Jaffe, P. R., and Mueller, R. T. (1991) *Organic Substances and Sediments in Water, Vol. 1*, Lewis Publisher, Chelsea, MI, pp. 201–230.
- [8] Tobia, R. J., Camacho, J. M., Augustin, P., Griffiths, R. A., and Frederick, R. M. (1994) Washing studies for PCP and creosote contaminated soil, *J. Hazard. Mater.*, **38**, 145–161.
- [9] Deitch, J. J., and Smith, J. A. (1995) Effect of Triton X-100 on the rate of trichloroethene desorption form soil to water, *Environ. Techol.*, **29**(4), 1069–1080.
- [10] Cirelli, D. P. (1978) Pentachlorophenol: Chemistry, Pharmacology and Environmental Toxicity, Plenum Press, New York.
- [11] Urum, K., Grigson, S., Pekdemir, T., and McMenamy, S. (2006) A comparison of the efficiency of different surfactants for removal of crude oil from contaminated soils, *Chemosphere*, **62**, 1403–1410.
- [12] Urum, K., Pekdemir, T., and Copur, M. (2004) Surfactants treatment of crude oil contaminated soils, *J. Colloids Interface Sci.*, **276**, 456–464.
- [13] Zhou, Q., Sun, F., and Liu, R. (2005) Joint chemical flushing of soils contaminated with petroleum hydrocarbons, *Environ. Int.*, **31**, 835–839.
- [14] Lee, M. H., Kang, H. M., and Do, W. H. (2005) Application of nonionic surfactant-enhanced *in situ* flushing to a diesel contaminated site, *Water Res.*, **39**, 139–146.
- [15] Verma, S., and Kumar, V. V. (1998) Relationship between oil-water interfacial tension and oily soil removal in mixed surfactant systems, *J. Colloids Interface Sci.*, **207**, 1–10.
- [16] Al-Sabagh, A. M., Ahmed, N. S., Nassar, A. M., and Gabr, M. M. (2003) Synthesis and evaluation of some polymeric surfactants for treating crude oil emulsions Part I: treatment of sandy soil polluted with crude oil by monomeric and polymeric surfactants, *Colloids Surfaces A: Physicochem. Eng. Aspects*, **216**, 9–19.
- [17] Park, S. K., and Bielefeldt, A. R. (2005) Non-ionic surfactant flushing of pentachlorophenol from NAPL-contaminated soil, *Water Research*, **39**, 1388–1396.
- [18] Urum, K., and Pekdemir, T. (2004) Evaluation of biosurfactants for crude oil contaminated soil washing, *Chemosphere*, **57**, 1139–1150.

- [19] Kuyukina, M. S., Ivshina, I. B., Makarov, S. O., Litvinenko, L. V., Cunningham, C. J., and Philp, J. C. (2005) Effect of biosurfactants on crude oil desorption and mobilization in a soil system, *Environ. Int.*, **31**, 155–161.
- [20] Sabaté, J., Viñas, M., and Solanas, A. M. (2004) Laboratory-scale bioremediation experiments on hydrocarbon-contaminated soils, *Int. Biodeterior. Biodegrad.*, **54**, 19–25.
- [21] Urum, K., Pekdemir, T., and Copur, M. (2004) Surfactants treatment of crude oil contaminated soils, *J. Colloids Interface Sci.*, **276**, 456–464.
- [22] Lee, D. H., Cody, R. D., Kim, D. J., and Choi, S. G. (2002) Effect of soil texture on surfactant-based remediation of hydrophobic organic-contaminated soil, *Environ. Int.*, **27**, 681–688.
- [23] Iturbe, R., Flores, C., Chávez, C., Ramírez, A., and Torres, L. G. (2004) *In situ* flushing of contaminated soils from a refinery: organic compounds and metal removals, *Wiley Interscience, Remediation Spring*, 141–152.
- [24] Kile, D. E., and Chiou, C. T. (1989) Water solubility enhancement of DDT and trichlorobenzene by some surfactants below and above the critical micelle concentration, *Environ. Sci. Technol.*, **23**, 832–838.
- [25] Liu, Z., Shonali, L., and Luthy, R. G. (1991) Surfactant solubilization of polycyclic aromatic hydrocarbon compounds in soil-water suspensions, *Wat. Sci. Technol.*, **23**, 475–485.
- [26] Haulbrook, W. R., Feerer, J. L., Hatton, T. A., and Tester, J. W. (1993) Enhanced solubilization of aromatic solutes in aqueous solutions of N-vinylpyrrolidone/styrene, *Environ. Sci. Technol.*, **27**, 2783–2788.
- [27] Fountain, J. C., Klimek, A., Beikirch, M. G., and Middleton, T. M. (1991) The use of surfactant for *in situ* extraction of organic pollutants from a contaminated aquifer, *J. Hazard. Mater.*, **28**, 295–311.
- [28] Weber, J. W., Jr., Huang, W., and Yu, H. (1998) Hysteresis in the sorption and desorption of hydrophobic organic contaminants by soil and sediments. 2. Effects of soil organic matter heterogeneity, *J. Contam. Hydrol.*, **31**, 149–165.
- [29] Liu, Z., Edwards, D. A., and Luthy, R. G. (1991) Sorption of non-ionic surfactants onto soil, *Water Res.*, **26**(10), 1337–1345.
- [30] Kommalapati, R. R., ValsaRaj, K. T., Constant, W. D., and Roy, D. (1997) Aqueous solubility enhancement and desorption of hexachlorobenzene from soil using a plant-based surfactant, *Water Res.*, **31**(9), 2161–2170.
- [31] Deshpande, S., Wesson, L., Wade, D., Sabatini, D. A., and Harwell, J. H. (2000) Dowfax surfactant components for enhancing contaminant solubilization, *Water Res.*, **34**(3), 1030–1036.

- [32] Zhao, D., Joseph, P. J., White, C. J., and Braida, W. (2001) Dual-mode modeling of competitive and concentration-dependent sorption and desorption kinetics of polycyclic aromatic hydrocarbon in soils, *Water Resour. Res.*, **37**(8), 2205–2212.
- [33] Doong, R., Lei, W., Chen, T., Lee C., and Chang, W. (1996) Effect of anionic and nonionic surfactants on sorption and micellar solubilization of monocyclic aromatic compounds, *Water Sci. Technol.*, **34**(7–8), 327–334.
- [34] Lee, F. J., Liao, P. M., Kuo, C.C., Yang, H. T., and Chiou, C. T. (2000) Influence of a nonionic surfactant (Triton X-100) on contaminant distribution between water and several soil solids, *J. Colloid Interface Sci.*, **229**, 445–452.
- [35] Grimberg, S.J., Nagel, J., and Aitken, M.D. (1995) Kinetic of phenanthrene dissolution into water in the presence of nonionic surfactant, *Environ. Sci. Technol.*, **29**, 1480–1487.
- [36] Sun, S., Inskeep, W. P., and Boyd, S. A. (1995) Sorption of nonionic organic compounds in soil-water system containing a micelle-forming surfactant, *Environ. Sci. Technol.*, **29**, 903–913.
- [37] Liu, G.G., Roy, D., and Rosen, M. J. (2000) A simple method to estimate the surfactant micelle-water distribution coefficients of aromatic hydrocarbons, *Langmuir*, **16**, 3595–3605.
- [38] Abriola, L. M., Dekker, J. T., and Pennell, K. D. (1993) Surfactant-enhanced solubilization of residual dodecane in soil columns. 2. Mathematical modeling, *Environ. Sci. Technol.*, **27**, 2341–2351.
- [39] Abdul, S. A., Gibson, T. L., and Rai, D. N. (1987) Statistical correlation for predicting the partition coefficient for nonpolar organic contaminants between aquifer organic carbon and water, *Hazard. Waste Hazard. Mater.*, **4**(3), 211–222.
- [40] Guha, S., Jaffe, P. R., and Peters, C. A. (1998) Solubilization of PAH mixtures by a nonionic surfactant, *Environ. Sci. Technol.*, **32**, 930–935.
- [41] Edwards, D.A., Adeel, Z., and Luthy, R. G. (1994) Distribution of nonionic surfactant and phenanthrene in a sediment/aqueous system, *Environ. Sci. Technol.*, **28**, 1550–1560.
- [42] Tounissou, P., Herbant, M., Rodehuser, L., and Tondre, C. (1996) Ultrafiltration of micellar solutions in the presence of electrolyte, *J. Colloid Interface Sci.*, **183**, 484–490.
- [43] Glass, J. E. (1997) *Technology for Waterborne Coatings*, ACS Symposium Series 663, American Chemical Society, Washington DC.

- [44] Song, M. -E., Kim, J. -Y., and Suh, K. -D. (1996) Preparation of UV-curable emulsions using PEG-modified urethane acrylates: the effect of nonionic and anionic groups, *J. Appl. Polym. Sci.*, **62**, 1775.
- [45] Kim, H. -D., and Kim, T. -W. (1998) Preparation and properties of UV-curable polyurethane acrylate ionomers, *J. Appl. Polym. Sci.*, **67**, 2153–2162.
- [46] Lee, K. H., and Kim, B. K. (1996) Structure-property relationships of polyurethane anionomer acrylates, *Polymer*, **37**, 2251–2257.
- [47] Kim, J. -Y., Kim, C. -H., Yoo, D. -J., and Suh, K. -D. (2000) Hydrophobic and hydrophilic aggregation of tailor-made urethane acrylate anionomers in various solvents and their network structures, *J. Polym. Sci. Part B: Polym. Phys.*, **38**, 1903–1916.
- [48] Kim, J. -Y., Shim, S. -B., and Shim, J. -K. (2004) Enhanced desorption of phenanthrene from aquifer sand using amphiphilic polyurethane nanoparticles, *J. Ind. Chem. Eng.*, **10**, 1043–1051.
- [49] Yeom, I. T., Ghosh, M. M., and Cox, C. D. (1996) Kinetic aspects of surfactant solubilization of soil-bound polycyclic aromatic hydrocarbons, *Environ. Sci. Technol.*, **30**, 1589–1595.
- [50] Yeom, I. T., Ghosh, M. M., Cox, C. D., and Robinson, K. G. (1995) Micellar solubilization of polycyclic aromatic hydrocarbons in coal tar-contaminated soils, *Environ. Sci. Technol.*, **29**, 3015–3021.
- [51] Jafvert, C. T. (1991) Sediment- and saturated-soil-associated reactions involving an anionic surfactant (dodecylsulfate). 2. Partition of PAH compounds among phases, *Environ. Sci. Technol.*, **25**, 1039–1045.
- [52] Chu, W., and So, W. S. (2001) Modeling the two stage of surfactant-aided soil washing, *Water Res.*, **35**(3), 761–767.
- [53] West, C. C., and Harwell, J. H. (1992) Surfactants and subsurface remediation, *Environ. Sci. Technol.*, **26**(2), 2324–2329.
- [54] Kim, J. -Y., Cohen, C., Shuler, M. L., and Lion, L. W. (2000) Use of amphiphilic polymer particles for *in-situ* extraction of sorbed phenanthrene from a contaminated aquifer material, *Environ. Sci. Technol.*, **34**, 4133–4139.

This page intentionally left blank

Chapter 3

USE OF AMPHIPHILIC NONIONIC POLYMER NANOPARTICLES FOR REMOVAL OF HYDROPHOBIC POLLUTANTS FROM SOIL

Juyoung Kim

*Department of Advanced Materials Engineering,
Kangwon National University, Samcheok, Kangwon 245-711,
South Korea*

juyoungk@kangwon.ac.kr

In the previous chapter, extraction of sorbed phenanthrene from aquifer materials using anionic amphiphilic cross-linked polymer (ACP) nanoparticles having the same microstructure of anionic surfactant micelles was presented. ACP nanoparticles were shown to adsorb weakly to a sandy aquifer in batch experiments, which is attributed to the chemically cross-linked nature of their microstructure. In this chapter, soil-washing performance of ACP nanoparticles having different surface property will be presented. Soil-washing performance of a surfactant strongly depends on the degree of sorption onto soil. In general, cationic surfactants having severe biotoxicity show relatively high degree of sorption because of negatively charged soil particles, so that the use of cationic surfactants in soil washing is highly restricted. Although the degree of sorption of anionic surfactants is much lower than that of cationic surfactants,

Advances in Nanotechnology and the Environment

Edited by Juyoung Kim

Copyright © 2012 by Pan Stanford Publishing Pte. Ltd.

www.panstanford.com

their toxicity to soil bacteria could hinder the whole remediation effort. Therefore, nonionic surfactants can be the most favorable materials for soil remediation because of their intermediate sorption and low biotoxicity. Several kinds of nonionic surfactants have been used for removal of various hydrophobic pollutants from the soil [1–10]. Representative nonionic surfactants, which have been the most widely used on soil remediation, are Triton X-100, Tween, and Brij series. All these nonionic surfactants have polyethylene oxide (PEO) chains or ethylene oxide (EO) component as hydrophilic segments within their backbone. Hydrophilic-lipophilic balance (HLB) of these surfactants can be controlled by the varying chain length of PEO or the number of EO in the backbone [11–13]. In aqueous phase, these surfactants form nano-aggregates, micelles, at the concentration higher than their own critical micelle concentration. Exterior of their micelles have PEO or EO chains expanded and oriented toward water phase, which provide dispersion stability and solubilization capability for the micelles.

To synthesis amphiphilic polymer nanoparticles having the same microstructure of nonionic surfactant micelles, nonionic amphiphilic polymers should have PEO segments as hydrophilic segment within their backbone. Although tremendous number of nonionic surfactants have been being developed and used, very few number of amphiphilic polymers having hydrophilic PEO have been commercialized. One of representative nonionic amphiphilic polymers is Pluronic® (polypropylene oxide (PPO)-PEO triblock copolymer). This polymer has been used in various fields as drug delivery carrier, dispersant, template of nanoparticles synthesis, etc., because of their amphiphilic property [14–21]. Even though Pluronic® has very versatile functions and applications, its application for environmental remediation has been rarely reported because of their expensive price.

These amphiphilic polymer nanoparticles containing hydrophilic PEO segments could also be synthesized using nonionic amphiphilic precursors, urethane acrylate nonionomers (UAN), which can be synthesized through much simple process. UAN chains have hydrophilic PEO pendant segment and PPO-based hydrophobic segment at the same backbone. In addition, UAN chains have reactive vinyl groups at the both ends of PPO-based hydrophobic segment, so that UAN chains can be converted into highly cross-linked amphiphilic

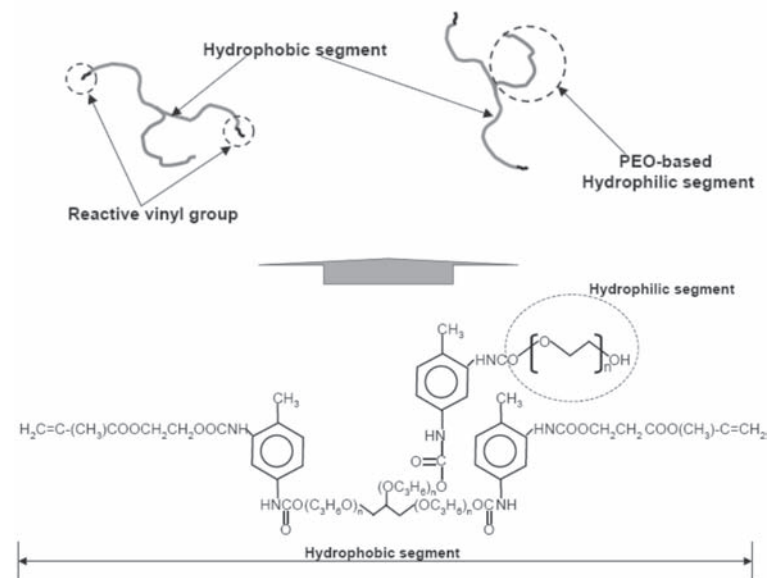
polymer through radical-initiated polymerization process. By mixing with water, UAN chains can form very stable amphiphilic oligomer nanoparticles in aqueous phase whose structure is similar to that of nonionic surfactant micelle. As UAA nanoparticles can be converted to anionic ACP nanoparticles via cross-linking polymerization process, these amphiphilic oligomer nanoparticles can be converted into nonionic ACP nanoparticles. This chapter will first represent interfacial activity and solubilization performance of nonionic ACP nanoparticles, which will be compared with three kinds of nonionic surfactants based on the microstructural difference between nonionic ACP nanoparticles and nonionic surfactant micelles. Desorption capability of nonionic ACP nanoparticles for sorbed hydrophobic pollutants from soil was also presented and compared with nonionic surfactants.

3.1 NONIONIC AMPHIPHILIC REACTIVE OLIGOMERS AND AMPHIPHILIC POLYMER NANOPARTICLES

As illustrated in Fig. 3.1, nonionic amphiphilic reactive oligomers, UAN chains, consist of PEO-based hydrophilic segment and PPO-based hydrophobic segments. These two segments are connected with each other through urethane linkage such as UAA chains. That is, OH groups of hydrophobic PPO triol was first reacted with excess amount of NCO groups of diisocyanate compounds such as toluene diisocyanate (TDI) or methylene bis(phenyl isocyanate) (MDI) to synthesis NCO-terminated PPO precursors. Then, OH groups of hydrophilic poly(ethylene glycol) and hydroxyethyl methacrylate (HEMA) are reacted with NCO groups of the obtained PPO precursors in a separate step. Through two- or three-step reaction between OH groups and NCO groups, hydrophilic PEO segments are connected with hydrophobic PPO segments containing reactive vinyl groups [22–29]. Detailed recipe and chemicals used for the synthesis of UAN chains are summarized in Table 3.1. Molecular weights of PPO triol and polyethylene glycol were varied to control the HLB of UAN. Nonionic ACP nanoparticles synthesized using UAN 700-1, 700-2, and 1000 chain are named as NACP 700-1, 700-2, and 1000 nanoparticle, respectively.

Table 3.1 Recipe for the synthesis of UAN chains and their molecular weights

Molar ratio of TDI/PPO triol/2-HEMA/PEG	Molecular weight of PPO triol (g/mol)	Molecular weight of PEG (g/mol)	Symbol	Molecular weight of UAN (g/mol)
3/1/2/1	700	600	UAN 700-1	3750
3/1/2/1	700	1500	UAN 700-2	4120
3/1/2/1	1000	1500	UAN 1000	6700

**Figure 3.1** Schematic presentation of urethane acrylate nonionomer.

As water is a good solvent for PEO segments in UAN chains but is not a solvent for PPO segments, on contacting with water, water-soluble PEO segments in UAN chains are microphase-separated from hydrophobic PPO segments and oriented toward water phase to form outer layer in the nanoparticles. At the same time, hydrophobic PPO-based segments are associated (hydrophobic association) with each other to form hydrophobic interior. Consequently, micelle-like nano-aggregates of UAN chains are formed in water. As UAA nanoparticles are converted to anionic ACP nanoparticles via emulsion polymerization process, UAN nanoparticles dispersed in water can

be easily transformed to amphiphilic polymer nanoparticles through conventional emulsion polymerization process where radicals formed in aqueous phase penetrate into hydrophobic interior and initiate radical polymerization. Potassium persulfate (KPS) dissolved in aqueous phase makes radicals, which penetrate from aqueous phase into oligomeric UAN nanoparticles to initiate radical polymerization reaction. As mentioned earlier, the interior of UAN nanoparticles dispersed in aqueous phase exclusively consists of hydrophobic PPO segments having reactive vinyl groups, so penetrated radicals initiate radical polymerization between vinyl groups located at hydrophobic interior of the nanoparticles but hydrophilic PEO segment located at outer layers of UAN nanoparticles remain intact. After the completion of radical cross-linking polymerization, hydrophobic interior of UAN nanoparticles is converted from oligomer to highly cross-linked polymer; as a consequence, oligomer nanoparticles are transformed to cross-linked amphiphilic polymer nanoparticles, which is schematically presented in Fig. 3.2 [26, 28–29].

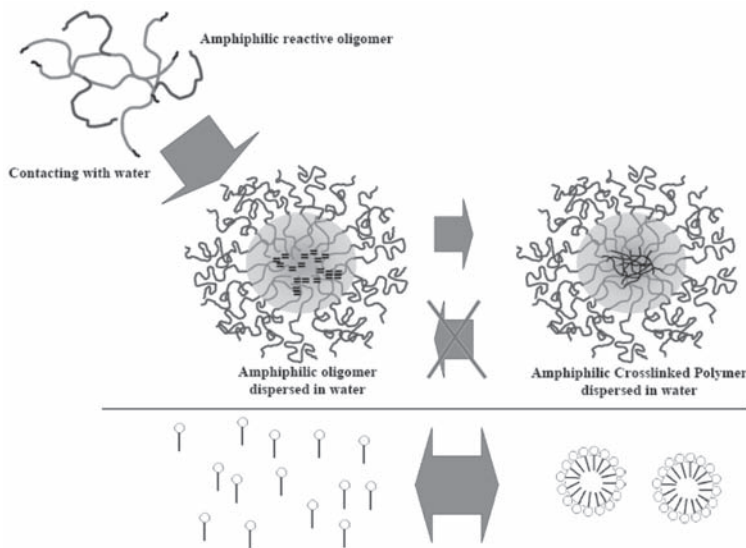


Figure 3.2 The postulated microstructure of NACP nanoparticles in water.

As hydrophilic and hydrophobic segments in UAN chains have relatively strong intermolecular and intramolecular interactions due to relatively high molecular weight compared to surfactant molecules,

UAN nanoparticles dispersed in water are much stable compared with surfactant micelles. After chemical cross-linking reaction, UAN chains were chemically cross-linked with each other within nanoparticles, so NACP nanoparticles cannot be breakdown and returned to single UAN chain in water. The size of the prepared NACP nanoparticles measured by dynamic light scattering measurement was in the range 23.4–32.10 nm.

3.2 SOLUBILIZATION OF PERFORMANCE OF NACP NANOPARTICLES

As mentioned in the previous chapter, solubilization performance of NACP nanoparticles for hydrophobic organic compounds (HOC) should be evaluated before using as washing material for soil remediation. As hydrophobic pollutants absorbed onto soil have strong interaction with hydrophobic organic matters in soil, washing materials in soil remediation should have strong affinity for hydrophobic compounds to extract these absorbed hydrophobic pollutants from soil. The affinity for hydrophobic compounds can be determined by solubilization performance of washing materials, which can be obtained by measuring the increased apparent solubility of hydrophobic compounds in water containing amphiphilic compounds. Increased apparent solubility of hydrophobic compounds in aqueous phase means increase in the amount of hydrophobic compounds solubilized within amphiphilic compounds in aqueous phase without increasing the amounts of hydrophobic compounds dissolved in pure water. So, increased apparent solubility of hydrophobic compounds in water can be used for evaluating solubilizing capacity of amphiphilic compounds such as NACP nanoparticles and surfactants. As mentioned in previous chapter, solubilization performance can be expressed in several ways such as MSR, micelle–water partition coefficient, and C/C_0 [30–33].

As the microstructure of NACP nanoparticles is similar to that of micelles of nonionic surfactant, apparent solubility of hydrophobic compounds in water in the presence of NACP nanoparticles should be examined and compared with a representative nonionic surfactant. So, the solubility of phenanthrene in Triton X-100 and NACP solutions was measured and compared with the solubility of phenanthrene in pure water. Triton X-100, one of the most widely used nonionic

surfactants in the soil remediation process, is the commercial name of polyoxyethylene (10) isoctylphenyl ether. Hydophilic-lipophilic balance (HLB) and molecular weight of Triton X-100 are presented in Table 3.2. Since, like anionic ACP nanoparticles, NACP nanoparticles have unlimited molecular weight, solubilization capability of NACP nanoparticles also has to be evaluated using C/C_0 , where C is the concentration of hydrophobic compound in aqueous solution containing NACP nanoparticles or a surfactant and C_0 is the concentration of hydrophobic compound in pure water phase. As mentioned in the previous chapter, this increased concentration of hydrophobic pollutant in water corresponds to C . C_0 is the original amount of hydrophobic compound dissolved in pure water. So, the ratio of C to C_0 (C/C_0) is the enhanced solubility of hydrophobic compound in water by aid of NACP nanoparticles.

Table 3.2 Characteristics of nonionic surfactants

Trade name	Chemical	Molecular weight (g/mol)	HLB	CMC (mg/L)
Brij 30	Polyoxyethylene (4) lauryl ether	363	9.7	20
Tween 80	Polyoxyethylene (20) sorbitan monooleate	1309	15.0	15.7
Triton X-100	Polyoxyethylene (10) isoctylphenyl ether	646	13.5	111

As described in previous chapter, this solubilization capacity can be measured using the following procedure [35–38]:

- (1) Concentrated phenanthrene solutions (35 g/L) prepared in methylene chloride are placed in a 25 mL glass scintillation vial equipped with open-top screw caps and Teflon-backed septa.
- (2) After evaporation of methylene chloride, Triton X-100 or NACP aqueous solutions (10 mL) of various concentrations are added to the vials. The concentrations of Triton X-100 and NACP nanoparticles in the aqueous solution were 93–2000 mg/L and 138–140,000 mg/L, respectively.
- (3) The vials were sealed and gently agitated with a rotary tumbler for 7 days. After completion of mixing, 5 mL of supernatant was withdrawn and centrifuged at an acceleration of $15000 \times g$.

(4) A 1 mL sample was transferred into a scintillation vial containing 10 mL of Ecolume cocktail, and the concentrations of ^{14}C -phenanthrene in the aqueous phase was measured using a liquid scintillation counter (LSC).

Figure 3.3 shows the enhanced solubility (C/C_0) of phenanthrene in the presence of NACP nanoparticles and Triton X-100. Enhanced solubility increases with the increase of NACP nanoparticle dose in aqueous solution, indicating NACP nanoparticles can solubilize phenanthrene within their hydrophobic interiors just like the solubilization of HOC in surfactant micelles. At the same concentration (2000 mg/L), Triton X-100 micelles and NACP nanoparticles can solubilize approximately 50 times and 3.7–4.8 times, respectively, the phenanthrene that an equal amount of pure water will solubilize. This result indicates that NACP nanoparticles can solubilize phenanthrene within their hydrophobic interior but the solubilizing capability of NACP nanoparticles for phenanthrene is worse than that of Triton X-100.

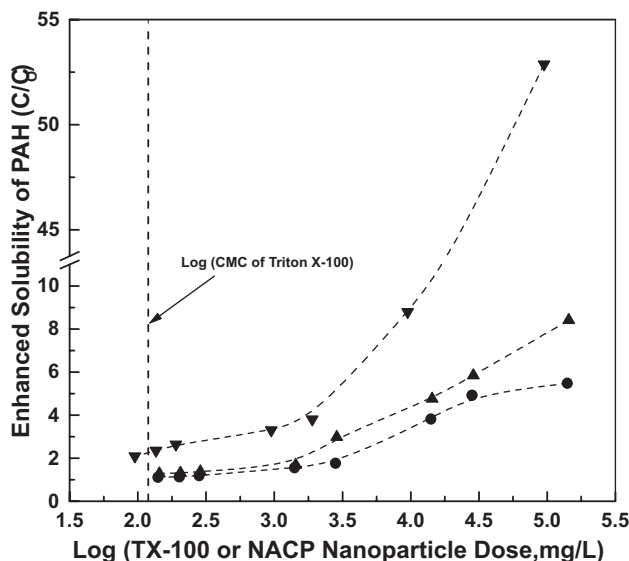


Figure 3.3 Enhanced solubility of phenanthrene in aqueous phase in the presence of Triton X-100 or NACP nanoparticles: - ● - NACP 700-2, - ▲ - NACP 1000, and - ▼ - Triton X-100. Reprinted from *J. Hazard. Mater.*, **B 98**, Kim, J. Y., Shim, S. B., and Shim, J. K., Effect of amphiphilic polyurethane nanoparticles on sorption-desorption of phenanthrene in aquifer material, 145–160, Copyright (2003), with permission from Elsevier.

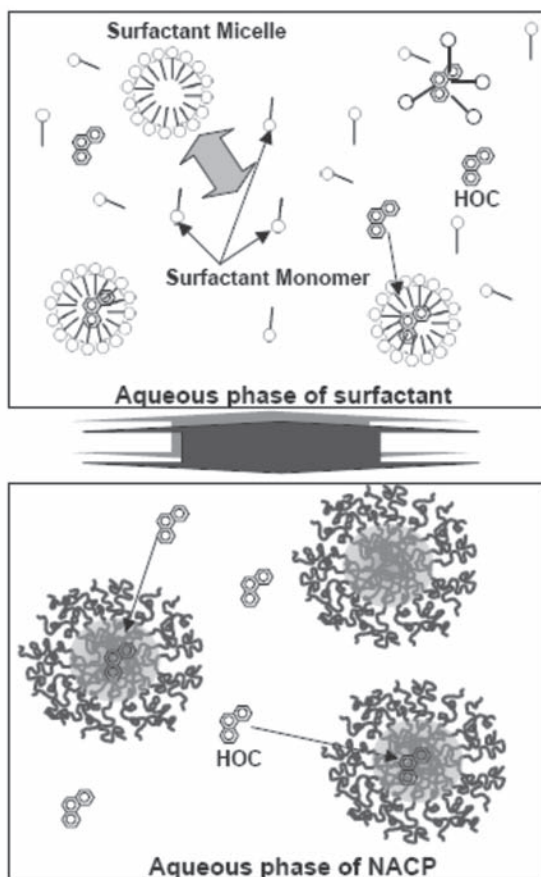


Figure 3.4 Difference of solubilization mechanism between surfactant molecules and NACP nanoparticles.

As mentioned in previous chapter, amphiphilic polymer nanoparticles and surfactant molecules absorb and solubilize phenanthrene molecules with very different ways. That is, micelle-like microstructure of NACP is permanently locked in by cross-linking polymerization, so solubilization of crystalline phenanthrene can be done only by direct contact of NACP nanoparticles with crystalline phenanthrene. However, for Triton X-100 aqueous solution, monomeric Triton X-100 molecules can easily contact with crystalline phenanthrene to solubilize phenanthrene and form micelles containing solubilized phenanthrene. Triton X-100 micelles

directly solubilize phenanthrene and are broken up to become monomeric Triton X-100 molecules, which are converted to micelles in the course of solubilization of phenanthrene, which makes solubilization performance of NACP nanoparticles less efficient and more difficult compared to Triton X-100 molecules. The difference in solubilization mechanism between surfactant molecules and NACP nanoparticles is schematically described in Fig. 3.4.

3.3 INTERFACIAL ACTIVITY OF NACP NANOPARTICLES

As presented in previous chapter, SDS and anionic ACP nanoparticles exhibited very different adsorption behavior at water/air interface because of difference in the formation mechanism of nano-aggregates between SDS and ACP nanoparticles. NACP nanoparticles are formed by almost same mechanism of formation of anionic ACP nanoparticle, so it can be expected that NACP nanoparticles exhibit similar adsorption behavior to that of anionic ACP nanoparticles. As shown in Fig. 3.5, surface tension of Triton X-100 and NACP aqueous solutions decreased with the increase of concentration of NACP nanoparticles in the solution, indicating that NACP nanoparticles have interfacial activity like nonionic surfactant Triton X-100 does.

At the same concentration, Triton X-100 solutions exhibited a greater decrease in surface tension compared to APU nanoparticles solutions, indicating that Triton X-100 molecules have higher interfacial activity. However, unlike Triton X-100 solutions showing constant value of surface tension after critical concentration, NACP nanoparticles did not exhibit discontinued decrease in surface tension. This very different adsorption behavior between NACP and Triton X-100 can be explained by microstructural difference between these molecules. As mentioned in previous chapter, surfactant molecules SDS and Triton X-100 have very different morphology before and after their own critical concentration for formation of micelles (CMC). At concentration lower than CMC, Triton X-100 molecules exist as dissolved single molecules in water. These single molecules adsorb at water-air interface, resulting in the decrease of surface tension of water. As the concentration of Triton X-100 increase, the number of molecules adsorbed at the interface increased, so that the surface tension of the aqueous solution continues to decrease.

However, at the concentration equal to or greater than CMC, the adsorption of Triton X-100 molecules at the interface is saturated, so that they start to aggregate with each other and form micelles in the aqueous phase. Consequently, the surface tension of Triton X-100 aqueous solution is practically constant regardless of increase of its concentration.

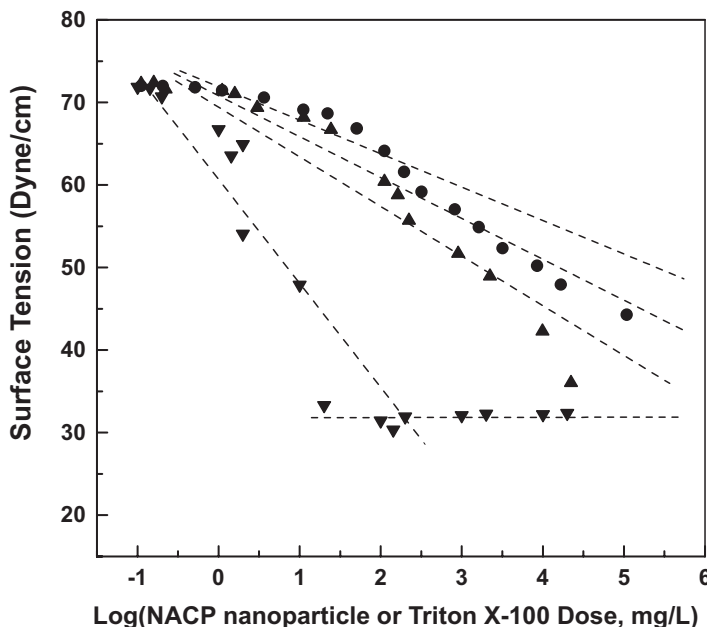


Figure 3.5 Surface tension for Triton X-100 and NACP nanoparticle solutions: -●- NACP 700-2, -▲- NACP 1000, and -▼-Triton X-100. Reprinted from *J. Hazard. Mater.*, **B 98**, Kim, J. Y., Shim, S. B., and Shim, J. K., Effect of amphiphilic polyurethane nanoparticles on sorption-desorption of phenanthrene in aquifer material, 145–160, Copyright (2003), with permission from Elsevier.

As UAN chains have much higher molecular weight of hydrophobic segments, their hydrophobic segments have much stronger hydrophobic interactions compared with those of surfactant molecules, which makes UAN chains insoluble in water even at extremely low concentration in water. Consequently, UAN chains exist as nano-aggregates in water even at extremely low concentration in water. In addition, after cross-linked polymerization, nano-aggregated structure of UAN nanoparticles is permanently

locked-in. So, UAN chains cannot be adsorbed at water–air interface as a dissolved single UAN chain in water. Decrease of surface tension of NACP aqueous solution can be only explained by adsorption of NACP nanoparticles at the interface. Unlike surfactant molecules that can be adsorbed in water as single molecules, NACP nanoparticles have to be located at the interface as nanoparticle because of extremely low water solubility and chemically locked-in structure. This microstructural difference between SDS and NACP aqueous solutions is schematically illustrated in Fig. 3.6.

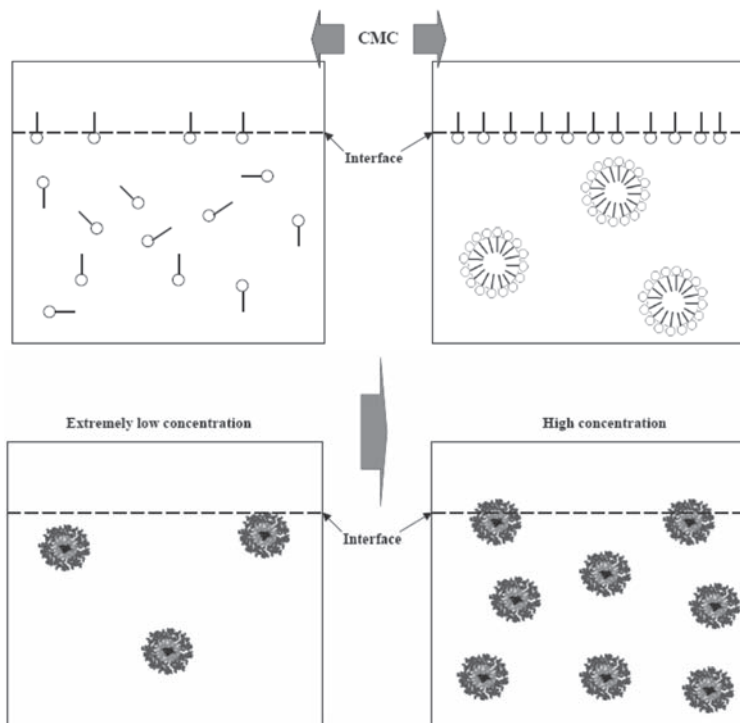


Figure 3.6 Schematic diagram of interfacial activity of surfactant molecules and NACP nanoparticles at critical micelle concentration.

NACP 1000 nanoparticles had a lower surface tension at the same concentrations and greater decrease in surface tension, compared to NACP 700-2, which is identical with the order of enhanced solubility of phenanthrene in NACP solutions. NACP nanoparticles used in this study were synthesized with different UAN chains having different

chain length of PEO and PPO segment, so that these nanoparticles have different hydrophilic/hydrophobic balances, resulting in different affinity with phenanthrene. NACP 1000 nanoparticles, having the longer PPO and PEO chains solutions, show a greater degree of decrease in surface tension than NACP 700-2.

When nonionic surfactant molecules (Brij 30 and Triton X-100) and NACP nanoparticles are mixed with two immiscible liquids such as toluene–water mixture, they form very different mixtures. As shown in Fig. 3.7, nonionic surfactants locate at interface between toluene and water and emulsify toluene to oil droplets around interface through emulsification mechanism. However, NACP nanoparticles also locate at the interface but do not form emulsion droplets, because NACP nanoparticles do not emulsify oil droplet but only solubilize oil within their hydrophobic core due to their chemically locked-in microstructure.



(a)



(b)



(c)

Figure 3.7 Pictures for toluene–water mixtures after adding surfactants or NACP nanoparticles: (a) Brij 30, (b) NACP nanoparticle, and (c) Triton X-100.

3.4 CHANGE IN DISTRIBUTION OF HOC MOLECULES BETWEEN AQUEOUS PHASE AND SOIL IN THE PRESENCE OF NACP NANOPARTICLES

As mentioned in previous chapter, many researchers have represented the sorption of HOC on the soil or sediment in terms of the distribution of compounds between the soil and aqueous solutions. The distribution of HOC between the aqueous phase and the soil is significantly changed with the addition of absorbents such as surfactant, active carbons, and clay minerals, because these compounds can absorb HOC in the aqueous phase resulting in reducing partitioning of HOC in soils. The partitioning of HOC in soil can be reduced by the surfactant molecules existing in aqueous phase. Consequently, this distribution of HOC compounds can be used as an index for evaluating the soil-washing performance of a surfactant and estimated as [10, 39, 40]:

$$K_d = [\text{HOC}]_s / ([\text{HOC}]_w + [\text{HOC}]_{\text{mic}}) = (\text{mol of HOC sorbed/g of solid}) / (\text{mol of HOC in aqueous and micellar solution/L})$$

where K_d is the partition coefficient of HOC between solid and aqueous-pseudophase, $[\text{HOC}]_s$ is the ratio of the moles of HOC sorbed per gram of solid (mole/g), $[\text{HOC}]_w$ is the ratio of the moles of HOC in water per liter of solution (mole/L), and $[\text{HOC}]_{\text{mic}}$ is the moles of HOC in micelles per liter of solution (mole/L) (see Fig. 2.9 of Chapter 2).

Figure 3.8 presents K_d of phenanthrene between aquifer material and aquifer phase in the absence and presence of amphiphilic materials determined using batch tests based on the same process described in previous chapter. That is, aquifer soil artificially contaminated by phenanthrene was mixed with nonionic surfactants and NACP aqueous solutions, and then change of phenanthrene concentration in aqueous phase was measured and described as K_d values. As described in previous section, the K_d is the partition coefficient of HOC molecules between soil and aqueous phase. Decrease of K_d values means sorbed HOC onto soil is extracted or moved into aqueous phase by amphiphilic molecules, so the degree of decrease in K_d values in the presence of nonionic surfactants and NACP nanoparticles corresponds to desorption capability of these materials for adsorbed HOC molecules.

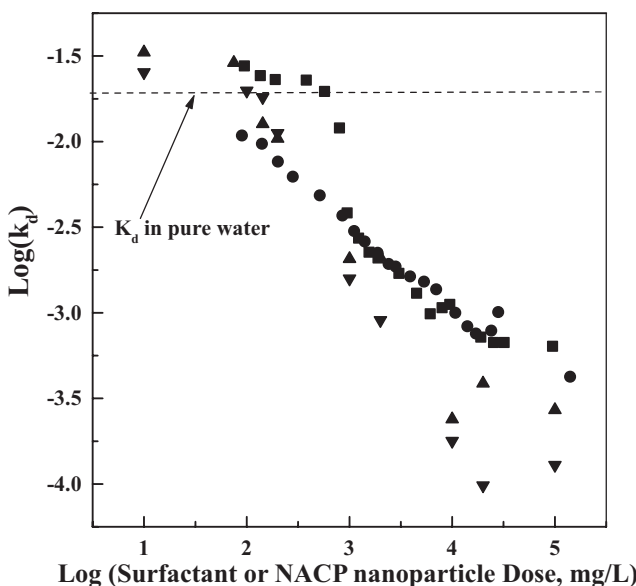


Figure 3.8 Distribution of phenanthrene between soil and aqueous pseudophase containing NACP nanoparticles and surfactants: - ■ - Triton X-100, - ● - NACP nanoparticles, - ▲ - Tween 80, and - ▼ - Brij 30. Reprinted from *J. Hazard. Mater.*, **B 116**, Kim, J. Y., Shim, S. B., and Shim, J. K., Comparison of amphiphilic polyurethane nanoparticles to nonionic surfactants for flushing phenanthrene from soil, 205, Copyright (2004), with permission from Elsevier.

Extraction and desorption of hydrophobic pollutants from soil highly depends on HLB and CMC, so three kinds of nonionic surfactants were used and compared their performance with NACP nanoparticles. HLB, molecular weight and CMC of nonionic surfactants were presented in Table 3.2.

As shown in Figure 3.8, the K_d values of phenanthrene decrease with an increase of NACP or nonionic surfactant concentration in aqueous phase, indicating that adsorbed phenanthrene on the soil was extracted and moved into the aqueous phase. However, NACP and nonionic surfactant showed very different desorption behavior with their concentrations. In the low concentration region (10–1000 mg/L), K_d values in nonionic surfactant aqueous solutions are higher than K_d values in pure water. This indicates that in this concentration region, nonionic surfactant molecules do not extract adsorbed phenanthrene from soil. Rather they cause an increase of the sorption of phenanthrene from aqueous phase to aquifer sand. However, in this

concentration region, K_d values in aqueous solution containing NACP nanoparticles are lower than K_d value in pure water and decrease with the increase of concentration of NACP nanoparticles, indicating that NACP nanoparticles can extract adsorbed phenanthrene in this concentration region. This interesting behavior is due to the microstructural difference between NACP and nonionic surfactants.

In low concentrations, most of the nonionic surfactant molecules dissolve in aqueous phase and exist as dissolved monomeric molecules, which are easily adsorbed onto soil. So, very few numbers of surfactant molecules can participate in desorption of phenanthrene. In addition, surfactant molecules adsorbed onto soil increase the adsorption of phenanthrene from aqueous phase to soil. Consequently, nonionic surfactant molecules cannot extract adsorbed phenanthrene from soil at the concentration lower or slightly greater than their CMC. It is reported that Brij 30 molecules have greater solubilization capability for phenanthrene compared with Triton X-100 because of lower HLB of Brij30 (9.7) compared with that of Triton X-100 (13.5). Surfactant having lower HLB has the higher affinity for hydrophobic compounds, and they have lower solubility in water, so they can form micelles at relatively low concentration in aqueous phase. As presented in Table 3.2, CMC of Brij 30 (20 mg/L) is much lower than that of Triton X-100 (111 mg/L). Thus, lower K_d values in Brij 30 aqueous solution can be explained by their higher affinity and lower CMC.

Even though Brij 30 showed better desorption capability than Tween 80 and Triton X-100, NACP aqueous solution showed lower K_d values than Brij 30 aqueous solution at this low concentration region, which means NACP nanoparticles have better desorption capability than Brij 30 molecules. That is, because UAN chain can form micelle-like nanoparticles (NACP nanoparticles) at extremely low concentration (practically no critical concentration for formation of NACP nanoparticles in aqueous phase) and micelle-like microstructure of NACP nanoparticles are permanently and chemically locked-in. So, at low concentration in aqueous phase, NACP nanoparticles can efficiently extract HOC molecules from soil and solubilize them within their hydrophobic interior despite their lower solubilization capability than nonionic surfactants.

In higher concentration regions, NACP and Triton X-100 solutions exhibited almost the same K_d values, indicating that NACP nanoparticles and Triton X-100 have the same extraction efficiency regardless of higher affinity of Triton X-100 for phenanthrene than NACP nanoparticles. Brij 30 aqueous solutions showed lower K_d

values than NACP nanoparticles and the other surfactant solutions at this concentration region. This can be explained by higher affinity for HOC molecules and lower CMC due to lower HLB. Brij 30 showed better desorption capability than NACP nanoparticles from the concentration greater than 10,000 mg/L, which is too high to be used in real field.

3.5 ADSORPTION OF SURFACTANT AND NACP NANOPARTICLES ONTO AQUIFER SOIL

At surfactant concentrations less than CMC, surfactant monomers can extract sorbed HOC but most of the surfactant monomers are easily sorbed onto the soil. These sorbed surfactants on a soil increase the soil's organic carbon content and solubilize HOCs as well, resulting in an enhanced sorption of HOC onto the soil [10, 39, 40]. In addition, the CMC of the surfactant in soil/water system is much greater than its CMC in pure water, due to high degree of surfactant sorption onto the soil. As a consequence, the surfactant can effectively extract sorbed hydrophobic pollutant only at concentrations much greater than its CMC in pure water. Consequently, Triton X-100 could extract sorbed phenanthrene from aquifer material only when the concentration is greater than 312 mg/L, which is three times greater than its CMC.

Figure 3.9 shows the sorption of NACP nanoparticles and Triton X-100 molecules onto the aquifer sand at various concentrations. In the low concentration region (93–600 mg/L), the sorption of Triton X-100 onto aquifer sand is much higher than the sorption of NACP 700-2 and NACP 1000 nanoparticles, that is, 30–40% of the Triton X-100 molecules are adsorbed, whereas 7–14% of APU nanoparticles are adsorbed onto aquifer materials. At higher concentrations (>700 mg/L), the sorption of Triton X-100 is also slightly greater than that of APU nanoparticles. This result is mainly due to the cross-linking nature of APU nanoparticles.

Below CMC, 100% of Triton X-100 molecules exist not as micelles but as monomeric molecules, whereas NACP aqueous phase consists of nano-sized particles only at this concentration. On contact with aquifer sand, monomeric molecules of Triton X-100 can be easily adsorbed onto the aquifer sand, whereas sorption of APU nanoparticles can be largely hindered due to their aggregated structure. At higher concentrations, even though Triton X-100 can form

aggregates (micelles) in aqueous phase, Triton X-100 exhibits greater sorption onto the aquifer material than NACP 700-2 and NACP 1000 nanoparticles. This result can be explained by the chemically cross-linked microstructure of NACP nanoparticles. Surfactant micelles formed by physical association of monomeric molecules tend to break up on contacting with soil or solid. However, NACP nanoparticles, nano-aggregates of UAN chains, cannot be easily destroyed because this aggregated structure is permanently locked in by chemical cross-linking reaction. As a consequence, NACP nanoparticles can remain intact due to their chemically cross-linked structure, yielding a lower degree of sorption of NACP 700-2 and NACP 1000 nanoparticles.

So, even at very low concentration in aqueous phase, NACP nanoparticles can efficiently extract sorbed phenanthrene from soil, even though Triton X-100 has a better solubilizing performance for phenanthrene compared to NACP nanoparticles. This indicates that desorption performance of amphiphilic materials in the mixture of water and soil containing hydrophobic pollutants is strongly influenced by the degree of sorption onto the soil.

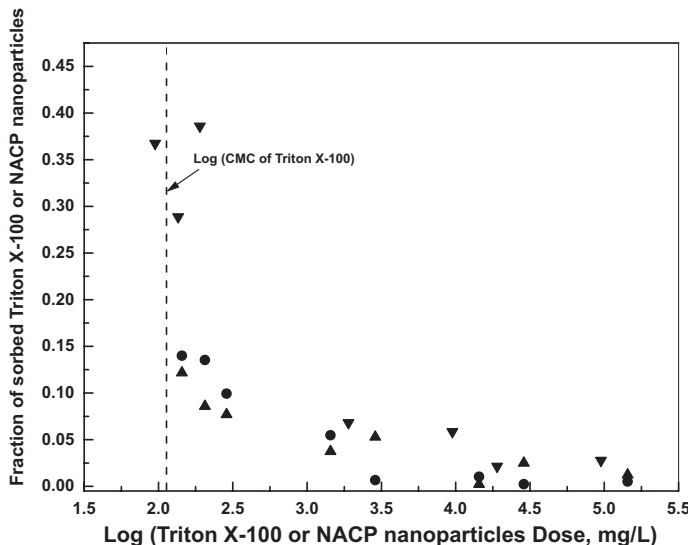


Figure 3.9 Sorption of Triton X-100 and NACP nanoparticles onto aquifer sand as a function of Triton X-100 or NACP nanoparticle dose: - ● - NACP 700-2, - ▲ - NACP 1000, and - ▼ - Triton X-100 Reprinted from *J. Hazard. Mater.*, **B 98**, Kim, J. Y., Shim, S. B., and Shim, J. K., Effect of amphiphilic polyurethane nanoparticles on sorption-desorption of phenanthrene in aquifer material, 145–160, Copyright (2003), with permission from Elsevier.

3.6 IN SITU SOIL WASHING USING NACP NANOPARTICLES AND NONIONIC SURFACTANTS

Batch isotherm experiments showed a better desorption capability of NACP nanoparticles compared with nonionic surfactants especially at low concentration region. At batch isotherm, desorption of adsorbed HOC from soil by NACP nanoparticles is evaluated as equilibrium concentration change after adding amphiphilic materials into the mixture of aqueous solution and soil where distribution of HOC between aqueous phase and soil is equilibrated. At *in situ* soil washing, washing solution containing amphiphilic materials flow through soil pores at relatively fast speed, so an aqueous solution containing amphiphilic materials move to new soil matrix before distribution of HOC molecules is equilibrated between aqueous phase and soil. Amphiphilic molecules could show very different soil-washing capability at *in situ* and batch soil-washing process. *In situ* soil-washing performance of a washing material can be generally evaluated as lab-scale using as soil column experiment. As described at previous chapter, washing solutions are added into soil column packed with contaminated soil to monitor soil-washing performance of amphiphilic molecules at various conditions [36, 41, 42].

Soil used for the preparation of soil column is aquifer sand obtained from a quarry in New Field, NY. The organic content of the sand was reported to be $0.049 \pm 0.012\%$. Also, 47.2% and 47.5% of the particles are in the fine (0.1–0.25 mm) and medium (0.25–0.5 mm) size range, respectively. The remaining constituents included very fine sand (0.05–0.1 mm) at 3.7%, coarse sand (>0.5 mm) at 0.2%, and silt and clay at 1.2%.

Figures 3.10 and 3.11 show the *in situ* soil-washing performance of NACP nanoparticles and Triton X-100 at various flow rate and concentrations in washing solution. As discussed in the previous section, Triton X-100 at a concentration less than 2000 mg/L does not extract sorbed phenanthrene from the aquifer soil, so the concentration of NACP and Triton X-100 solutions was fixed at 4000 mg/L. At the higher flow rate (0.12 mL/min), after 18 pore volumes of washing with NACP and Triton X-100 solution, 32.6% and 46.9% of the phenanthrene was removed from the soil column, respectively. This result indicates that the *in situ* extraction efficiency of Triton X-100 is better than that of NACP nanoparticles at this concentration and flow rate.

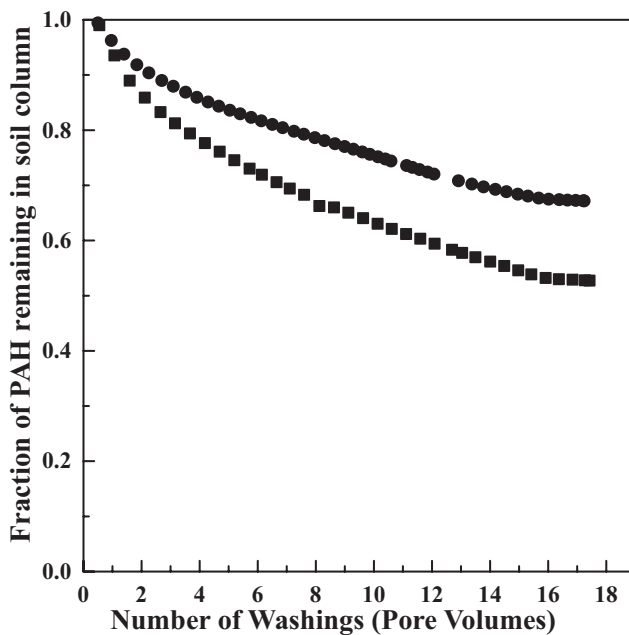


Figure 3.10 Extraction of sorbed phenanthrene (PAH) from a soil column using NACP nanoparticles and Triton X-100 solutions at a higher flow rate (0.12 mL/min): - ■ - Triton X-100, and - ● - NACP nanoparticles. Reprinted from *J. Hazard. Mater.*, B116, Kim, J. Y., Shim, S. B., and Shim, J. K., Comparison of amphiphilic polyurethane nanoparticles to nonionic surfactants for flushing phenanthrene from soil, 205, Copyright (2004), with permission from Elsevier.

However, as shown in Fig. 3.11, at the same concentration (4000 mg/L), extraction performance of NACP nanoparticles and Triton X-100 with lower flow rate of washing (0.02 mL/min) was better than the soil washing with at higher flow rate (0.12 mL/min). At lower flow rate, washing materials have longer contact time with soil grains absorbing phenanthrene, which increase desorption of phenanthrene by washing materials. The interesting phenomenon is that NACP nanoparticles showed better *in situ* extraction efficiency than did Triton X-100 at the same concentration, which is very opposite to the results of Fig. 3.10. By decreasing flow rate from 0.12 mL/min to 0.02 mL/min at the same concentration (4000 mg/L), extraction performance of Triton X-100 slightly increased, whereas NACP nanoparticles showed greater increase in extraction performance. That is, NACP nanoparticles washed out 21% of

phenanthrene after 18 pore volumes of washing with 0.12 mL/min of flow rate, but 88% of phenanthrene was extracted from soil column using nine pore volumes of washing with 0.02 mL/min at the same concentration. This indicates that extraction performance of NACP nanoparticles can be largely enhanced by increasing their contact time with soil matrix.

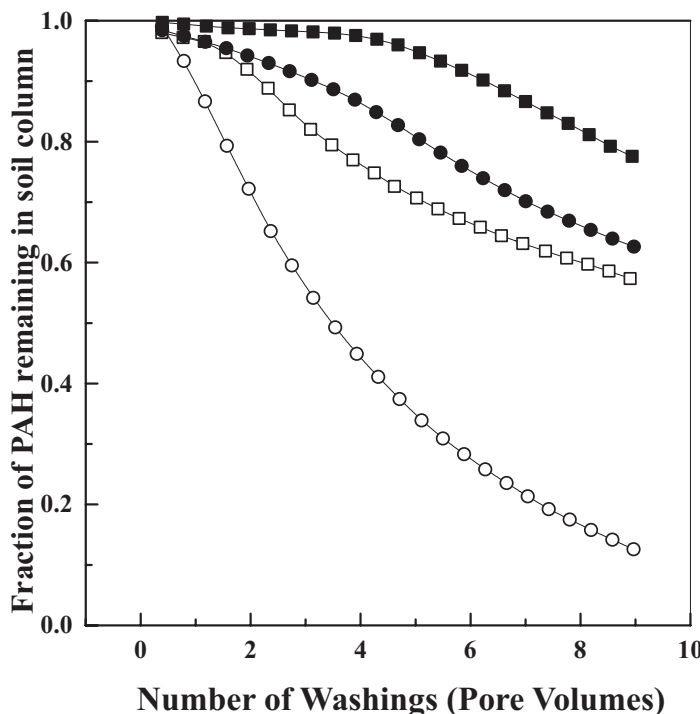


Figure 3.11 Extraction of sorbed phenanthrene (PAH) from a soil column using APU nanoparticle and Triton X-100 solutions at a lower flow rate (0.02 mL/min) using two different concentrations: - ■ - Triton X-100 (100 mg/L), - ● - NACP nanoparticles (100 mg/L), - □ - Triton X-100 (4000 mg/L), and - ○ - NACP nanoparticles (4000 mg/L). Reprinted from *J. Hazard. Mater.*, **B116**, Kim, J. Y., Shim, S. B., and Shim, J. K., Comparison of amphiphilic polyurethane nanoparticles to nonionic surfactants for flushing phenanthrene from soil, 205, Copyright (2004), with permission from Elsevier.

Increasing the contact time of washing materials with soil matrix can cause increase in the degree of sorption onto the soil. As mentioned earlier, Triton X-100 molecules are easily sorbed onto soil matrix owing to the vulnerable structure of their micelles.

So, decreasing the flow rate of Triton X-100 aqueous solution at soil column can increase its contact time with soil matrix, which is offset by increased sorption of Triton X-100 onto soil. Consequently, extraction performance of Triton X-100 was slightly increased even with much lower flow rate in the soil column. However, the degree of sorption of NACP nanoparticles onto the soil slightly increased at highly reduced flow rate, due to chemically cross-linked structure of NACP nanoparticles, which makes soil-washing performance of NACP nanoparticles largely increased.

As mentioned earlier, even though NACP nanoparticles have lower solubilization capacity than Triton X-100, desorption performance of NACP nanoparticles for absorbed phenanthrene is higher than that of Triton X-100. Especially, at low concentration, NACP nanoparticles showed much better extraction efficiency compared with Triton X-100. At lower flow rates, the better *in situ* extraction performance of NACP nanoparticles can be explained by the lower degree of sorption of NACP nanoparticles within the soil column. Lower flow rates increase the contact time between amphiphilic materials (NACP nanoparticles and Triton X-100) and soil grains, and their remaining times within soil pores. Consequently, NACP nanoparticles having physically strong microstructure have relatively lower degree of sorption onto the soil, resulting in a better extraction performance.

In situ flushing efficiency of NACP nanoparticles was compared with that of several nonionic surfactants such as Triton X-100, Brij 30, and Tween 80. As presented in Table 3.2, Brij 30 and Tween 80 have much lower CMC compared with Triton X-100. It means these surfactants can form micelles at very low concentration in aqueous phase. HLB of Brij 30 (9.7) is lower than that of Triton X-100 (13.5). Lower HLB surfactants have strong affinity for hydrophobic molecules, so it can be expected that Brij 30 has much better solubilization performance compared with Triton X-100. Figure 3.12 shows the *in situ* extraction efficiency of NACP and surfactant solutions at the same washing condition (0.02 mL/min of flow rate and 100 mg/L of concentration). After nine pore volumes of washing, NACP washed out a larger amount of phenanthrene (about 40%) from the soil column than did Brij 30 (18%), Triton X-100 (18%), and Tween 80 (4.5%). As illustrated in Fig. 3.13, at a higher concentration of washing solution (4000 mg/L), NACP nanoparticles also showed higher *in situ* extraction performance compared with the surfactants.

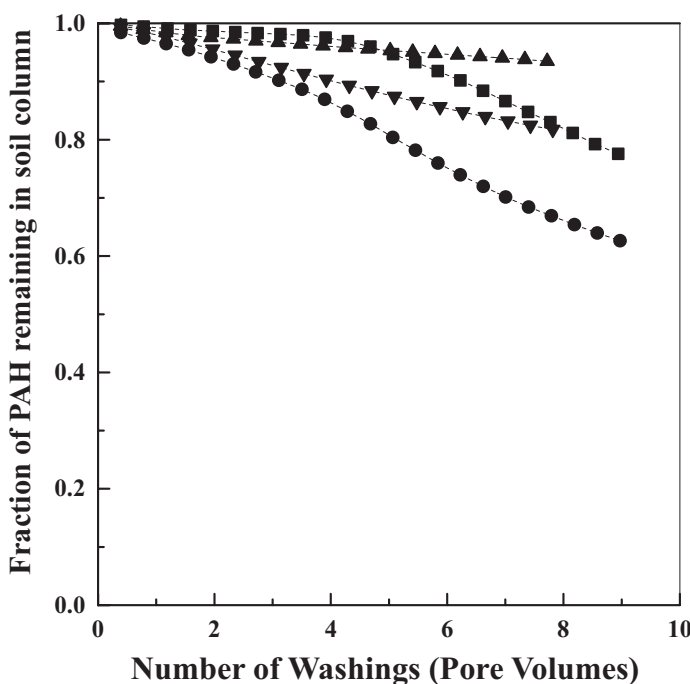


Figure 3.12 Extraction of sorbed phenanthrene (PAH) from a soil column using NACP nanoparticles and surfactant solutions at the same flow rate (0.02 mL/min) and concentration (100 mg/L): - ■ - Triton X-100, - ● - NACP nanoparticles, - ▲ - Tween 80, and - ▼ - Brij 30. Reprinted from *J. Hazard. Mater.*, **B116**, Kim, J. Y., Shim, S. B., and Shim, J. K., Comparison of amphiphilic polyurethane nanoparticles to nonionic surfactants for flushing phenanthrene from soil, 205, Copyright (2004), with permission from Elsevier.

As mentioned earlier, the solubilization capacity of Triton X-100 for phenanthrene is eight times higher than that of NACP nanoparticles. In addition, it was reported that the solubilization efficiency of Brij 30 is 2.5 times greater than that of Triton X-100 [38]. So, it can be expected that all surfactants, especially Brij 30, would exhibit better extraction efficiency for sorbed phenanthrene than NACP nanoparticles. However, NACP nanoparticles exhibited better soil-washing performance than did all surfactants. This result indicates that the lower degree of sorption of NACP nanoparticles due to chemically cross-linked structure make them more efficient material in *in situ* soil washing.

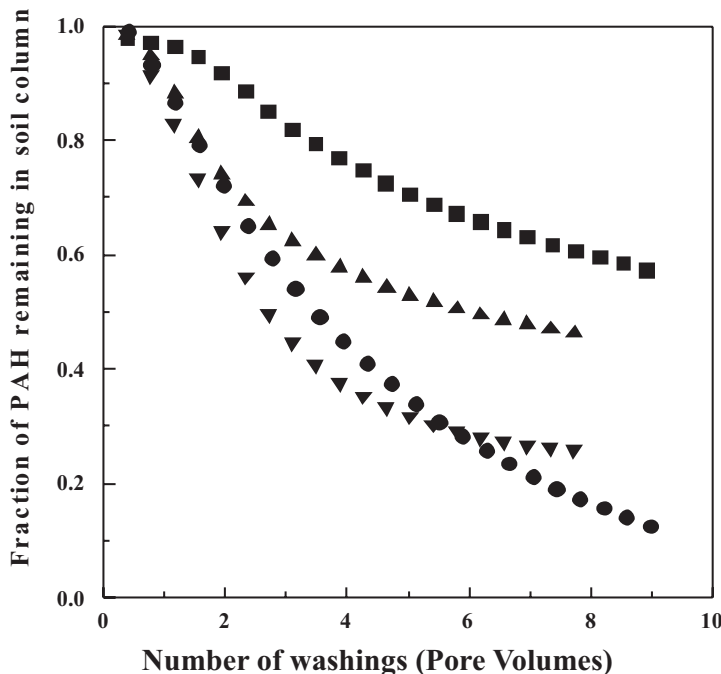


Figure 3.13 Extraction of sorbed phenanthrene (PAH) from a soil column using NACP nanoparticle and surfactant solutions at the same flow rate (0.02 mL/min) and concentration (4000 mg/L): -■- Triton X-100, -●- NACP nanoparticles, -▲- Tween 80, and -▼- Brij 30. Reprinted from *J. Hazard. Mater.*, **B116**, Kim, J. Y., Shim, S. B., and Shim, J. K., Comparison of amphiphilic polyurethane nanoparticles to nonionic surfactants for flushing phenanthrene from soil, 205, Copyright (2004), with permission from Elsevier.

3.7 FLOW BEHAVIOR OF SURFACTANT AND NACP NANOPARTICLES SOLUTIONS WITHIN SOIL COLUMN

As mentioned in previous section, in batch condition, NACP nanoparticles have better extraction efficiency than surfactant molecules, because of lower degree of sorption onto soil due to their chemically cross-linked microstructure. NACP nanoparticles also have better *in situ* washing performance especially with lower flow rate and concentrations, which can be also explained by lower degree of

sorption onto soil matrix while they flow through it. Degree of sorption of surfactant molecules and NACP nanoparticles can be monitored by measuring their relative concentration (C_0/C) in effluents. C_0 is the initial concentration of surfactant or NACP nanoparticles in washing solutions, which are added to soil column. C is the concentration of surfactant or NACP nanoparticles in effluents, which are flow out from soil column. If the relative concentration of an effluent is close to 1 ($C/C_0 \leq 1$), most of surfactant molecule or NACP nanoparticles added at soil column are eluted out without sorption onto soil matrix.

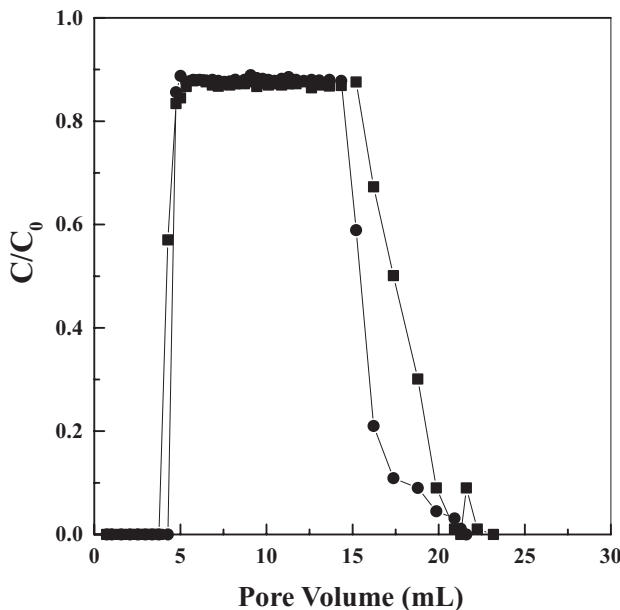


Figure 3.14 Elution of Triton X-100 and NACP nanoparticles from a soil column at a lower flow rate (0.02 mL/min): - ■ - Triton X-100 (4000 mg/L) and - ● - NACP nanoparticles (4000 mg/L). Reprinted from *J. Hazard. Mater.*, **B116**, Kim, J. Y., Shim, S. B., and Shim, J. K., Comparison of amphiphilic polyurethane nanoparticles to nonionic surfactants for flushing phenanthrene from soil, 205, Copyright (2004), with permission from Elsevier.

The relative concentration of Triton X-100 and APU nanoparticles solutions (with $C_0 = 4000$ mg/L) flowing through the soil column is illustrated in Figs. 3.14 and 3.15. C_0 is the initial concentration of Triton X-100 or APU nanoparticles in the elutant. C is the concentration of Triton X-100 or NACP nanoparticles of a sample eluted from the soil

column. After adding 2.5 pore volumes (10.67 mL) of NACP and Triton X-100 solution to the soil-packed column, rinse water was added to the column to recover NACP nanoparticles and Triton X-100 from the soil column. As shown in Fig. 3.14, at a high flow rate (0.12 mL/min), Triton X-100 and NACP nanoparticles exhibited almost identical breakthrough curves. That is, NACP and Triton X-100 solution exhibited almost the same relative concentration (C/C_0), indicating that APU and Triton X-100 have almost the same degree of sorption within the soil column under the given conditions. However, as shown in Fig. 3.15 for a low flow rate (0.02 mL/min), the two solutions exhibited different breakthrough curves. The relative concentration, C/C_0 , of NACP nanoparticle is higher than that of Triton X-100. This indicates that the degree of sorption of NACP nanoparticle onto the soil column is lower than that of Triton X-100.

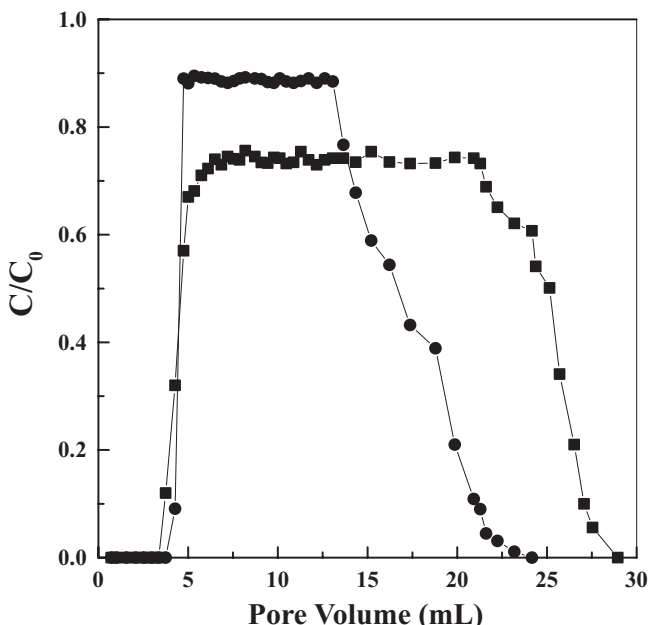


Figure 3.15 Elution of Triton X-100 and APU nanoparticles from a soil column at a lower flow rate (0.02 mL/min): - ■ - Triton X-100 (4000 mg/L) and - ● - APU nanoparticles (4000 mg/L). Reprinted from *J. Hazard. Mater.*, **B116**, Kim, J. Y., Shim, S. B., and Shim, J. K., Comparison of amphiphilic polyurethane nanoparticles to nonionic surfactants for flushing phenanthrene from soil, 205, Copyright (2004), with permission from Elsevier.

As schematically shown in Fig. 3.16, because of chemically cross-linked microstructure of NACP nanoparticles, NACP nanoparticles maintain their individual structure, so that smaller amount of NACP nanoparticles remain within the soil column in the course of soil washing, resulting in higher C/C_0 . However, Triton X-100 molecules and their micelles are easily adsorbed onto soil while they flow through it because of their vulnerable structures, so that larger amount of Triton X-100 molecules remains within the soil column after soil washing, resulting in lower C/C_0 .

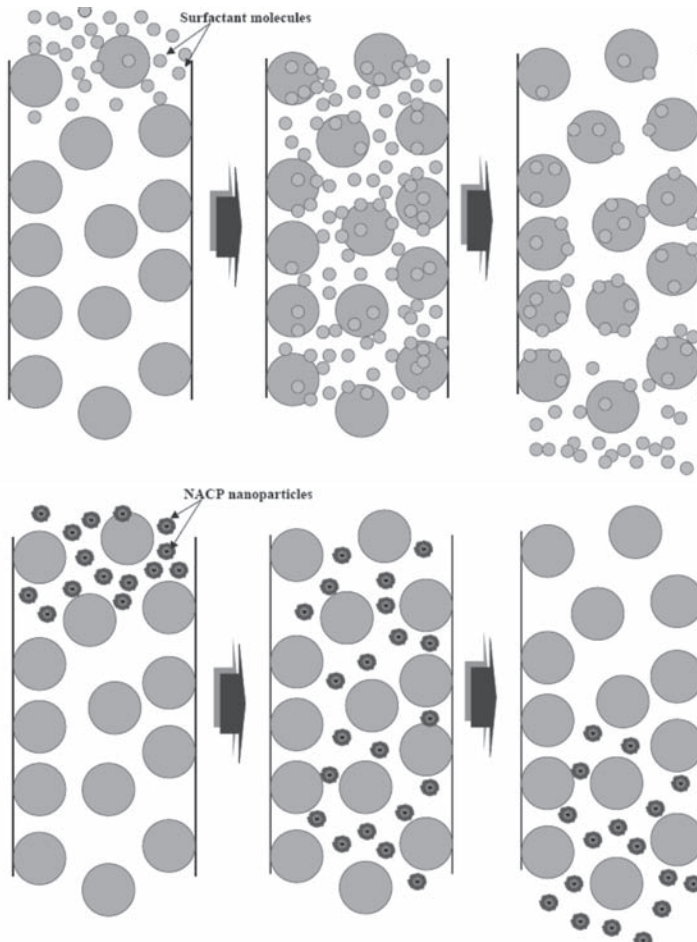


Figure 3.16 Schematic diagram of flow behavior of surfactant molecules and NACP nanoparticles.

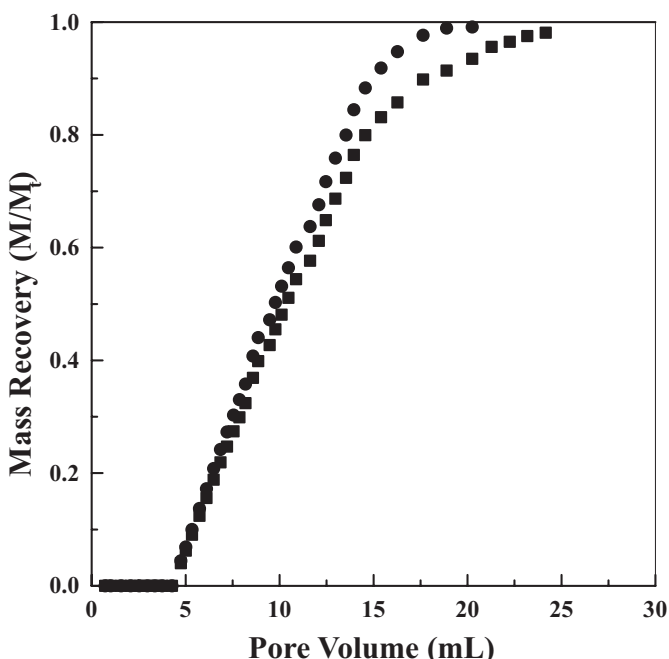


Figure 3.17 Mass recovery of Triton X-100 and NACP nanoparticles from a soil column at a higher flow rate (0.12 mL/min): - ■ - Triton X-100 (4000 mg/L) and - ● - NACP nanoparticles (4000 mg/L). Reprinted from *J. Hazard. Mater.*, **B116**, Kim, J. Y., Shim, S. B., and Shim, J. K., Comparison of amphiphilic polyurethane nanoparticles to nonionic surfactants for flushing phenanthrene from soil, 205, Copyright (2004), with permission from Elsevier.

In Figs. 3.17 and 3.18, the mass recovery of the NACP nanoparticles and Triton X-100 from the soil column is plotted as a function of the volume of the aqueous solution added to the soil column. Here, M_T represents the total mass of NACP nanoparticles or Triton X-100 added to the column and M is the accumulated mass of NACP nanoparticles or Triton X-100 eluted from the column. At a high flow rate (Fig. 3.17), over 98% of Triton X-100 and NACP nanoparticles was recovered with the almost same amount of rinse water. At a low flow rate (Fig. 3.18), over 98% of NACP nanoparticles was recovered after 12.81 mL of rinse water, but only 96% of Triton X-100 could be recovered with 19.22 mL of rinse water. That is, at a high flow rate, Triton X-100 and NACP nanoparticles have almost the same degree of sorption onto the soil, and so Triton X-100 and NACP

nanoparticles could be recovered with almost the same amount of rinse water. At a low flow rate, Triton X-100 and NACP nanoparticles have longer contact time with the soil, and so more Triton X-100 and NACP nanoparticles were adsorbed onto the soil. Consequently, more rinse water was needed to recover over 98% of Triton X-100 and NACP nanoparticles. However, less rinse water was used for the recovery of NAPU nanoparticles, which can be interpreted as being due to the lower degree of sorption of NACP nanoparticles. Hence, it can be thought that the cross-linked structures of NACP nanoparticles make it possible for the particles to maintain their structure when in contact with soil for a longer contact time, which causes a lower degree of sorption onto the soil column.

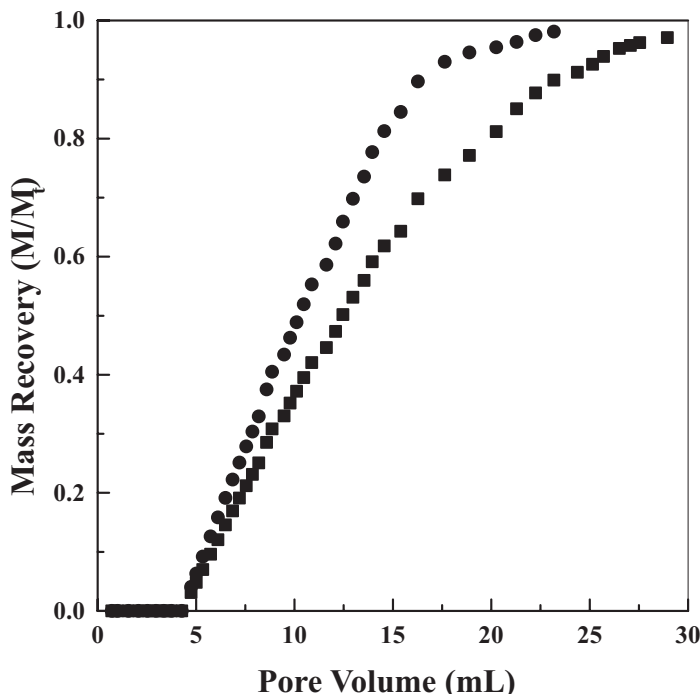


Figure 3.18 Mass recovery of Triton X-100 and NACP nanoparticles from a soil column at a higher flow rate (0.12 mL/min): - ■ - Triton X-100 (4000 mg/L) and - ● - NACP nanoparticles (4000 mg/L). Reprinted from *J. Hazard. Mater.*, **B116**, Kim, J. Y., Shim, S. B., and Shim, J. K., Comparison of amphiphilic polyurethane nanoparticles to nonionic surfactants for flushing phenanthrene from soil, 205, Copyright (2004), with permission from Elsevier.

3.8 CONCLUSIONS

Even though surfactant molecules have a stronger affinity for phenanthrene and better phenanthrene solubilizing performance than NACP nanoparticles, NACP nanoparticles exhibited better extraction performance and had a greater reduction of phenanthrene sorption especially in low concentration regions. Also, these two aqueous solutions portrayed relatively small differences in extraction efficiency of phenanthrene in the higher concentration region. So, it can be concluded that the soil-washing performance strongly depends not on the affinity with phenanthrene but on the degree of sorption of interfacial agents onto the soil. The price of UAN chains could be more expensive than that of commercialized surfactants. This higher cost, however, would be compensated by better extraction performance at a relatively low concentration, and low degree of sorption of NACP nanoparticles onto the soil. Furthermore, as described in the following chapter, 100 % of the applied NACP nanoparticles could be recovered through a membrane separation process, which makes NACP nanoparticles more efficient material as a soil-washing material.

References

- [1] Park, S. -K., and Bielefeldt, A. R. (2003) Aqueous chemistry and interactive effects of non-ionic surfactant and pentachlorophenol sorption to soil, *Water Res.*, **37**, 4663–4672.
- [2] Deitch, J. J., and Smith, J. A. (1995) Effect of Triton X-100 on the rate of trichloroethene desorption form soil to water, *Environ. Sci. Technol.*, **29**(4), 1069–1080.
- [3] Urum, K., Grigson, S., Pekdemir, T., McMenamy, S. (2006) A comparison of the efficiency of different surfactants for removal of crude oil from contaminated soils, *Chemosphere*, **62**, 1403–1410.
- [4] Laha, S., Tansel, B., and Ussawarujikulchai, A. (2009) Surfactant-soil interactions during surfactant-amended remediation of contaminated soils by hydrophobic organic compounds: a review, *J. Environ. Management*, **90**, 95–100.
- [5] Lee, M. H., Kang, H. M., and Do, W. H. (2005) Application of nonionic surfactant-enhanced in situ flushing to a diesel contaminated site, *Water Res.*, **39**, 139–146.

- [6] Park, S. K., and Bielefeldt, A. R. (2005) Non-ionic surfactant flushing of pentachlorophenol from NAPL-contaminated soil, *Water Res.*, **39**, 1388–1396.
- [7] Kile, D. E., and Chiou, C. T. (1989) Water solubility enhancement of DDT and trichlorobenzene by some surfactants below and above the critical micelle concentration, *Environ. Sci. Technol.*, **23**, 832–838.
- [8] Liu, Z., Edwards, D. A., and Luthy, R. G. (1991) Sorption of non-ionic surfactants onto soil, *Water Res.*, **26**(10), 1337–1345.
- [9] Deshpande, S., Wesson, L., Wade, D., Sabatini, D. A., and Harwell, J. H. (2000) Dowfax surfactant components for enhancing contaminant solubilization, *Water Res.*, **34**(3), 1030–1036.
- [10] Edwards, D. A., Adeel, Z., and Luthy, R. G. (1994) Distribution of nonionic surfactant and phenanthrene in a sediment/aqueous system, *Environ. Sci. Technol.*, **28**, 1550–1560.
- [11] Schick, M. J. (1987) *Nonionic Surfactants: Physical Chemistry*, Marcel Dekker Inc., New York and Basel.
- [12] Myers, D. (1988) *Surfactant Science and Technology*, VCH, New York.
- [13] Rosen, M. J. (2004) *Surfactants and Interfacial Phenomena*, Wiley-Interscience, Hoboken, NJ.
- [14] Rafael, B. L., Lev, B., Marina, T., Alan, H. T., Angel, C., and Carmen, A. L. (2004) Solubilization and stabilization of camptothecin in micellar solutions of pluronic-g-poly(acrylic acid) copolymers, *J. Controlled Release*, **97**, 537–549.
- [15] Amiji, M. M., and Park, K. N. (2005) Analysis on the surface adsorption of PEO/PPO/PEO triblock copolymers by radiolabelling and fluorescence techniques, *J. Appl. Polym. Sci.*, **52**, 539–544.
- [16] James-Smith, M. A., Shekhawat, D., Cheung, S., Moudgil, B. M., Shah, D. O. (2008) Role of ethylene oxide and propylene oxide groups of pluronics in binding of fatty acid to pluronics in microemulsions, *J. Surfactants Deterg.*, **11**, 237–242.
- [17] Causse, J., Lagerge, S., de Menorval, L.C., Faure, S. (2006) Micellar solubilization of tributylphosphate in aqueous solutions of Pluronic block copolymers. Part I. Effect of the copolymer structure and temperature on the phase behavior, *J. Colloid Interface Sci.*, **300**, 713–723.
- [18] Jain, T. K., Foy, S. P., Erokwu, B., Dimitrijevic, S., Flask, C. A., and Labhasetwar, V. (2009) Magnetic resonance imaging of multifunctional pluronic stabilized iron-oxide nanoparticles in tumor-bearing mice, *Biomaterials*, **30**, 6748–6756.

- [19] Batrakova, E. V., and Kabanov, A.V. (2008) Pluronic block copolymers: evolution of drug delivery concept from inert nanocarriers to biological response modifiers, *J. Controlled Release*, **130**, 98–106.
- [20] Zhao, J., Gou, M., Dai, M., Li, X. Y., Cao, M., Huang, M. J., Wen, Y. J., Kan, B., Qian, Z. Y., and Wei, Y. Q. (2009) Preparation, characterization, and in vitro cytotoxicity study of cationic PCL-Pluronic-PCL (PCFC) nanoparticles for gene delivery, *J. Biomedical Mater. Res. Part A*, **90**, 506–513.
- [21] Chen, S., Guo, C., Hu, G. H., Liu, H. Z., Liang, X. F., Wang, J., Ma, J. H., and Zheng, L. (2007) Dissipative particle dynamics simulation of gold nanoparticles stabilization by peo-ppo-peo block copolymer micelles, *Colloid Polym. Sci.*, **285**, 1543–1552.
- [22] Kim, J. Y., Shin, D. H., and Shim, S. B. (2001) Korea Patent No. 0420371.
- [23] Kim, J. Y., Shin, D. H., and Shim, S. B. (2001) Korea Patent No. 0420372.
- [24] Kim, J. Y., Oh, Y. H., and Kim, J. H. (2007) Korea Patent No. 10-0868728.
- [25] Kim, J. Y. (2008) Korea Patent No. 10-0788848-0000.
- [26] Kim, J. Y., Wainina, J., Kim, J. H., and Shim, J. K. (2007) Use of polymer nanoparticles as functional nano-absorbents for low-molecular weight hydrophobic pollutants, *J. Nanosci. Nanotechnol.*, **7**(11), 4000–4004.
- [27] Kim, J. Y., Kim, H. M., Shin, D. H., and Ihn, K. J. (2006) Synthesis of CdS nanoparticles dispersed within poly(urethane acrylate-co-styrene) films using amphiphilic urethane acrylate nonionomer, *Macromol. Chem. Phys.*, **207**, 925–932.
- [28] Lee, K. T., Choi, H. S., Kim, J. Y., and Ahn, I. S. (2003) Distribution of phenanthrene between soil and an aqueous phase in the presence of anionic micelle-like amphiphilic polyurethane particles, *J. Hazard. Mater.*, **B 105**, 179–197.
- [29] Kim, J. Y., Shim, S. B., and Shim, J. K. (2003) Effect of amphiphilic polyurethane nanoparticles on sorption-desorption of phenanthrene in aquifer material, *J. Hazard. Mater.*, **B 98**, 145–160.
- [30] Kim, J. Y., Shim, S. B., and Shim, J. K. (2004) Comparison of amphiphilic polyurethane nanoparticles to nonionic surfactants for flushing phenanthrene from soil, *J. Hazard. Mater.*, **B116**, 205.
- [31] Liu, Z., Shonali, L., and Luthy, R. G. (1991) Surfactant solubilization of polycyclic aromatic hydrocarbon compounds in soil-water suspensions, *Water Sci. Technol.*, **23**, 475–485.
- [32] Haulbrook, W. R., Feerer, J. L., Hatton, T. A., and Tester, J. W. (1993) Enhanced solubilization of aromatic solutes in aqueous solutions of N-vinylpyrrolidone/styrene, *Environ. Sci. Technol.*, **27**, 2783–2788.

- [33] Kommalapati, R. R., ValsaRaj, K. T., Constant, W. D., Roy, D. (1997) Aqueous solubility enhancement and desorption of hexachlorobenzene from soil using a plant-based surfactant, *Water Res.*, **31**(9), 2161–2170.
- [34] Doong, R., Lei, W., Chen, T., Lee C., and Chang, W. (1996) Effect of anionic and nonionic surfactants on sorption and micellar solubilization of monocyclic aromatic compounds, *Water Sci. Technol.*, **34**(7–8), 327–334.
- [35] Grimberg, S. J., Nagel, J., and Aitken, M. D. (1995) Kinetic of phenanthrene dissolution into water in the presence of nonionic surfactant, *Environ. Sci. Technol.*, **29**, 1480–1487.
- [36] Zhao, D., Joseph, P. J., White, C. J., and Braida, W. (2001) Dual-mode modeling of competitive and concentration-dependent sorption and desorption kinetics of polycyclic aromatic hydrocarbon in soils, *Water Resour. Res.*, **37**(8), 2205–2212.
- [37] Yeom, I. T., Ghosh, M. M., and Cox, C. D. (1996) Kinetic aspects of surfactant solubilization of soil-bound polycyclic aromatic hydrocarbons, *Environ. Sci. Technol.*, **30**, 1589–1595.
- [38] Yeom, I. T., Ghosh, M. M., Cox, C. D., and Robinson, K. G. (1995) Micellar solubilization of polycyclic aromatic hydrocarbons in coal tar-contaminated soils, *Environ. Sci. Technol.*, **29**, 3015–3021.
- [39] Jafvert, C. T. (1991) Sediment- and saturated-soil-associated reactions involving an anionic surfactant (dodecylsulfate). 2. Partition of PAH compounds among phases, *Environ. Sci. Technol.*, **25**, 1039–1045.
- [40] Chu, W., and So, W. S. (2001) Modeling the two stage of surfactant-aided soil washing, *Water Res.*, **35**(3), 761–767.
- [41] West, C. C., and Harwell, J. H. (1992) Surfactants and subsurface remediation, *Environ. Sci. Technol.*, **26**(2), 2324–2329.
- [42] Kim, J.-Y., Cohen, C., Shuler, M. L., and Lion, L. W. (2000) Use of amphiphilic polymer particles for in situ extraction of sorbed phenanthrene from a contaminated aquifer material, *Environ. Sci. Technol.*, **34**, 4133–4139.

This page intentionally left blank

Chapter 4

ADSORPTION AND CONCENTRATION OF ORGANIC CONTAMINANTS BY CARBON NANOTUBES FROM ENVIRONMENTAL SAMPLES

Hongyun Niu and Yaqi Cai

*State Key Laboratory of Environmental Chemistry and Ecotoxicology,
Research Center for Eco-Environmental Sciences,
Chinese Academy of Sciences, Beijing, China*

hnyiu@rcees.ac.cn; cayaqi@rcees.ac.cn

4.1 ADSORPTION OF ORGANIC COMPOUNDS TO CNTs

Since the discovery of carbon nanotubes (CNTs) by Iijima, fundamental research on CNTs and various potential applications has been proposed. CNTs are carbon macromolecules consisting of sheets of carbon atoms covalently bonded in hexagonal arrays that seamlessly rolled into a hollow, cylindrical shape with both ends normally capped by fullerene-like tips. Based on the structure, CNTs are categorized into two main classes: single-walled carbon nanotubes (SWCNT) and multiwalled carbon nanotubes (MWCNT). The lengths of CNTs can range from several hundred nanometers to several micrometers, and the diameters from 0.2 to 2 nm for SWCNT and from 2 to 100 nm for coaxial MWCNT. Nanotubes are characterized by their high surface areas and good electrical, chemical, mechanical, and

Advances in Nanotechnology and the Environment

Edited by Juyoung Kim

Copyright © 2012 by Pan Stanford Publishing Pte. Ltd.

www.panstanford.com

conducting properties. CNTs are extremely hydrophobic and prone to aggregation as bundles (especially SWCNT) or ropes due to the strong van der Waals interactions along the length axis. Aggregation is a characteristic that differentiate CNTs from other carbonaceous materials (e.g., activated carbons, carbon fibers, etc.).

CNTs synthesis techniques may be classified into three major categories: laser ablation, catalytic arc discharge, and chemical vapor deposition. No matter which method is used, the as-produced CNTs are usually contaminated with residual metal catalyst and carbon species such as carbon nanoparticles, fullerenes, carbon nano-onions, and amorphous carbon. Purification of CNTs is usually necessary for its further use. The most commonly employed purification technique is oxidation by acid treatment (concentrated acids and acid mixtures (HNO_3 , H_2SO_4), and other strong oxidizers (H_2O_2 , KMnO_4)) or dry-air oxidation. Since CNTs have reactive sites at defects and their strained caps, the tubes can be functionalized during the purification procedures, giving rise to various oxygen-containing functional groups (e.g., $-\text{COOH}$, $-\text{OH}$, or $-\text{C=O}$) on CNTs surface and alter the properties of CNTs considerably.

The characteristic structures and electronic properties of CNTs allow them to interact strongly with organic molecules. The surface, made up of hexagonal arrays of carbon atoms in graphene sheets, interacts strongly with the benzene ring of aromatic compounds. In 2001, Long and Yang observed that dioxins, which present two benzene rings, were strongly adsorbed on MWCNT. The authors suggested that MWCNT were an ideal adsorbent for dioxin removal. Since this initial work, plenty of studies have been carried out on the application potential of CNTs to eliminate organic pollutants from environment. Similar to the adsorption of organic compounds on activated carbon, the affinity of CNTs to adsorbate molecules is determined mainly by hydrophobic, $\pi-\pi$, H-bonding, and electrostatic interactions. There are four possible groups of adsorption sites on bundles: interior of individual tubes, interstitial channels between nanotubes, external groove sites, and the outer surface sites of individual tubes on the peripheral surface of the bundles. The interior of individual tubes is only available in open-ended tubes, the interstitial channels are applied for large tube diameters, while grooves and the external surface are of most importance for adsorption, and it may also significantly impact their adsorption properties. The adsorption may be affected by the surface areas, pore size or pore volume, and surface chemistry property of CNTs.

Surface functionalization can change the accessibility and affinity of CNTs to adsorbate molecules. The former can be attributed to the change in the aggregation due to increase in the wettability of CNTs surfaces and/or the number of available adsorption sites by either opening (removal of the end tips of CNTs by oxidation) or blocking (with functional groups or water clusters formed around the clusters formed around the functional groups) of the inner cavities.

4.1.1 Adsorption of Aromatic Compounds on CNTs From Aqueous Solution

Cyclic aromatics consist of one or more carbon rings, the planar arrangement of its atoms creates the conditions for filling the in-plane sp^2 hybrid orbitals of C and creating a resonant bond shared by all six C atoms. Besides this aromatic bond, there is a set of π orbitals transverse to the molecular plane. Each carbon atom in a CNT has a π electron orbit perpendicular to the CNT surface. Therefore, the aromatic molecules/CNT systems can be viewed as two interacting π systems. Hence, aromatic compounds interacting with CNTs are of particular interest. Noncovalent sidewall CNTs functionalization with aromatic organic molecules has attracted increasing attention. Aromatic compounds have relatively higher sorption affinity to CNTs than nonaromatics. Moreover, aromatic compounds represent an important group of organic contaminants in various environmental matrixes and structural components of large organic molecules in biological system. An increasing number of theoretical (calculation or simulation) and experimental studies have been carried out to understand systematically the interaction between CNT and aromatic compounds. However, researches in this area are still fragmentary and not complete enough for making clear conclusion. By far, the studies indicate that the interactions between CNTs and aromatic compounds can be influenced by many factors (such as property of adsorbate and CNTs, and environmental conditions).

4.1.1.1 Effect of number of benzene ring

Zhao et al. have suggested that the hybridization of π electrons between nanotubes and molecules is the common feature of all aromatic molecules adsorbed on CNTs. The $\pi-\pi$ bond has been recognized as a dominating interaction force for the adsorption of aromatic compounds on CNTs. Consequently, sorption affinity of chemicals

containing benzene rings by CNTs increase with increasing number of aromatic rings, e.g., the adsorption affinity of cyclohexanol, phenol, phenylphenol, and naphthalol to CNTs follow the order of cyclohexanol < phenol < 2-phenylphenol < 1-naphthalol; for nonpolar PAHs, the adsorption coefficient (K) is found to increase with the benzene ring numbers, for instance, naphthalene < phenanthrene < pyrene.

4.1.1.2 Effect of organic functional groups of aromatic compounds

Benzene derivatives are obtained by substituting one or more hydrogen atoms in the benzene ring with a functional group such as hydroxyl, methyl nitro, or amino. These derivatives have a common π structure from the hexagonal carbon ring, but they have distinct properties, such as permanent dipole moments and different electron affinities from the functional groups. The most widely recognized influence of organic chemical functional groups on organic chemical–CNT interactions is on the electron donor–acceptor (EDA) π – π interaction. Electron-donating substituent on an aromatic ring can strengthen the π – π interaction between organic compounds and CNTs. The graphene surfaces on CNT sidewalls are of high electronic polarizability, and CNTs may act as amphoteric adsorbate π -acceptors to the electron-rich graphene surface area near edged and π -donors to the central regions being relatively electron poor. The substituents on benzene ring provide different inductive and resonance effects. Benzene is a weak charge donor, and the donor strength can be increased with the substitutes of hydroxyl group, methyl group, and amino group on benzene ring. Pan et al. report that the K/K_{HW} values of endocrine disrupting chemical (EDCs) 17a-ethinyl estradiol (EE2) and bisphenol A (BPA) on MWCNT were six order of magnitude higher than PAHs (phenanthrene and pyrene) due to the presence of hydroxyl groups (π -electron donors) on EDCs, although the number of benzene ring of EE2 and BPA was lower than that of PAHs. Both Wang and Chen observed that the K_d of naphthalene (ca. 6000 L/Kg) was about three times lower than 1-naphthalol at a similar equilibrium concentration, confirming the importance of -OH substitution on the interaction of aromatics and CNTs. Amino group (-NH₂) is a strong electron-donating group (stronger than -OH), the unshared pair of electrons of nitrogen can result in strong electron conjugation with π -electron in the benzene rings, making the benzene rings electron rich. As a result, the adsorption affinity of 1-naphthylamine on CNTs is significantly higher than those of 1-naphthalol and naphthalene. Both

chlorine atoms and nitro group exhibit strong electron-withdrawing ability and cause the chloro- or nitro-substituted benzene rings to be electron depleted and hence function as π -electron acceptors, which interact strongly with the π -electron rich sites (π -electron donors) of the graphene surface of CNTs. Therefore, the adsorptions of nitroaromatic and chloroaromatic compounds are much stronger than those of benzene and toluene. Generally, the relative electron-donating trends of the alternative groups decrease with the order of $\text{NH}_2 > \text{OH} > \text{OCH}_3 > \text{Cl} > \text{NO}_2$. As a result, $-\text{NO}_2$, $-\text{Cl}$, or $-\text{CH}_3$ groups on benzene, phenol, or aniline will enhance their adsorption on CNTs and follow the order nitro group > chloride group > methyl group.

The number of groups could significantly influence the adsorption, showing that the substitution with more groups has the higher adsorption affinity. For example, adsorption affinity of chlorobenzenes on CNTs increases with the chlorine atom in benzene ring, and follows the order 1,2,4,5-tetrachlorobenzene > 1,2,4-trichlorobenzene > 1,2-dichlorobenzene > chlorobenzene. For chlorophenols, the adsorption ability of 2,4-dichlorophenol is much higher than that of 2-chlorophenol and 4-chlorophenol. The position of groups on phenol and aniline can also influence the adsorption; however, adsorption effects from group position are weaker than those from the group types. The group position effects on adsorption cannot be interpreted directly by the group position.

Besides hydrophobic interactions and EDA π - π interaction, hydrogen bonds and electrostatic interactions are also important mechanism for the adsorption of organic compounds on CNTs. The contribution of hydrogen bonding to aromatic chemical adsorption on CNTs is generally considered to be negligible by most researchers. However, Yang et al. developed a linear quantitative relationship combining Polanyi theory-based Dubinin–Astakhov (DA) model parameters with solute solvatochromic parameters to evaluate the adsorptive behaviors of nondissociated phenol and aniline substituents on CNTs. They proposed that H-bonding interactions played an important role on the adsorption of phenols and anilines by CNTs, where the solutes might act as hydrogen-bonding donors and the CNTs acted as the hydrogen-bonding acceptors. The π -electron polarizability might also be important for phenol or aniline adsorption, but its effects were weaker than that of hydrogen-bonding donor ability. Chen suggested that Lewis acid-base interaction was likely an extra important mechanism contributing to the stronger adsorption of 1-naphthylamine than 2-naphthol

to CNTs. Liu et al. found that cation organic dye AO showed much higher affinity to MWCNT than the other azo-containing dyes OG and PAN. The authors concluded that electrostatic attraction was likely to play the dominant role in the noncovalent interaction between dyes and MWCNT in aqueous environment.

4.1.1.3 Effect of surface chemical property of CNTs

Surface property of CNTs can affect the adsorption of aromatic-containing compounds. Researchers suggest that the presence of oxygen and hydrogen within the surface groups crucially affect the adsorptive properties of the adsorbent. Oxygen-containing functional groups can act as electron-withdrawing groups and localize the π -electron system of CNTs, lowering the dispersive force with π -electron of adsorbate. Additionally, the introduction of the oxygen-containing function groups is favorable for water molecules adsorption by means of hydrogen bonding, which can hinder the target molecules accessing to the surface of CNTs, and is unfavorable for the adsorption of organic analytes. Finally, the carboxylic, hydroxyl groups on CNTs surface can be ionized at high solution pH, thus make CNTs negatively charged and provide electrostatic repulsion to ionizable organic adsorbate such as phenol and its derivatives. Decreased adsorption capacity of xylene, resorcinol, pentachlorophenol, and aniline had been observed on the surface-functionalized CNTs. Cho et al. reported that a 10% increase in oxygen concentration led to a 71% decrease in maximum sorption capacity of naphthalene. The authors described the relationship between the increasing oxygen concentration on MWCNT and decreasing adsorption capacity of naphthalene using an equation: $q_{ad,max} = 118 - 6.6(\%)O$. They deduced that each additional percentage of surface oxides could lead to 5.9% sorption capacity reduction of naphthalene. They further predicted based on this equation that no naphtnalene sorption would be obtained with >18% surface oxygen on MWCNT.

However, reverse effect of oxygen-containing groups on aromatic compounds adsorption by CNTs was also reported. In the study by Gotovac et al., the adsorption capacities of phenanthrene and tetracene on SWCNT were found to increase by 5–6 times after SWCNT was treated with nitric acid. They suggested that π – π -interacted phenanthrene or tetracene molecules on the SWCNT surface could be stabilized with the additional interaction with the carboxylic groups. Some researchers propose that the negatively charged

-COO- group is a strong electron donor, and can enhance the $\pi-\pi$ EDA interactions of π -electron acceptors. In Chen and Zhu's study, they observed that increase in solution pH did not affect adsorption of naphthalene but enhanced the adsorption of 1,3-dinitrobenzene and trinitrobenzene by 2–3 times. Lu et al. found that the adsorption capacity of BTEX on CNTs enhanced with the increase in the density of surface carboxylic groups. The authors supposed that the $\pi-\pi$ EDA mechanism involving the carboxylic oxygen atom of CNT surface as the electron donor and the aromatic ring of BTEX as the electron acceptor was responsible for the uptake of BTEX by CNTs.

4.1.1.4 Effect of molecular configuration of adsorbate and property of CNTs

Molecular configuration determines the availability of different adsorption sites on CNTs. The effect of molecular configuration on the adsorption affinity of aromatic compounds to CNTs has been discussed by some researchers. The favorable adsorption states of phenanthrene (PNT) and planar tetracene molecules on SWCNT have been attributed to the so-called "bridge positions" (i.e., the PAH molecules aligned along the nanotube axis under an intensive $\pi-\pi$ interaction between PAH and SWCNT surface). As the PNT and tetracene molecules are rigid, the longitudinally parallel external surface and interstitial channels of the SWCNT can provide more accessible adsorption sites for PNT or tetracene than the short, entangled MWCNT. Therefore, SWCNT show significantly higher adsorption capacities and site energies for planar compounds than the MWCNT. Whereas, for nonplanar BP and 2PP, the molecular configurations can be adjusted to better pack in the tubular spaces of MWCNT with diameter several times larger than their widths, hence smaller adsorption capacity and site energy difference for BP and 2PP between SWCNT and MWCNT was observed. Liu et al. have observed the structure-dependent interaction between organic dyes and CNTs. They found that molecular morphology was the dominant factor for the attachment of dyes on MWCNT. The molecules with large planar aromatic polynuclear structure (such as AO, AR, AN, and RB) were strongly adsorbed onto CNT sidewalls, because the planar molecules were easy to approach MWCNTs via a face-to-face conformation, which was favorite for $\pi-\pi$ interaction between the conjugated aromatic chromophore skeleton and nanotubes. On the contrary, the nonplanar molecules were kept apart from MWCNT due to the spatial restriction, resulting in low $\pi-\pi$ interaction with MWCNT.

4.1.1.5 Effect of aqueous solution chemistry

The apparent pH influence on organic chemical adsorption depends on how the increase in attractive forces (e.g., EDA) counteracts the increase of repulsive forces (e.g., charge repulsion) and/or the decline of certain attractive interactions (e.g., H-bond formation and hydrophobic interaction). Valuable data may also be derived by comparing solution pH, the pKa of the organic chemical, and the pH_{pzc} (point of zero charge) of CNTs. Low adsorption would be expected at pH greater than pKa and pH_{pzc} because both adsorbent and adsorbate are negatively charged and electrostatic repulsion may be one of the dominant mechanisms. On the other hand, the organic chemical would show high adsorption under conditions with pH_{pzc} > pH > pKa because of their electrostatic attraction with CNTs.

In environmental samples, organic contaminants are present together with a complex suit of natural organic matter (NOM), heavy metals, alkali and alkaline cations and anions. The coexisting solutes can be adsorbed/complexed to the surface of CNTs and thus impact adsorption of organic contaminants. Therefore, a single-solute system may not adequately represent the majority of mixed contaminant systems commonly encountered in the environment. Adsorption of mixed pollutants (including metals and organic chemicals) has not been widely investigated, and several works involve only in the competitive adsorption between metal or between organic contaminants on CNTs. The inhibition effects of coexisting metal cations to organic chemicals adsorption on CNTs have been observed. Chen et al. reported that adsorption of 2,4,6-trichlorophenol (TCP) by oxidized MWCNT decreased markedly when 6.5 (15%) or 65 (30%) mg/L of Cu(II) coexisted in solution; whereas, TCP adsorption on as-grown MWCNT was slightly suppressed with the presence of Cu(II). Yang investigated the competitive sorption of pyrene, phenanthrene, and naphthalene on MWCNT. The author found that the observed competitive sorption depended on the relative equilibrium concentrations of both primary solutes and cosolutes. Significant competition was observed at relatively low concentrations of primary solute and high concentrations of competitors, while competition was much weaker in the case of relatively high concentrations of primary solute and low competitor concentrations. When the relative concentration of primary solute (C_e/C_s , C_e the equilibrium aqueous concentration; C_s the water solubility) approached 1, competition by other solutes seemed to disappear.

The effect of NOM such as humic acid (HA) on organic chemical adsorption on CNTs is rather complex. Chen observed that the presence of HA at 50 mg/L moderately reduced adsorption of NPHA, DNB, and TNB (K_d lowered by 29–35%, 35–44%, and 47–57% for NPAH, DNB, and TNB, respectively). Wang et al. reported that the adsorption of Phen and 1-Naph was remarkably decreased with low level of HA concentrations; the adsorption was less affected with increasing HA concentrations. They ascribed this un conspicuous suppression effect of HA to the possible dispersion of CNTs induced by the sorbed HA molecules thus creating new sites for organic chemical sorption. The HA-suppressed adsorption of organic compounds to CNTs is likely based on two major mechanisms: competitive adsorption and pore blockage. In addition, NOM themselves can adsorb organic chemicals with high hydrophobicity such as PAH and PCB. The presence of NOM will enhance the solubility of organic chemicals and decrease their adsorption on CNTs. Therefore, HA shows higher competition with Phen on CNTs than 1-Naph. Generally, the improvement or suppression effect of NOM on organic chemicals adsorption on CNTs depends on the balance of these two opposite factors.

4.1.2 Adsorption of Aromatic Chemicals by CNTs in Comparison With Activated Carbon

The experimental isotherms of analytes on CNTs have been described with different adsorption models such as Langmuir, Freundlich, and Polanyi–Manes models (Table 4.1). Their adsorption on CNTs generally fits well with the Freundlich model and the Polanyi–Manes model (PMM). The Freundlich isotherm model is an empirical relationship describing the adsorption of solutes from a liquid to a solid surface, and assumes that different sites with several adsorption energies are involved. The PMM theory is developed to describe the physical adsorption to microporous adsorbents and involved a pore-filling mechanism and the concept of a variable adsorption potential in response to pore filling. This theory has been used to describe the adsorption isotherms of organic chemicals by ACs and charcoal. It is also applicable to examine the adsorption behavior of organic chemicals on CNTs by PMM mode as the bundles of CNTs formed in aqueous media and the spaces between the tubes within the bundles can be regarded as pores. Furthermore, PMM theory is suitable for either pore filling or flat surface adsorption.

Table 4.1 Adsorption models used to fit the experimental isotherms of analytes on CNTs

Name	Abbrev.	Equation	Capacity term
Freundlich model	FM	$q_e = K_f C_e^{1/n}$	q_e [mg/g], equilibrium sorbed concentration; C_e [mg/L], equilibrium solution phase concentration; Q^0 [mg/g], sorbed capacity; C_s [mg/L], aqueous water solubility; K_f [(mg/g)/(mg/L) $^{1/n}$], Freundlich affinity coefficient; $1/n$, Freundlich exponential coefficient; K_d [mg/L], affinity coefficient; K_p [L/g], partition coefficient
Langmuir model	LM	$q_e = \frac{Q_0 C_e}{K_d + C_e}$	Q^0_1 [mg/g] and Q^0_2 [mg/g], sorbed capacity of site populations 1 and 2, respectively;
Dual-model Model	DMM	$q_e = K_p C_e + \frac{Q_0 C_e}{K_d + C_e}$	K_{d1} [mg/L] and K_{d2} [mg/L], affinity coefficient of site populations 1 and 2, respectively;
Dual-Langmuir Model	DLM	$q_e = \frac{Q^0_1 C_e}{K_{d1} + C_e} + \frac{Q^0_2 C_e}{K_{d2} + C_e}$	ε_{sw} [kJ/mol], effective adsorption potential; V_s [cm 3 /mol], molar volume of solute; E [kJ/mol], the “correlating divisor”; α [(cm 3) $^{b+1}$ /(Kg Jb)] and b , fitting parameters; R [8.314E-3 kJ/mol K], universal gas constant; T [K], absolute temperature
Polanyi–Manes Model	PMM	$\log q_e = \log Q^0 + \alpha(\frac{\varepsilon_{sw}}{V_s})^b$ $\varepsilon_{sw} = RT \ln(C_s / C_e)$	
Dubinin–Ashtakhov Model	DA	$\log q_e = \log Q^0 - (\varepsilon/E)^b$ $\varepsilon = RT \ln(C_s / C_e)$	

The thermodynamic study shows that the adsorption of aromatic chemicals on CNTs is mainly a physisorption process, and the interaction between adsorbate and CNTs is exothermic. Hence, increased adsorption capacity of aniline, atrazine, and PCP on as-prepared CNTs is observed as the temperature decreases. On oxidized CNTs, the standard enthalpy change is reported to be positive by some researchers, implying that the adsorption is endothermic. Accordingly, decreased adsorption of aniline, atrazine, and PCP on oxidized CNTs is reported.

Adsorption heterogeneity and hysteresis are two widely recognized features of organic chemical–CNT interactions. The hysteresis might be caused by the strong π – π coupling of benzene-ring-containing chemicals with the CNT surface and capillary condensation, and alteration of adsorbent structure or reorganization after adsorption. Adsorption/desorption hysteresis is observed for small molecules (such as organic vapors of methane, ethylene, and benzene). However, a lack of hysteresis is reported for butane, PAHs, and atrazine. Different hysteresis phenomena result in different opinions on CNT-related risk. For example, high adsorption capacity and reversible desorption of organic chemicals on CNTs imply the potential release of organic chemicals after intake by animals or human. In this case, CNTs act like pollutant collectors and thus pose high health risk. However, significant adsorption/desorption hysteresis can make CNTs pollutant sinks. This would result in decreased organic chemical mobility, bioavailability, and environmental risk. Therefore, proper understanding of hysteresis mechanisms is a key step toward assessing CNT-led risk and application.

The adsorptions of some selected aromatic compounds on CNTs are listed in Tables 4.2–4.4. Comparison of various commercial carbonaceous materials for the adsorption of these compounds is shown in Table 4.5. For some selected organic chemicals, ACs show higher capacity than CNTs, however, if the uptake of adsorbates per unit surface area instead of per gram is compared, the removal capacity of CNTs is 3–5 times higher than ACs. Moreover, the adsorption coefficients of organic chemicals on CNTs are usually higher than on ACs. As the adsorption by ACs is dependent on the porous structure, it takes time for adsorbates to diffuse through pores; while the adsorption on CNTs is almost 20–300 times quicker than on ACs, suggesting the high adsorption efficiency of CNTs in unit time and significant potential in removal of organic contaminants from water. Compared with ACs, CNTs can be regenerated much easier and more efficiently by desorbing adsorbates using acid, alkaline solution, organic solvent, or heat treatment.

Table 4.2 Adsorption of phenol and phenol derivates on CNTs

Adsorbate	Adsorbent	Property of adsorbents						K_d (L/g)	Q (mg/g)	Source
		OD	ID	SSA	V_{meso}	V_{micro}	O %			
2,4,6-TCP	MWCNT8	<8	2.0-5	559	1.69	0.085			$10^{2.26}$ (PMM)	Chen, 2009
	MWCNT15A	10-15	5-8	279	0.57	0.026	3.92	15.24 (30 mg/L) 2.25 (100 mg/L)	$10^{1.88}$ (PMM)	
	MWCNT15	10-15	5-8	181	0.41	0.016	1.52	10.37 (30 mg/L) 1.15 (100 mg/L)	$10^{1.75}$ (PMM)	
	MWCNT20	10-20	5-10	167	0.55	0.016			$10^{1.6}$ (PMM)	
	MWCNT30	30-50	5-15	91	0.3				$10^{1.93}$ (PMM)	
	MWCNT50	>50	5-15	68	0.16				$10^{1.97}$ (PMM)	
o-CP	p-MWCNT		10.3	157	0.401				73.5 (LM)	Liao, 2008
	MWCNT (NH ₃)		9.2	195	0.419				110.3 (LM)	
2-CP	MWCNT15	8-15	3-5	174	0.597	0.068			$10^{2.02}$ (DA)	Yang, 2008
4-CP	MWCNT15	8-15	3-5	174	0.597	0.068			$10^{1.88}$ (DA)	
2,4-DCP	MWCNT15	8-15	3-5	174	0.597	0.068		3.20 (200 mg/L) 0.088 (2000 mg/L)	$10^{2.14}$ (DA)	

Table 4.2 continued

Adsorbate	Adsorbent	Property of adsorbents						K_d (L/g)	Q (mg/g)	Source
		OD	ID	SSA	V_{meso}	V_{micro}	O %			
PCP	MWCNT (KMnO ₄)			106					26.2 (FM) 8.18 (LM)	Salam, 2008
	MWCNT (HNO ₃)			140					4.58 (FM) 5.06 (LM)	
	MWCNT (H2O2)			144					4.13 (FM) 4.75 (LM)	
phenol	MWCNT15	8-15	3-5	174	0.597	0.068			10 ^{1.81} (DA)	Yang, 2008
phenol	MWCNT	15-65		72	0.41	0.008			17.24 (FM) 15.88 (LM)	Liao, 2008
phenol	MWCNT10	9.4		357	0.951	0.142	1.1	788 (0.1mM) 154 (2.0mM)	224 (FM)	Lin, 2008
	MWCNT100	70.1		58	0.114	0.023	2	123 (0.1mM) 25.2 (2.0mM)	36.4 (FM)	
catechol	MWCNT10	9.4		357	0.951	0.142	1.1	3200 (0.1mM) 308 (2.0mM)	530 (FM)	
	MWCNT100	70.1		58	0.114	0.023	2	511 (0.1mM) 52.6 (2.0mM)	89.1 (FM)	

Table 4.2 continued

Adsorbate	Adsorbent	Property of adsorbents						K_d (L/g)	Q (mg/g)	Source
		OD	ID	SSA	V_{meso}	V_{micro}	O %			
catechol	MWCNT	15-65		72	0.41	0.008			16.49 (FM) 14.2 (LM)	Liao, 2008
pyrogallol	MWCNT10	9.4		357	0.951	0.142	1.1	11500 (0.1mM) 2090 (2.0mM)	3100 (FM)	Lin, 2008
	MWCNT100	70.1		58	0.114	0.023	2	3850 (0.1mM) 801 (2.0mM)	1150 (FM)	
pyrogallol	MWCNT	15-65		72	0.41	0.008			38.71 (FM) 33.61 (LM)	Liao, 2008
2-PP	MWCNT10	9.4		357	0.951	0.142	1.1	4370 (0.1mM) 512 (2.0mM)	841 (LM)	Liao, 2008
	MWCNT100	70.1		58	0.114	0.023	2	931 (0.1mM) 70.6 (2.0mM)	128 (LM)	
1-naphthol	MWCNT10	9.4		357	0.951	0.142	1.1	20300 (0.1mM) 1960 (2.0mM)	3370 (LM)	
	MWCNT100	70.1		58	0.114	0.023	2	3220 (0.1mM) 349 (2.0mM)	584 (LM)	
cyclohexanol	MWCNT10	9.4		357	0.951	0.142	1.1	122 (0.1mM) 45 (2.0mM)	57 (LM)	
	MWCNT100	70.1		58	0.114	0.023	2	25.2 (0.1mM) 11.2 (2.0mM)	13.5 (LM)	

Table 4.2 continued

Adsorbate	Adsorbent	Property of adsorbents						K_d (L/g)	Q (mg/g)	Source
		OD	ID	SSA	V_{meso}	V_{micro}	O %			
2-PP	SWCNT	1-2		486		0.031	3.66		71 (FM)	Zhang, 2009
	SWCNT-OH	1-2		420		0.023	5.41		56 (FM)	
	SWCNT-COOH	1-2		386		0.023	4.46		62 (FM)	
	MWCNT	8-15	3-5	164		0.06	1.53		22 (FM)	
	MWCNT-OH	8-15	3-5	192		0.07	6.39		16 (FM)	
	MWCNT-COOH	8-15	3-5	134		0.05	6.71		16 (FM)	
2-NP	MWCNT15	8-15	3-5	174	0.597	0.068			10^2 (DA)	Yang, 2008
3-NP	MWCNT15	8-15	3-5	174	0.597	0.068			$10^{1.9}$ (DA)	
4-NP	MWCNT15	8	3-5	174	0.597	0.068			$10^{1.8}$ (DA)	
4-MP	MWCNT15	8	3-5	174	0.597	0.068			$10^{1.84}$ (DA)	Yang, 2008
BPA	SWCNT	1-2	0.8-1.6	541	0.82	0.201		$10^{4.69}$	455 (LM) 591 (PMM)	Pan, 2008
	MWCNT15	8-15	3-5	174	0.597	0.0677		$10^{4.11}$	102 (LM) 121 (PMM)	

Table 4.2 continued

Adsorbate	Adsorbent	Property of adsorbents						K_d (L/g)	Q (mg/g)	Source
		OD	ID	SSA	V_{meso}	V_{micro}	O %			
BPA	MWCNT30	20-30	5-10	107	0.278	0.0391		$10^{3.92}$	61.6 (LM) 77 (PMM)	Pan, 2008
	MWCNT50	30-50	5-15	94.7	0.217	0.0364		$10^{3.90}$	73.9 (LM) 103 (PMM)	
EE2	SWCNT	1-2	0.8-1.6	541	0.82	0.201		$10^{6.30}$	276 (LM)	
	MWCNT15	8-15	3-5	174	0.597	0.0677		$10^{5.82}$	119 (LM) 133 (PMM)	
	MWCNT30	20-30	5-10	107	0.278	0.0391		$10^{5.66}$ (0.01Cs)	81.5 (LM) 89.5 (PMM)	
	MWCNT50	30-50	5-15	94.7	0.217	0.0364		$10^{5.53}$ (0.01Cs)	74.1 (LM) 78.4 (PMM)	

OD, outer diameter (nm); ID, inner diameter (nm); SSA, specific surface area (m^2/g); V_{meso} , mesopore volume (cm^3/g); V_{micro} , micropore volume (cm^3/g); O (%), oxygen atom content on CNTs surface; K_d , distribution coefficient at a given equilibrium concentration; PCP, pentachlorophenol; 2,4,6-TCP, 2,4,6-trichlorophenol; 2,4-DCP, 2,4-dichlorophenol; 4-CP, 4-chlorophenol; 2-CP, 2-chlorophenol; o-CP, ortho-chlorophenol; 2-NP, 2-nitrophenol; 3-NP, 3-nitrophenol; 4-NP, 4-nitrophenol; 4-MP, 4-methylphenol; BPA, bisphenol A; EE2, 17 α -ethinyl estradiol; 2-PP, 2-phenylphenol.

Table 4.3 Adsorption of nonionic organic chemicals on CNTs

Adsorbate	Adsorbent	Property of adsorbents						<i>Q</i> (mg/g)	Source
		OD	ID	SSA	<i>V</i> _{meso}	<i>V</i> _{micro}	O %		
Naph	MWCNT	15±5	7±2	283			3.3	36.1 (FM)	Cho, 2008
	MWCNT-O (HNO ₃)						6	21.4 (FM)	
							7.4	20.8 (FM)	
							8.9	14.7 (FM)	
							10.9	16.3 (FM)	
							12.2	11.3 (FM)	
							13.1	11.8 (FM)	
Naph	MWCNT-O (KMnO ₄)						13.5	9.4 (FM)	Yang. 2006
	MWCNT-O (H ₂ O ₂)						14	14.6 (FM)	
Naph	MWCNT15	8-15	3-5	174	0.597	0.0677		10 1.11 (FM); 395.3 (LM) 10 1.87 (PMM)	Yang. 2006
Naph	SWCNT			370			17.2	1420 (FM) in 0.02 M NaNO ₃ solution 1330 (FM) in 50 mg/L Cu ²⁺ solution 1220 (FM) in 50 mg/L HA solution	Chen. 2008

Table 4.3 continued

Adsorbate	Adsorbent	Property of adsorbents						Q (mg/g)	Source
		OD	ID	SSA	V_{meso}	V_{micro}	O %		
Phen	SWCNT	1-2	0.8-1.6	541	0.82	0.201		$10^{2.52}$ (FM); 40000 (LM); $10^{2.42}$ (PMM)	Yang, 2006
	MWCNT8	<8	2-5	348	0.689	0.127		$10^{2.07}$ (FM); 4673 (LM); $10^{1.94}$ (PMM)	
Phen	MWCNT15	8-15	3-5	174	0.597	0.0677		$10^{1.94}$ (FM); 6098 (LM) $10^{1.62}$ (PMM)	Yang, 2006
	MWCNT30	20-30	5-10	107	0.278	0.0391		$10^{1.68}$ (FM); 4065 (LM) $10^{1.43}$ (PMM)	
	MWCNT50	30-50	5-15	94.7	0.217	0.0364		$10^{1.68}$ (FM); 1773 (LM) $10^{1.37}$ (PMM)	
Phen	SWCNT	1-2		486		0.031	3.66	285 (FM)	Zhang, 2009
	SWCNT-OH	1-2		420		0.023	5.41	238 (FM)	
	SWCNT-COOH	1-2		386		0.023	4.46	206 (FM)	
	MWCNT	8-15	3-5	164		0.06	1.53	58 (FM)	
	MWCNT-OH	8-15	3-5	192		0.07	6.39	48 (FM)	
	MWCNT-COOH	8-15	3-5	134		0.05	6.71	39 (FM)	
pyrene	MWCNT15	8-15	3-5	174	0.597	0.0677		$10^{2.37}$ (FM); 9709 (LM) $10^{1.63}$ (PMM)	Yang, 2006

Table 4.3 continued

Adsorbate	Adsorbent	Property of adsorbents					<i>Q</i> (mg/g)	Source
		OD	ID	SSA	<i>V</i> _{meso}	<i>V</i> _{micro}	O %	
1,3-DNB	SWCNT			370			17.2	Chen, 2008
1,3,5-TNB	SWCNT			370			17.2	
BP	SWCNT	1-2		486		0.031	3.66	Zhang, 2009
	SWCNT-OH	1-2		420		0.023	5.41	
	SWCNT-COOH	1-2		386		0.023	4.46	
	MWCNT	8-15	3-5	164		0.06	1.53	
Phen	MWCNT-OH	8-15	3-5	192		0.07	6.39	Chin, 2007
	MWCNT-COOH	8-15	3-5	134		0.05	6.71	
o-xylene	SWCNTs	1.2-1.5		248		0.05	68.493 (LM)	Chin, 2007
	P-SWCNT			284		0.092	59.527 (LM)	
p-xylene	SWCNTs	1.2-1.5		247.6		0.05	77.519 (LM)	
	P-SWCNT			284		0.092	85.47 (LM)	

OD, outer diameter (nm); ID, inner diameter (nm); SSA, specific surface area (m^2/g); V_{meso} mesopore volume (cm^3/g); V_{micro} micropore volume (cm^3/g); O (%), oxygen atom content on CNTs surface; Phen, phenanthrene; Naph, naphthalene; BP, biphenyl; 1,3,5-TNB, 1,3,5-trinitrobenzene; 1,3-DNB, 1,3-dinitrobenzene.

Table 4.4 Adsorption of aniline and some herbicides CNTs

Adsorbate	Adsorbent	Property of adsorbents						Q (mg/g)	Model used	Source
		OD	ID	SSA	V_{meso}	V_{micro}	O%			
aniline	MWCNT	30						9.82 (25°C) 9.25 (50°C) 7.56 (75°C)	LM	Xie, 2007
								1.93 (25°C) 1.04 (50°C) 0.741 (75°C)	FM	
	MWNCT-O citric acid							15 (25°C) 60 (50°C) 94.9 (75°C)	LM	
								0.825 (25°C) 0.913 (50°C) 1.60 (75°C)	FM	
	MWNCT-O nitric acid							17.1 (25°C) 19.6 (50°C) 29.1 (75°C)	LM	
								1.57 (25°C) 1.67 (50°C) 1.78 (75°C)	FM	

Table 4.4 continued

Adsorbate	Adsorbent	Property of adsorbents						Q (mg/g)	Model used	Source
		OD	ID	SSA	V_{meso}	V_{micro}	0%			
aniline	MWNCT-O KMnO ₄							46.7 (25°C) 50.3 (50°C) 34.76 (75°C)	LM	Xie, 2007
	MWCNT	30						0.844 (25°C) 0.549 (50°C) 0.417 (75°C)	FM	
aniline	MWCNT15	8-15	3-5	174	0.597	0.068		$10^{2.06}$	DA	Yang, 2008
4-chloroaniline	MWCNT15	8-15	3-5	174	0.597	0.068		$10^{2.00}$	DA	
2-nitroaniline	MWCNT15	8-15	3-5	174	0.597	0.068		$10^{1.79}$	DA	
3-nitroaniline	MWCNT15	8-15	3-5	174	0.597	0.068		$10^{1.71}$	DA	
4-nitroaniline	MWCNT15	8-15	3-5	174	0.597	0.068		$10^{1.71}$	DA	
atrazine	MWCNT8	<8	2-5	559	1.69	0.085		110.9 (FM) 170.6 (LM) $10^{1.98}$ (PMM)		Chen, 2008
	MWCNT30	30-50	5-15	91	0.3	nd		11.14 (FM) 41.97 (LM) $10^{1.48}$ (PMM)		

Table 4.4 continued

Adsorbate	Adsorbent	Property of adsorbents						Q (mg/g)	Model used	Source
		OD	ID	SSA	V_{meso}	V_{micro}	0%			
atrazine	MWCNT50	>50	5-15	68	0.16	nd		8.43 (FM) 37.21 (LM) $10^{1.44}$ (PMM)		Chen, 2008
	MWCNT-O	10-20	5-10	167	0.619	0.016	0.85	14.89 (FM) 47.63 (LM) $10^{1.59}$ (PMM)		
	MWCNT-O	10-20	5-10	178	0.629	0.015	2.16	15.89 (FM) 36.05 (LM) $10^{1.55}$ (PMM)		
	MWCNT-O	10-20	5-10	185	0.756	0.024	7.07	7.30 (FM) 20.12 (LM) $10^{1.30}$ (PMM)		
atrazine	SWCNT20	10-20		167	0.417			17.25 (18°C) 16.21 (25°C) 12.83 (30°C)	FM	Yan, 2008
								33.43 (18°C) 31.37 (25°C) 28.21 (30°C)	LM	
								$10^{1.46}$ (18°C) $10^{1.39}$ (25°C) $10^{1.32}$ (30°C)	PMM	

Table 4.4 continued

Adsorbate	Adsorbent	Property of adsorbents						Q (mg/g)	Model used	Source
		OD	ID	SSA	V_{meso}	V_{micro}	O%			
	r-MWCNT	20-40		300	0.794			57.81 (18°C)	FM	
								52.53 (25°C) 53.2 (30°C)		
atrazine	r-MWCNT	20-40		300	0.794			110.8 (18°C) 100.43 (25°C) 97.05 (30°C)	LM	Yan, 2008
								10 ^{1.99} (18°C) 10 ^{1.97} (25°C) 10 ^{1.91} (30°C)		
atrazine	MWCNT-O	10-20	5-10	167	0.619	0.016	0.85	61.1	PMM	Chen, 2009
	MWCNT-O	10-20	5-10	178	0.629	0.015	2.16	36.6	FM	
	MWCNT-O	10-20	5-10	185	0.756	0.024	7.07	25.6	LM	
2,4,5-T	MWCNT	10-30		40-600				0.49 (pH1) 0.47 (pH3) 0.48 pH7	FM	Pyrzynska, 2007
dicamba	MWCNT	10-30		40-600				0.48 (pH1) 0.48 (pH3) 0.37 (pH7)		

OD, outer diameter (nm); ID, inner diameter (nm); SSA, specific surface area (m^2/g); V_{meso} mesopore volume (cm^3/g); V_{micro} micropore volume (cm^3/g); O (%), oxygen atom content on CNTs surface; 2,4,5-T, 2,4,5-trichlorophenoxyacetic acid.

Table 4.5 Adsorption of selected organic chemicals on different adsorbents

Adsorbate	Adsorbent	Property of adsorbents			Q (mg/g)	Model used	Source
		OD	ID	SSA			
o-CP	GAC	0.7-1.7 (mm)	3.6	1000	134.9	LM	Aktaş, 2007
	PAC	7-75 (mm)	4.4	1400	140.8	LM	
BPA	fullerene	~10	~0.35	7.21	0.108 0.984	LM PMM	Pan, 2008
EE2	fullerene	~10	~0.35	7.21	0.287 0.228	LM PMM	
Naph	natural char			46	7.4	FM	Cho, 2008
	AC			1004	212.8	FM	
Naph	graphite			4.5	50 in 0.02 M NaNO ₃ solution 15 in 50mg/L HA solution	FM	Chen, 2008

Table 4.5 continued

Adsorbate	Adsorbent	Property of adsorbents			Q (mg/g)	Model used	Source
		OD	ID	SSA			
Phen	fullerene	~10	~0.35	7.21	$10^{-1.24}$	FM	Yang, 2008
					0.62	LM	
					$10^{-1.17}$	PMM	
1,3-DNB	graphite			4.5	64 in 0.02 M NaNO_3 solution 1 in 50mg/L HA solution	FM	Chen, 2008
1,3,5-TNB	graphite			4.5	90 in 0.02 M NaNO_3 solution 1 in 50mg/L HA solution	FM	Chen, 2008
2,4,5-T	GCB			100	0.49 (pH1) 0.20 (pH3) 0.19 (pH7)	FM	Pyrzynska, 2007
	C ₁₈				0.14 (pH3) 0.19 (pH7)		
dicamba	GCB			100	0.49 (pH1) 0.19 (pH3) 0.17 (pH7)		
	C ₁₈				0.07 (pH3) 0.14 (pH7)		

Table 4.5 continued

Adsorbate	Adsorbent	Property of adsorbents			Q (mg/g)	Model used	Source
		OD	ID	SSA			
phenol	GAC			1100	350	LM	Sulaymon and Ahmed, 2008
	APET			1200-1500	262	LM	Laszlo 2005
	G-BAC			1170	235.4	LM	Kim 2006
	CCM200			647	140	LM	Kim 2006
aniline	APET			1200-1500	283.6	LM	Laszlo 2005
4-CP	GAC			1100	319.9	LM	Sulaymon and Ahmed, 2008
resorcinol	GAC			579	34.83 142.82	FM LM	Kumar 2003
catechol	GAC			579	42.4 143.47	FM LM	

OD, outer diameter (nm); ID, inner diameter (nm); SSA, specific surface area (m^2/g); 2,4,5-T, 2,4,5-trichlorophenoxyacetic acid.

GAC, granular activated carbon; PAC, powdered activated carbon; AC, activated carbon; GCB, graphite carbon black; APET, microporous carbons prepared from poly(ethyleneterephthalate) (PET) based activated carbon by chemical (HNO_3) and thermal (700 °C) post-treatment; G-BAC, activated carbon; CCM200, carbon cryogel microspheres.

4.2 ADSORPTION OF VOLATILE ORGANIC COMPOUNDS

Volatile organic compounds (VOCs) have received a great deal of attention in the field of environmental control for a number of reasons. First, VOCs are ubiquitous in the environment, workplace, and consumer products. Humans can, therefore, be easily exposed to VOCs through skin contact, breathing, and eating. Second, VOCs are suspected to have primary and secondary harmful effects due to prolonged exposure. These include eye and throat irritation, liver damage, and damage to the central nervous system. Third, VOCs can form photochemical smog, which contains ozone and other toxic byproducts, by reacting with other atmospheric chemicals such as nitrogen oxides. Moreover, VOCs are emitted by landfill leachate and industrial effluent. Leakage into groundwater can cause serious contamination problems. Therefore, the development of effective treatments to remove these organic chemicals is necessary. Among VOCs, the aromatic compounds, especially benzene, toluene, xylene and dichlorobenzene, are of particular interest. All of the aromatic VOCs are known or suspected to be carcinogenic. Furthermore, these compounds have no safety threshold dose for carcinogenic effects. Thus, even low-level exposure poses a finite risk. In fact, benzene, toluene, and xylenes, known as BTX, are the markers for human exposure to VOCs.

In recent years, CNTs have been proposed as adsorbents for a variety of gases, such as hydrogen, NH_3 , and NO_2 gas by SWCNT, as well as ethanol, *n*-hexane, *n*-nonane, and CCl_4 . A few experimental studies have described adsorption isotherms for toluene, benzene, xylene, dichlorobenzene, methyl ethyl ketone, hexane, cyclohexene, methanol, and methane; adsorption coefficients of trichloroethylene, benzene, *n*-hexane, and acetone; adsorption kinetics of acetylene, ethanol, isopropanol, cyclohexane, benzene, thiophene, and hexane onto a variety of CNTs. The results indicate that the adsorption capacity or affinity of aromatic VOCs are higher than that of alkanes (including linear and cyclic). For example, Agnihotri observed that the adsorption capacities of organic vapor on SWCNT were in the order of toluene > MEK > hexane > cyclohexane. Shih reported that the adsorption coefficients of VOCs on MWCNT decreased in the order benzene = trichloroethylene > *n*-hexane. However, the author also observed that the polar acetone showed much larger adsorption coefficients on

MWCNT than benzene, *n*-hexane, and trichloroethylene. Sone et al. compared the elimination of 23 VOCs by highly crystalline MWCNT (HC-MWCNT) including 1-dichloroethylene, dichloromethane, *trans*-1,2-dichloroethylene, *cis*-1,2-dichloroethylene, chloroform, 1,1,1-trichloroethane, carbon tetrachloride, 1,2-dichloroethane, benzene, trichloroethylene, 1,2-dichloropropane, bromodichloromethane, *cis*-1,3-dichloropropene, toluene, *trans*-1,3-dichloropropene, 1,1,2-trichloroethane, tetrachloroethylene, dibromochloromethane, *m*-xylene, *p*-xylene, *o*-xylene, bromoform, and *p*-dichlorobenzene. The authors found that HC-MWCNT showed high selectivity and high affinity for adsorbing aromatic VOCs, and the affinity of VOCs on HC-MWCNT followed the order of *p*-dichlorobenzene > *o*-xylene > *m,p*-xylene > toluene > benzene > the other aliphatic VOCs.

The adsorption mechanisms of VOCs on CNTs are also discussed by some researchers. Díaz suggested that the dispersive interactions of several VOCs on MWCNT mainly control the adsorption process. Shih suggested that the van der Waals interactions dominated the sorption process between three VOCs (benzene, *n*-hexane, and trichloroethylene) and the surface of MWCNT since the adsorption coefficients of these compounds decreased slightly with a decreasing trend of their molecular weight. However the π - π EDA interaction between VOCs (such as benzene and trichloroethylene) and CNTs also was proposed in the two studies. In fact, the π - π EDA interaction between aromatic VOC and CNTs was so strong that selective adsorption of aromatic VOCs could be achieved by passing the air samples containing 6 aromatic and 17 aliphatic VOCs through a cartridge packed with highly crystalline MWCNT. Sone et al. suggested that HC-MWCNT adsorbed aromatic compounds according to Fukui's frontier theory, which is based on the interactions between the highest occupied molecular orbital (HOMO) and the lowest unoccupied molecular orbital (LUMO) of the aromatic VOCs and those of the HC-MWCNT. The π -electrons can transfer from the HOMO of the HC-MWCNT to the LUMO of the aromatic VOCs. The frontier electrons (HOMO) of the aromatic VOCs repel the π -electrons transferring to the LUMO. Then a compound with a small HOMO-LUMO gap will have a higher affinity toward the HC-MWCNT. Therefore, the authors found that the order of the affinities of the aromatic VOCs for the HC-MWCNT (*p*-dichlorobenzene > *o*-xylene > *m,p*-xylene > toluene > benzene) was identical to the order of the HOMO-LUMO gap values. The adsorption of most VOCs decreases

with the increase of temperature, which is indicative of exothermic physisorption on the surface of CNTs. In the case of the polar acetone, the curvature and topological defect sites are of great importance to the adsorption process of acetone. Several studies have indicated the strong chemisorption of acetone molecules on the surface of CNTs.

Adsorption of VOCs on CNTs can occur in the hollow space inside nanotubes, the interstitial space between nanotubes, and the curved surface of nanotube bundles (Fig. 4.1). A few studies have treated the effect of gas adsorption on the structure of the bundle. Recent calculations predict that gas atoms such as H₂ enter interstitial channels, separating perfect monodisperse nanotubes and slightly dilate the bundle lattice. However, most interstitial channels are inaccessible to the bigger molecules such as Xe, CCl₄, and SF₆. The adsorption kinetics of VOCs molecules and their different adsorption sites on CNTs can be investigated using an ultra-high vacuum surface science temperature ramping technique (thermal desorption spectroscopy, TDS). In the TDS spectra of nonpolar alkanes and CCl₄, three distinct peaks can be discerned, which are assigned to the adsorption on interior, groove, and external adsorption sites. For polar VOCs such as thiophene and alcohols, the distinct CNTs-induced TDS features cannot be observed. But the co-adsorption TDS of alkane-thiophene or alkane-alcohol reveals that the polar molecules can also adsorb on these adsorption sites of CNTs. The simulation and experimental studies indicate that the VOC molecules preferentially adsorb on the most attractive sites of CNTs. The highest binding energy adsorption site corresponds to adsorption inside nanotubes, followed by the groove sites between adjacent nanotubes in bundles, and the weaker binding energy sites are attributed to adsorption on the outer surface. Babaa et al. reported that CCl₄ adsorbed first inside the tubes and in the external grooves, and next on the convex external surface of the bundles. In the case of as-produced CNT, the tubes are generally closed at both ends, CCl₄ adsorbed first in the external grooves and then on the convex external surface of the bundles. Muris et al. reported neutron-diffraction studies of CD4 and D2 adsorbed on SWCNT, which showed that the molecules were first condensed in the grooves, and simultaneously in the interstitial channels forming linear and zigzag chains, and then the less attractive sites on the convex outer surface of the bundles were occupied until the bundles were completely covered by a single quasi-hexagonal monolayer. Agnihotri et al. observed that organic vapors (benzene, hexane, cyclohexane, and MEK) saturated the internal volume of nanotubes at lower values

of relative pressures ($p/p^0 \leq 10^{-2}$, p was the actual vapor pressure and p^0 was the saturation pressure of the organic vapor), and at $p/p^0 > 10^{-2}$ adsorption occurred only on the outer surface of the bundles (i.e., in the void spacing between the bundles).

Owing to the heterogeneity of CNTs adsorption sites, the Freundlich isotherm equation fitted the experimental data more closely than the Langmuir or DR equations. The contributions of these multiple sites to overall adsorption could differ from sample to sample depending on the percentage of open-ended nanotubes in a sample, surface defects, and chemical functional groups. Amorphous carbon can enhance the adsorption capacity of VOCs on CNTs. Hilding and Grulke indicated that amorphous carbon associated with raw CNTs was a strong adsorbent for hydrocarbons. Several studies indicate that CNTs have small interaction potential toward VOCs compared with the activated carbon. However, Crespo and Yang showed that the adsorption capacity of SWCNT for thiophene was larger than that of activated carbons, and Chen et al. reported that oxidized CNTs showed much higher adsorption capacities for nicotine and tar from the mainstream smoke of cigarettes than activated carbon.

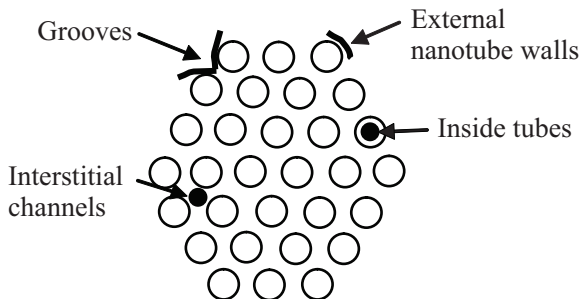


Figure 4.1 The location of the four possible adsorption sites on a bundle of CNTs.

4.3 CONCENTRATION OF ORGANIC CONTAMINANTS AS SOLID-PHASE EXTRACTION ADSORBENTS

Solid-phase extraction (SPE) is a widely used sample preparation technique for the isolation of selected analytes, usually from a mobile phase (gas, fluid or liquid). SPE is initially developed as a

complement or replacement for liquid–liquid extraction (LLE). It is now the most common sampling technique in many areas of chemistry, including environmental, pharmaceutical, clinical, food, and industrial chemistry. In SPE, the analytes to be extracted are partitioned between a solid phase and a liquid phase, and these analytes must have greater affinity for the solid phase than for the sample matrix. The choice of sorbent is therefore a key point in SPE because it can control parameters such as selectivity, affinity and capacity. This choice depends strongly on the analytes of interest and the interactions of the chosen sorbent through the functional groups of the analytes. The unique properties and adsorption behaviors to organic compounds make CNTs as potential adsorbents for preconcentration of organic pollutants from environmental samples, including rapid equilibrium rates, high adsorption capacity, effectiveness over a broad pH range, consistency with BET, Langmuir, or Freundlich isotherms, and lack of adsorption/desorption hysteresis. There are plenty of examples in the literature of the use of CNTs as SPE adsorbents for preconcentrating trace analytes from samples with various matrixes in the format of cartridge/column, SPE disks or solid-phase microextraction (SPME) fibers (Fig. 4.2)

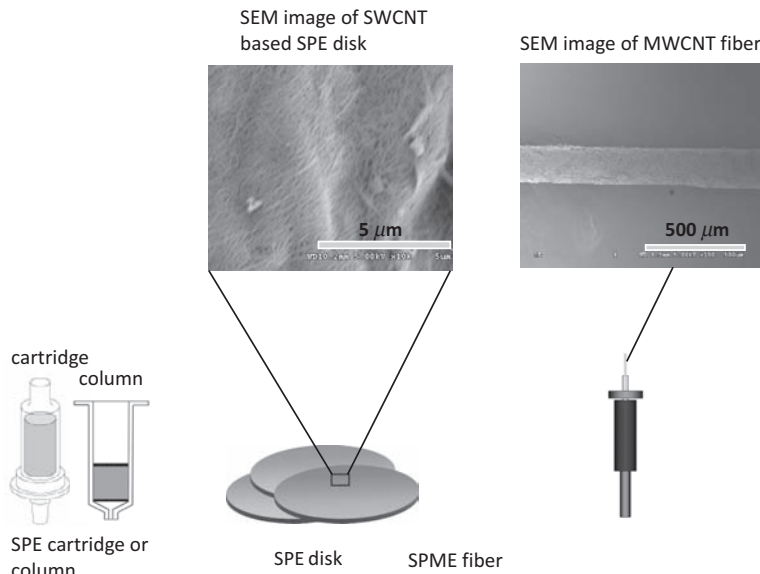


Figure 4.2 CNTs used as solid-phase extraction adsorbents in different formats.

4.3.1 SPE Cartridge or Column

Cartridges or columns are easily prepared in the laboratory and are cheaper and simpler than the disks. Therefore, cartridge is the often used form of SPE in routine applications. By far, most of the studies about application potentials of CNTs to preconcentrate organic contaminants from environmental or biological samples are performed in the cartridges or columns form. In 2003, the initial work was carried out by Cai group to enrich endocrine disruptors (BPA, NP, and OP) from water samples by using MWCNT-packed column. This study and the following works proved that MWCNT could be a potential alternative adsorbent to preconcentrate trace level of analytes with different polarity (such as bisphenol A, 4-*n*-nonylphenol and 4-*tert*-octylphenol, phthalate esters, chlorophenols, antibiotics, and multiphenol compounds). Compared with the commercial *n*-alkylsilica adsorbents, CNTs adsorbents demonstrate high ability in isolating polar molecules with high solubility in water (>1 g/L). These types of solutes are the most difficult to extract because of their low affinity for most reversed-phase sorbents. Compared with other carbonaceous nanomaterials (activated carbon or graphitized carbon blacks), CNTs possess more efficient surface areas and provide more adsorptive sites to analytes; therefore, CNTs show higher extraction efficiency to diverse organic compounds. Additionally, irreversible adsorption is seldom observed on CNTs, which results in the bad reputation of carbon materials (especially activated carbon) for being “difficult to elute.” Similar to the common SPE procedure, the enrichment performance using CNTs cartridges (or column) can be influenced by several experimental conditions such as mass of adsorbent, eluent and its volume, flow rate of sample loading, pH of sample solution, and volume of sample solution.

4.3.1.1 Adsorbent mass

Adsorbent mass can affect the SPE efficiency of CNTs to organic analytes. Enhancing the amount of adsorbent led to an increase in the percentage of the analyte adsorbed, but may decrease the flow rate owing to the increase in bed size. Generally, the mass of CNTs (usually in the range 20–200 mg) is fairly less than other commercial SPE adsorbents to obtain the satisfactory enrichment

efficiency of analytes (Table 4.6). El-Sheikh et al. have compared the enrichment efficiency of MWCNT, C₁₈ silica, and activated carbon toward some pesticides (triazine, propoxur, and methidathion) from environmental waters. The results showed that the required mass of MWCNT (200 mg) was obviously less than that of activated carbon (300 mg) and C₁₈ silica (400 mg) given the same level of analyte concentration and volume of water samples, and the recoveries of target analytes in real water samples extracted with MWCNT were higher than those of the other two adsorbents.

4.3.1.2 Sample volume

For water samples, the adsorbent mass is associated with the breakthrough volume of each analyte in SPE method. BTV is dependent on the adsorption ability of analytes to CNTs. For nonpolar polyhalogenated pollutants, BTV can be larger than 2000 mL even with 20 mg of MWCNT. For polar sulfonylurea herbicides, the recoveries obtained with 100 mg MWCNT can maintain constant as sample is up to 2000 mL (Table 4.6). In the literature, the breakthrough volume for many analytes such as PAHs, atrazine, simazine, phthalate esters, alkylphenols, diazinon, and so on, are higher than 1000 mL. Then, the concentration factor of 1000–4000 for these target analytes can be achieved easily. Combined with the commonly used instruments such as HPLC-UV, HPLC-DAD, GC-ECD, or GC-FID, the detection limits for target analytes can be less than 10 ng/L, which are comparable to those obtained by the expensive and sensitive analytical technologies LC-MS, LC-MS-MS, GC-MS, or GC-MS-MS.

4.3.1.3 Desorption of analytes

In SPE procedures, different elution efficiencies can be obtained when different solvents are used because of the chemical and physical properties of the organic solvents, the nature of the extracted analytes, and the characteristics of the adsorbents used as the SPE material. CNTs cannot dissolve in any organic solvent; therefore, this material can resist most solvents. Hexane, dichloromethane, tetrahydrofuran, acetone, acetonitrile, and methanol have been adopted to desorb analytes from CNTs. For example, acetone is more potent than hexane and methanol in

the desorption of polyhalogenated organic pollutants (TCP, PCP, PCB77, and PBB52) from pristine and C₁₈ modified MWCNT due to the hydrophobicity of the two materials and the partial polarity of analytes. In the case of PEG-modified MWCNT (MWCNT-PEG), methanol has the highest efficiency, followed by acetone and then hexane. The authors suggested that there might be hydrogen bonds between polar solvents and hydroxyl groups (-OH) either from the PEG chains or from the unfunctionalized carboxylic or phenolic groups on MWCNT, which led to more efficient desorption of analytes by methanol followed by acetone than hexane. Generally, methanol and acetonitrile are most frequently used solvents among the studies, and the volume of eluents is usually less than 5–6 mL.

4.3.1.4 Effect of solution pH

pH value plays an important role in the extraction of organic compounds in environmental water samples because the pH value of the sample solution determined the existing state of analytes and the analytes can only be adsorbed in molecule form. For nonpolar analytes (such as PAHs, phthalate esters, or alkylphenol), pH has no effect on their extraction efficiency by CNTs adsorbents, and the enrichment of analytes can be conducted in the pH range 3–11. With regard to polar or moderate polar compounds, the optimal pH range is dominantly determined by the dissociation constant (pKa) of analytes. For example, dramatic decrease in recoveries of bisphenol A, benzene acid, and chlorophenols are observed as solution pH is higher than pH 8.0. The CNT-OH or CNT-COOH materials contain multiple binding sites due to the presence of the oxygen-containing groups on adsorbent surface with mixed adsorption mechanisms, e.g., ion exchange dispersion, hydrophobic interaction, and hydrogen bonding. However, these interactions might be conflicted. For example, at lower pH value, aromatic amines with lower pKa (pKa of 0.99 for 4-NA, pKa of -0.26 for 2-NA, pKa of 2.64 for 2-CA, and pKa of 2.00 for 2,4-DCA) are highly protonated, which favors for electrostatic interaction but hinders the formation of hydrogen bond and hydrophilic/hydrophobic interactions. At higher pH values, the oxygen groups of MWCNT-COOH can easily be ionized and more negative charged, which becomes a disadvantage for extraction of the compounds.

4.3.2 SPE Disks

By far, few studies have been performed to prepare CNTs SPE disks perhaps because disks are hard to be manufactured in laboratory. CNTs in the format of sheet or film have been reported and used as alternative actuators, electrolytes, artificial muscle, and sensors. A CNT sheet, also called as “bucky paper,” is typically produced by the vacuum filtration of certain volume of CNTs suspension through a filter. The sheet can be peeled from the filter and possesses good tenacity and suitable mechanical properties, which allow it to be enfolded or rolled up. The sheet can be readily assembled from SWCNT but are much more difficult to produce consistently from the more rigid MWCNT. The SWCNT sheet has a much larger specific surface area than the SWCNT particles, and a sheet (47 mm in diameter) made from ~30 mg of SWCNT is typically 60 μm in thickness with a specific surface area of ~700 m^2/g . It has been packed into a metal tube as preconcentrator to trap organic vapors (methyl ethyl ketone, toluene, and dimethyl methylphosphonate).

Using SWCNT sheet, Cai group has tried to develop SPE disk with a simple method. The disks are prepared by filtering suitable amount of highly dispersed SWCNT suspension in 2.5% SDS surfactant solution through a qualitative filter paper, followed by washing and drying. In order to improve the mechanical properties of the disk, the sheet is not peeled from the filter. The strong interactions between individual SWCNT ensure that nanotubes can be fixed onto the filter surface without leaking or peeling during the processes of filtration or sample loading. The group investigated the properties of the SWCNT disks by enriching organic compounds with different polarity including phthalate esters, BPA, NP, OP, chlorophenols, and sulfonylurea herbicides from large volumes of water samples. The reproducibility of different disks is satisfactory (RSDs < 15%, $n = 7$), and the flow rate can be as high as 100 mL/min without decreasing the extraction efficiency to target analytes. If one liter of aqueous solution is pretreated by the disk within 10–100 min, the recoveries almost remain constant. Two or three disks can be stacked to enhance the adsorption capacity of the disks since there is only 30 mg of SWCNT in one disk. The detection limits for BPA, OP, NP, and five sulfonylurea herbicides are 1.1–38 ng/L under

optimized conditions (Table 4.6). The extraction efficiency of SWCNT disk to these analytes is comparable to that of commercial C₁₈ disk and activated carbon disk. However, the analytes retained by SWCNT disk can be desorbed with 8–15 mL of methanol or acetone/nitrole solvent, while they are hardly eluted from activated carbon disks regardless of the type and volume of organic solvents. Although the SWCNT disk produced by this simple method can be used to pretreat water samples, much effort must be made to improve the quality of SWCNT disk, such as increasing the amount of SWCNT in one disk.

4.3.3 SPME

Solid-phase microextraction (SPME) is a solvent-free sample preparation technique that uses a fused silica fiber coated with an appropriate stationary phase attached to a modified microsyringe. SPME can integrate sampling, extraction, and sample introduction into a single step and become an attractive alternative to most of the conventional sampling techniques. The extraction efficiency of SPME is determined by the distribution of analytes between the matrix and the coating. As the fiber coating plays a key role in SPME, development of fiber coating for highly efficient extraction of the analytes of interest is an important research direction in SPME. High porosity and large adsorption area are two of main characteristics of CNTs, which make a suitable candidate for SPME coating in the case of analysis over a wide range of concentration. In addition, the more thermal and physical resistance of CNTs in comparison with commercial SPME coatings are the other important characteristics from a practical point of view. CNTs or functionalized CNTs have been successfully used as the SPME fiber coating for analysis of organic compounds, such as phenols, polybrominated diphenyls, organochlorine pesticides, MTBE, and so on (see Table 4.7). Compared with the commercial SPME fiber, the CNTs-coated fiber exhibits higher extraction efficiency to analytes, better thermal stability (300–350°C), and longer life span (over 200 times). Wang et al. reported that the MWCNT-coating fiber gave much higher enhancement factor for five PBDEs targets (616–1756) than

poly(5% dibenzene–95% dimethylsiloxane) coating (139–384) and activated carbon coating (193–423), and 30-min extraction of 10 mL of sample solution using the MWCNT-coated fiber for GC-ECD determination yielded the limits of detection of 3.6–8.6 ng/L and exhibited good linearity of the calibration functions. In another study, Zhang et al. have prepared hydroxyl-terminated silicone oil (TSO-OH)-functionalized SWCNT fiber, and using this SPME fiber coupled with GC-ECD detection, the detection limits for seven PBDEs were decreased to 0.08–0.8 ng/L ($S/N = 3$).

4.3.4 Application of CNT Adsorbents to Different Matrixes and Comparison with Other Adsorbents

4.3.4.1 Water samples

The suitability of CNTs for adsorption of different pollutants have been demonstrated in various complex matrixes including surface water samples, wastewater sludge, and biological sample (such as eggs, pork, honey, milk, olive oil, and urine). However, most CNTs applications published have been developed for the extraction of water samples, which are probably the less complex samples to work with. Off-line extractions have been described using CNTs cartridges for the extraction of nonpolar or moderate polar analytes such as PAH, phthalate esters, chlorophenols, PCBs (Table 4.6), and high-performance liquid chromatography (HPLC) with ultraviolet detector (UV) or diode array detector (DAD) or fluorescence detector (FLD) and gas chromatography (GC) with ECD, FID or NPD detector are the most commonly used instruments. Through the sample treatment step with MWCNT cartridge or SWCNT disks, the sensitivity of the analytical method with LC or GC for these analytes has been enhanced significantly.

Half of the applications of CNTs cartridge deal with the extraction of neutral or basic pesticides over a wide range of polarity and including polar pesticides or their degradation products. Using the SPE-LC-UV technique, the detection limits for metalaxyl, diethofencarb, myclobutanil, prometryn, and tebuconazole were much lower than 10 ng/L (0.8–4.1 ng/L), and for DDT and its

degradation products are in the range 4–13 ng/L after they were enriched from 500 mL of water samples with a CNTs cartridge packed with 100 mg of MWCNT. With SPE-GC-ECD analytical method, the detention limits for acetochlor, alachlor, metolachlor, and butachlor ranged in 10–30 ng/L, and the recoveries were 82–88% in river water and wastewater samples. A reliable multiresidue method based on SPE with MWCNT as adsorbent was developed for determination and quantitation of 12 pesticides in surface water by GC-MS. The detection limits of the proposed method could reach 10–30 ng/L based on the ratio of chromatographic signal to baseline noise ($S/N = 3$). Good recoveries achieved with 500 mL of spiked water samples were in the range 82–104%. The potential of CNTs for the extraction of very polar and water-soluble compounds is shown with the trace determination of simazine, atrazine, their degradation products, and a few polar pesticides such as sulfonylurea herbicides (shown in Table 4.8).

The potential of on-line SPE with CNTs adsorbents to LC, GC, or electrophoresis (CE) for the determination of various kinds of analytes has also been investigated. On-line coupling of SPE to GC or GC/MS can be realized readily with SPME fibers by inserting the fibers into the GC injector directly after sampling. The MWCNT or polymer-functionalized SWCNT SPME fibers have been used to detect phenol compounds or PBDEs coupled with GC-FID or GC-ECD from water samples. As a result, the MWCNT fiber was more efficient for the preconcentration of PBDEs than activated carbon fiber and poly (5% dibenzene–95% dimethylsiloxane) fiber. The developed method could be successfully applied for the analysis of real samples including river water and wastewater samples.

For the typical on-line SPE-LC system, it is easy to perform in any laboratory using simple switching valves and commercial precolumns and their holds. This system is also named column-switching LC in the literature. Instead of precolumns, in-tube SPME, an alternative SPME method, was adapted to couple directly to HPLC separation system for the determination of substituted aniline compounds in water samples. The oxidized MWCNT was coated on the outer surface of the fused silica tube and inserted in the polyether ether ketone (PEEK) tubing, and then fixed directly on

the six-port injection valve to substitute for the sample loop. High extraction capacity was achieved for the target analytes and great improvement of the detection limits (ranged from 40 to 130 ng/L) was obtained in comparison with other method. Micro-solid-phase extraction (μ -SPE) is a solvent-reducing extraction technique by miniaturizing conventional SPE to smaller beds and solvent volumes, which is comparable to SPME.

4.3.4.2 Biological samples

Concerning the application of CNTs for the extraction of organic compounds from complex matrices (different from waters), they have been focused on the extraction of nonsteroidal anti-inflammatory drugs, methyl *tert*-butyl ether, ethyl *tert*-butyl ether, and methyl *tert*-amyl ether from urine; polibrominated diphenyl ethers from milk; barbital, amobarbital, and phenobarbital residues from pork; sulfonamides from eggs and pork; atrazine and its principal metabolites from soil samples; atrazine and simazine in olive oil samples; and organophosphorus pesticides from fruit juices, soil, and olive oil samples. These research works involve both off-line extraction and on-line SPE (in the format of fiber or precolumn) coupling to LC, GC, or CE. As shown in Table 4.9, the matrix effect on the determination of analytes can be observed especially in pork and egg samples. In the pork and/or egg matrix, the recoveries of sulfonamides were in the range 66–80%, and recoveries of benzodiazepine drugs including diazepam, estazolam, alprazolam and triazolam, and barbiturates such as barbital, amobarbital, and phenobarbital were in the range 75–100%. While the recoveries of target analytes in other matrix were rather satisfactory (85–100%). However, the extraction efficiencies of polar analytes such as sulfonamides, simazine, atrazine, and its metabolites are relatively lower than other concerned organic compounds. Anyway, from the revision of this relatively low number of works it is clear that CNTs have a high potential for the extraction of organic compounds of different nature from very complex matrixes and that further applications are highly necessary in order to expand their possibilities as new extracting systems.

Table 4.6 Extraction efficiency of CNTs cartridge or disks to different analytes from environmental water samples

Analytes	Adsorbent (mg)	BTV (mL)	LOD (ng/L)	Recovery (%)		Sample volume (mL)	Instrument	Source
				Surface water	Wastewater			
Nap	MWCNT (100 mg)	1000	21	100	113	500	HPLC	Wang, 2007
Acy		>1500	58	91-96	79-81			
Flo		1000	26	94-117	98.2			
Ph		1000	9	90-116	103			
An		1000	5	108	99.6			
Fl		1000	34	108	87			
Py		1000	36	109	111			
BaA		1000	13	111	101.5			
BbF		1000	9	108	83-87			
BkF		>1500	15	115	89-110			
BPA	MWCNT (500 mg)	1000 (recovery >90%)	83	101		500	HPLC-FLD	Cai, 2003
4-OP			24	100	90.4			
4-NP			18	98.4	90.1			
DEP	MWCNT (500 mg)	2000-3000	18	82-92	83-91 ^a	1000	HPLC-UV	Cai, 2003
DPP			23	85-97	80-95			
DBP			48	92-94	87-95			
DCP			86	68-95	97-105			

Table 4.6 continued

Analytes	Adsorbent (mg)	BTV (mL)	LOD (ng/L)	Recovery (%)		Sample volume (mL)	Instrument	Source
				Surface water	Wastewater			
C10-LAS	CMWCNT (200 mg)	1500	20	84.8	94	500	HPLC-UV	Guan, 2008
C11-LAS			30	89.7	97.8			
C12-LAS	CMWCNT (200 mg)	1500	30	91.1	103	500	HPLC-UV	Guan,2008
C13-LAS			2000	20	95.8			
BPA	SWCNT disk (60 mg)	1000	7	95-99	59-67	1000	HPLC-FLD	Niu, 2008
4-OP		>2000	25	97-98	69-84			
4-NP		>2000	38	97-98	81-86			
4-CP	MWCNT (300 mg)	200	80	100	100	200	HPLC-UV	Cai, 2005
3-CP		200	100	99	103			
DCP		500	100	93	100			
TCP		500	200	88	100			
PCP		500	800	109	97			

^a sea water, BTV, breakthrough volume.

Nap, naphthalene; Acy, acenaphthylene; Flo, fluorine; Ph, phenanthrene; An, anthracene; Fl, fluoranthene; Py, pyrene; BaA, ben[a]anthracene; BbF, benzo[b]fluoranthene; BkF, benzo[k]fluoranthene; BPA, bisphenol A; 4-OP, 4-tert-octylphenol; 4-NP, 4-n-nonylphenol; 4-CP, 4-chlorophenol; 3-CP, 3-chlorophenol; DCP, 2,4-dichlorophenol; TCP, 2,4,6-trichlorophenol; PCP, pentachlorophenol; DEP, diethyl-phthalate; DPP, di-n-propyl-phthalate; DBP, di-iso-butyl-phthalate; DCP, di-cyclohexyl-phthalate; LAS, linear alkylbenzene sulfonate.

Table 4.7 Extraction efficiency of MWCNTs fiber to different analytes from environmental water samples

Analytes	LOD (ng/L) (<i>S/N</i> =3)	Recovery (%)		Instrument	Source
		Surface water	Wastewater		
phenol	50	94.4	98.9	GC	Liu, 2009
o-methylphenol	50	73.5	100		
p-methylphenol	50	93.8	115		
o-ethylphenol	5	98.5	145		
2,5-dimethylphenol	5	85.4	128		
p-ethylphenol	5	104	142		
2,3-dimethylphenol	5	80.7	106		
2-nitrophenol	3000	81-104.9	56.1-81.2	HPLC	Sae-Khow, 2009
2,6-dichloroaniline	1000				
naphthalene	100			HPLC	Liu, 2008
4-nitroaniline	70				
2-nitroaniline	40				
2-chloroaniline	130				
2,4-dichloroaniline	80				

Table 4.7 continued

Analytes	LOD (ng/L) (<i>S/N</i> =3)	Recovery (%)		Instrument	Source
		Surface water	Wastewater		
BDE-47	3.6	94	90	GC-ECD	Wang, 2006
BDE-99	4.9	93	91		
BDE-100	5.9	97	90		
BDE-153	7.7	97	95		
BDE-154	8.6	94	98		
BDE-35	0.08	92-107		GC-ECD	Zhang 2009
BDE-47	0.2	74-109			
BDE-77	0.2	78-103			
BDE-99	0.2	83-103			
BDE-100	0.2	75-93			
BDE-153	0.8	75-85			
BDE-154	0.4	77-81			

Table 4.8 Extraction efficiency of CNTs cartridge or disks to herbicides and antibiotics analytes from environmental water samples

Analyte	Adsorbent (mg)	BTW (mL)	Recovery (%)			Sample volume (mL)	Instrument	Source
			LOD (ng/L) ^a	Surface water	Wastewater			
metalaxyl	MWCNT (100mg)	>1500	3	103	78.7	500	HPLC	Zhou 2007
diethofencarb			3.7	108	104			
myclobutanol			4.1	98	96.3			
prometryn			0.8	89.8	100			
tebuconazole				100	83.8			
diazinon	MWCNT (50 mg)	>1000	60	95.2 ^b		200	HPLC	Katsumata, 2008
methidathion	MWCNT (300 mg)		2000	95-97 ^b	86-93 ^c	600	UV	Al-Degsa, 2009
propoxur			3000	95-103	85-91			
atrazine			3000	94-104	84.3-93			
propoxur	MWCNT (200 mg)	400	220	82-102	85-107 ^c		HPLC	El-Sheikh, 2008 and 2007
atrazine			58	81-105	93-108			
methidathion			36	81-101	96-104			
atrazine	MWCNT (100 mg)	1000	33	82.6	58	500	HPLC	Zhou 2006
simazine	(100 mg)	1000	9	98.4	72			

Table 4.8 continued

Analyte	Adsorbent (mg)	BTV (mL)	Recovery (%)			Sample volume (mL)	Instrument	Source
			LOD (ng/L) ^a	Surface water	Wastewater			
carbofuran	MWCNT (100 mg)	>2000	20	94-98		500	GC-MS	Wang 2007
iprobenfos			10	94-98				
parathion-methyl			30	95-98				
prometryn			20	100-105				
fenitrothion	MWCNT (100mg)	>2000	30	95-98		500	GC-MS	Wang 2007
parathion-ethyl			20	92-96				
isocarbofos			10	94-98				
phenthroate			30	89-93				
methidathion			10	97-101				
endrin			30	93-98				
ethion			20	92-95				
methoxychlor			20	88-92				
atrazine	MWCNT (100 mg)		20	88-92		100	GC-MS	Min, 2008
deisopropyl-atrazine			40	86-105				
deethyl-atrazine			50	90-110				

Table 4.8 continued

Analyte	Adsorbent (mg)	BTW (mL)	Recovery (%)			Sample volume (mL)	Instrument	Source
			LOD (ng/L) ^a	Surface water	Wastewater			
p,p'-DDD	MWCNT (100 mg)	>2000	4	89.7	>100	500	HPLC-UV	Zhou, 2006
p,p'-DDE		>2000	9	100	~100			
p,p'-DDT		>2000	5	92	~100			
o,p'-DDT		750	13	90	~100			
sulfathiazole	MWCNT (100 mg)	500	27	55	66-88 ^d	500	HPLC-UV	Niu, 2007
sulfadiazine			34	75-87	80-92			
sulfapyridine			38	87-95	95-102			
sulfamethazine			29	89-91	100			
metsulfuron-methyl	SWCNT disk 90 mg)	1500	6.2	93	79 ^d	500	HPLC-UV	Niu, 2009
chlorsulfuron		>3000	1.1	97	84			
bensulfuron-methyl		2500	6.5	95	76			
pyrazosulfuron-ethyl		>3000	2.8	101	85			
chlorimuron-ethyl		>3000	7.2	99	91			
acetochlor	MWCNT (100mg)	>1000	10	83.4	83.4	500	GC-ECD	Dong, 2009
alachlor			20	84.6	81.6			
metolachlor			30	87.7	82.5			
cyanazine	MWCNT (100mg)	>1500	15	104	101	250	HPLC	Zhou, 2007
chlorotoluron			12	93.8	87.8			
chlorobenzuron			34	101	105			

BTW: breakthrough volume; ^a LOD S/N=3; ^b tap water; ^c reservoir water; ^d: river water.

Table 4.9 Extraction efficiency of CNTs cartridges or fibers to different analytes from biological samples

Analytes	Matrix	Adsorbent (mg)	LOD ($\mu\text{g}/\text{kg}$)	Recovery (%)	Instrument	Source
diazepam	pork	MWCNT (200 mg)	2	75-90	GC-MS	Wang, 2006
estazolam			5	85-104		
alprazolam			5	85-97		
triazolam			5	89-103		
ketoprofen	urine	c-SWCNT immobilized on glass	1.9 ^a	99-102	CE-MS	Suárez, 2007
tolmetin			1.6 ^a	99-100		
indomethacine			2.6 ^a	98-102		
ethopropofos	forestry soil	MWCNT (100mg)	3.49	102	GC-NPD	Asensio-Ramos, 2009
	ornamental soil		3.06	105		
	agricultural soil		4.19	90		
diazinon	forestry soil	MWCNT (100mg)	2.97	87		
	ornamental soil		3.1	109		
	agricultural soil		3.14	98		
chlorpyriphosmethyl	forestry soil	MWCNT (100mg)	5.65			
	ornamental soil		6.02			
	agricultural soil		4.22			
fenitrothion	forestry soil	MWCNT (100mg)	5.6	90		
	ornamental soil		6.06	105		
	agricultural soil		5.04	103		
malathion	forestry soil		4.1	98		

Table 4.9 continued

Analytes	Matrix	Adsorbent (mg)	LOD ($\mu\text{g/kg}$)	Recovery (%)		Instrument	Source
malathion	ornamental soil	MWCNT (200 mg)	3.92	106		GC-NPD	Asensio-Ramos, 2009
	agricultural soil		3.5	102			
chlorpyriphos	forestry soil		19.9				
	ornamental soil		27.6				
	agricultural soil		17.7				
buprofezin	forestry soil		52.2				
	ornamental soil		72.4				
	agricultural soil		37.4				
phosmet	forestry soil		8.66	90			
	ornamental soil		9.49	108			
	agricultural soil		8.06	106			
babital	pork	MWCNT (250 mg)	0.2	76-85		GC-MS-MS	Zhao, 2007
amobarbital			0.1	91-94			
phenobarbital			0.1	89-96			
atrazine	soil	MWCNT (100 mg)	300	85-89		GC-MS	Min, 2008
deisopropyl-atrazine			1000	72-74			
deethyl-atrazine			800	77-78			

Table 4.9 continued

Analytes	Matrix	Adsorbent (mg)	LOD ($\mu\text{g/kg}$)	Recovery (%)		Instrument	Source
sulfadiazine	eggs and pork		5.9 ^b	72-79 ^c	73-79 ^d	HPLC	Fang 2006
sulfathiazole			4.6 ^b	72-77	69-74		
sulfamerazine			4.9 ^b	70-73	66-78		
sulfamoxol	eggs and pork		9.3 ^b	72-77	73-79	HPLC	Fang 2006
sulfamethizole			5.1 ^b	70-75	70-79		
sulfadimidine			7.6 ^b	72-76	78-79		
sulfamethoxypyridazine			7.1 ^b	72-79	71-76		
sulfachlorpyridazine			4.1 ^b	77-79	71-79		
sulfadoxin			4.5 ^b	71-80	74-80		
sulfasoxazole			10 ^b	80-81	80-86		
MEBE	urine	SWCNT	10 ^b	90-95		GC/MS	Rastkari, 2009
ETBE			10 ^b	92-94			
TAME			10 ^b	90-93			

Table 4.9 continued

Analytes	Matrix	Adsorbent (mg)	LOD ($\mu\text{g/kg}$)	Recovery (%)		Instrument	Source
BDE-47	milk	MWCNT fiber	3.6 ^b	98-117		GC-ECD	Wang, 2006
BDE-99			4.9 ^b	95-115			
BDE-100			5.9 ^b	93-105			
BDE-153			7.7 ^b	99-119			
BDE-154			8.6 ^b	91-104			
chlortoluron	oil	MWCNT (30 mg)	1.8 ^a	101		GC/MS	López-Feria, 2009
diuron			2.4 ^a	79			
terbutylazin-desethyl			1.5 ^a	105			
dimetoathe			1.5 ^a	97			
simazine	oil	MWCNT (30 mg)	2.4 ^a	99		GC/MS	López-Feria, 2009
atrazine			2.1 ^a	98			
malathion			3 ^a	99			
parathion			3 ^a	98			

^a $\mu\text{g/kg}$; ^b ng/L; ^c eggs sample; ^d pork sample ; C-SWCNT: SWCNT-COOH.

References

- Agnihotri S, Rood M J, Rostam-Abadi M. Adsorption equilibrium of organic vapors on single-walled carbon nanotubes. *Carbon* 2005, 43, 2379–2388.
- Sood, and RostamAbadi (2005):Aktaş Ö, Çeçen F. Adsorption, desorption and bioregeneration in the treatment of 2-chlorophenol with activated carbon. *J. Hazard. Mater.* 2007, 141(3), 769–777.
- Al-Degsa Y S, Al-Ghouti M A, El-Sheikh A H. Simultaneous determination of pesticides at trace levels in water using multiwalled carbon nanotubes as solid-phase extractant and multivariate calibration. *J. Hazard. Mater.* 2009, 169, 128–135.
- Asensio-Ramos M, Hernández-Borges J, Borges-Miquel T M, Rodríguez-Delgado M A. Evaluation of multi-walled carbon nanotubes as solid-phase extraction adsorbents of pesticides from agricultural, ornamental and forestal soils. *Anal. Chim. Acta* 2009, 647, 167–176.
- Babaa M R, Dupont-Pavlovsky N, McRae E, Masenelli-Varlot K. Physical adsorption of carbon tetrachloride on as-produced and on mechanically opened single walled carbon nanotubes. *Carbon* 2004, 42, 1549–1554.
- Béguin F. Thermodynamic properties of benzene adsorbed in activated carbons and multi-walled carbon nanotubes. *Chem. Phys. Lett.* 2006, 421, 409–414.
- Bittner E W, Smith M R, Bockrath B C. Characterization of the surfaces of single-walled carbon nanotubes using alcohols and hydrocarbons: a pulse adsorption technique. *Carbon* 2003, 41, 1231–1239.
- Breza M. Model studies of SOCl₂ adsorption on carbon nanotubes. *J. Mol. Struc. THEOCHEM* 2006, 767, 159–163.
- Burghaus U, Bye D, Cosert K, Goering J, Guerard A, Kadossov E, Lee E, Nadoyama Y, Richter N, Schaefer E, Smith J, Ulness D, Wymore B. Methanol adsorption in carbon nanotubes. *Chem. Phys. Lett.* 2007, 442, 344–347.
- Cai Y Q, Cai Y E, Mou S F, Lu Y Q. Multi-walled carbon nanotubes as a solid-phase extraction adsorbent for the determination of chlorophenols in environmental water samples. *J. Chromatogr. A* 2005, 1081, 245–247.
- Cai Y Q, Jiang G B, Liu J F, Zhou Q X. Multi-walled carbon nanotubes packed cartridge for the solid-phase extraction of several phthalate esters from water samples and their determination by high performance liquid chromatography. *Anal. Chim. Acta* 2003, 494, 149–156.
- Cai Y Q, Jiang G B, Liu J F, Zhou Q X. Multiwalled carbon nanotubes as a solid-phase extraction adsorbent for the determination of bisphenol

- A, 4-n-nonylphenol, and 4-tert-octylphenol. *Anal. Chem.* 2003, 75, 2517–2521.
- Chen G C, Shan X Q, Wang Y S, Pei Z G, Shen X E, Wen B, Owens G. Effects of copper, lead, and cadmium on the sorption and desorption of atrazine onto and from carbon nanotubes. *Environ. Sci. Technol.* 2008, 42, 8297–8302.
- Chen G C, Shan X Q, Wang Y S, Wen B, Pei Z G, Xie Y N, Liu T, Pignatello J J. Adsorption of 2,4,6-trichlorophenol by multi-walled carbon nanotubes as affected by Cu(II). *Water Res.* 2009, 43, 2409–2418.
- Chen G C, Shan X Q, Zhou Y Q, Shen X E, Huang H L, Khan S U. Adsorption kinetics, isotherms and thermodynamics of atrazine on surface oxidized multiwalled carbon nanotubes. *J. Hazard. Mater.* 2009, 169, 912–918.
- Chen J Y, Chen W, Zhu D Q. Adsorption of nonionic aromatic compounds to single-walled carbon nanotubes: effects of aqueous solution chemistry. *Environ. Sci. Technol.* 2008, 42, 7225–7230.
- Chen W, Duan L, Zhu D Q. Adsorption of polar and nonpolar organic chemicals to carbon nanotubes. *Environ. Sci. Technol.* 2007, 41, 8295–8300.
- Chen Z G, Zhang L S, Tang Y W, Jia Z J. Adsorption of nicotine and tar from the mainstream smoke of cigarettes by oxidized carbon nanotubes. *Appl. Surf. Sci.* 2006, 252, 2933–2937.
- Chin C J M, Shih L C, Tsai H J, Liu T K. Adsorption of *o*-xylene and *p*-xylene from water by SWCNTs. *Carbon* 2007, 45, 1254–1260.
- Cho H H, Smith B A, Wnuk J D, Fairbrother D H, Ball W P. Influence of surface oxides on the adsorption of naphthalene onto multiwalled carbon nanotubes. *Environ. Sci. Technol.* 2008, 42, 2899–2905.
- Díaz E, Ordóñez S, Vega A. Adsorption of volatile organic compounds onto carbon nanotubes, carbon nanofibers, and high-surface-area graphites. *J. Colloid Interface Sci.* 2007, 305, 7–16.
- Dong M F, Ma Y Q, Zhao E C, Qian C F, Han L J, Jiang S R. Using multiwalled carbon nanotubes as solid phase extraction adsorbents for determination of chloroacetanilide herbicides in water. *Microchim. Acta* 2009, 165, 123–128.
- El-Sheikh A H, Insisi A A, Sweileh J A. Effect of oxidation and dimensions of multi-walled carbon nanotubes on solid phase extraction and enrichment of some pesticides from environmental waters prior to their simultaneous determination by high performance liquid chromatography. *J. Chromatogr. A* 2007, 1164, 25–32.

- El-Sheikh A H, Sweileh J A, Al-Degs Y S, Insisi A A, Al-Rabady N. Critical evaluation and comparison of enrichment efficiency of multi-walled carbon nanotubes, C18 silica and activated carbon towards some pesticides from environmental waters. *Talanta* 2008, 74, 1675–1680.
- Fagan S B, Souza Filho A G, Lima, J O G, Mendes Filho J, Ferreira O P, Mazali I O, Alves O L, Dresselhaus M S. First principles study of 1,2-Dichlorobenzene interacting with carbon nanotubes. *Nano Lett.* 2004, 7, 1285–1288.
- Fagan, S B, Girao E C, Mendes Filho J, Souza Filho A G. Dichlorobenzene adsorption on metallic carbon nanotubes. *Int. J. Quantum Chem.* 2006, 106, 2558–2563.
- Fang G Z, He J X, Wang S. Multiwalled carbon nanotubes as sorbent for online coupling of solid-phase extraction to high-performance liquid chromatography for simultaneous determination of 10 sulfonamides in eggs and pork. *J. Chromatogr. A* 2006, 1127, 12–17.
- Gauden P A, Terzyk A P, Rychlicki G, Kowalczyk P, Lota K, Raymundo-Pinero E, Frackowiak E, Goering J, Burghaus U. Adsorption kinetics of thiophene on single-walled carbon nanotubes (CNTs). *Chem. Phys. Lett.* 2007, 447, 121–126.
- Gotovac S, Honda H, Hattori Y, Takahashi K, Kanoh H, Kaneko K. Effect of nanoscale curvature of single-walled carbon nanotubes on adsorption of polycyclic aromatic hydrocarbons. *Nano Lett.* 2007, 7, 583–587.
- Guan Z, Huang Y M, Wang W D. Carboxyl modified multi-walled carbon nanotubes as solid-phase extraction adsorbents combined with high-performance liquid chromatography for analysis of linear alkylbenzene sulfonates. *Anal. Chim. Acta* 2008, 627, 225–231.
- Hennion M C. Solid-phase extraction: method development, sorbents, and coupling with liquid chromatography. *J. Chromatogr. A* 1999, 856, 3–54.
- Hyung H, Fortner J, Hughes J, Kim J H. Natural organic matter stabilizes carbon nanotubes in the aqueous phase. *Environ. Sci. Technol.* 2007, 41, 179–184.
- Hyung H, Kim J H. Natural organic matter (NOM) adsorption to multi-walled carbon nanotubes: effect of NOM characteristics and water quality parameters. *Environ. Sci. Technol.* 2008, 42, 4416–4421.
- Katsumata H, Matsumoto T, Kaneco S, Suzuki T, Ohta K. Preconcentration of diazinon using multiwalled carbon nanotubes as solid-phase extraction adsorbents. *Microchem. J.* 2008, 88, 82–86.

- Komarneni M, Sand A, Lu M, Burghaus U. Adsorption kinetics of small organic molecules on thick and thinner layers of carbon nanotubes. *Chem. Phys. Lett.* 2009, 470 (4–6), 300–303, doi:10.1016/j.cplett.2009.02.002.
- Kim S I, Yamamoto T, Endo A, Ohmori T, Nakaiwa M. Adsorption of phenol and reactive dyes from aqueous solution on carbon cryogel microspheres with controlled porous structure. *Microporous Mesoporous Mater.* 2006, 96, 191–196.
- Kondratyuk P, Wang Y, Johnson J K, Yates J T, Jr. Observation of a one-dimensional adsorption site on carbon nanotubes: adsorption of alkanes of different molecular lengths. *J. Phys. Chem. B* 2005, 109, 20999–21005.
- Kumar A, Kumar S, Kumar S. Adsorption of resorcinol and catechol on granular activated carbon: Equilibrium and kinetics. *Carbon* 2003, 41, 3015–3025.
- Laszlo, K. Adsorption from aqueous phenol and aniline solutions on activated carbons with different surface chemistry. *Colloids Surf. A: Physicochem. Eng. Asp.* 2005, 265, 32–39.
- Li Q L, Yuan D X, Lin Q M. Evaluation of multi-walled carbon nanotubes as an adsorbent for trapping volatile organic compounds from environmental samples. *J. Chromatogr. A* 2004, 1026, 283–288.
- Liao Q, Sun J, Gao L. Adsorption of chlorophenols by multi-walled carbon nanotubes treated with HNO₃ and NH₃. *Carbon* 2008, 46, 553–555.
- Liao Q, Sun J, Gao L. The adsorption of resorcinol from water using multi-walled carbon nanotubes. *Colloids Surf., A* 2008, 312, 160–165.
- Lin D H, Xing B S. Adsorption of phenolic compounds by carbon nanotubes: role of aromaticity and substitution of hydroxyl groups. *Environ. Sci. Technol.* 2008, 42, 7254–7259.
- Lin D H, Xing B S. Tannic acid adsorption and its role for stabilizing carbon nanotube suspensions. *Environ. Sci. Technol.* 2008, 42, 5917–5923.
- Liu C H, Li J J, Zhang H L, Li B R, Guo Y. Structure dependent interaction between organic dyes and carbon nanotubes. *Colloids Surf., A* 2008, 313–314, 9–12.
- Liu H M, Li J B, Liu X, Jiang S X. A novel multiwalled carbon nanotubes bonded fused-silica fiber for solid phase microextraction–gas chromatographic analysis of phenols in water samples. *Talanta* 2009, 78(3), 929–935, doi:10.1016/j.talanta.2008.12.061.
- Liu X Y, Ji Y S, Zhang H X, Liu M C. Highly sensitive analysis of substituted aniline compounds in water samples by using oxidized multiwalled carbon nanotubes as an in-tube solid-phase microextraction medium. *J. Chromatogr. A* 2008, 1212, 10–15.

- Long R Q, Yang R T. Carbon nanotubes as superior sorbent for dioxin removal. *J. Am. Chem. Soc.* 2001, 123, 2058–2059.
- López-Feria S, Cárdenas S, Valcárcel M. One step carbon nanotubes-based solid-phase extraction for the gas chromatographic–mass spectrometric multiclass pesticide control in virgin olive oils. *J. Chromatogr. A* 2009, 1216(43), 7346–7350, doi:10.1016/j.chroma.2009.02.060.
- Lu C Y, Su F S. Adsorption of natural organic matter by carbon nanotubes. *Sep. Purif. Technol.* 2007, 58, 113–121.
- Mauter M S, Elimelech M. Environmental applications of carbon-based nanomaterials. *Environ. Sci. Technol.* 2008, 42, 5843–5859.
- Min G, Wang S, Zhu H P, Fang G Z, Zhang Y. Multi-walled carbon nanotubes as solid-phase extraction adsorbents for determination of atrazine and its principal metabolites in water and soil samples by gas chromatography–mass spectrometry. *Sci. Total Environ.* 2008, 396, 79–85.
- Muris M, Dufau N, Bienfait M, Dupont-Pavlovsky N, Grillet Y, Palmari J P. Methane and krypton adsorption on single-walled carbon nanotubes. *Langmuir* 2000, 16, 7019–7022.
- Niu H Y, Cai Y Q, Shi Y L, Wei F S, Liu J M, Jiang G B. A new solid-phase extraction disk based on a sheet of single-walled carbon nanotubes. *Anal. Bioanal. Chem.* 2008, 392, 927–935.
- Niu H Y, Cai Y Q, Shi Y L, Wei F S, Liu J M, Mou S F, Jiang G B. Evaluation of carbon nanotubes as a solid-phase extraction adsorbent for the extraction of cephalosporins antibiotics, sulfonamides and phenolic compounds from aqueous solution. *Anal. Chim. Acta* 2007, 594, 81–92.
- Niu H Y, Shi Y L, Cai Y Q, Wei F S, Jiang G B. Solid-phase extraction of sulfonylurea herbicides from water samples with single-walled carbon nanotubes disk. *Microchim. Acta* 2009, 164(3–4), 431–438, doi:10.1007/s00604-008-0079-1.
- Onyestyáka Gy, Valyona J, Hernádib K, Kiricsi I, Rees L V C. Equilibrium and dynamics of acetylene sorption in multiwalled carbon nanotubes. *Carbon* 2003, 41, 1241–1248.
- Pan B, Lin D H, Mashayekhi H, Xing B S. Adsorption and hysteresis of bisphenol A and 17 α -ethinyl estradiol on carbon nanomaterials. *Environ. Sci. Technol.* 2008, 42, 5480–5485.
- Pan B, Xing B S. Adsorption mechanisms of organic chemicals on carbon nanotubes. *Environ. Sci. Technol.* 2008, 42, 9005–9013.
- Peng X J, Li Y H, Luan Z K, Di Z C, Wang H Y, Tian B H, Jia Z P. Adsorption of 1,2-dichlorobenzene from water to carbon nanotubes. *Chem. Phy. Lett.* 2003, 376, 154–158.

- Poole C F. New trends in solid-phase extraction. *Trends Anal. Chem.* 2003, 22, 362–373.
- Pyrzynska K, Stafiej A, Biesaga M. Sorption behavior of acidic herbicides on carbon nanotubes. *Microchim. Acta* 2007, 159, 293–298.
- Rastkari N, Ahmadkhaniha R, Yunesian M. Single-walled carbon nanotubes as an effective adsorbent in solid-phase microextraction of low level methyl *tert*-butyl ether, ethyl *tert*-butyl ether and methyl *tert*-amyl ether from human urine. *J. Chromatogr. B* 2009, 877, 1568–1574.
- Ridgway K, Lalljie S P D, Smith R M. Sample preparation techniques for the determination of trace residues and contaminants in foods. *J. Chromatogr. A* 2007, 1153, 36–53.
- Sae-Khow O, Mitra S. Carbon nanotubes as the sorbent for integrating μ -solid phase extraction within the needle of a syringe. *J. Chromatogr. A* 2009, 1216, 2270–2274.
- Salam M A, Burk R C. Thermodynamics of pentachlorophenol adsorption from aqueous solutions by oxidized multi-walled carbon nanotubes. *Appl. Surf. Sci.* 2008, 255, 1975–1981.
- Shih Y H, Li M S. Adsorption of selected volatile organic vapors on multiwall carbon nanotubes. *J. Hazard. Mater.* 2008, 154, 21–28.
- Sidorenko I G, Markitan O V, Vlasova N N, Zagorovskii G M, and Lobanov V V. The adsorption of biogenic amines on carbon nanotubes. *Russ. J. Phys. Chem. A* 2009, 83, 1002–1005.
- Sone H, Fugetsu B, Tsukada T, Endo M. Affinity-based elimination of aromatic VOCs by highly crystalline multi-walled carbon nanotubes. *Talanta* 2008, 74, 1265–1270.
- Suárez B, Simonet B M, Cárdenas S, Valcárcel M. Determination of non-steroidal anti-inflammatory drugs in urine by combining an immobilized carboxylated carbon nanotubes minicolumn for solid-phase extraction with capillary electrophoresis-mass spectrometry. *J. Chromatogr. A* 2007, 1159, 203–207.
- Sulaymon, A H, Ahmed, K W. Competitive adsorption of furfural and phenolic compounds onto activated carbon in fixed bed column. *Environ. Sci. Technol.* 2008, 42, 392–397.
- Valentini L, Armentano I, Lozzi L, Santucci S, Kenny J M. Interaction of methane with carbon nanotube thin films: role of defects and oxygen adsorption. *Mater. Sci. Eng. C* 2004, 24, 527–533.
- Wang J X, Jiang D Q, Gu Z Y, Yan X P. Multiwalled carbon nanotubes coated fibers for solid-phase microextraction of polybrominated diphenyl ethers in water and milk samples before gas chromatography with electron-capture detection. *J. Chromatogr. A* 2006, 1137, 8–14.

- Wang L P, Zhao H X, Qiu Y M, Zhou Z Q. Determination of four benzodiazepine residues in pork using multiwalled carbon nanotube solid-phase extraction and gas chromatography-mass spectrometry. *J. Chromatogr. A* 2006, 1136, 99–105.
- Wang S, Zhao P, Min G, Fang G Z. Multi-residue determination of pesticides in water using multi-walled carbon nanotubes solid-phase extraction and gas chromatography-mass spectrometry. *J. Chromatogr. A* 2007, 1165, 166–171.
- Wang W D, Huang Y M, Shu W Q, Cao J. Multiwalled carbon nanotubes as adsorbents of solid-phase extraction for determination of polycyclic aromatic hydrocarbons in environmental waters coupled with high-performance liquid chromatography. *J. Chromatogr. A* 2007, 1173, 27–36.
- Wang X L, Lu J L, Xing B S. Sorption of organic contaminants by carbon nanotubes: influence of adsorbed organic matter. *Environ. Sci. Technol.* 2008, 42, 3207–3212.
- Wang X L, Tao S, Xing B S. Sorption and competition of aromatic compounds and humic acid on multiwalled carbon nanotubes. *Environ. Sci. Technol.* 2009, 43(16), 6214–6219, doi: 10.1021/es901062t.
- Woods L M, Bădescu ř C, Reinecke T L. Adsorption of simple benzene derivatives on carbon nanotubes. *Phys. Rev. B* 2007, 75, 155415-1–155415-9.
- Xie X F, Gao L, Sun J. Thermodynamic study on aniline adsorption on chemical modified multi-walled carbon nanotubes. *Colloids Surf., A* 2007, 308, 54–59.
- Yan X M, Shi B Y, Lu J J, Feng C H, Wang D S, Tang H X. Adsorption and desorption of atrazine on carbon nanotubes. *J. Colloid Interface Sci.* 2008, 321, 30–38.
- Yang K, Wang X L, Zhu L Z, Xing B S. Competitive sorption of pyrene, phenanthrene, and naphthalene on multiwalled carbon nanotubes. *Environ. Sci. Technol.* 2006, 40, 5804–5810.
- Yang K, Wu W H, Jing Q F, Zhu L Z. Aqueous adsorption of aniline, phenol, and their substitutes by multi-walled carbon nanotubes. *Environ. Sci. Technol.* 2008, 42, 7931–7936.
- Yang K, Xing B S. Adsorption of fulvic acid by carbon nanotubes from water. *Environ. Pollut.* 2009, 157(4), 1095–1100, doi:10.1016/j.envpol.2008.11.007.
- Yang K, Xing B S. Desorption of polycyclic aromatic hydrocarbons from carbon nanomaterials in water. *Environ. Pollut.* 2007, 145, 529–537.

- Yang K, Zhu L Z, Xing B S. Adsorption of polycyclic aromatic hydrocarbons by carbon nanomaterials. *Environ. Sci. Technol.* 2006, 40, 1855–1861.
- Ye C, Gong Q M, Lu F P, Liang J. Adsorption of uraemic toxins on carbon nanotubes. *Sep. Purif. Technol.* 2007, 58, 2–6.
- Zhang S J, Shao T, Bekaroglu S S K, Karanfil T. The impacts of aggregation and surface chemistry of carbon nanotubes on the adsorption of synthetic organic compounds. *Environ. Sci. Technol.* 2009, 43 (15), 5719–5725 doi: 10.1021/es900453e.
- Zhang W Y, Sun Y, Wu C Y, Xing J, Li J Y. Polymer-functionalized single-walled carbon nanotubes as a novel sol-gel solid-phase microextraction coated fiber for determination of polybrominated diphenyl ethers in water samples with gas chromatography-electron capture detection. *Anal. Chem.*, 2009, 81(8), 2912–2920, doi: 10.1021/ac802123s.
- Zhao H X, Wang L P, Qiu Y M, Zhou Z Q, Zhong W K, Li X. Multiwalled carbon nanotubes as a solid-phase extraction adsorbent for the determination of three barbiturates in pork by ion trap gas chromatography–tandem mass spectrometry (GC/MS/MS) following microwave assisted derivatization. *Anal. Chim. Acta* 2007, 586, 399–406.
- Zhou Q X, Ding Y J, Xiao J P. Simultaneous determination of cyanazine, chlorotoluron and chlorbenzuron in environmental water samples with SPE multiwalled carbon nanotubes and LC. *Chromatographia* 2007, 65, 25–30.
- Zhou Q X, Wang W D, Xiao J P, Wang J H, Liu G G, Shi Q Z, Guo G L. Comparison of the enrichment efficiency of multiwalled carbon nanotubes, C18 silica, and activated carbon as the adsorbents for the solid phase extraction of atrazine and simazine in water samples. *Microchim. Acta* 2006, 152, 215–224.
- Zhou Q X, Xiao J P, Ding Y J. Sensitive determination of fungicides and prometryn in environmental water samples using multiwalled carbon nanotubes solid-phase extraction cartridge *Anal. Chim. Acta* 2007, 602, 223–228.
- Zhou Q X, Xiao J P, Wang W D, Liu G G, Shi Q Z, Wang J H. Determination of atrazine and simazine in environmental water samples using multiwalled carbon nanotubes as the adsorbents for preconcentration prior to high performance liquid chromatography with diode array detector. *Talanta* 2006, 681, 1309–1315.
- Zhou Q X, Xiao J P, Wang W D. Using multi-walled carbon nanotubes as solid phase extraction adsorbents to determine dichlorodiphenyl-trichloroethane and its metabolites at trace level in water samples by high performance liquid chromatography with UV detection. *J. Chromatogr. A* 2006, 1125, 152–158.

Chapter 5

EFFICIENT REMOVAL OF ORGANIC POLLUTANTS AND METAL IONS USING AMPHIPHILIC POLYMER NANOPARTICLES

Jin Kie Shim

*Korea Packaging Center, Korea Institute of Industrial Technology,
Bucheon-si, Gyeonggi-do, 421-742, Korea*

jkshim@kitech.re.kr

5.1 INTRODUCTION

In the wake of technical innovation, the industry has been able to increase the efficiency of recycle and reuse for their waste and process waters, and to save a cleaning cost for groundwater and soil contamination as macro porous polymer was used to remove pollutants such as aromatics, aliphatics, chlorinated hydrocarbons, poly aromatics (PAHs), and heavy metal ions to below 1 ppb. Presently, most of the governments have promoted environmental guidelines and regulations that become more encompassing and progressively stricter in relation to their responsible care and environmental policies such as ISO 14000. As a next step, to increase the efficiency of removal pollutants, polymeric colloidal particle with hollow interiors has been considered a best volunteer, which plays an important role in micro-encapsulation [1]. Micellar-enhanced ultrafiltration (MEUF) [2–8] and surfactant-enhanced soil remediation (SESR) [9–17] have

Advances in Nanotechnology and the Environment

Edited by Juyoung Kim

Copyright © 2012 by Pan Stanford Publishing Pte. Ltd.

www.panstanford.com

been known as the most effective environmental process for removal of low molecular weight hydrophobic pollutants from soil and water. In both the processes, nano-sized aggregates of surfactant molecules (micelles) absorb and solubilize pollutants from soil and aqueous phase, which move through soil pores or separated from aqueous phase through separation membranes, resulting in improved washing and separation efficiency of conventional soil washing and filtration process. However, the real field application of these processes was still limited by the fatal drawbacks of MEUF and SESR process: (1) very easy breakage, (2) too small size of surfactant micelles, and (3) strong sorption of surfactant to soil and membrane cause secondary contamination. Thus, it has been strongly demanded to develop a new type of micelle-like nanoparticles to overcome these drawbacks and highly improve the efficiency of SESR and MEUF process. Micelle-like nanoparticles could be prepared using amphiphilic molecules such as surfactant and amphiphilic block copolymers (ABCs). For ABCs, they can form micelle-like nanoparticles at extremely low concentration in aqueous phase and maintain stable dispersion even at extremely high dilution, and their nanoparticles are much more stable compared to surfactant micelles, which makes ABCs a useful and potential alternative material for surfactant [18]. As a very promising material for cleaning water, amphiphilic polymer nanoparticle has

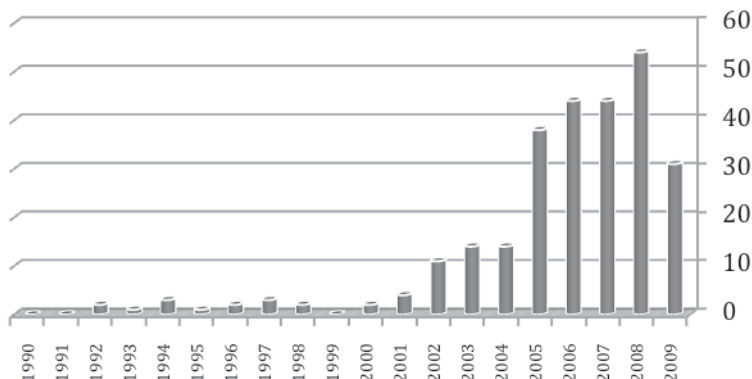


Figure 5.1 Number of annual patents on amphiphilic polymer nanoparticle related to pollutant removal technology. (Searched at US Patent Office, World Intellectual Property Organization (WIPO), European Patent Office and UK Patent Office; Key words: amphiphilic nanoparticle, water and hydrocarbon; Search on Oct. 30, 2009.)

received intensive interests from industries over the last couple of decades. Figure 5.1 shows that the number of patents on pollutant removal applications has increased exponentially and exceeded 50 articles in 2008. However, these polymers are very expensive and can be obtained only by extremely difficult synthetic processes, which make their practical application limited. In this chapter, a new ultrafiltration process is presented for removal of pollutants from water using designed amphiphilic polymer nanoparticles.

5.2 AMPHIPHILIC POLYMER NANOPARTICLE AS A NANO-ABSORBENT

Contamination of soil and groundwater by hydrophobic organic carbons (HOCs) is caused by leakage from storage tanks, spillage, or improper disposal of wastes. Once in the soil matrix, HOCs are a source of dissolved contaminants [19–23]. Among HOCs, polyaromatic hydrocarbons (PAHs) are of special interest because they are strongly sorbed onto soil or sediment. Consequently, sorbed PAHs may act as a long-term source of groundwater contamination. Many researchers have been using surfactants to enhance the desorption of sorbed PAHs from soil through solubilization of sorbed PAHs in surfactant micelles [24–31]. However, surfactant-enhanced remediation techniques have some disadvantages because of micelle breakage and loss of surfactant through sorption to soil. Therefore, surfactant-enhanced desorption and washing are effective only when the surfactant dose is much greater than its critical micelle concentration (CMC) [26–29, 32–34]. As a result, recent research has been directed toward the design of a surfactant that minimizes such losses and also toward the development of surfactant recovery and recycling techniques.

Amphiphilic polymers, which have hydrophilic and hydrophobic moieties on the same carbon backbone, have been widely used in various fields. In fact, parallels can be drawn between typical surfactants and amphiphilic polymers, and both materials have been used as emulsifiers, dispersants, foamers, thickeners, rinse aids, and compatibilizers [35–37]. The CMC of amphiphilic polymers is extremely low and their dispersion efficiency is retained even at extremely high dilution, hence amphiphilic polymers can be used as an alternative for the removal of absorbed hydrophobic pollutants

from the soil. There are several types of amphiphilic polymers, such as nonionic, anionic, or cationic homopolymers, random copolymers, and diblock-copolymers. It has been generally recognized that amphiphilic block or graft copolymers are very effective and versatile.

In this chapter, a new process is suggested for the enhanced desorption of sorbed phenanthrene (PAHs), which uses amphiphilic polyurethane (APU) nanoparticles that had been synthesized via soap-free emulsion polymerization of amphiphilic urethane acrylate nonionomer chains (UAN) or amphiphilic urethane acrylate anionomer chains (UAA). Unlike surfactant molecules that completely dissolve in water below its CMC, UAN and UAA chains cannot be dissolved in water but are just dispersed in water to form nano-aggregates (APU nanoparticles) even at extremely low concentrations, because whole UAN and UAA chains are insoluble in water.

5.2.1 Synthesis of a New Type of Amphiphilic Polymer Nanoparticle

To be used in MEUF process without blocking membrane pores, UAA (UAN) precursor chains needed to be prepared in nano-sized particles to allow them to flow through the soil bed and maximize the contact area. UAA and UAN chains were first emulsified through the phase inversion emulsification process without using any external surfactant, because a surfactant may affect the adsorption of cross-linked amphiphilic polymer (CAP) nanoparticles onto soil. The UAA (UAN) precursor was synthesized from poly(tetramethylene glycol) (PTMG, Mw = 1000), 2,4-toluene diisocyanate (TDI), 2-hydroxyethyl methacrylate (2-HEMA). The dimethylol propionic acid (DMPA) was used as received. CAP dissolved 90 g of deionized water are slowly dropped into the homogeneous mixture of UAA (UAN), triethylamine (TEA) and 2,2-azobisiso-butyronitrile (AIBN). TEA played a neutralizing reagents. After the formation of UAA (UAN) nanoparticles dispersed at water, cross-linking polymerization of UAA (UAN) nanoparticles was carried out at 80°C for 5 h with stirring at 200 rpm to obtain CAP nanoparticles. Postulated microstructure of CAP is represented in Fig. 5.2. The CAP nanoparticle can be synthesized with various lengths of UAA (UAN) as shown in Table 5.1. As a result, the sizes of the obtained CAP are in the range 32–61 nm.

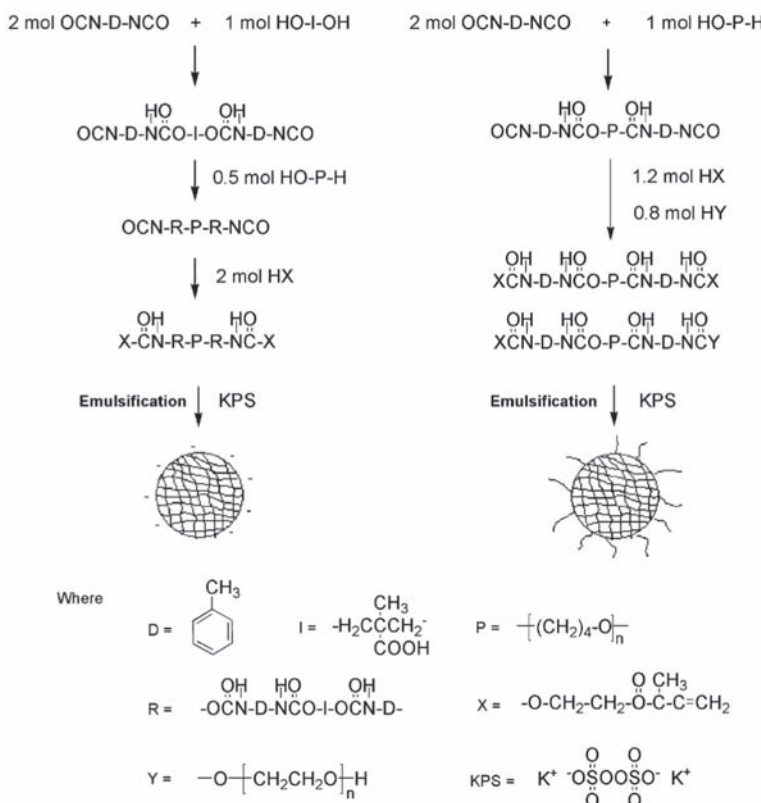


Figure 5.2 Reaction sequence used in the preparation of (a) UAA and (b) UAN precursor chains and nanoparticles.

After the completion of polymerization, the CAP emulsions were poured into 100 mL beaker containing CaCl_2 aqueous solution to aggregate CAP nanoparticles. After collecting via filtration, and aggregated CAP nanoparticles were immersed in acetone/water mixture to remove unreacted materials and initiators, etc., and dried for 24 h in a vacuum oven. The conversion from UAA to CAP nanoparticles was determined using the following equation:

$$\text{Conversion (wt\%)} = \left(\frac{W_d}{W_t} \times \text{TSC} \right) \times 100$$

where, W_d and W_t are collected sample weight (g) and sample weight after washing and drying (g), respectively. TSC is theoretical

solid content value per gram of collected sample at 100% conversion. Conversions for UAA (UAN) chains were in the range 92–95%.

Table 5.1 Recipe for synthesis of CAP nanoparticles

CAP nanoparticles	UAA chain	Molar ratio of PTMG/DMPA/TDI/2-HEMA	Mn (g/mol)	Particle size (nm)
CAP64	UAA 64	0.6/0.4/1.5/1	6700	61.20
CAP55	UAA 55	0.5/0.5/1.5/1	5670	58.32
CAP28	UAA 28	0.2/0.8/1.5/1	3750	32.40

Water is a good solvent for PEO segments in UAA (UAN) chains but is not a solvent for PPO chains. On contacting with water, water-soluble PEO segments in UAA (UAN) chains are microphase-separated from hydrophobic segment and oriented toward water phase to form outer layer. Hydrophobic PPO-based segments are associated with each other to form hydrophobic interior, leading to form micelle-like nano-sized aggregates of UAA (UAN) chains (APU nanoparticles). Finally, this aggregate structure of APU nanoparticles is permanently locked-in by chemical cross-linking reaction. Figure 5.3 shows a UAN and a UAA.

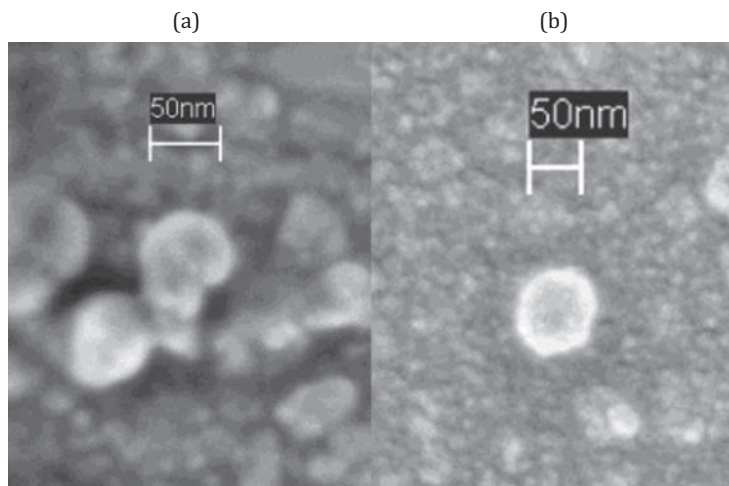


Figure 5.3 Scanning electron micrographs of (a) UAN and (b) UAA particles. Reprinted with permission from W. Tungittiplakorn (2004). Engineered polymeric nanoparticles for soil remediation, *Environ. Sci. Technol.*, 38, 1605. Copyright 2004 American Chemical Society.

5.2.2 Filtration Experiments

The ultrafiltration was carried out using cross-flow ultrafiltration unit (Millipore, USA) fitted with mixed cellulose esters (MCE) ultrafiltration flat membranes, having effective membrane area of 13.4 cm^2 and pore size of 0.025 mm. Pressure in the cell was maintained by nitrogen gas. Stirring speed was kept constant at 250–300 rpm using magnetic stirrer. All the experiments were conducted at room temperature. The schematic diagram of ultrafiltration unit is presented in Fig. 5.4. Ultrafiltration was carried out for 10 min at various transmembrane pressures. Before ultrafiltration of aqueous solutions containing pollutants, pure Triton X-100 and APU aqueous solution were filtrated to examine rejection of these materials from permeated aqueous solution at the same ultrafiltration condition. Concentration of APU and Triton X-100 were varied in the range 125–1000 mg/L and operating pressure was fixed at 2 kgf/cm^2 . The rejection (R) is defined as follows:

$$R = 1 - \frac{C_{per}}{C_{feed}}$$

where C_{feed} and C_{per} are the concentrations of solute in feed and permeate solutions, respectively.

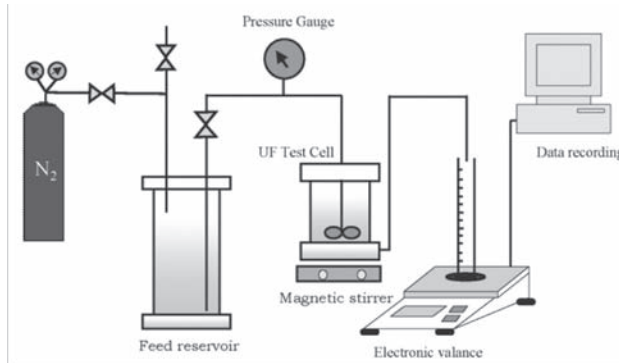


Figure 5.4 Schematic presentation of a dead-end stirred cell filtration system. Reprinted from *J. Ind. Eng. Chem.*, 13(6), K. Shim, I. -S. Park, and J. -Y. Kim, Use of amphiphilic polymer nanoparticles as a nano-absorbent for enhancing efficiency of micelleenhanced ultrafiltration process, 917, Copyright (2007), with permission from Elsevier.

For ultrafiltration of aqueous solution containing pollutants, hydrophobic pollutants and metal ions were added to APU aqueous

solutions and, then mixed by magnetic stirrer over 12 h. Prepared aqueous solutions were ultrafiltrated under the same condition used for ultrafiltration of neat APU aqueous solutions. To investigate the effects of APU concentration on rejection ratio of pollutants, four different concentrations of APU aqueous solution (125, 250, 500, and 1000 mg/L) were used at the constant concentration of hydrophobic pollutants (1000 mg/L) and metal ionic concentration (1000mg/L). The rejection (R) of hydrophobic pollutants and metal ions was also measured using previously mentioned equation. Concentrations of APU and hydrophobic pollutants at permeate solution were analyzed by total organic carbon analyzer (TOC) and UV-vis spectrophotometer. Concentration of metal ions was determined using inductively coupled plasma optical emission spectrometers (ICP-OES).

5.3 SOLUBILIZING PERFORMANCE AND INTERFACIAL ACTIVITY OF APU NANOPARTICLES

5.3.1 *In situ* Extraction Efficiency of APU Nanoparticles Compared with Other Surfactants

Amphiphilic molecules, surfactant, can increase the solubility of hydrophobic organic compounds (HOC) in water phase because the hydrophobic core of surfactant micelles can accommodate a certain amount of lipophilic organic compound. This solubilization capability of the surfactant makes it as a useful material for soil-washing process and wastewater treatment process. So, the enhanced solubility of a certain HOC by a surfactant can be used as an index for evaluating a surfactant for soil-washing process and wastewater treatment process of sorbed and solubilized HOC [39–42]. Especially, in MEUF process, surfactant molecules added in aqueous phase should solubilize HOC and be separated by ultrafiltration membrane to remove HOC from water (as illustrated in Fig. 5.3a) [43]. That is, solubilization performance of surfactant for HOC is a very decisive factor for determining the efficiency of a MEUF process. So, to be used at MEUF process instead of a surfactant, CAP nanoparticles should solubilize HOC and be separated by ultrafiltration membrane (see Fig. 5.5b). As follows, solubilizing efficiency of CAP nanoparticles for HOC (phenanthrene) was evaluated and compared with that of SDS.

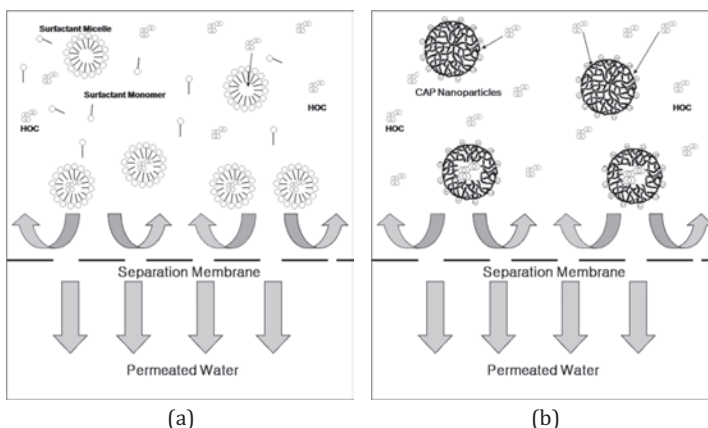


Figure 5.5 Schematic presentation of MEUF filtration mechanism containing (a) surfactant and (b) CAP nanoparticles. Reprinted from *J. Ind. Eng. Chem.*, 13(6), K. Shim, I.-S. Park, and J.-Y. Kim, Use of amphiphilic polymer nanoparticles as a nano-absorbent for enhancing efficiency of micelleenhanced ultrafiltration process, 917, Copyright (2007), with permission from Elsevier.

Solubilization efficiency of a surfactant is generally described in molar solubilization ratio (MSR) or weight solubilization ratio (WSR), but molecular weight of CAP nanoparticles could not be calculated because those particles were formed by cross-linking polymerization of UA. That is, molecular weight of cross-linked polymer can be considered infinite. Solubilization efficiency of CAP nanoparticles as enhanced solubility of phenanthrene in water can be described by the ratio of C/C_0 , where C is the concentration of phenanthrene in aqueous solution containing CAP nanoparticles or SDS and C_0 is the concentration of phenanthrene in pure water phase. So, C/C_0 of CAP nanoparticles should be greater than 1 in order to be a useful material for absorbing and removing phenanthrene dissolved in water. Enhanced solubility (C/C_0) of phenanthrene at various concentrations of SDS or CAP nanoparticles in aqueous solutions is given in Fig. 5.6.

C/C_0 of CAP aqueous solution increased with the increase of concentration of CAP nanoparticles. Even at the lowest concentration (143 mg/L), C/C_0 of CAP nanoparticles was greater than 1, indicating that CAP nanoparticles can solubilize phenanthrene within their hydrophobic interiors just like the solubilization of phenanthrene in surfactant micelles. At the highest concentration (38,000 mg/L), SDS micelles and CAP nanoparticles can solubilize approximately 12

times and 28 times the phenanthrene that an equal amount of pure water will solubilize.

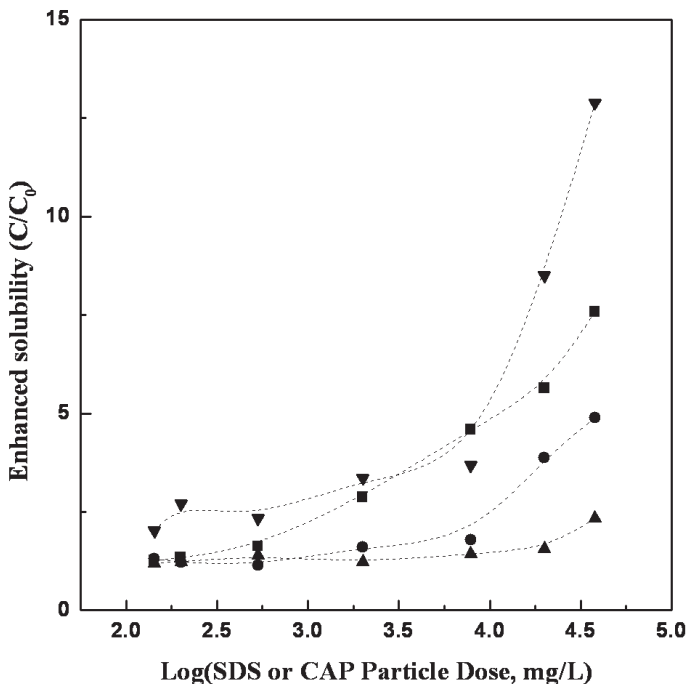


Figure 5.6 Enhanced solubility of phenanthrene at aqueous phase in the presence of SDS or CAP nanoparticles: ■ CAP 64, ● CAP 55, ▲ CAP 28, and ▼ SDS. Reprinted from *J. Ind. Eng. Chem.*, 13(6), K. Shim, I. -S. Park, and J. -Y. Kim, Use of amphiphilic polymer nanoparticles as a nano-absorbent for enhancing efficiency of micelleenhanced ultrafiltration process, 917, Copyright (2007), with permission from Elsevier.

CAP 64 nanoparticles show a better enhanced solubilization performance than CAP 55 and CAP 28 nanoparticles. This difference may be due to the difference of hydrophilicity or hydrophobicity among these nanoparticles. For the synthesis of UAA chains, DMPA introduces hydrophilic carboxylic groups to hydrophobic PTMG-based UA chain backbone, which make water-insoluble urethane acrylate chains dispersible in water and form nanoparticles in water. As the molar ratio of DMPA to PTMG increases in the synthesis of UAA chains, the hydrophilicity of UAA chains increase, resulting in the formation of smaller CAP nanoparticles having higher hydrophilicity. So, UAA 64

chain used in the preparation of CAP 64 nanoparticles was synthesized at the highest molar ratio of PTMG/DMPA, so that CAP 64 nanoparticles have the highest hydrophobicity among CAP nanoparticles, resulting in the highest enhanced solubilization performance of CAP 64.

For the same sense, because UAN chains have two immiscible hydrophilic and hydrophobic segments as parts of the same backbone just like nonionic surfactants have, UAN chains are associated with each other on contacting with water and form micelle-like UAN nanoparticles having polypropylene oxide-based hydrophobic interior and polyethylene oxide-based hydrophilic outer layers. Micelle-like microstructure of UAN nanoparticles was also permanently locked-in by chemical cross-linking polymerization, resulting in the formation of CAP nanoparticles in water. To apply CAP nanoparticles as nano-absorbent for removal of hydrophobic pollutant from water, CAP nanoparticles should have interfacial activity and solubilize hydrophobic molecules. Thus, materials used in MEUF process should also have interfacial activity to solubilize and absorb hydrophobic pollutants effectively. So, surface tensions of SDS and CAP aqueous solutions were examined at various concentrations and has been presented in Fig. 5.7. Like SDS solution, CAP solutions show a decrease of surface tension with the increase of concentration of CAP in the solution. This indicates that CAP nanoparticles also have interfacial activity like surfactants do. Unlike surfactants exhibiting abrupt decrease in surface tension at certain concentration, CAP nanoparticle solutions show gradual and linear decrease in surface tension with the increase of CAP concentration. This very different result between SDS and CAP solution can be interpreted as due to the difference of aqueous pseudophase between SDS and CAP solutions.

For surfactant molecules, at the concentration below CMC, surfactant molecules dissolve in water and exist as monomeric molecules. At the concentration equal to or greater than CMC, surfactant molecules form aggregates (micelle) by the association of surfactant molecules. Surface tension of surfactant solutions shows abrupt change and almost constant values at this CMC. Surfactant micelles are not permanent structure but can break into monomeric surfactant molecules. So, there coexists dissolved surfactant molecules and micelles in aqueous pseudophase of surfactant molecules.

UAN chains have extremely low solubility in water (practically water insoluble), so on contacting with water, UAN chains associate with each other and form nano-aggregates (CAP nanoparticles) at extremely low concentration. That is, UAN chains do not have a certain

concentration for the formation of aggregates; as a consequence, CAP solutions did not show abrupt change in surface tension with the change of CAP concentration.

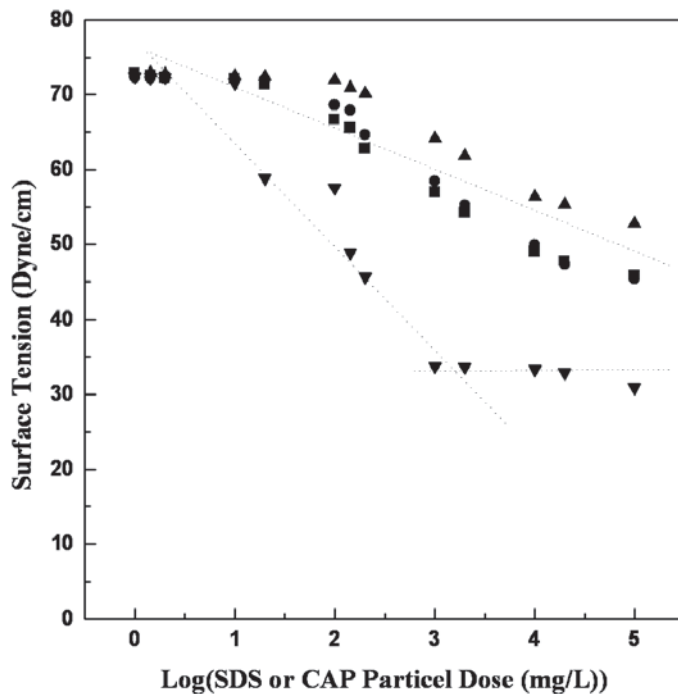


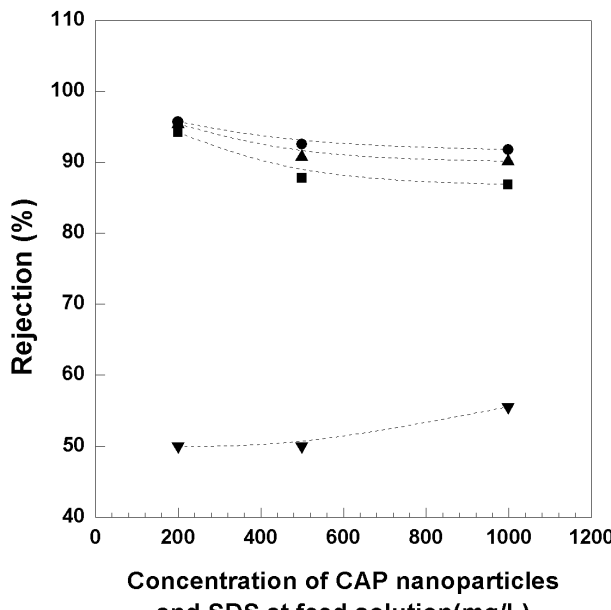
Figure 5.7 Surface tension for SDS and CAP nanoparticle solutions: ■ CAP64, ● CAP 55, ▲ CAP 28, and ▼ SDS. Reprinted from *J. Ind. Eng. Chem.*, 13(6), K. Shim, I. -S. Park, and J. -Y. Kim, Use of amphiphilic polymer nanoparticles as a nano-absorbent for enhancing efficiency of micelleenhanced ultrafiltration process, 917, Copyright (2007), with permission from Elsevier.

5.3.2 Rejection Ratio of SDS and CAP Nanoparticles in UF Membrane

To effectively remove dissolved hydrophobic organic pollutants from water via MEUF process, absorbing material should show very high rejection in UF process. That is, rejection behavior of an absorbing material is the most important factor for efficiency of UF process. So, the rejection behavior of SDS and CAP nanoparticles using the same UF membrane and at the same condition should be examined. Figure

5.8a shows the rejection percentage of CAP and SDS with various concentrations at a constant pressure of 2 kgf/cm^2 through the same UF membrane. The concentration of SDS and CAP nanoparticles was varied from 200–1000 mg/L to examine the removal efficiency of SDS and CAP nanoparticles. At all concentrations, SDS solution shows a very low rejection ratio (below 50%), but all CAP nanoparticle solutions exhibit a higher rejection ratio (almost higher than 90%). This indicates that the UF membrane used in this study can effectively separate CAP nanoparticles only at used condition.

Figure 5.8b shows the rejection percentage of CAP nanoparticles and SDS at different transmembrane pressures, where the concentration of CAP nanoparticles and SDS solution is 200 mg/L. Rejection percentage of CAP nanoparticles is also higher than that of SDS at all transmembrane pressures. CAP nanoparticles show almost constant rejection percentage with the increase of applied transmembrane pressure. This can be explained as due to no change of morphology and size of CAP nanoparticles at higher applied pressure. As CAP nanoparticles have chemically cross-linked structure, they can maintain their morphology and size at higher applied pressure. However, SDS solution showed a little increase of rejection percentage at higher applied pressure, which can be explained as due to the breakage of surfactant micelles and adsorption onto the membrane surface.



(a)

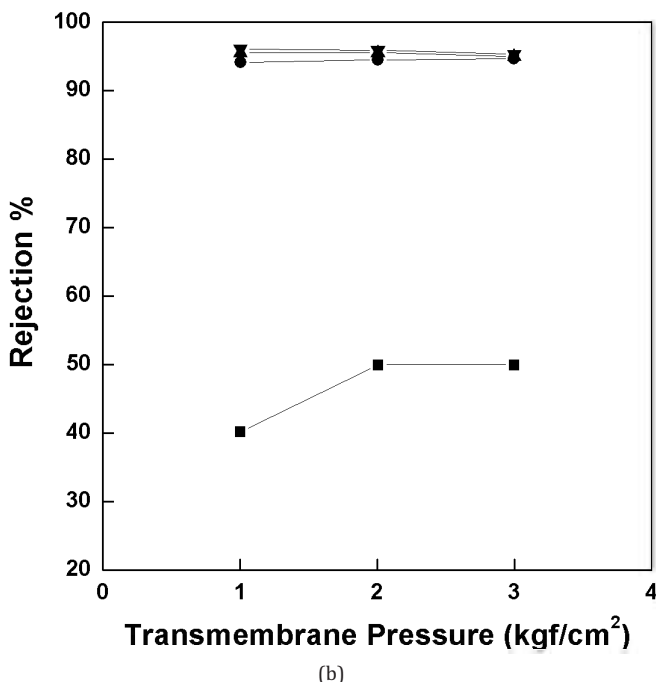
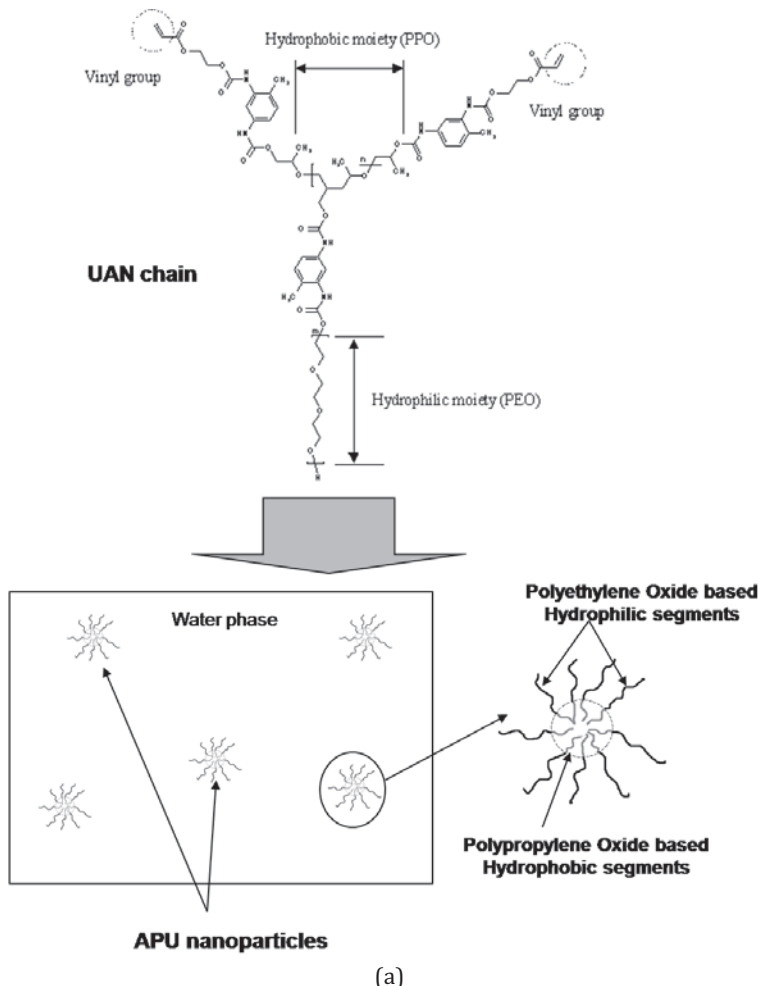


Figure 5.8 (a) Rejection % of SDS and CAP nanoparticles as a function of concentration at a constant pressure of 2 kgf/cm² in the absence of phenanthrene. (b) Rejection % of SDS and CAP nanoparticles as a function of transmembrane pressure at a constant concentration of SDS and CAP nanoparticles (200 mg/L) (● CAP 28, ▲ CAP55, ■ CAP 64. ▼ SDS solution). Reprinted from *J. Ind. Eng. Chem.*, 13(6), K. Shim, I.-S. Park, and J.-Y. Kim, Use of amphiphilic polymer nanoparticles as a nano-absorbent for enhancing efficiency of micelleenhanced ultrafiltration process, 917, Copyright (2007), with permission from Elsevier.

The sizes of APU nanoparticles and Triton X-100 micelles were 42 nm and 5.76–7.62 nm, respectively. Pore size of UF membrane used in our system was 0.025 mm (25 nm), which was smaller than APU nanoparticles but bigger than Triton X-100 micelles. So, it can be thought that the bigger size of APU nanoparticles, capable of solubilizing hydrophobic molecules, caused much higher rejection recovery of APU nanoparticles. Triton X-100 micelles formed by physical association of Triton X-100 monomeric molecules are not permanent structure, so their micelles are easily breakdown into monomeric molecules, which penetrate through membrane pores.

However, even though APU nanoparticles are formed by physical association of UAN chains, the microstructures of APU nanoparticles are permanently locked-in by chemical cross-linking reaction, so that the APU nanoparticles can maintain their microstructure during filtration process. As a consequence, there are no dissolved UAN chains that can go through the membrane pores in aqueous feed solutions. This difference of size and microstructure between Triton X-100 and APU nanoparticles is schematically presented in Fig. 5.9.



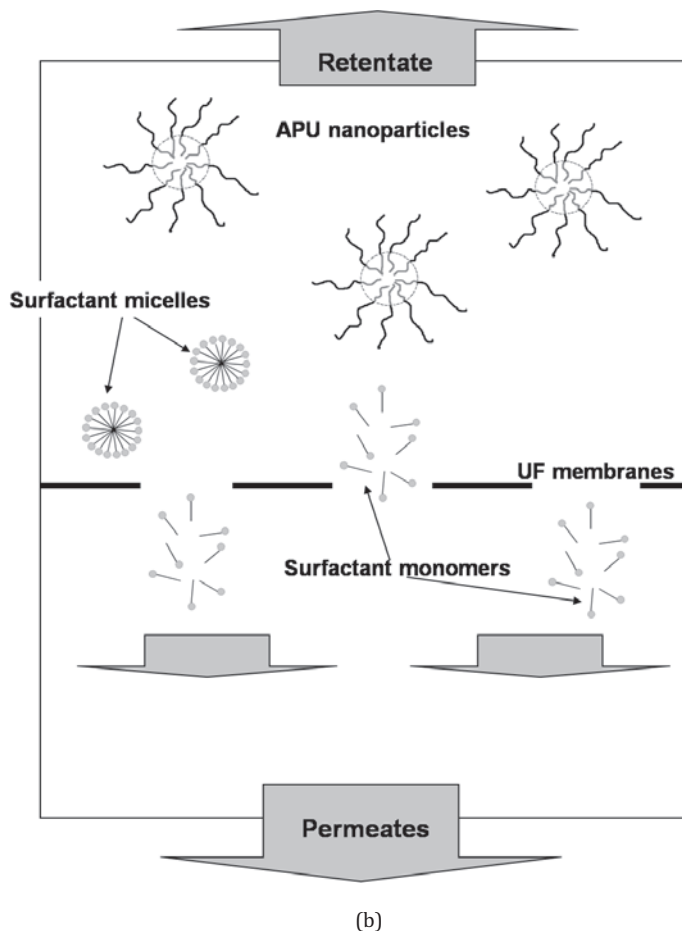


Figure 5.9 Schematic presentation of (a) molecular structure of UAN chains and APU nanoparticles dispersed in water and (b) MEUF filtration mechanism containing Triton X-100 and APU nanoparticles. Reprinted from *J. Ind. Eng. Chem.*, 14, S. -I. Noh, J. K. Shim, and J. -Y. Kim, New amphiphilic polymer nanoparticle-enhanced UF process for removal of organic pollutants and metal ions, 480, Copyright (2008), with permission from Elsevier.

5.3.3 Rejection Ratio of Metal Ions in the Presence of APU Nanoparticles

Amphiphilic polyurethane nanoparticles, formed by amphiphilic urethane acrylate, represent a microphase-separated structure similar to that of surfactant micelles and can form very stable

dispersions in aqueous phase. In the case of anionic cross-linked polyurethane nanoparticles dispersed in aqueous phase for the extraction of sorbed phenanthrene from aquifer materials, these nanoparticles were shown to adsorb weakly to a sandy aquifer in batch experiments, which is attributed to the chemically cross-linked nature of their microstructure. In most of the tests with the anionic cross-linked polyurethane nano-network emulsions, a very high level (95%) of the hydrophobic tested pollutant (phenanthrene) was extracted from the aquifer sand with extremely low loss of the applied nanoparticles. Relatively few pore volume washings were needed to achieve a high level of remediation. However, these anionic polyurethane nanoparticles were easily and rapidly aggregated in the presence of ionic compounds such as CaCl_2 , MgCl_2 , etc. This finding indicate that polyurethane nanoparticles can be stable in aqueous solution containing large amount of ionic compounds. A new kind of amphiphilic urethane acrylate nonionomer (UAN) chain that has hydrophilic polyethylene oxide (PEO) pendant chain and polypropylene oxide (PPO)-based hydrophobic backbone is synthesized. This chain can form very stable amphiphilic polyurethane (APU) nanoparticles in aqueous phase whose structure is similar to that of nonionic surfactant micelle.

Figure 5.10 shows rejection ratio of metal ions having various electron valences through UF process in the presence of APU nanoparticles. The trans membrane pressure and concentration of metal ions were also fixed as 2 kgf/cm^2 and 1000 mg/L , respectively. At the same electron valence (bivalent ions), the order of rejection ratio was Mg^{2+} , Ni^{2+} , and Cu^{2+} . Comparing rejection ratio at various electron valences, higher rejection ratio was obtained at higher electron valence, that is, Cr^{3+} ions showed higher rejection ratio than Ni^{2+} and Cs^+ ions in the same UF condition. These results can be explained as due to difference of affinity between metal ions and APU nanoparticles. It has been known that polyethylene oxide chain can make complex with various metal ions, and polymers or oligomers containing polyethylene oxide chains can dissolve various metal salts without the use of a solvent [44, 45]. So, rejection of metal ions through UF in the presence of APU nanoparticles can be interpreted as due to the formation of complex between metal ions and hydrophilic polyethylene oxide segments of APU nanoparticles. As illustrated in Fig. 5.9a, UAN chains have hydrophobic polypropylene oxide (PPO)-based segment and hydrophilic polyethylene oxide (PEO) segment at the same chain. Water is a good solvent for PEO segments in UAN chains but nonsolvent for PPO chains. On contacting with water, PEO

segments in UAN chains are microphase separated from hydrophobic segment and oriented toward water phase to form outer layer, while hydrophobic PPO-based segments are associated with each other to form hydrophobic interior, leading to form micelle-like nano-sized aggregates of UAN chains in water. These aggregate structures of APU nanoparticles are permanently locked-in by chemical cross-linking reaction and form micelle-like polymer nanoparticles (APU nanoparticles). On contacting APU nanoparticles with metal ions, PEO segments in outer layer of APU nanoparticles make complex with metal ions, a consequence, metal ions are rejected through UF process. So, difference in rejection ratio between metal ions can be explained as difference in the affinity between metal ions and PEO segments of APU nanoparticles.

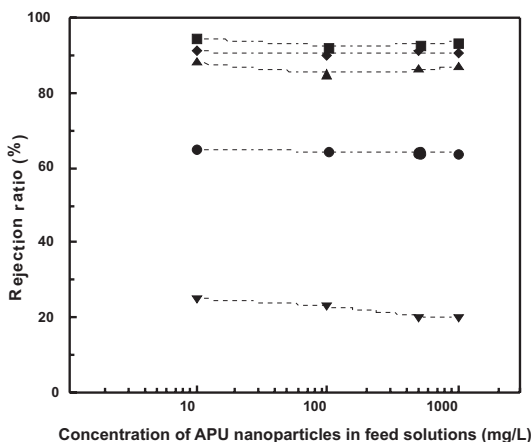


Figure 5.10 Rejection of metal ions via ultrafiltration as a function of concentration at a constant pressure of 2 kgf/cm² ((■) Mg²⁺, (●) Cu²⁺, (▲) Ni²⁺, (▼) Cs⁺, and (◆) Cr³⁺). Reprinted from *J. Ind. Eng. Chem.*, 14, S.-I. Noh, J. K. Shim, and J.-Y. Kim, New amphiphilic polymer nanoparticle-enhanced UF process for removal of organic pollutants and metal ions, 480, Copyright (2008), with permission from Elsevier.

5.4 CONCLUSION

Even though surfactants have a better solubilization efficiency for phenanthrene, in the low concentration range, APU nanoparticles dispersed in an aqueous phase exhibited better extraction performance than did the surfactants in both batch and column tests. The soil-washing performance of APU nanoparticles was

better than those of the surfactants, especially at longer soil contact times. This is because a smaller amount of APU nanoparticles was sorbed on the soil, owing to their chemically cross-linked structure. It can be concluded that the chemically cross-linked structure of APU nanoparticles causes its lower degree of sorption on the soil, even at longer residence times within soil column, which results in better *in situ* soil-washing performance compared with surfactants that have a higher degree of sorption on the soil. As the size of APU nanoparticles is much greater than that of surfactant micelles, APU nanoparticles could be recovered 100% through ultrafiltration process at greater pore size of separation membrane. Low concentration and degree of sorption to the soil would make soil-washing process using APU nanoparticles economical and useful in practical applications. Consequently, the APU nanoparticles are as follows:

1. Cheaper and easier (simpler) synthetic process than amphiphilic block copolymer (ABCs).
2. Bigger than surfactant micelle (20–100 nm).
3. Easy to vary length and ratio of hydrophilic/hydrophobic segments.
4. Very strong nano-structure owing to chemical cross-linking.
5. Lower degree of sorption onto a soil.
6. Extremely low CMC and adsorption.

There are needs for the investigation about *in situ* extraction of pollutants and recycling and reuse of APU nanoparticles at field scale in future work.

References

- [1] S. Hyuk Im et al. (2005). Polymer hollow particles with controllable holes in their surfaces, *Nature Mat.*, **4**, 671.
- [2] R. O. Dunn Jr., J. F. Scamehorn, S. D. Christian (1985). Ultrafiltration and alumina adsorption of micelles for the preconcentration of copper(II) in water, *Sep. Sci. Technol.*, **20**, 257.
- [3] R. O. Dunn Jr., J. F. Scamehorn, S. D. Christian (1987). Concentration polarization effects in the use of micellar-enhanced ultrafiltration to remove dissolved organic pollutants from wastewater, *Sep. Sci. Technol.*, **22**, 763.
- [4] M. K. Purkait, S. DasGupta, S. De (2005). Separation of aromatic alcohols using micellar-enhanced ultrafiltration and recovery of surfactant, *J. Membr. Sci.*, **250**, 47.

- [5] F. I. Talens-Alesson, R. Urbanski, J. Szymanowski (2001). Evolution of resistance to permeation during micellar enhanced ultrafiltration of phenol and 4-nitrophenol, *Colloid Surf. A*, **178**, 71.
- [6] J. Sabate, M. Pujola, J. Llorens (2002). Comparison of polysulfone and ceramic membranes for the separation of phenol in micellar-enhanced ultrafiltration, *J. Colloids Interface Sci.*, **246**, 157.
- [7] S. R. Jadhav, N. Verma, A. Sharma, P. K. Bhattacharya (2001). Flux and retention analysis during micellar enhanced ultrafiltration for the removal of phenol and aniline, *Sep. Purif. Technol.*, **24**, 541.
- [8] K. H. Choo, S. C. Han, S. J. Choi (2007). Use of chelating polymers to enhance manganese removal in ultrafiltration for drinking water treatment, *J. Ind. Eng. Chem.*, **13**(2), 163.
- [9] D. A. Edwards, Z. Adeel, R. G. Luthy (1994). Distribution of nonionic surfactant and phenanthrene in a sediment/aqueous system, *Environ. Sci. Technol.*, **28**, 1550.
- [10] J. W. Tester, H. R. Holgate, F. J. Armellini, P. A. Webley, W. R. Killiea, H. E. Barner, G. T. Hong, in: D. W. Tedder, F. G. Pohland (eds) (1993). Emerging technologies in hazardous waste management, ACS Symposium Series, 518, American Chemical Society, Washington, DC.
- [11] B. Krebbs-Yuill, J. H. Harwell, D. A. Sabatini, R. C. Knox (1995). Surfactant-enhanced subsurface remediation: Emerging technologies, ACS Symposium Series 594: American Chemical Society, Washington, DC.
- [12] D. Zhao, J. J. Pignatello, J. C. White, W. Braida, F. Ferrandino (2001). Dual-mode modeling of competitive and concentration-dependent sorption and desorption kinetics of polycyclic aromatic hydrocarbons in soils, *Water Resour. Res.*, **37**(8), 2205.
- [13] S. Deshpande, L. Wesson, D. Wade, D. A. Sabatini, J. H. Harwell (2000). DOWFAX surfactant components for enhancing contaminant solubilization, *Water Res.*, **34**(3), 1030.
- [14] K. D. Pennell, L. M. Abriolar, W. J. Weber Jr. (1993). Surfactant-enhanced solubilization of residual dodecane in soil columns, *Environ. Sci. Technol.*, **27**, 2332.
- [15] C. C. West, and J. H. Harwell (1992). Surfactants and subsurface remediation, *Environ. J. Sci. Technol.*, **26**(12), 2324.
- [16] D. A. Edwards, R. G. Luthy, and Z. Liu (1991). Solubilization of polycyclic aromatic hydrocarbons in micellar non-ionic surfactant solutions, *J. Environ. Sci. Technol.*, **25**, 127.
- [17] G. N. Kim, W. K. Choi, C. H. Jung (2007). Development of a washing system for soil contaminated with radionuclides around TRIGA reactors, *J. Ind. Eng. Chem.*, **13**, 406.

- [18] S. Förster, and M. Antonietti (1998). Amphiphilic block copolymers in structure-controlled nanomaterial hybrids, *Adv. Mater.*, **10**(3), 195.
- [19] L. W. Canter, and R. C. Knox (1986). *Ground Water Pollution Control*, Lewis Publishers Inc., Chelsea, MI.
- [20] J. L. Haley, B. Hanson, C. Enfield, and J. Glass (1991). Evaluating the effectiveness of groundwater extraction systems. *Ground Water Monit. Rev.*, **11**, 119.
- [21] J. H. Harwell (1992). Transport and remediation of subsurface contaminants, in: Sabatini, D.A., Knox. R.C. (eds), ACS Symposium Series 491, American Chemical Society, Washington, DC, p. 124
- [22] Douglas M. Mackay, John A. Cherry (1989). Groundwater contamination: pump-and-treat remediation, *Environ. Sci. Technol.*, **23**(6), 630.
- [23] J. F. McCarthy, J. M. Zachara (1989). Subsurface transport of contaminants, *Environ. Sci. Technol.*, **23**(3), 496.
- [24] I. T. Yeom, M. M. Ghosh, C. D. Cox (1996). Kinetics aspects of surfactant solubilization of soil-bound polycyclic aromatic hydrocarbons, *Environ. Sci. Technol.*, **30**, 1589.
- [25] W. H. Noordman, J. -W. Bruining, P. Wietzes, and D. B. Janssen (2000). Facilitated transport of a PAH mixture by a rhamnolipid biosurfactant in porous silica matrices, *J. Contam. Hydrol.*, **44**, 119.
- [26] R. R. Kommalapati, R. T. Valsaraj, W. D. Constant, D. Roy (1997). Aqueous solubility enhancement and desorption of hexachlorobenzene from soil using a plant-based surfactant, *Water Res.*, **31**(9), 2161.
- [27] G. G. Liu, D. Roy, M. J. Rosen (2000). A simple method to estimate the surfactant micelle-water distribution coefficients of aromatic hydrocarbons, *Langmuir*, **16**, 3595.
- [28] Jiunn-Fwu Lee, P. M. Liao, C. C. Kuo, H. T. Yang, C. T. Chiou (2000). Influence of a nonionic surfactant (Triton X-100) on contaminant distribution between water and several soil solids, *J. Colloid Interf. Sci.*, **229**, 445.
- [29] W. Chu, W. S. So (2001). Modeling the two stages of surfactant-aided soil washing, *Water Res.*, **35**(3), 761.
- [30] D. Zhao, J. J. Pignatello, J. C. White, W. Braida, F. Ferrandino (2001). Sorption and desorption kinetics of polycyclic aromatic hydrocarbons in soils, *Water Resourc. Res.*, **37**(8), 2205.
- [31] S. Deshpande, L. Wesson, D. Wade, D. A. Sabatini, J. H. Harwell (2000). Dowfax surfactant components for enhancing contaminant solubilization, *Water Res.*, **34**(3), 1030.
- [32] K. Urum, T. Pekdemir, M. Copur (2004). Surfactants treatment of crude oil contaminated soils, *J. Colloid Interf. Sci.*, **276**, 456.

- [33] Zhongming Zhen, Jeffrey P. Obbard (2002). Evaluation of an elevated non-ionic surfactant critical micelle concentration in a soil/aqueous system, *Water Res.*, **36** 2667.
- [34] R. A. Doong, W. G. Lei (2003). Solubilization and mineralization of polycyclic aromatic hydrocarbons by *pseudomonas putida* in the presence of surfactant, *J. Hazard. Mater.*, **96**, 15.
- [35] S. Forster, M. Antonietti (1998). Amphiphilic block copolymers in structure-controlled nanomaterial hybrids, *Adv. Mater.*, **10**(3), 195.
- [36] A. B. R. Mayer (2001). Colloidal metal nanoparticles dispersed in amphiphilic polymers, *Polym. Adv. Technol.*, **12**, 96.
- [37] R. Gangopadhyay, and D. Amitabha (2000). Conducting polymer nanocomposites: a brief overview, *Chem. Mater.*, **12**, 608.
- [38] W. Tungittiplakorn, L. W. Lion, C. Cohen, and J. Y. Kim (2004). Engineered polymeric nanoparticles for soil remediation, *Environ. Sci. Technol.*, **38**, 1605.
- [39] D. Rouse, D. A. Sabatini, and J. H. Harwell (1993). Minimizing surfactant losses using twin-head anionic surfactants in subsurface remediation, *Environ. Sci. Technol.*, **27**, 2072.
- [40] B. J. Shiau, D. Sabatini, J. H. Harwell (1994). Solubilization and microemulsification of chlorinated solvents using direct food additive (edible) surfactants, *Ground Water*, **32**, 561.
- [41] B. Krebbs-Yuill, J. H. Harwell, D. A. Sabatini, and R. C. Knox (1995). Surfactant-enhanced subsurface remediation: Emerging technologies; ACS Symposium Series 594, American Chemical Society, Washington, DC.
- [42] G. N. Kim, M. Narayan, and H. J. Won (2006). Separation of hot particulate from a PFC decontamination solution for reuse by filtration equipment, *Korean Ind. Eng. Chem.*, **12**, 531.
- [43] J. K. Shim, I. -S. Park, and J. -Y. Kim (2007). Use of amphiphilic polymer nanoparticles as a nano-absorbent for enhancing efficiency of micelle-enhanced ultrafiltration process, *J. Ind. Eng. Chem.*, **13**(6), 917.
- [44] S. -I. Noh, J. K. Shim, and J. -Y. Kim (2008). New amphiphilic polymer nanoparticle-enhanced UF process for removal of organic pollutants and metal ions, *J. Ind. Eng. Chem.*, **14**, 480.
- [45] J. -Y. Kim, H. M. Kim, D. H. Shin, and K. J. Ihn (2006). Synthesis of CdS nanoparticles dispersed within poly(urethane acrylate-co-styrene) films using an amphiphilic urethane acrylate nonionomer, *Macromol. Chem. Phys.*, **207**, 925.

Chapter 6

NANOPARTICLES FOR FUEL CELL APPLICATIONS

Chang Hyun Lee

*Macromolecules and Interfaces,
Virginia Polytechnic Institute and State University,
Blacksburg, VA 24061, USA
changlee@vt.edu*

Well-dispersed nanoparticles contribute to improved thermal/mechanical/chemical/electrochemical properties of proton-conductive polymer electrolytes for fuel cells such as proton exchange membrane fuel cell (PEMFC) and direct methanol fuel cell (DMFC) via the combination with intrinsic properties derived from polymers themselves (synergistic effect). These enhanced properties are vital to high electrochemical fuel cell performance for a long period of time.

6.1 THE USE OF NANOPARTICLES FOR FUEL CELL APPLICATIONS

Fuel cells are environment friendly and highly efficient energy generation systems, which directly convert the chemical energy of various fuels, such as hydrogen, methane, methanol, and even gasoline, to electric energy (Health & Revfsz, 1973; Jacobson et al., 2005). The fuel cells can replace the internal combustion engine in vehicles as well as power generation system in stationary and

Advances in Nanotechnology and the Environment

Edited by Juyoung Kim

Copyright © 2012 by Pan Stanford Publishing Pte. Ltd.

www.panstanford.com

portable power applications. Some important issues must be addressed for fuel cell technology to gain a considerable share of the electric power market. These issues include feasible material selection such as electrocatalysts for anode and cathode and proton-conductive electrolyte (e.g., proton exchange membrane (PEM)) (Steele & Heinzel, 2001). The polymer electrolytes need following properties: (1) high proton conductivity under various fuel cell operation conditions including high temperature and/or low humidity, (2) good mechanical, chemical, and thermal strength, (3) low fuel permeability (i.e., hydrogen/oxygen and methanol in PEMFC and DMFC, respectively), and (4) low production cost.

Until now, there have been a variety of approaches to meet these requirements. They include:

- (1) Modified perfluorosulfonic acid ionomers (PFSI, e.g., Nafion®) (Zaluski & Xu, 1994; Yang & Rajendran, 2005; Tsang et al., 2007; Gibon et al., 2008);
- (2) Sulfonated hydrocarbon polymers (Wang et al., 2002; Zhou et al., 2006; Norsten et al., 2006; Yamaguchi et al., 2007; Miyatake et al., 2007);
- (3) Acid-based complexes (Jiang et al., 2006; Argun et al., 2008);
- (4) Organic–inorganic hybrids or composites (Chen et al., 2005; Pereira et al., 2008).

Here, the designation of “composite” is used to describe all membranes comprising an inorganic and an organic component. Meanwhile, the term “hybrid” is reserved for membranes with the fabrication history of *In situ* formation of the inorganic component in the state of the polymer membrane or solution.

Recently, adding inorganic fillers and particles to organic polymer electrolytes that serve as the matrix components has been a subject of growing interest in fuel cell researches since the inorganic additives can induce improved electrolyte properties to a certain level when used appropriately. Potential candidates are silica (Li & Nogami, 2002; Chen et al., 2005), zeolite (McKeen et al., 2008), heteropolyacids (Kim et al., 2003; Ponce et al., 2003), carbon nanotube (Kannan et al., 2008), and so on. Most of the inorganic components have high surface area, large porous volume, and excellent mechanical and thermal stability.

The most important concern in making corresponding organic–inorganic composites is to disperse the inorganic components

homogeneously in polymer matrices and to minimize their self-agglomeration occurred owing to physical interaction derived from inorganic surface functionalities (e.g., $-\text{CH}_3$, $-\text{OH}$, $-\text{COOH}$, or $-\text{SO}_3\text{H}$). Generally, well-dispersed inorganic solids can form good interface between inorganic and organic components and, also, improve the probability of materials synergism. However, the aggregated inorganic components may induce nonselective cavities or uneven distribution in the polymers, leading to uncontrolled or decreased PEM properties as well as mechanical brittleness.

In this chapter, some approaches to enhance inorganic dispersion for desirable composite formation are described. Furthermore, detailed investigation to correlate macroscopic properties of composite membranes (water retention property, fuel barrier property, improved dimensional stability, proton-conducting properties, and comprehensive electrochemical properties) with identity, shape, and size of inorganic components and the nature of the interaction between organic and inorganic components was conducted.

6.2 DIRECT MIXING OF INORGANIC AND ORGANIC COMPONENTS

6.2.1 Simple Direct Mixing

This method employs a successive procedure of the simple mixing of prepared inorganic oxides or conductors (Tables 6.1 and 6.2) in the powder form with a polymer solution, solution casting, and film formation after drying. Both proton-conducting ionomers (e.g., sulfonated polymers) and nonsulfonated polymers can be used as polymer matrices. When the inorganic fillers (<5 wt.%) are added into the proton-conducting polymer media, the main roles of the inorganic components are to improve water management and/or to reduce fuel crossover (H_2 , O_2 , or methanol), since proton conductivity of the polymeric components is sufficiently high to be applied for fuel cells. However, the amount of inorganic conductors (e.g., 30–70 wt.%) in nonsulfonated polymers should be high to secure desirable proton conduction level, which may be accompanied by mechanical brittleness.

The direct mixing gives rise to heterogeneity in both the size of inorganic agglomerates and dispersion state, which disturbs the manifestation of reproducible physico-chemical properties. For example, heteropolyacids (Zaidi et al., 2000) and boron phosphate (Mikhailenko et al., 2001) were heterogeneously dispersed in sulfonated poly(ether ether ketone) (SPEEK) matrix with different agglomerate size ranges of 50–150 nm and 100–300 nm, respectively. In the corresponding composites, membrane porosity significantly increased (pore diameter = 3–10 μm) showing irregular pore distribution (Fig. 6.1).

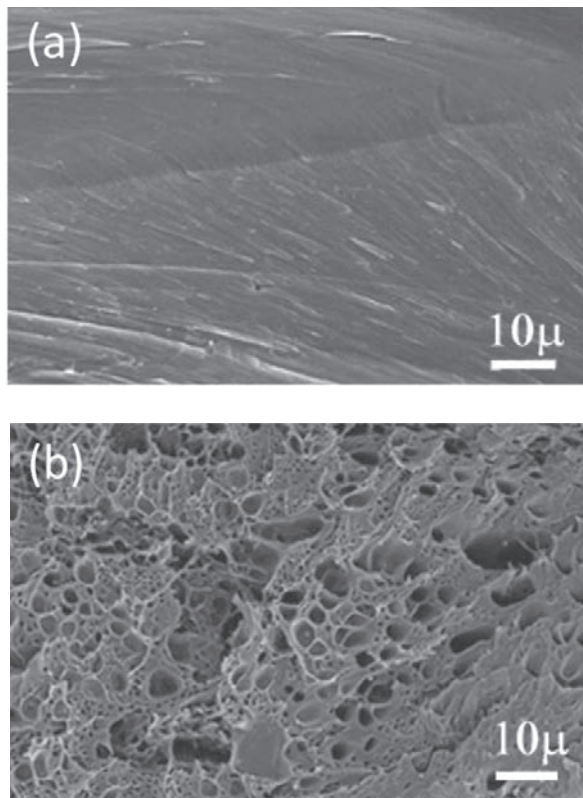


Figure 6.1 Scanning electron microscopy (SEM) images of (a) pure PEEK and (b) BPO₄-SPEEK composite with 40 wt.% content of BPO₄). Reprinted from *Cat. Today*, 67, Mikhailenko, S. D., Zaidi, S. M. J. and Kaiaguine, S., Sulfonated polyether ether ketone based composite polymer electrolyte membranes, 225–236, Copyright (2001), with permission from Elsevier.

Table 6.1 Inorganic oxides and acids used for organic–inorganic composite formation and their proton-conduction capability

	Inorganic components	Proton conductivity [Scm ⁻¹]	Testing condition	References
Inorganic oxides	Zr(O ₃ PC ₂ H ₅) _{1.15} Y _{0.85}	6×10 ⁻⁷ 2×10 ⁻³ 4×10 ⁻⁶	100°C and 0% RH 100°C and 60% RH 170°C and 0% RH	Alberti and Casciola (1997)
	(P ₂ O ₅) ₄ (ZrO ₂) ₃ glass	1×10 ⁻²	90°C and 50% RH	Grot and Rajendran (1999)
	P ₂ O ₅ –ZrO ₂ –SiO ₂ glass	5×10 ⁻³	90°C and 50% RH	Nogami et al. (1997)
	Ba ₂ YSnO _{5.5}	1×10 ⁻⁴ 1×10 ⁻⁵	120°C and 0% RH 200°C and 0% RH	Kreuer (1997)
	Tetraethylorthosilicate (TEOS)	NA	–	Wilkes et al. (1990)
	Montmorillonite (MMT)		–	Hasani-Sadrabadi et al. (2008)
	TiO ₂		–	Watanabe et al. (1996)
	ZrO ₂		–	Aricò et al. (2004)
	SiO ₂ (Aerosil®)		–	Lee et al. (2007, 2010); Mulmi et al. (2009); Park et al. (2009); Kim et al. (2006)
Inorganic acids	CsDSO ₄	5×10 ⁻⁶ 5×10 ⁻²	140°C and 0% RH 152°C and 0% RH	Kirpichnikova et al. (1997)
	CsHSO ₄	3×10 ⁻⁷ 1×10 ⁻² 2×10 ⁻²	130°C and 0% RH 150°C and 0% RH 200°C and 0% RH	Pawlowski et al. (1990)
	BPO ₄	7×10 ⁻²	30°C and 100% RH	Mikhailenko et al. (2001)

Table 6.2 Heteropolyacids used for organic–inorganic composite formation and their proton-conduction capability.

Inorganic components	Proton conductivity (Scm ⁻¹)	Testing condition	References
$\alpha\text{-Zr(O}_3\text{PCH}_2\text{OH)}_{1.27}(\text{O}_3\text{PC}_6\text{H}_4\text{SO}_3\text{H})_{0.73}\cdot n\text{H}_2\text{O}$	8×10^{-3} 1×10^{-5}	100°C and 60% RH 180°C and 0% RH	Alberti et al. (1992a, 1992b) Alberti et al. (1992b)
$\gamma\text{-Zr(PO}_4\text{)(H}_2\text{PO}_4\text{)}_{0.54}(\text{HO}_3\text{PC}_6\text{H}_4\text{SO}_3\text{H})_{0.46}\cdot n\text{H}_2\text{O}$	5×10^{-2}	100°C and 95% RH	Alberti et al. (1996)
$\text{Zr(O}_3\text{PCH}_2\text{OH)}_{1.27}\text{Y}_{0.73}\cdot n\text{H}_2\text{O}$	1×10^{-5} 1×10^{-2}	100°C and 0% RH 100°C and 60% RH	Alberti and Casciola (1997)
$\alpha\text{-Zr(O}_3\text{PC}_6\text{H}_4\text{SO}_3\text{H)}\cdot 3.6\text{H}_2\text{O}$	2×10^{-2}	105°C and 85% RH	Stein et al. (1996)
$\alpha\text{-Zr(O}_3\text{POH)}\cdot \text{H}_2\text{O}$	5×10^{-6} 1×10^{-4}	100°C and 60% RH 100°C and 95% RH	Casciola et al. (1993)
$\beta\text{-Cs}_3(\text{HSO}_4)_2(\text{H}_x\text{(P,S)O}_4)$	3×10^{-5} 1×10^{-2} 1.6×10^{-2}	90°C and 0% RH 150°C and 0% RH 200°C and 0% RH	Haile et al. (1997)
Phosphotungstic acid	-	-	Staiti et al. (2001)
Silicotungstic acid	-	-	Staiti et al. (2001)
Tungstophosphoric acid ($\text{H}_3\text{PW}_{12}\text{O}_{40}\cdot 29\text{H}_2\text{O}$)	2×10^{-1}	Liquid water at 30°C	Zaidi et al. (2000)
Molybdophosphoric acid ($\text{H}_3\text{PO}_4\cdot 12\text{MoO}_3\cdot x\text{H}_2\text{O}$)	-	-	Zaidi et al. (2000)

A facile way for good inorganic dispersion within polymer matrices is to use adequate surface-functionalized nanoparticles (hydrophilic or hydrophobic characteristics). Hydrophilic inorganic components show high compatibility with sulfonated polymers. The hydrophilic functional groups on inorganic surface may drive physical interaction (e.g., ionic and hydrogen bond) with polymer matrices. For instance, hydrophilic silica (SiO_2) with hydroxyl (-OH) groups on its surface was relatively easily mixed after ultrasonic or homogenizer treatment with dispersed or suspended sulfonated polymers (e.g., Nafion® or sulfonated polystyrenes) in hydrophilic solvents (e.g., methanol, ethanol, isopropyl alcohol, and butanol) (Watanabe et al., 1996; Stonehart & Watanabe, 1996). The well-dispersed SiO_2 was advantageous to maintaining high water retention level at high temperatures over 130°C and, also, to lowering methanol permeation to the level of 10^{-3} of unmodified Nafion® when the composite was used for DMFC. Even in this way, the concentration of inorganic components to polymer components acts as an important factor in determining the mechanical properties and free volume elements for accessible water and/or ion transport. High concentration of the inorganic components leads to unfavorable loss in mechanical properties.

6.2.1 Advanced Direct Mixing Based on Dispersants

A new strategy is to maximize additive effects by incorporating the smallest amount of inorganic nanoparticles with amphiphilic surfactants. A representative surfactant is a family of triblock copolymer (ABA block, A = polyethylene oxide (PEO) and B = polypropylene oxide (PPO), e.g., Pluronic®), which has been used as detergent, forming agent, lubricant, and drug delivering agent (Velichkova & Christova, 1995; Kabanov et al., 2002; Causse et al., 2005; Ortona et al., 2006; Rajam & Ho, 2006). The amphiphilic surfactant was also used as a dispersant with hydrophilic and hydrophobic balance for distributing nanosized inorganic particles (e.g., hydrophilic or hydrophobic SiO_2) (Lee et al., 2007, 2010). Over critical micelle concentration (e.g., 4.3 mg/mL in *m*-cresol determined by a dynamic light scattering, Lee et al., 2010), the surfactant forms micelle structures composed of hydrophobic core (PPO segments) and hydrophilic outer shells (PEO segments) in aqueous medium (Fig. 6.2) (Alexandridis & Hatton, 1995; Yang et al., 2000; Mata et

al., 2005; Portehault et al., 2006). The micelle diameter of surfactant (e.g., Pluronic® L64)-SiO₂ (Aerosil® 200 with the diameter size of 12 nm) mixture becomes bigger than that of the surfactant, indicating the coverage of the nanoparticles with L64 micelle. It prevents SiO₂ nanoparticle agglomeration even after mixing with viscous polymer solution.

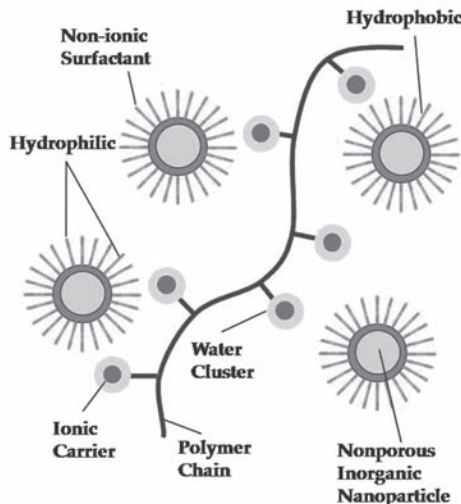


Figure 6.2 Nanoscale dispersion of surface-functionalized inorganic particles around hydrophilic segments of polymer matrix via micelle formation using surfactants.

Figure 6.3 shows the change of SiO₂ distribution patterns depending on the use of the surfactant (Lee et al., 2010). In spite of the use of -OH functionalized SiO₂ (e.g., Aerosil® 200) in a sulfonated polymer, a small amount of SiO₂ (1 wt.% per polymer) caused local agglomeration of the fine particle (Fig. 6.3a), resulting in nonselective cavity formation at the interface between the nanoparticles and polymer matrix. In contrast, the agglomeration disappeared after using the surfactant. The existence of silicon element derived from SiO₂ was confirmed by using Si-mapping images (white dots, Fig. 6.3b) and transmission electron microscopy (TEM) images (black dots, Fig. 6.3c,d). The average particle sizes of SiO₂ were not largely changed when compared with their initial particle sizes (12 and 7 nm to hydrophilic and hydrophobic SiO₂, respectively). It means the surfactant assists the inorganic dispersion, regardless of the

hydrophilicity of the inorganic components due to its hydrophilic–hydrophobic balance. In particular, the well-distributed hydrophilic SiO₂ particles improved the proton conductivity and chemical durability in the nanocomposite membranes. This trend was significantly observed at high SiO₂ content. This peculiar characteristic is associated with the combination of two different factors: (1) –Si-OH groups on hydrophilic SiO₂ surface were converted to –Si-(OH₂)⁺ groups in acidic medium (Hunter, 1993) (e.g., PEM, pH = 0–1), which act as additional proton conductor, and (2) the content of bound water, which can interact with hydrophilic groups (e.g., –SO₃H and –OH groups in sulfonated polymer and SiO₂, respectively) in the corresponding composites, increased with high inorganic loading content. Both methanol permeation and water uptake decreased at low SiO₂ content (<1 wt.%) as shown in those in Maxwell's composite model (Barrer et al., 1962; Qiu et al., 2007). SiO₂ nanoparticles began to aggregate over 1 wt.% SiO₂. It physically disrupted the polymer chain packing structure and induced increased free volume elements for methanol permeation and water absorption. It means that the optimum content for methanol barrier property is 1 wt.% in this system. The maximum DMFC performance was observed at the nanocomposite membrane containing 1 wt.% hydrophilic SiO₂. Its single cell performance was similar to that of Nafion® 117 (~200 mAcm⁻² at 0.4 V, catalyst loading = 3 mgcm⁻²) and superior to that of the pure polymer matrix (~130 mAcm⁻² at 0.4 V) under the same operation condition (temperature = 90°C and fuel flow rate = 1 mLmin⁻¹ of 1 M methanol and 200 mLmin⁻¹ of oxygen).

The surfactant was also effective in dispersing SiO₂ nanoparticles within another polymer matrix with hydrocarbon backbone (e.g., sulfonated poly(arylene ether sulfone, SPAES) (Lee et al., 2007). Surface properties of SiO₂ nanoparticles (surface area (150, 200, 300, and 380 m²g⁻¹) and average particle size (7, 12, and 14 nm)) were so important to determine molecular transport behavior as well as membrane durability to free radicals. Hydrophilic SiO₂ (e.g., Aerosil® 380) with small size (7 nm) and large surface area (380 m²g⁻¹) was advantageous to proton conductivity and fuel barrier property. The corresponding nanocomposite exhibited excellent resistance to attack of free radicals, which are caused by hydrogen peroxide (H₂O₂) formed via catalytic reaction during fuel cell operation and lead to membrane degradation (Pianca et al., 1999; Curtin et al., 2004; Gonon et al., 2005).

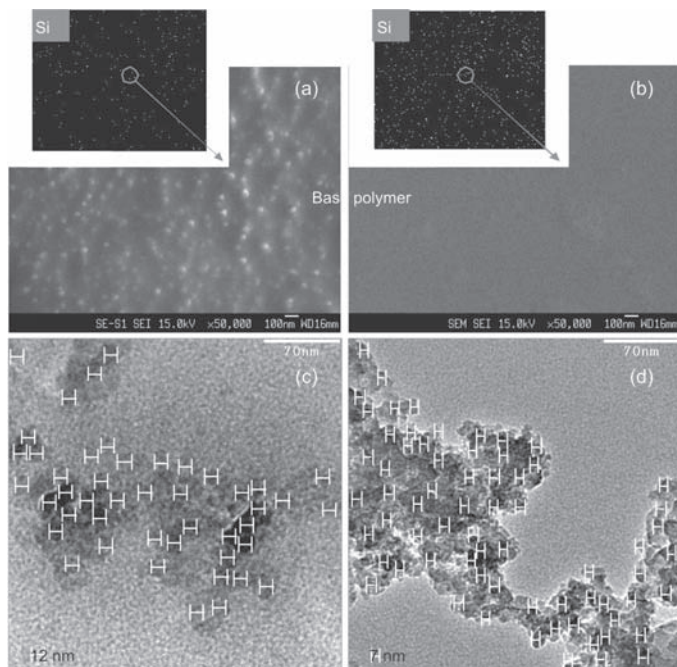


Figure 6.3 SEM images of (a) sulfonated polyimide (SPI)- SiO_2 without surfactant and (b) SPI/ SiO_2 /surfactant and TEM images of (c) SPI/hydrophilic SiO_2 (average diameter size = 12 nm)/surfactant, and (d) SPI/hydrophobic SiO_2 (average diameter size = 7 nm)/surfactant. Here, Si-mapping EDS images were taken with magnification of 1000. Reprinted from *J. Power Sources*, 195, Lee, C. H., Park, H. B., Park, C. H., Lee, S. Y., Kim, J. Y., McGrath, J. E. and Lee, Y. M., Preparation of high-performance polymer electrolyte nanocomposites through nanoscale silica particle dispersion, 1325-1332, Copyright (2010), with permission from Elsevier.

The hydrocarbon surfactant is not always useful for all composite membrane formation. The surfactant should be selected by considering chemical ingredient (particularly, polymer nature) of a polymer component as a mixed matrix. When perfluorinated sulfonic acid ionmers (e.g., Nafion®) instead of sulfonated hydrocarbons are used as polymer matrices, the use of fluorosurfactants is desirable rather than using hydrocarbon surfactants such as Pluronic® to improve the compatibility between polymer matrices and surfactants (Mulmi et al., 2009; Park et al., 2009). Fluorosurfactants (Zonyl® FSP: $[\text{F}(\text{CF}_2\text{CF}_2)_n\text{CH}_2\text{CH}_2\text{O}]_m\text{P}(\text{O})(\text{ONH}_4)_n$); Zonyl® TBS: $\text{F}(\text{CF}_2\text{CF}_2)_n\text{CH}_2\text{CH}_2\text{SO}_3\text{H}$) with different ionic character (phosphonic acid and sulfonic acid) contributed to additional transport of protons and,

simultaneously, the homogeneous dispersion of SiO_2 nanoparticles within recast Nafion[®] matrix. Accordingly, the Nafion-hydrophilic SiO_2 nanocomposite membrane containing Zonyl[®] TBS ($\sim 1600 \text{ mAcM}^{-2}$ at 0.6 V) showed PEMFC performance higher than Nafion[®] 112 and recast Nafion[®] ($\sim 1000 \text{ mAcM}^{-1}$ at 0.6 V) under the same operation condition (temperature = 80°C, fuel flow rate = 200 mLmin⁻¹ of O₂ and H₂, and catalyst loading content = 0.3 mgcm⁻²) (Mulmi et al., 2009). Furthermore, when hydrophobic SiO_2 was added with Zonyl[®] TBS into recast Nafion[®], the composite membrane exhibited reduced water uptake and enhanced methanol barrier property (Park et al., 2009). Consequently, their DMFC performances even at high temperature (90°C) were continuously promoted (350–540 mAcM⁻² at 0.4 V) as the methanol concentration increased (1–5 M).

Another well-known dispersant for inorganic distribution is urethane acrylate nonionomer (UAN) with the chemical structure composed of a hydrophilic PEO segment and a hydrophobic PPO segment, similar to that of Pluronic[®] (Fig. 6.4). Furthermore, UAN has two kinds of reactive groups: (1) vinyl groups (C=C) at the terminal end of PPO segments, and (2) a hydroxyl (–OH) group at the terminal end of PEO segment as shown in Fig. 6.4.

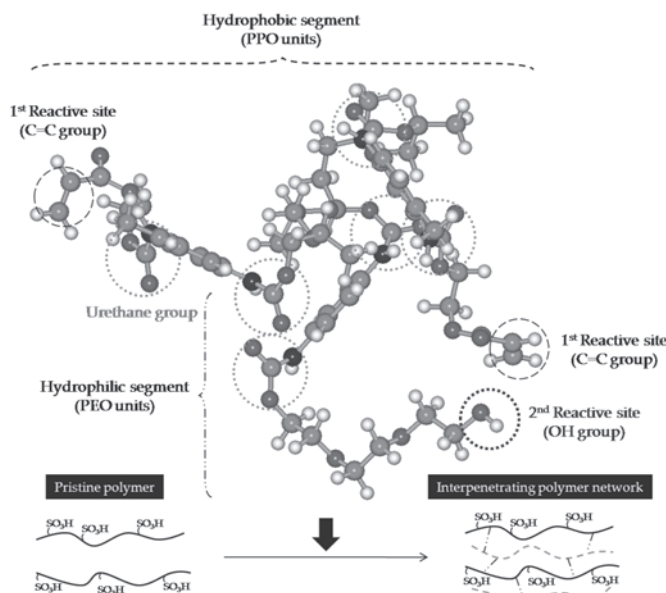


Figure 6.4 Basic chemical structure of UAN and formation of IPN structure.

In addition to its role as an inorganic dispersant, UAN can form peculiar chemical structures and morphology depending on its chemical circumstances. For instance, the vinyl groups are polymerized under AIBN as an initiator and form interpenetrating polymer network (IPN) structure within polymer matrices. When there exist another functional group (e.g., $-COOH$) in the polymer matrices, which can react with $-OH$ group, crosslinked structure is secondly accompanied (Lee et al., 2006). The resultant sulfonated polymer- SiO_2 nanocomposite membranes displayed high proton conductivity, hydrolytic durability, and low fuel permeability as compared with those in its pristine polymer via synergistic effect of the tuned structures and SiO_2 incorporation. Moreover, high amphiphilic balance of UAN enables sulfonated monomer (hydrophilic) and nonsulfonated monomer (hydrophobic) with big solubility differences to be highly miscible for their polymerization even under the existence of inorganic particles (e.g., SiO_2) (Kim et al., 2006). As PEO chain length in UAN is longer, hydrophilic domain size is larger. It leads to improved proton conductivity (Kim et al., 2008).

6.3 *IN SITU FORMATION OF INORGANIC COMPONENTS*

6.3.1 *In situ Local Growth of Inorganic Component Within Polymer Membrane*

Inorganic sublattice is locally formed within swollen sulfonated polymer membranes (particularly in their hydrophilic domains) via ion exchange or permeation of appropriate precursors, which is followed by hydrolysis or precipitation, aging and drying processes. Consequently, inorganic components are developed preferentially in the hydrophilic domains of the polymer membrane matrices (Fig. 6.5).

In the hybrid membrane formation described in Fig. 6.5, Nafion® with the quasi-ordered nanophase-separated morphology was used as a template for *In situ* sol-gel reaction of ZrO_2 precursor (i.e., TBZ). The ionic clusters composed of $-SO_3H$ groups (acid catalysts) in Nafion® act as nanoreactors (Mauritz, 1998; Gummaraju et al., 1996). When the precursors (e.g., silicon, zirconium, titanium, or aluminum oxides) are permeated from one side of thick Nafion® membrane,

compositional inorganic concentration profile is created. As a result, inorganic oxide nanoparticles are asymmetrically distributed, showing growth pattern to be less branched and more linear and, then, interlinked. The resulting hybrid membranes showed improved membrane properties. For example, the proton conductivity of Nafion®-SiO₂ hybrid membrane (~ 100 mScm⁻¹ at 80°C and 100% RH) is higher than that of Nafion® (74 mScm⁻¹) under the same measurement condition (Baradie et al., 2000). However, its methanol permeation behavior similar to that of Nafion® due to nonselective and porous SiO₂ network formation.

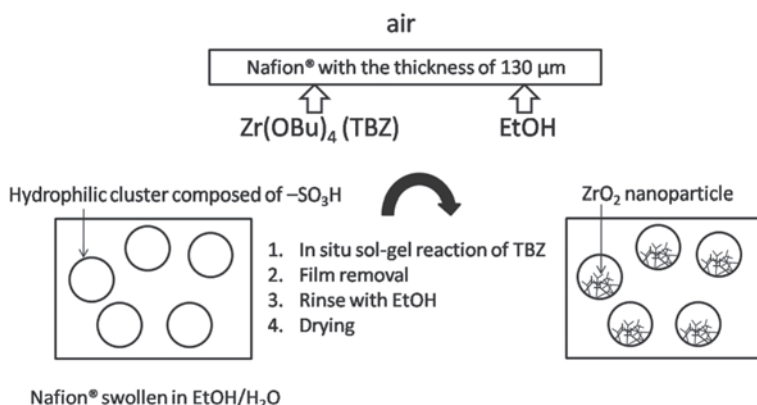


Figure 6.5 Schematic diagram of Nafion®/ZrO₂ hybrid membrane formulation. Here, ZrO₂ has asymmetric concentration profile owing to one-side permeation of tetrabutylzirconate (Zr(OBu)₄ or TBZ). Reprinted from *Mater. Sci. Eng. C*, 6, Mauritz, K. A., Organic-inorganic materials: perfluorinated ionomers as sol-gel polymerization templates for inorganic alkoxides, 121–133, Copyright (1998), with permission from Elsevier.

SO₃H groups in the polymer templates including Nafion® do act not only as acid catalysts for *In situ* sol-gel transition but also as active centers for inorganic particle growth, when metal ions are added by ion exchanging or conditioning in appropriate metal ion-containing solution in the system (Yang et al., 2001). This method has been used to make Nafion®- and hydrocarbon-based hybrid membranes using layered metal (IV) hydrogenphosphate M(IV)(HPO₄)₂·nH₂O (M = Zr, Ti, and Sn). The membrane properties including morphology are controlled by the concentrations of metal salts for ion-exchange reaction and phosphoric acid concentration for the precipitation

of the layered phosphate as well as temperature and reaction time. The incorporated layered phosphate caused improved proton conductivity at low humidity (>65% RH) and high temperature (<150°C) together with excellent single cell performance (max. power densities of 380 and 260 mWcm⁻² under dry oxygen and air feed at 150°C, respectively).

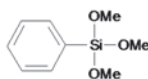
6.3.2 Sol-gel Transition of Inorganic Alkoxide Monomer in Polymer Solution

Previous method based on *in situ* sol-gel transition that occurred mainly in hydrophilic domains of sulfonated polymers has a critical limitation in making organic-inorganic hybrid membranes with high inorganic content. In the system, the content of inorganic components is highly restricted by both ion-exchange capacity (IEC) of polymer matrices and their permeation property to alkoxide precursors in appropriate solutions. For instance, in case of ion exchange, the limitation of zirconium phosphate (ZrP), which can be grown in sulfonated polyether ether ketone (SPEEK) with IEC value of 1.3 meqg⁻¹, is about 30 wt.%. The limitation of the inorganic content obtained from permeation is around 40 wt.%.

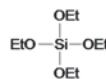
However, those intrinsic limitations can be overcome via inorganic growth in the polymer solution state Novak (1993). The membrane characteristics can be theoretically controlled from pure organic to pure inorganic as the inorganic content increases. Until now, a lot of polymers have been used as polymer matrices for this *In situ* sol-gel transition. They include polydimethylsiloxane (Langley et al., 1991), poly(methylmethacrylate) (Philipp & Schmidt, 1984), epoxy resins (Philipp & Schmidt, 1986), polyimides (Nandi et al., 1991, Cornelius & Marand, 2002), Nafion® (Zoppi et al., 1997, Zoppi & Nunes, 1998), polyvinyl alcohol (Nagarale et al., 2004; Kim et al., 2004), polyethylene glycol (PEG) (Chang & Lin, 2003), polystyrene (Aparicio et al., 2005), and sulfonated polystyrene (Tamaki & Chujo, 1999). In the majority of cases, polymer/SiO₂ hybrids are prepared using silica precursors as shown in Fig. 6.6. Their mechanical properties are generally higher than those of pure polymer matrices.

Macroscopic properties (e.g., morphology and proton conductivity) of the polymer-SiO₂ hybrid membranes are highly affected by a variety of factors including alkoxide structure, pH of the sol-gel reaction medium, solvents, the ratio of water and catalyst to

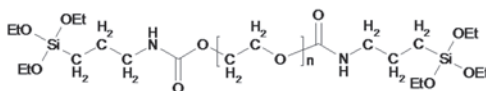
the alkoxides, reaction temperature and pressure, and stoichiometry of monomers. For example, Nafion®-SiO₂ hybrid membranes were prepared with different SiO₂ contents (6–54 wt.%) and alkoxides (TEOS and 1,1,3,3-tetramethyl-1,3-diethoxydisiloxane (TMDES)) (Zoppi et al., 1997; Zoppi & Nunes, 1998). Here, Nafion® solution in ethanol/water containing the precursors was catalyzed with some amount of acids (e.g., HNO₃ or HCl). After inorganic polymerization, the microstructure of Nafion® was diversely changed depending on the content of SiO₂. The hybrid with 6.5 wt.% showed band-like structure of SiO₂ with a width of 1.2 μm in the direction of solvent evaporation. When 10% of TEOS was substituted with TMDES having flexible and hydrophobic characteristics, laminar structure was observed. In addition to morphological tuning effect, TMDES resulted in promoted mechanical properties of the corresponding hybrid membranes. While Nafion-TEOS hybrid (SiO₂ content = 22 wt.%) was brittle, Nafion®-hybrid with 15–20% substituted TMDES exhibited storage and dissipative moduli similar to Nafion®. The proton conductivity of hybrid membranes was in the range 10⁻⁷–10⁻⁵ S cm⁻¹ under dry argon at 100°C.



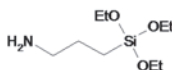
Monophenyl trimethoxysilane (PTMOS)



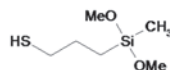
Tetraethyl orthosilicate (TEOS)



Alkoxy silane-end-capped PEG precursor



3-Aminopropyltriethoxysilane



Mercaptopropylmethylethoxysilane

Figure 6.6 SiO₂ precursors for *In situ* sol–gel reaction.

Most of hybrid membranes do not have sufficient proton conductivity applicable to fuel cell system. There have been some

efforts to improve proton transport property of the hybrid membranes. One way is to dope acidic moieties (e.g., 4-dodecylbenzene sulfonic acid (DBSA), Chang and Lin (2003)/tungstophosphoric acid, Aparicio et al. (2005)) into the inorganic network. The increase of DBSA content in PEG-SiO₂ hybrid led to improved proton conductivity (2.8×10^{-3} to $2.4 \times 10^{-2} \text{ Scm}^{-1}$ in liquid water at 25°C) without a big change of IEC value. At the same time, their methanol permeability (2.2×10^{-8} to $9.5 \times 10^{-7} \text{ cm}^2\text{sec}^{-1}$ under 3% methanol at 35°C) was reduced to the level of one order of magnitude lower than that of Nafion® ($7.5 \times 10^{-6} \text{ cm}^2\text{sec}^{-1}$) owing to the formation of SiO₂ network as methanol barrier. Meanwhile, the combination of SiO₂ and tungstophosphoric acid provided resulting polystyrene-SiO₂ hybrid membrane with enhanced water retention properties. The tungstophosphoric acid-doped hybrid membranes displayed excellent proton conductivity (max. $6.2 \times 10^{-1} \text{ Scm}^{-1}$) at 120°C and 87% RH.

6.4 CONCLUSIONS

Organic-inorganic composite membranes have a lot of advantages over their polymer counterparts in a variety of PEM properties such as proton conduction at high temperature and/or low humidity, high fuel barrier property (e.g., methanol crossover for DMFC application), high water retention property, excellent chemical resistance to water, fuels, and byproducts (e.g., radical or H₂O₂), and comprehensive electrochemical properties. These properties have been of particular interest in fuel cell systems targeting harsh operation (high temperature and/or low humidification, and hydrocarbon fuel-based reforming system). The important issue in organic-inorganic composite membrane researches for fuel cells is how to make homogeneously distributed inorganic phase within the polymer matrices and to maximize membrane performances with minimum amount of inorganic components at the same time. Recent researches include ionic cross-linking or interpenetration between organic and inorganic components or networks.

References

- Alberti, G., Casciola, M., Costantino, U., Peraio, A. and Montoneri, E. (1992a). Protonic conductivity of layered zirconium phosphonates containing –SO₃H groups. I. Preparation and characterization of a mixed

- zirconium phosphonate of composition $\text{Zr}(\text{O}_3\text{PR})_{0.73}(\text{O}_3\text{PR}')_{1.27}\cdot n\text{H}_2\text{O}$, with R= $-\text{C}_6\text{H}_4-\text{SO}_3\text{H}$ and R'= $-\text{CH}_2-\text{OH}$, *Solid State Ionics*, 50, pp. 315–322.
- Alberti, G., Casciola, R., Palombari, R. and Peraio, A. (1992b). Protonic conductivity of layered zirconium phosphonates containing $-\text{SO}_3\text{H}$ groups. II. Ac conductivity of zirconium alkyl-sulphophenyl phosphonates in the range of 100–200°C, in the presence or absence of water vapor, *Solid State Ionics*, 58, pp. 339–344.
- Alberti, G., Boccali, L., Casciola, M., Massinelli, L. and Montoneri, E. (1996). Protonic conductivity of layered zirconium phosphonates containing $-\text{SO}_3\text{H}$ groups. III. Preparation and characterization of γ -zirconium sulfoaryl phosphonates, *Solid State Ionics*, 84, pp. 97–104.
- Alberti, G. and Casciola, M. (1997). Layered metal IV phosphonates, a large class of inorganic-organic proton conductor, *Solid State Ionics*, 97, pp. 177–186.
- Alexandridis, P. and Hatton, T.A. (1995). Poly(ethylene oxide)-poly(propylene oxide)-poly(ethylene oxide) block copolymer surfactants in aqueous solution and at interfaces: thermodynamics, structure, dynamics, and modeling, *Colloids Surf. A: Phys. Eng. Aspects*, 96, pp. 1–46.
- Aparicio, M., Castro, Y. and Duran, A. (2005). Synthesis and characterization of proton conducting styrene-co-methacrylate-silica sol-gel membranes containing tungstophosphoric acid, *Solid State Ionics*, 176, pp. 330–340.
- Aricò, A. S., Baglio, V., Blasi, A., Di, Modica, E., Antonucci, P. L. and Antonucci, V. (2004). Surface properties of inorganic fillers for application in composite membranes-direct methanol fuel cells, *J. Power Sources*, 128, pp. 113–118.
- Argun, A. A., Ashcraft, J. N. and Hammond, P. T. (2008). Highly conductive, methanol resistant polyelectrolyte multilayers, *Adv. Mater.*, 20, pp. 1539–1543.
- Baradie, B., Dodelet, J. P. and Guay, D. (2000). Hybrid Nafion®-inorganic membrane with potential applications for polymer electrolyte fuel cells, *J. Electroanal. Chem.*, 489, pp. 101–105.
- Barrer, R. M., Barrie, J. A. and Raman, N. K. (1962). Solution and diffusion in silicone rubber II-The influence of fillers, *Polymer*, 3, pp. 605–614.
- Casciola, M., Marmottini, F. and Peraio, A. (1993). Ac conductivity of α -layered zirconium phosphate in the presence of water vapor at 100–200°C, *Solid State Ionics*, 61, pp. 125–129.
- Causse, J., Lagerge, S., Ménorval, L. C. de, Faure, S. and Fournel, B. (2005). Turbidity and ^1H NMR analysis of the solubilization of tributylphosphate

- in aqueous solutions of an amphiphilic triblock copolymer (L64 pluroinc), *Colloids Surf. A: Phys. Eng. Aspects*, 252, pp. 51–59.
- Chang, H. Y. and Lin, C. W. (2003). Proton conducting membranes based on PEG/SiO₂ nanocomposites for direct methanol fuel cells, *J. Membr. Sci.*, 218, pp. 295–306.
- Chen, S. L., Xu, K. Q. and Dong, F. (2005). Preparation of three-dimensionally ordered inorganic/organic bi-continuous composite proton conducting membranes, *Chem. Mater.*, 17, pp. 5880–5883.
- Cornelius, C. J. and Marand, E. (2002). Hybrid inorganic-organic materials based on a 6FDA-6FpDA-DABA polyimide and silica: physical characterization studies, *Polymer*, 43, pp. 2385–2400.
- Curtin, D. E., Lousenberg, R. D., Henry, T. J., Tangeman, P. C. and Tisack, M. E. (2004). Advanced materials for improved PEMFC performance and life, *J. Power Sources*, 131, pp. 41–48.
- Gibon, C. M., Norvez, S., Girault, S. T. and Goldbach, J. T. (2008). Control of morphology and crystallization in polyelectrolyte/polymer blends, *Macromolecules*, 41, pp. 5744–5752.
- Gonon, L., Perrot, C., Gebel, G., Morin, A., Escribano, S. and Marestin, K. (2005). Degradation mechanism of alternative polymers to Nafion used as proton exchange membrane in fuel cell, in: Proceedings of the 1st European Fuel Cell Technology and Application Conference, p. 188.
- Grot, W. G. and Rajendran, G. (1999). Membranes containing inorganic fillers and membrane and electrode assemblies and electrochemical cells employing same, US Patent 5,919,583.
- Gummaraju, R. V., Moore, R. B. and Mauritz, K. A. (1996). Asymmetric [Nafion®]/[silicon oxide] hybrid membranes via the in situ sol-gel reaction for tetraethyoxysilane, *J. Polym. Sci. B, Polym. Phys.*, 34, pp. 2383–2392.
- Hasani-Sadrabadi, H. M., Emami, S. H., Ghaffarian, R. and Moaddel, H. (2008). Nanocomposite membranes made from sulfonated poly(ether ether ketone) and montmorillonite clay for fuel cell applications, *Energy Fuels*, 22, pp. 2539–2542.
- Health, C. E. and Revfsz, A. G. (1973). Fuel cells, *Science*, 180, pp. 542–544.
- Hunter, R. J. (1993). *Introduction to Modern Colloid Science*, Oxford Science Publication, Oxford University Press: New York, NY.
- Jacobson, M. Z., Colella, W. G. and Golden, D. M. (2005). Cleaning the air and improving health with hydrogen fuel-cell vehicles, *Science*, 308, pp. 1901–1905.

- Jiang, S. P., Liu, Z., and Tian, Z. Q. (2006). Layer-by-layer self-assembly of composite polyelectrolyte-Nafion membranes for direct methanol fuel cells, *Adv. Mater.* 18, pp. 1068–1072.
- Kabanov, A. V., Batrakova, E. V. and Alakhov, V. Y. (2002). Pluronic® block copolymers for overcoming drug resistance in cancer, *Adv. Drug Deliver. Rev.*, 54, pp. 759–779.
- Kannan, R., Kakade, B. A. and Pillai, V. K. (2008). Polymer electrolyte fuel cells using Nafion-based composite membranes with functionalized carbon nanotubes, *Angew. Chem. Int. Ed.*, 47, pp. 2653–2656.
- Kim, D. S., Park, H. B., Rhim, J. W. and Lee, Y. M. (2004). Preparation and characterization of crosslinked PVA/SiO₂ hybrid membranes containing sulfonic acid groups for direct methanol fuel cell applications, *J. Membr. Sci.*, 240, pp. 37–48.
- Kim, J. Y., Mulmi, S., Lee, C. H., Park, H. B., Chung, Y. S. and Lee, Y. M. (2006). Preparation of organic-inorganic nanocomposite membrane using a reactive polymeric dispersant and compatibilizer: proton and methanol transport with respect to nano-phase separated structure, *J. Membr. Sci.*, 283, pp. 172–181.
- Kim, J. Y., Mulmi, S., Lee, C. H., Lee, Y. M. and Ihn, K. J. (2008). Synthesis of microphase-separated poly(styrene-co-sodium styrene sulfonate) membranes using amphiphilic urethane acrylate nonionomers as an reactive compatibilizer, *J. Appl. Polym. Sci.*, 107, pp. 2150–2158.
- Kim, Y. S., Wang, F., Hickner, M., Zawodzinski, T. A. and McGrath, J. E. (2003). Fabrication and characterization of heteropolyacid (H₃PW₁₂O₄₀)/directly polymerized sulfonated poly(arylene ether sulfone) copolymer composite membranes for higher temperature fuel cell applications, *J. Membr. Sci.*, 212, pp. 263–282.
- Kirpichnikova, L., Polomska, M., Wolak, J. and Hilczer, B. (1997). Polarized light study of the CsHSO₄ and CsDSO₄ superprototypic crystals, *Solid State Ionics*, 97, pp. 135–139.
- Kreuer, K. D. (1997). On the development of proton conducting materials for technological applications, *Solid State Ionics*, 97, pp. 1–15.
- Langley, N. R., Mbah, G. C., Freeman, H. A., Huang, H. H., Siochi, E. J., Ward, T. C. and Wilkes, G. (1991). Physical structure of polysilicate particles in organic media, *J. Colloid Interface Sci.*, 143, pp. 309–317.
- Lee, C. H., Hwang, S. Y., Sohn, J. Y., Park, H. B., Kim, J. Y. and Lee, Y. M. (2006). Water-stable crosslinked sulfonated polyimide-silica nanocomposite containing interpenetrating polymer network, *J. Power Sources*, 163, pp. 339–348.

- Lee, C. H., Min, K. A.; Park, H. B., Hong, Y. T., Jung, B. O. and Lee, Y. M. (2007). Sulfonated poly(arylene ether sulfone)-silica nanocomposite membrane for direct methanol fuel cell (DMFC), *J. Membr. Sci.*, 303, pp. 258–266.
- Lee, C. H., Park, H. B., Park, C. H., Lee, S. Y., Kim, J. Y., McGrath, J. E. and Lee, Y. M. (2010). Preparation of high-performance polymer electrolyte nanocomposites through nanoscale silica particle dispersion, *J. Power Sources*, 195, pp. 1325–1332.
- Li, H. and Nogami, M. (2002). Pore-controlled proton conducting silica films, *Adv. Mater.*, 14, pp. 912–914.
- Mata, J. P., Majhi, P. R., Guo, C., Liu, H. Z. and Bahadur, P. (2005). Concentration, temperature, and salt-induced micellization of a triblock copolymer Pluronic L64 in aqueous medium, *J. Colloid Interface Sci.*, 292, pp. 548–556.
- Mauritz, K. A. (1998). Organic-inorganic materials: perfluorinated ionomers as sol-gel polymerization templates for inorganic alkoxides, *Mater. Sci. Eng. C*, 6, pp. 121–133.
- McKeen, J. C., Yan, Y. S. and Davis M. E. (2008). Proton conductivity in sulfonic acid-functionalized zeolite beta: effect of hydroxyl group, *Chem. Mater.*, 20, pp. 3791–3793.
- Mikhailenko, S. D., Zaidi, S. M. J. and Kaiaguine, S. (2001). Sulfonated polyether ether ketone based composite polymer electrolyte membranes, *Cat. Today*, 67, pp. 225–236.
- Miyatake, K., Chikashige, Y., Higuchi, E. and Watanabe, M. (2007). Tuned polymer electrolyte membranes based on aromatic polyesters for fuel cell applications, *J. Am. Chem. Soc.*, 129, pp. 3879–3887.
- Mulmi, S., Park, C. H., Kim, H. K., Lee, C. H., Park, H. B. and Lee, Y. M. (2009). Surfactant-assisted polymer electrolyte nanocomposite membranes for fuel cells, *J. Membr. Sci.*, 344, pp. 288–296.
- Nagarale, R. K., Gohil, G. S., Shahi, V. K. and Rangarajan, R. (2004). Organic-inorganic hybrid membrane: thermally stable cation-exchange membrane prepared by the sol-gel method, *Macromolecules*, 37, 10023–10030.
- Nandi, M., Conklin, J. A., Salvati Jr, L. and Sen, A. (1991). Molecular level ceramic/polymer composites. 2. Synthesis of polymer-trapped silica and titania nanoclusters, *Chem. Mater.*, 3, pp. 201–206.
- Nogami, M., Miyamura, K. and Abe, Y. (1997). Fast protonic conductors of water-containing $P_2O_5\text{-ZrO}_2\text{-SiO}_2$ glasses, *J. Electrochem. Soc.*, 144, pp. 2175–2178.

- Norsten, T. B., Guiver, M. D., Murphy, J., Astill, T., Navessin, T., Holdcroft, S., Frankamp, B. L., Rotello, V. M. and Ding, J. (2006). Highly fluorinated comb-shaped copolymers as proton exchange membranes (PEMs): improving PEM properties through rational design, *Adv. Func. Mater.*, 16, pp. 1814–1822.
- Novak, B. M. (1993). Hybrid nanocomposite materials-between inorganic glasses and organic polymers, *Adv. Mater.*, 5, pp. 422–433.
- Ortona, O., D'Errico, G., Paduano, L. and Vitagliano, V. (2006). Interaction between cationic, anionic, and non-ionic surfactants with ABA block copolymer Pluronic PE6200 and with BAB reverse block copolymer Pluronic 25R4, *J. Colloid Interface Sci.*, 301, pp. 63–77.
- Park, C. H., Kim, H. K., Lee, C. H., Park, H. B. and Lee, Y. M. (2009). Nafion® nanocomposite membranes: effect of fluorosurfactants on hydrophobic silica nanoparticle dispersion and direct methanol fuel cell performance, *J. Power Sources*, 194, pp. 646–654.
- Pawlowski, A., Pawlaczyk, Cz. and Hilczer, B. (1990). Electric conductivity in crystal group $\text{Me}_3\text{H}(\text{SeO}_4)_2$ (M: NH_4^+ , Rb^+ , Cs^+), *Solid State Ionics*, 44, pp. 17–19.
- Pereira, F., Vallé, K., Belleville, P., Morin, A., Lambert, S. and Sanchez, C. (2008). Advanced mesostructured hybrid silica-Nafion membranes for high-performance PEM fuel cell, *Chem. Mater.*, 20, pp. 1770–1718.
- Philipp, G. and Schmidt, H. (1984). New materials for contact lenses prepared from Si- and Ti-alkoxides by the sol–gel process, *J. Non-Cryst. Solids*, 63, pp. 283–292.
- Philipp, G. and Schmidt, H. (1986). The reactivity of TiO_2 and ZrO_2 in organically modified silicates, *J. Non-Cryst. Solids*, 82, pp. 31–36.
- Pianca, M., Barchiesi, E., Esposto, G. and Radice, S. (1999). End groups in fluoropolymers, *J. Fluorine Chem.*, 95, pp. 71–84.
- Ponce, M. L., Prado, L., Ruffmann, B., Richau, K., Mohr, R. and Nunes, S. P. (2003). Reduction of methanol permeability in polyetherketone-heteropolyacid membranes, *J. Membr. Sci.*, 217, pp. 5–15.
- Portehault, D., Petit, L., Pantoustier, N., Ducouret, G., Lafuma, F. and Hourdet, D. (2006). Hybrid thickeners in aqueous media, *Colloids Surf. A: Phys. Eng. Aspects*, 278, pp. 26–32.
- Qiu, J., Zheng, J. M. and Peinemann, K. V. (2007). Gas transport properties of poly(trimethylsilylpropyne) and ethylcellulose filled with different molecular weight trimethylsilylsaccharides: impact on fractional free volume and chain mobility, *Macromolecules* 40, pp. 3213–3222.
- Rajam, S. and Ho, C. C. (2006). Graft coupling of PEO to mixed cellulose esters microfiltration membranes by UV irradiation, *J. Membr. Sci.*, 281, pp. 211–218.

- Haile, S. M., Calkins, P. M. and Boysen, D. (1997). Superprotonic conductivity in β -Cs₃(HSO₄)₂(H_x(P,S)O₄), *Solid State Ionics*, 97, pp. 145–151.
- Staiti, P., Aricò, A. S., Baglio, V., Lufrano, F., Passalacqua, E. and Antonucci, V. (2001). Hybrid Nafion-silica membranes doped with heteropolyacids for application in direct methanol fuel cells, *Solid State Ionics*, 145, pp. 101–107.
- Steele, B. C. H. and Heinzel, A. (2001). Materials for fuel-cell technologies, *Nature*, 414, pp. 345–352.
- Stein, E. W., Clearfield, A. and Subramanian, M. A. (1996). Conductivity of group IV metal sulfophosphonates and a new class of interstratified metal amine-sulfophosphonates, *Solid State Ionics*, 83, pp. 113–124.
- Stonehart, P. and Watanabe, M. (1996). Polymer solid-electrolyte composition and electrochemical cell using the composition, US Patent 5,523,181.
- Tamaki, R. and Chujo, Y. (1999). Synthesis of polystyrene and silica gel polymer hybrids utilizing ionic interactions, *Chem. Mater.*, 11, pp. 1719–1726.
- Tsang, E. M. W., Zhang, Z., Shi, Z., Soboleva, T., Holdcroft, S. (2007). Consideration of macromolecular structure in the design of proton conducting polymer membranes: Graft versus diblock polyelectrolytes, *J. Am. Chem. Soc.*, 129, pp. 15106–15107.
- Velichkova, R. S. and Christova, D. C. (1995). Amphiphilic polymers from macromonomers and telechelics, *Prog. Polym. Sci.* 20, pp. 819–887.
- Wang, F., Hickner, M., Kim, Y. S., Zawodzinski, T. A. and McGrath, J. E. (2002). Direct polymerization of sulfonated poly(arylene ether sulfone) random (statistical) copolymers: candidates for new proton exchange membranes, *J. Membr. Sci.*, 197, pp. 231–242.
- Watanabe, M., Uchida, H., Seki, Y., Emori, M. and Stonehart, P. (1996). Self-humidifying polymer electrolyte membranes for fuel cells, *J. Electrochem. Soc.*, 143, pp. 3847–3852.
- Wilkes, G. L., Huang, H. and Glaser, R. H. (1990). Silicon-based polymer science: a comprehensive resources: advances in chemistry ser. 224, American Chemical Society, Washington, DC, pp. 207.
- Yamaguchi, T., Zhou, H., Nakazawa, S. and Hara, N. (2007). An extremely low methanol crossover and highly durable aromatic pore-filling electrolyte membrane for direct methanol fuel cells, *Adv. Mater.*, 19, pp. 592–596.
- Yang, C., Srinivasan, S., Aricò, A. S., Cretì, P., Baglio, V. and Antonucci, V. (2001). Composite Nafion/zirconium phosphate membranes for direct methanol fuel cell operation at high temperature, *Electrochim. Solid-State Lett.*, 4, pp. A31–A34.

- Yang, L., Alexandridis, P., Steytler, D. C., Kositza, M. J. and Holzwarth, J. F. (2000). Small-angle neutron scattering investigation of the temperature-dependent aggregation behavior of the block copolymer Pluronic L64 in aqueous medium, *Langmuir*, 16, pp. 8555–8561.
- Yang, Z.Y. and Rajendran, R. G. (2005). Copolymerization of ethylene, tetrafluoroethylene, and an olefin-containing fluorosulfonyl fluoride: synthesis of high-proton-conductive membranes for fuel-cell applications, *Angew. Chem. Int. Ed.*, 44, pp. 564–567.
- Zaidi, S. M. J., Mikhailenko, S.D., Robertson, G. P., Guiver, M. D. and Kaliaguine, S. (2000). Proton conducting composite membranes from polyether ether ketone and heteropolyacids for fuel cell applications, *J. Membr. Sci.*, 173, pp. 17–34.
- Zaluski, C. and Xu, G. (1994). Blends of Nafion and Dow perfluorosulfonated ionomer membranes, *Macromolecules*, 27, pp. 6750–6754.
- Zhou, Z., Dominey, R. N., Rolland, J. P., Maynor, B. W., Pandya, A. A., and DeSimone, J. M. (2006). Molded, high surface area polymer electrolyte membranes from cured liquid precursors, *J. Am. Chem. Soc.*, 128, pp. 12963–12972.
- Zoppi, R.A., Yoshida, I.V.P. and Nunes, S.P. (1997). Hybrids of perfluorosulfonic acid ionomer and silicon oxide by sol-gel reaction from solution: morphology and thermal analysis, *Polymer*, 39, pp. 1309–1315.
- Zoppi, R. A. and Nunes, S. P. (1998). Electrochemical impedance studies of hybrids of perfluorosulfonic acid ionomer and silicon oxide by sol-gel reaction from solution, *J. Electroanal. Chem.*, 445, pp. 39–45.

This page intentionally left blank

Chapter 7

THE OCCURRENCE, BEHAVIOR, AND EFFECTS OF ENGINEERED NANOMATERIALS IN THE ENVIRONMENT

Bernd Nowack

Empa — Swiss Federal Laboratories for Materials Science and Technology

Lerchenfeldstrasse 5, CH - 9014 St. Gallen, Switzerland

nowack@empa.ch

The behavior and effects of engineered nanomaterials (ENM) in the environment have received a lot of attention in recent years. A variety of different ENM enter the environment from a multitude of sources either directly, e.g., during a groundwater remediation, or indirectly, e.g. by release from products and through wastewater treatment plants. This chapter gives an overview on the occurrence, the behavior and effects of ENM in the environment. The first ENM have been detected in environmental samples (wastewater treatment plant effluent and urban drainage), indicating that ENM indeed do end up in the environment. However, as quantitative, ENM-specific trace analytical methods are not yet available, only modeling can give us any indications as to where and at which concentrations ENM can be expected in the environment. It is also discussed how ENM behave during waste incineration and wastewater treatment, two important entry points for ENM into the environment. An overview is given of how ENM are altered by environmental factors and how aggregation affects their behavior. The effects of ENM on organisms

Advances in Nanotechnology and the Environment

Edited by Juyoung Kim

Copyright © 2012 by Pan Stanford Publishing Pte. Ltd.

www.panstanford.com

are also summarized, highlighting the importance of distinguishing between the effects of ENM themselves and the solubilized metals.

7.1 INTRODUCTION

The potential effects of engineered nanomaterials (ENM) have received quite a lot of attention in the recent years. Although human health issues clearly dominate, environmental aspects are also getting increasing attention. Government agencies, media, and NGO call for information on whether ENM pose a threat to the environment. The current situation is characterized by relatively little scientific information on this topic, although the field is growing with astonishing speed. A good sign of this rapid development is that the first report about the detection of an ENM in the environment has been published: Kaegi et al. (2008a) have shown that nano-TiO₂ is leached out of house facades painted with TiO₂ containing paint. They traced the particles from the house facades into receiving waters and found concentrations in the range of a few µg/L of titanium in a small stream. These concentrations lie within the range of nano-TiO₂ predicted for the water compartment by Mueller and Nowack (2008) in their exposure modeling of ENM. These authors have used the available knowledge about nanoparticle production and use and information on the product lifecycles of the nano-products to model the environmental concentrations of nanoparticles in water, air, and soil. Studies by Kaegi et al. (2008a) and Mueller and Nowack (2008) have shifted the discussion about ENM and the environment to a much more quantitative level. For the first time we know that ENM actually end up in the environment and we also have first ideas about the expected concentrations.

The investigation of the behavior and effects of nanoparticles in the environment is thus no longer in its infancy. Our knowledge of this subject is increasing almost exponentially, caused by a massive investment in nano-risk-related research (Guzman et al., 2006). However, the field is by far from mature, and many investigations still have explorative character and raise more new questions than they answer. It is also noteworthy that despite the infancy of the field, a large number of reviews are already available that focus on environmental behavior and ecotoxicity (Lead and Wilkinson, 2006; Nowack and Bucheli, 2007; Baun et al., 2008; Handy et al., 2008a,

2008b; Ju-Nam and Lead, 2008; Klaine et al., 2008; Navarro et al., 2008a; Farre et al., 2009; Simonet and Valcarcel, 2009). These reviews try to combine the available knowledge and to estimate the behavior and effects of nanoparticles based on the fragmentary information that we already have.

The aim of this chapter is to provide an overview on the current knowledge about the release of nanoparticles into the environment, the detection and modeling of their environmental concentrations, and to present the current state of knowledge about their potential effects on organisms.

7.2 THE OCCURRENCE OF ENGINEERED NANOMATERIALS IN THE ENVIRONMENT

One major difficulty is that the ENM need to be separated from the natural nanoparticles, e.g., organic matter and minerals, and quantified at trace levels. Figure 7.1 shows an example of natural nanoparticles sampled from a lake (Buffle and Leppard, 1995). The intimate interplay of inorganic and organic particles can be clearly seen. Man-made nanoparticles have to be detected and identified in this matrix of natural particles. Currently, there is a lack of studies that are able to quantify trace concentrations of ENM under environmental conditions (Hasselov et al., 2008; Tiede et al., 2008). First attempts to isolate ENM from natural samples have been published, e.g., using chemothermal oxidation to isolate CNT from the natural organic matter present in sediments and soils (Sobek and Bucheli, 2009). Also, chromatographic methods (Tiede et al., 2009) or field flow fractionation (Dubascoux et al., 2008) have been used to separate ENM from other particles.

The analysis of ENM in natural systems is further complicated because many ENM have closely related natural counterparts with the same composition and mineralogy. For example, natural nanosized TiO₂ particles have been detected in river water affected by mining wastes (Wigginton et al., 2007). Also, iron(hydr)oxides, aluminum(hydr)oxides, and silica nanoparticles have natural counterparts, which may be present in high concentrations (Waychunas et al., 2005; Hasselov and von der Kammer, 2008; Theng and Yuan, 2008; Waychunas and Zhang, 2008). A similar problem also exists in air where sensitive methods are available to count

nanoparticles, but they do not reveal the identity of the particles. Due to the large background of natural and inadvertently produced nanoparticles (Anastasio and Martin, 2001; Buseck and Adachi, 2008), it is very difficult to identify and detect small numbers of ENM. This has to date only been possible in occupational exposures where, e.g., nano-TiO₂ has been detected inside a factory handling this material (Peters et al., 2009).

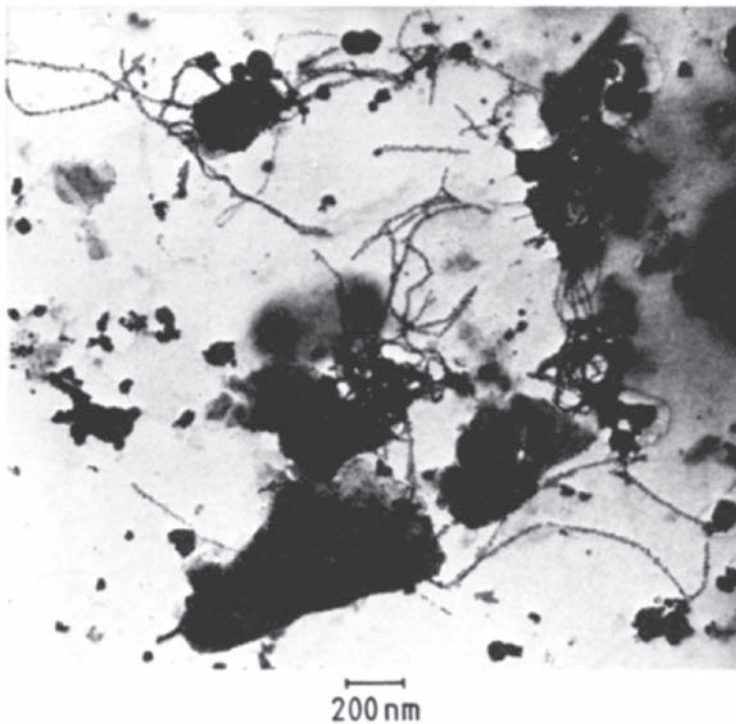


Figure 7.1 Typical example of colloidal materials in an eutrophic lake observed by transmission electron microscopy (TEM). The picture shows inorganic colloids, in particular clay (large angular particles) and iron oxyhydroxide globules aggregated together by a mesh of organic filaments. Reprinted with permission from Buffle and Leppard (1995). Copyright 1995 American Chemical Society.

The difficulties discussed above can explain why almost no quantitative measurements of ENM in the environment are available. To date almost all studies have used electron microscopy to detect natural and engineered nanoparticles in the environment. In some

studies a fractionation based on sedimentation (Kaegi et al., 2008a, 2008b) or filtration (Kiser et al., *in press*) was used to separate the smallest size fraction, thus leading to a clean-up of the fraction containing the nanoparticles.

Engineered nano-TiO₂ is the most widely used ENM (Mueller and Nowack, 2008), and two recent publications show that it is indeed present in natural water samples: Kaegi et al. (2008a) observed engineered nano-TiO₂ in surface water and traced the origin of the particles to leaching from facades that had been treated with nano-TiO₂ containing paint. Electron microscopy of the facades and the released particles showed that they were still partially embedded in the organic binder, but that many single particles were also observed that stemmed from aged facades (Fig. 7.2). These authors used a sedimentation/centrifugation-based pretreatment to exclusively collect particles below 200 nm and to remove a large fraction of the larger particles present in natural waters. This procedure allowed the authors to identify and detect small concentrations of single nanoparticles.

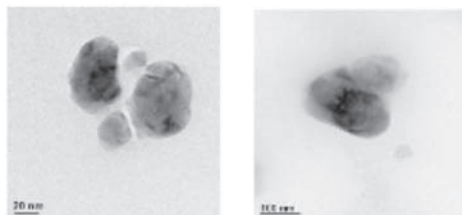


Figure 7.2 Nano-TiO₂ detected in runoff of a house facade (left) and in urban runoff (right). Reprinted from Kaegi et al. (2008a). Copyright 2008, with permission from Elsevier.

In the second study, Kiser et al. 2009 detected nano-TiO₂ in WWTP effluents (Fig. 7.3). Only few particles were found in the effluent samples, but those observed were often aggregates of a few hundred nanometers composed of several primary particles less than 100 nm that were made solely of Ti and O. The primary particles were often spherical in shape and some single TiO_x nanoparticles were observed. The shape and size of these Ti materials were stated by the authors to be consistent with TiO₂ synthesized for industrial/food applications. Filtration was used to distinguish between large particles and small nano-TiO₂, which was supposed to pass through

the pores of the filter ($0.7\text{ }\mu\text{m}$). The concentration of filterable TiO_2 in the effluent of different wastewater treatment plants was in the range 5–15 $\mu\text{g/L}$, thus representing a maximal value for nano- TiO_2 .

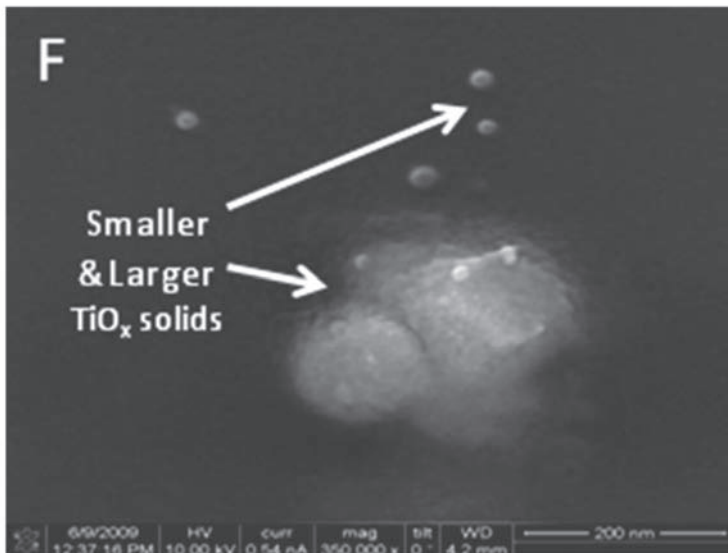


Figure 7.3 SEM analysis of nanoscale TiO_2 in WWTP tertiary effluent. Reprinted with permission from Kiser et al. 2009 Copyright 2009 American Chemical Society.

The study by Kaegi et al. (2008a) reports both the release of ENM from a material as well as its detection in the environment. The release part is very important because before ENM can be detected in the environment they need to be released either during production of the material itself or the product they are used in or during the use or disposal of the product. Experimental data on the release of ENM during the use or disposal are very scarce. The release of nano- TiO_2 from coatings on wood, polymers, and tiles has been reported to be the highest from coated tile, and UV-light increased the release of ENM (Hsu and Chein, 2007). Initial results about the abrasion of nanomaterial-containing products, e.g., of ZnO -containing coatings, have been presented (Vorbau et al., 2009). Silver nanoparticles were found to be released during washing from nano-Ag containing textiles (Benn and Westerhoff, 2008) and were also found to be chemically changed during washing (Impellitteri et al., 2009). Such investigations provide the necessary information

as to in what amounts and forms the ENM are released into the environment and thus should form the basis of any risk assessment of the environmental effects of ENM.

7.3 THE BEHAVIOR OF ENGINEERED NANOMATERIALS IN THE ENVIRONMENT

7.3.1 Waste Incineration and Wastewater Treatment

ENM can enter the environment from a multitude of sources, either directly, e.g., during groundwater remediation (Nowack, 2008), or indirectly, e.g., by abrasion during product use. The pathway of ENM from the product into the environment often leads through the wastewater treatment plant or the waste incineration plant. These facilities act as filters between the product and the environment, and depending on their ability to remove ENM, they can stop or at least diminish the disposal of ENM into the environment.

Most waste incineration plants are equipped with different types of filters, but most have a multistage flue gas cleaning system consisting of electrofilters, a flue gas scrubber and a catalytic NO_x /furan/dioxin removal system. The concentration of particles smaller than 100 nm is lowered by such filters by around 99.9% and in the subsequent wet filter by another 95% (Burtscher et al., 2002). There is no information available yet about the behavior of ENM during waste incineration. However, we can assume that even if ENM become airborne during combustion, they are efficiently removed in the filters. Exposure of the air to ENM released from incineration plants is thus expected to be very low. The slag or the filter residues containing residues of ENM that were not incinerated are usually landfilled, and thus their release into the environment through this pathway can be considered to be low. However, no studies about the behavior of ENM under the conditions present in landfills have been published so far.

Also, not much is known about the fate of ENM during wastewater treatment. Some information about the removal of silica nanoparticles originating from chemical mechanical polishing from the semiconductor industry is available (Huang et al., 2004; Chang et al., 2006; Chin et al., 2006; Den and Huang, 2006). It was shown that biological treatment was almost entirely ineffective in removing

the silica particles (Chang et al., 2007). Even addition of Al-coagulant only removed about 9% of the nanoparticulate silica. For quantum dots it was found that adding Al-coagulant removed up to 90% of the ENM by sedimentation (Zhang et al., 2008b). For a variety of metal oxide ENM (TiO_2 , Fe_2O_3 , ZnO , NiO , silica), it was found that they were removed by 20–60% after alum addition and sedimentation (Zhang et al., 2008a). Silica was the ENM with the lowest removal from water.

So far, only one study has investigated in detail the behavior of an ENM during wastewater treatment (Limbach et al., 2008). In this work a model wastewater treatment plant was used to study the removal of CeO_2 . It was found that the majority of the nanoparticles could be captured through adhesion to sewage sludge and only a small fraction of about 6% was discharged with the treated water. Most of the CeO_2 in the effluent was present as large aggregates or adsorbed to microorganisms. Scanning transmission electron micrographs of sludge after contact with the CeO_2 showed aggregated nanoparticles together with the microorganism (Fig. 7.4).

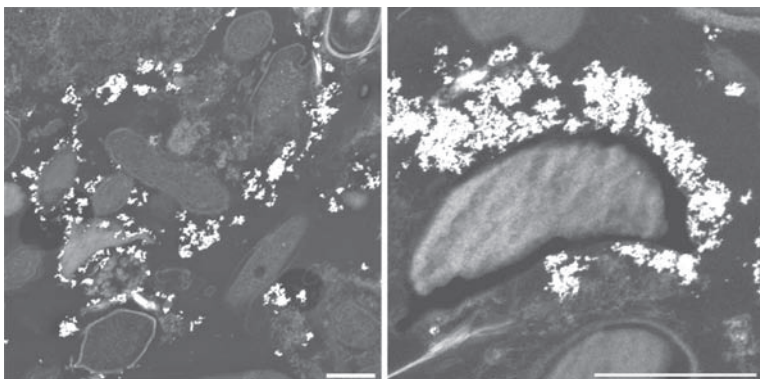


Figure 7.4 Scanning transmission electron micrograph of sewage sludge exposed to CeO_2 nanoparticles. The high-density cerium oxide nanoparticles appear bright. Reprinted with permission from Limbach et al. (2008). Copyright 2008 American Chemical Society.

7.3.2 Changes in the Environment

Once in the environment the released ENM are affected by environmental factors such as light, oxidants, or microorganisms. These factors can result in chemical or biological modifications or a degradation of the surface functionalization and the embedding

matrix that may result in free nanoparticles. The surface of uncoated ENM can also be modified by environmental factors and, e.g., coated by natural organic matter or functionalized by chemical or biological processes. It has been shown, however, that the polyelectrolyte coating of nZVI remains stable for several months with little changes in transport behavior over that time (Kim et al., 2009). The desorption of large molecules of polyaspartate, carboxymethyl cellulose, and polystyrene sulfonate was very slow with less than 30% desorbed after 4 months. Nothing is known so far about the environmental stability of other coatings usually used for ENM in commercial products. QDs comprise an important group of ENM that are in most cases capped with organic ligands. The capping ligands are the key factor in determining their fate in water (Zhang et al., 2008b).

Illumination of fullerenes with light lead to the production of currently unknown breakdown products (Hou and Jafvert, 2009). TOC analysis of the samples indicated that water-soluble products formed and that with continued light exposure these intermediates eventually mineralized, volatilized, or were converted into other products not quantified by TOC. The presence of oxygen was required for the reaction to occur. Fullerenes are also oxidized by ozone and again water-soluble products are formed, resulting in the dissolution of the fullerenes aggregates (Fortner et al., 2007).

Many nanoparticles are soluble and can dissolve under natural conditions. This can either alter their surface or result in complete disappearance of the ENM. Four types of nanoparticles are strongly affected by dissolution: nano-Ag, nano-ZnO, nano-CuO, and quantum dots (QD). For all these particles the dissolution yields dissolved metals (Ag^+ , Zn^{2+} , Cu^{2+} , Cd^{2+}) that are toxic to organisms.

Although the dissolution of many ENM is undesirable, the release of dissolved Ag from Ag nanoparticles is required for the intended biocidal effect (Ratte, 1999). In their modeling of silver flows into the environment, Blaser et al. (2008) only considered emissions of dissolved Ag from nano-Ag products and no particulate emissions. So far, most results about any dissolution of these nanoparticles come from toxicological experiments where high concentrations of nanoparticles were added to the media. Data obtained under realistic, environmentally relevant concentrations are missing so far, as are any data on the influence of natural compounds, e.g., DOC, on the dissolution rate. Relatively low dissolution of Ag nanoparticles is

often found during exposure in growth media (Griffitt et al., 2008), but little quantitative information is available on this reaction. It has been shown that nano-Ag dissolves by less than 1% in different natural waters (Gao et al., 2009) and in algal growth media (Navarro et al., 2008b).

Some metal oxide ENM such as ZnO are relatively soluble. Very significant dissolution of ZnO was observed in growth media (Franklin et al., 2007; Heinlaan et al., 2008). However, even if a particle such as ZnO should theoretically completely dissolve at near-neutral pH in pure water, it may well be stable if a corrosion layer is formed, which shields the particles from further dissolution. It has been shown that the easily soluble PbO was stable in soils for several months, either by a coating of less-soluble Zn carbonates or by a layer of pyromorphite (Birkefeld et al., 2007). Some particles remained virtually unaltered at pH 6.5 for more than a year. The products of dissolution and phase transfer can be different for nanoparticles compared with micron-sized particles (Xia et al., 2006).

As QDs typically consist of metals that are known to be toxic, almost all studies looking at QD toxicity also looked at dissolution and metal release, e.g., the studies by Gagne et al. (2008) and King-Heiden et al. (2009). Mahendra et al. (2008) exposed QD to high and low pH to mimic weathering in the environment. Significant release of the organic coating, Zn, and Cd was observed. Metz et al. (2009) used simulated oxidative conditions, based on the extracellular hydroquinone-driven Fenton's reaction used by lignolytic fungi, to transform QDs. Again significant release of metals was observed, indicating that QD may not be stable under natural conditions and that the toxicity of the altered products needs to be investigated.

Also, ENM that do not dissolve may be affected by dissolution if they contain impurities. An example could be CNT that contain metal impurities from the manufacturing process. These metals can dissolve during exposure in water and can thus be a source of toxic metals (Hull et al., 2009).

ENM are also under the influence of biota in the environment. Roberts et al. (2007) examined the interactions between *Daphnia magna* and a water-soluble, lysophosphatidylcholine-coated single-walled CNT. The *Daphnia* were able to ingest the CNT through normal feeding behavior and utilize the lysophosphatidylcholine coating as a food (Fig. 7.5). They excreted uncoated CNT, which precipitated and

formed black clumps (Fig. 7.5, 20 hours). The *Daphnia* had thus a dramatic effect on the physical properties of the CNT and thus on their environmental behavior. The *Daphnia* changed a completely water-soluble CNT within few hours into a completely insoluble form that formed large aggregates that are able to sediment out of the water column.

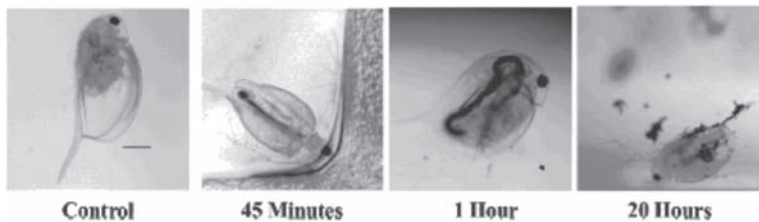


Figure 7.5 Micrographs of *Daphnia magna* exposed to 5 mg/L of lysophosphatidylcholine-coated single-walled nanotubes after different exposure time. Reprinted with permission from Roberts et al. (2007). Copyright 2007 American Chemical Society.

The catalytic biodegradation of CNT *in vitro* by oxidative activity of horseradish peroxidase and low concentrations of hydrogen peroxide (40 µM) has been reported (Allen et al., 2008). Figure 7.6 shows how the CNT were progressively shortened with exposure time and that globular material appeared. The resulting material had no more CNT-like characteristics, indicative of almost complete oxidative degradation. This reaction indicates that CNTs could possibly be degraded under environmental conditions.

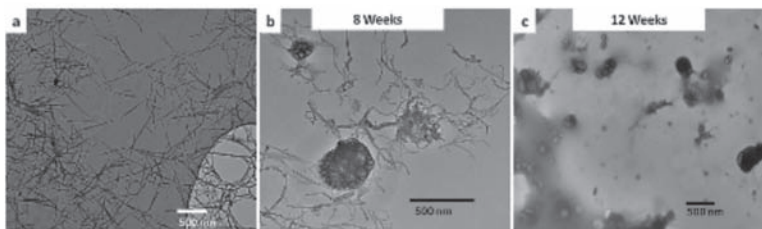


Figure 7.6 TEM micrograph showing the biodegradation of carbon nanotubes as incubation time increases. (a-c) Length decrease is seen at week 8 with some globular material, while at week 12 mostly globular material is present. Reprinted with permission from Allen et al. (2008). Copyright 2008 American Chemical Society.

7.3.3 Aggregation

Aggregation of single nanoparticles to larger aggregates is one of the most important reactions affecting the behavior, fate, and effects of ENM in the environment. Buffle et al. (1998) concluded that the formation of aggregates in aquatic systems can be understood by mainly considering the roles of three types of colloids: (i) compact inorganic colloids; (ii) large, rigid biopolymers; and (iii) fulvic compounds or refractory organic matter (Fig. 7.7). In most natural aquatic systems, the fulvic compounds will stabilize the inorganic colloids, whereas the rigid biopolymers will destabilize them. The concentration of stable colloids in an aquatic system was stated to depend on the relative proportions of these three components. These complexation processes between polyelectrolytes are an essential aspect to describe the stabilization/destabilization and have been modeled in detail (Ulrich et al., 2004; Seijo et al., 2006; Ulrich et al., 2006). The aggregation of nanoparticles is modified by adsorption processes (Fukushi and Sato, 2005) and the surface charge plays a dominant role (Kallay and Zalac, 2001, 2002).

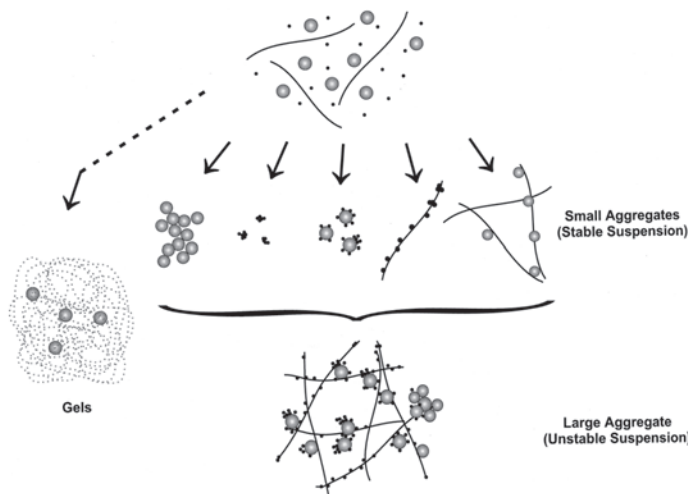


Figure 7.7 Major types of aggregates formed in the three-colloidal component system: inorganic colloids (circles), fulvic compounds (small points), and rigid biopolymers (lines). Both fulvic compounds and polysaccharides can also form gels, which are represented here as gray areas into which inorganic colloids can be embedded. Reprinted with permission from Buffle et al. (1998). Copyright 1998 American Chemical Society.

Owing to the importance of aggregation for the stability and behavior of ENM in the environment, numerous aggregation studies have been performed with inorganic and organic ENM in different media, both with and without natural organic matter. In the absence of humic acids, iron oxide ENM form open, porous aggregates with a fractal dimensions indicative of a diffusion-limited aggregation mechanism, whereas in the presence of humic acids, they form compact aggregates with a fractal dimension indicative of a rate-limited aggregation (Baalousha et al., 2008). For nano-TiO₂ it was found that nanoparticle dispersions were often stable for under environmentally relevant conditions of fulvic acids, pH, and ionic strength, suggesting that in the natural environment TiO₂ dispersion might occur to a greater extent than expected (Domingos et al., 2009). Divalent cations are very effective in aggregating 5-nm-sized nano-TiO₂ particles into micron-sized branching aggregates (French et al., 2009).

The particle size distribution of metal and oxide nanoparticles is strongly affected by the composition of the medium. In natural waters of different composition the average particle size of nano-Ag, nano-Cu, and fullerenes was found to vary by up to a factor of 100 from about 100 to 10,000 nm (Gao et al., 2009). Both changes in ionic strength and DOC content were responsible for the differences.

Organic matter stabilizes CNT suspensions by coating the hydrophobic CNTs with organic matter (Hyung et al., 2007; Hyung and Kim, 2008). The enhanced MWNT stability in the presence of humic acid was attributed to steric repulsion imparted by adsorbed humic acid macromolecules (Saleh et al., 2008). As a result of NOM adsorption, a fraction of the CNT formed a stable suspension in water and the concentration of CNT in suspension depended on the amount of NOM adsorbed per unit mass of CNT (Hyung and Kim, 2008). The amount of CNT suspended in water was also affected by ionic strength and pH. Similar effects were observed for fullerenes (Terashima and Nagao, 2007). In Figure 7.8 the effect of humic acids on the debundling of single-walled CNT is shown (Liu et al., 2007). Although in the absence of HA the CNT form thick strings of individual CNT glued together, the presence of HA results in a debundling of the aggregates and the formation of single dispersed CNT.

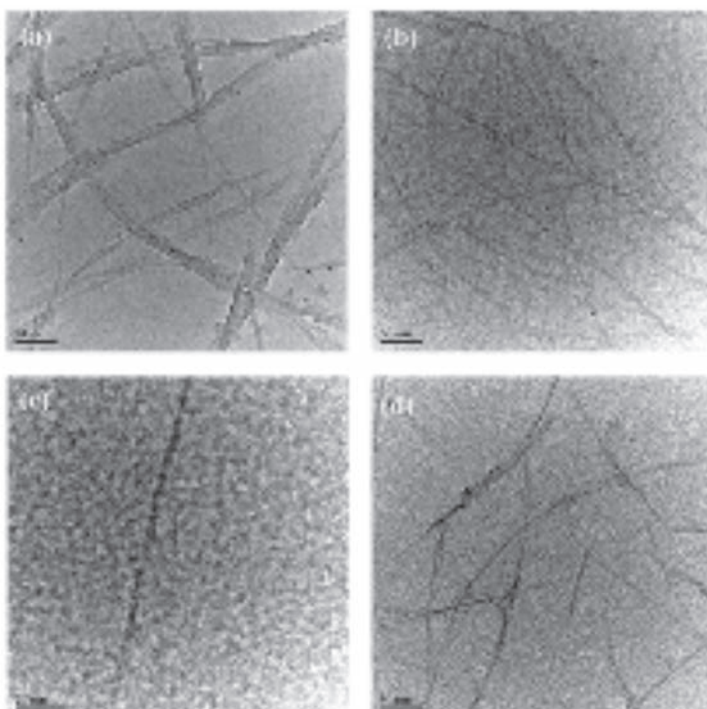


Figure 7.8 Influence of natural compounds on the debundling of single-walled CNT. Shown are TEM images of SWNTs dispersed in water (a) without dispersants, (b and c) with 0.15 g/L SLS, and (d) with 0.15 g/L HA. Reproduced with permission from Liu et al. (2007). Copyright 2007 IOP Publishing Ltd.

The presence of NOM was also found to greatly enhance fullerene dispersion (Li et al., 2009). At typical NOM concentrations found in natural waters, dissolved fullerene concentrations in the range of 10 mg/L can be obtained within 10 days of mixing, regardless of their extremely low water solubility.

7.3.4 Transport in Porous Media

The transport of colloids in porous media and the colloid-facilitated transport of contaminants has received a lot of attention in the past (McGechan and Lewis, 2002; Sen and Khilar, 2006). The movement of colloids in porous media is affected by two processes: straining or physical filtration where the particle is larger than the pore and

is trapped, and true filtration where the particle is removed from the solution by interception, diffusion, and sedimentation. However, particles removed from the solution by such processes can readily become resuspended upon changes in the chemical or physical conditions (e.g., changes in pH, ionic strength, flow rate) (Grolimund et al., 1998; Sen and Khilar, 2006).

Several studies have investigated the transport of a wide range of engineered ENM in porous media: fullerenes (Lecoanet and Wiesner, 2004; Espinasse et al., 2007; Li et al., 2008; Wang et al., 2008a; Wang et al., 2008b), TiO₂ (Lecoanet et al., 2004; Lecoanet and Wiesner, 2004; Dunphy Guzman et al., 2006; Choy et al., 2008; Fang et al., 2009), CNT (Lecoanet et al., 2004; Lecoanet and Wiesner, 2004; Jaisi et al., 2008), zero-valent iron (Kanel et al., 2005; Hydutsky et al., 2007; Kanel et al., 2007; Yang et al., 2007; Kanel et al., 2008; Zhan et al., 2008), aluminum (Doshi et al., 2008), and silica (Lecoanet et al., 2004; Lecoanet and Wiesner, 2004). Particles smaller than 100 nm are predicted to have very high efficiencies of transport to collector surfaces due to Brownian diffusion. If all particle-collector contacts were to result in particle attachment to the collector, these small particles would be retained to a large extent by the porous medium. However, nano-sized silica particles were not appreciably removed and also anatase ENM were only removed between 55% and 70%, depending on the flow velocity (Lecoanet and Wiesner, 2004). These studies show that the collector efficiency for ENM can be very different and that especially the surface-modified ENM displayed high mobilities. Also, the environmental conditions are important and efficient removal of titania ENM was observed close to the pH at the point of zero charge (Dunphy Guzman et al., 2006). pH also played a dominant role in the transport of metallic Al nanoparticles with much greater transport at pH 4 compared to pH 7 (Doshi et al., 2008).

7.4 MODELING ENVIRONMENTAL CONCENTRATIONS OF NANOMATERIALS

In Section 7.2 it was shown that only a few studies have measured ENM in the environment and these were not really quantitative. Owing to the lack of analytical measurements of ENM in the environment, the expected environmental concentrations have to be modeled based on the information on nano-product use. Different

approaches have been used so far, but they are all based on the same principle of distributing an input of ENM into environmental compartments. They differ in the way the input is derived and in the completeness of the system. In most cases these models do not assume any special “nano-properties” but use dilution and transfer factors to derive concentrations in well mixed compartments. These models are often based on the established procedures for the risk assessment of chemicals (ECB, 2003).

The first study was done for the UK based on the assumed market penetrations of nano-products and the known usage of these products (Boxall et al., 2007). Only certain consumer products, mainly household and cosmetic products, were included in the study. Concentrations of 11 different ENM including TiO₂, Ag, ZnO, fullerenes, and SiO₂ were modeled in water, air, sludge, and soil. For the 10% market penetration model, which probably overestimates current exposure levels, concentrations of silver, aluminum oxide, and fullerene were predicted to be in ng/L in wastewaters, whereas nano-TiO₂, silica, ZnO, and hydroxyapatite were predicted to be in µg/L range. These estimates are, however, based on simple modeling parameters and do not take into account any persistence, sedimentation, or accumulation of ENM in the environment.

Blaser et al. (2008) modeled Ag emissions from nano-Ag containing biocidal products and compared the expected concentrations coming from nano-products to those coming from other silver uses. The authors concluded that nano-Ag is only responsible for a small share of the total Ag flow in the environment. In this study no emissions of nanoparticles were considered and the nano-Ag products only served as a source of dissolved silver to the environment. Also, Luoma (2008) tried to estimate Ag concentrations in the environment based on the use of nano-Ag products. Again no distinction was made between the release of dissolved Ag and nano-Ag.

Park et al. (2008) modeled concentrations of CeO₂ in air and soils around highways originating from the use of CeO₂ in fuels. No other uses of CeO₂ were considered.

Another study used a lifecycle perspective to model the quantities of engineered nanoparticles released into the environment (Mueller and Nowack, 2008). Nano-Ag, nano-TiO₂, and CNT were quantified in the environment based on a substance flow analysis from products to air, soil, and water in Switzerland. The lifecycle of the nano-products formed the basis for assessing the mass flows of the ENM from the

products to the environment. The following parameters were used as model inputs: estimated worldwide production volume, allocation of the production volume to product categories, particle release from products, and flow coefficients within the environmental compartments. Figure 7.9 shows the resulting material flows from the products into the environment for nano-TiO₂ in Switzerland. The main flow goes from the product to the wastewater treatment plant and then to waste incineration because all sewage sludge is burnt in Switzerland.

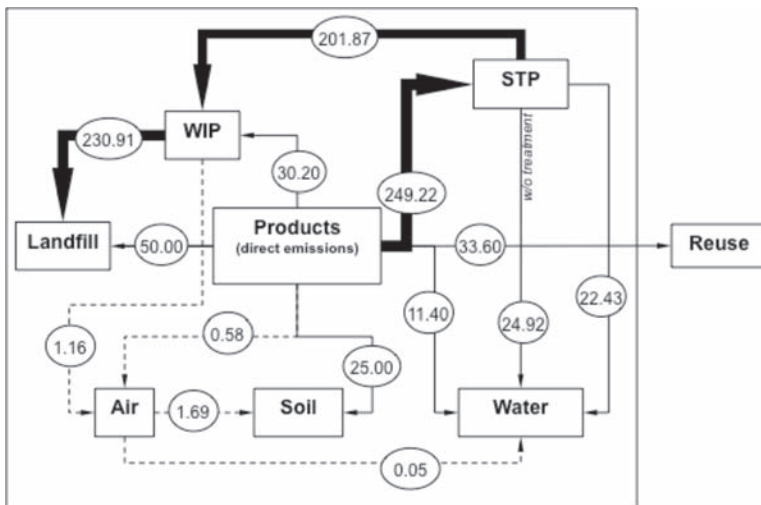


Figure 7.9 Nano-TiO₂ flows from the products to the different environmental compartments, WIP, STP, and landfill in tons per year. Reprinted with permission from Mueller and Nowack (2008). Copyright 2008 American Chemical Society.

Gottschalk et al. (2009, 2010) used an approach similar to that of Mueller and Nowack (2008), but applied a probabilistic model to cope with the high uncertainty in the knowledge available on the production, use, and behavior of ENM. In this work all possible uses of TiO₂, ZnO, Ag, CNT, and fullerenes were considered and concentrations were calculated for wastewater, surface water, sludge, sediments, soils, sludge-treated soils, and air.

In Table 7.1 the results from the different studies are shown. It can be seen that rather large differences exist between the predicted concentrations of the different models. The concentrations can vary

Table 7.1 Modeled environmental concentrations of some ENM in different compartments

ENM	Water (ng/L)	Wastewater (µg/L)	Sludge (mg/kg)	Soil (µg/kg)	Sludge-treated soil (µg/kg)	Sediment (µg/kg)	Remarks	References
TiO ₂	245,000		701		1030		10% market penetration	Boxall et al. (2007)
TiO ₂	700–16,000			0.4–4.8				Mueller and Nowack (2008)
TiO ₂	2–85	1.34–16.3	100–802	0.21–4.45	35–310	44–2382		Gottschalk et al. (2009, 2010)
ZnO	76,000		2172		3194		10% market penetration	Boxall et al. (2007)
ZnO	1–60	0.22–1.42	13.6–64.7	0.026–0.66	1.6–23.1	0.49–56		Gottschalk et al. (2009, 2010)
Ag	10		0.29		0.43		10% market penetration	Boxall et al. (2007)
Ag	30–80			0.02–0.1				Mueller and Nowack (2008)

ENM	Water (ng/L)	Wastewater (µg/L)	Sludge (mg/kg)	Soil (µg/kg)	Sludge-treated soil (µg/kg)	Sediment (µg/kg)	Remarks	References
Ag	0.09–2.6	0.016–0.13	1.29–6.24	0.006–0.06	0.5–4.1	10.15–10.1		Gottschalk et al. (2009, 2010)
Ag	40–340					2000–14000	Only Ag ⁺ considered	Blaser et al. (2008)
Ag	26–190					3000	Ag ⁺ and nano-Ag	Luoma (2008)
fullerenes	310		8.94		13.4		10% market penetration	Boxall et al. (2007)
fullerenes	<0.0005–0.24	0.002–0.026	0.008–0.68	0.00002–0.0006	0.001–0.022	<0.001–0.8		Gottschalk et al. (2009, 2010)
CNT	0.5–0.8			0.01–0.02				Mueller and Nowack (2008)
CNT	0.0006–0.025	0.006–0.032	0.05–0.15	0.0004–0.004	0.024–0.157	0.04–1.56		Gottschalk et al. (2009, 2010)
CNT						1–2000	Lake sediments	Koelmans et al. (2009)
CeO ₂				280–1120			Roadside soils	Park et al. (2008)

for one ENM and one compartment by up to five orders of magnitude for different models, e.g., for TiO₂ in water from 2 to 245000 ng/L. This is in part caused by the different approaches: some studies only considered few applications (Boxall et al., 2007; Park et al., 2008) while other attempted to cover all nano-products (Mueller and Nowack, 2008; Gottschalk et al., 2009, 2010). The inclusion or omission of removal during water treatment or sedimentation in natural waters has a profound influence on surface water concentrations. Although Mueller and Nowack (2008) and Boxall et al. (2007) did not consider sedimentation, Gottschalk et al. (2009, 2010) and Koelmans et al. (2009) included sedimentation into the models. The latter models predicted much lower surface water concentrations. Models using a market penetration approach (Boxall et al., 2007; Luoma, 2008) also predict much higher environmental concentrations than models based on worldwide production volumes (Mueller and Nowack, 2008; Gottschalk et al., 2009, 2010). However, Table 7.1 gives some first indications about the expected concentrations of ENM in the environment that can now be used to guide the development of analytical methods and that can form the basis for a first risk assessment of ENM.

7.5 EFFECTS OF NANOMATERIALS ON THE ENVIRONMENT

Although more information is available about the human toxicity of ENM than about ecotoxicity, there is a rapidly growing body of research devoted to the ecotoxicity of these materials and several reviews on this topic are already available (Oberdörster et al., 2006; Helland et al., 2007; Baun et al., 2008; Handy et al., 2008b; Klaine et al., 2008; Navarro et al., 2008a). The results so far show that ENM can be taken up by organisms and exert a toxic response, albeit normally only at relatively high concentrations (often in the high mg/L range).

The uptake ENM into cells has been observed for several organisms. Nano-sized ZnO, e.g., was internalized by bacteria (Brayner et al., 2006; Huang et al., 2008) (Fig. 7.10). The interaction of ENM with the cells is size dependent (Morones et al., 2005) and also seems to depend on the shape of the particles (Pal et al., 2007). However, effects on cells can also be observed without the uptake

of particles. Figure 7.11 shows that Au nanoparticles are not able to permeate the cell membranes of algae (Renault et al., 2008) although effects were observed.

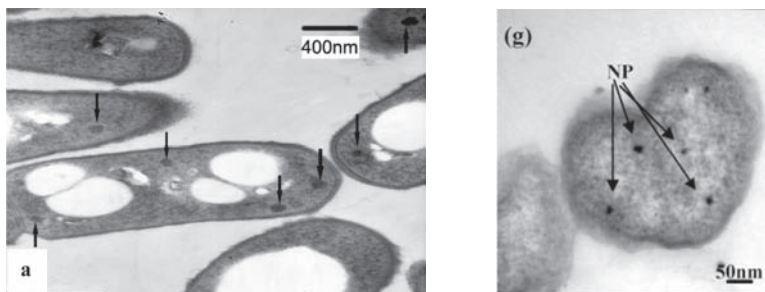


Figure 7.10 Left: TEM images of bacterial thin sections in the presence of ZnO nanoparticles. Reprinted with permission from Huang et al. (2008). Copyright 2008 American Chemical Society. Right: TEM micrographs of *E. coli* thin sections: NP; ZnO nanoparticles. Reprinted with permission from Brayner et al. (2006). Copyright 2006 American Chemical Society.

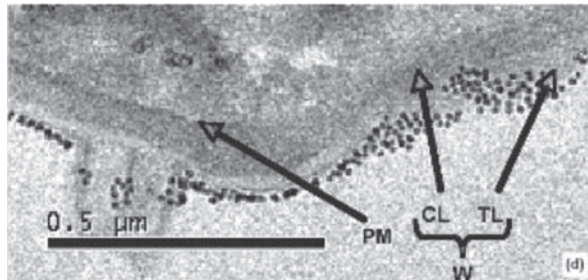


Figure 7.11 TEM observations of ultra-thin slices of *S. subspicatus* exposed to gold nanoparticles. Penetration of the cell wall, but not of the plasma membrane, is visible (CL: cellulosic layer, PM: plasmic membrane, TL: trilaminar layer, and W: cell wall). Figure taken from Renault et al. (2008).

Very little is known about the actual internalization of nanoparticles by higher organisms. Figure 7.12 shows one example where an uptake of Ag nanoparticles into zebrafish embryos has been shown. The Ag nanoparticles were found in different organs and tissues, proving that uptake from the surrounding water and transport within the organism took place.

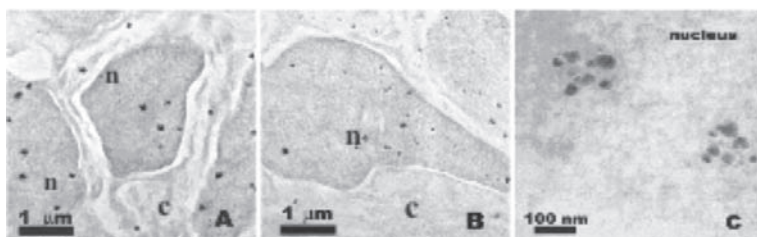


Figure 7.12 TEM images of thin sections of zebrafish embryos exposed to Ag nanoparticles. Deposition of the ENM in the cytoplasm (A) and nucleus (B) of the cells near the trunk and tail, respectively. Magnified images of the nucleus (C) showing nanoparticle deposition. The nucleus is indicated by “n” and cytoplasm by “c.” Reprinted with permission from Asharani et al. (2008b). Copyright 2008 IOP Publishing Ltd.

A lot of studies have identified dose–response relationships for ENM and different organisms. Although bulk TiO₂ is considered to have no health effects on aquatic organisms, that is clearly the case for nano-sized TiO₂ (Lovern and Klaper, 2006). The lowest concentrations where ENM were found to have an effect are summarized in Table 7.2. However, there are many studies that did not find any toxic effects of nano-TiO₂; for example, even at 20 g/L it was not toxic to the bacterium *Vibrio fischeri* and to the crustacean *Daphnia magna* (Heinlaan et al., 2008). Also, studies with zebrafish did not find any toxic effect of either nano-TiO₂ or bulk-TiO₂ at 500 mg/L concentration (Zhu et al., 2008). Nano-TiO₂ was also found not to have any behavioral effects on *Daphnia magna* at concentrations of 2 mg/L (Lovern et al., 2007).

The lowest effect concentrations observed in sediments and soils are very high with at least 100 mg/kg and in several cases no effects were found even at the highest tested concentration.

The toxicity of ENM is dependent on the surface functionalization of the nanomaterial. Functionalization significantly affected the response of *Daphnia pulex* to fullerenes, by significant production of the toxicity biomarkers glutathione-S-transferase and catalase (Klaper et al., 2009). Also, for QD, it was shown that different functionalizations can have very different effects on the organisms (King-Heiden et al., 2009).

Table 7.2 Lowest LC50 or NOEC from ecotoxicity studies

ENM	Compartment	Test species	Endpoint	Concentration	References
Nano-Ag	Water	<i>C. dubia</i>	LC50	0.696 µg/L	Gao et al. (2009)
CNT	Sediment	<i>Leptocheirus plumulosus</i>	LC50	68 g/kg	Kennedy et al. (2008)
	Water	<i>Danio rerio</i>	NOEC	40 mg/L	Asharani et al. (2008a)
	Soil	<i>Eisenia Veneta</i>	EC50	176 mg/kg	Scott-Fordsmand et al. (2008)
Fullerenes	Water	<i>Daphnia Magna</i>	NOEC	0.2 mg/L	Lovern and Klaper (2006)
	Soil	Microbial community	No effect observed	1000 mg/kg	Tong et al. (2007)
Nano-TiO ₂	Water	<i>Daphnia magna</i> , <i>Pseudokirchneriella subcapitata</i>	NOEC	1 mg/L	Hund-Rinke and Simon (2006); Aruoja et al. (2009)
	Soil	<i>P. scaber</i>	No effect observed	1000 mg/kg	Drobne et al. (2009)
Nano-ZnO	Water	<i>Pseudokirchneriella subcapitata</i>	EC50	40 µg/L	Aruoja et al. (2009)

Environmental factors can affect the toxicity of ENM. The most important factors are the composition of the medium, the aging of the particles, organism-induced changes, and light. As TiO₂ has a photocatalytic activity, the effect of light on toxicity was investigated (Hund-Rinke and Simon, 2006). A difference in toxicity to algae and daphnids was reported for illuminated and nonilluminated assays. Inorganic nanoparticulate TiO₂, SiO₂, and ZnO had a toxic effect on bacteria, and the presence of light was a significant factor increasing the toxicity (Adams et al., 2006). Phenrat et al. (2009) showed that partial or complete oxidation of nano zero-valent iron (nZVI) due to prolonged exposure in water reduced its redox activity, agglomeration, sedimentation rate, and toxicity. The surface modifications decreased nZVI toxicity by reducing sedimentation, which limited particle exposure to the cells. Extended freshwater storage of oxidized CNTs did not lessen cell membrane destruction or cell death (Panessa-Warren et al., 2009). However, storing oxidized CNTs for several years in NOM-containing solution significantly reduced CNT-induced cell membrane damage and increased cell survival to control levels (Panessa-Warren et al., 2009).

Water chemistry affects the suspension/solubility of ENM as well as the particle size distribution, resulting in a wide range of biological responses. Depending on the type of toxicity test, increased DOC resulted in either increased or decreased toxicity to nano-Cu (Gao et al., 2009).

For soluble ENM it is not yet clear how much of the observed toxic effects are due to dissolution of the particles and how much to the nanoparticles themselves. Dissolution and toxicity by the dissolved metal ion has been shown for nano-ZnO, which had comparable toxicity to bulk ZnO and dissolved Zn (Franklin et al., 2007). The toxicity was solely attributed to the dissolution of the ENM and toxicity by dissolved Zn²⁺ (Heinlaan et al., 2008). Also, for nano-CuO, the toxicity could be largely attributed to free Cu²⁺ (Heinlaan et al., 2008). However, another study with metallic Cu nanoparticles and zebrafish showed that only a small part of the toxic effect could be attributed to toxicity of Cu²⁺ (Griffitt et al., 2007). Also, metal catalysts leached from fullerenes or CNT can be toxic to organisms, complicating the assessment of the toxicity of the nanomaterial itself (Hull et al., 2009). Navarro et al. (2008b) observed that the toxicity of Ag nanoparticles appeared to be much higher than that of AgNO₃ when compared as a function of the Ag⁺ concentration. The ionic Ag⁺

measured in the nanoparticle suspensions could not fully explain the observed toxicity.

7.6 CONCLUSIONS

This chapter has shown that there is already quite a lot of information available about the environmental behavior and effects of ENM. The largest knowledge gap is the almost complete absence of quantitative analytical results of environmental concentrations. However, exposure modeling can give some first clues about the range of expected concentration in different environmental compartments. The modifications of ENM in the environment by abiotic and biotic factors have to date only received little attention but are of crucial importance regarding environmental behavior and the effects on the organisms.

References

- Adams, L.K., Lyon, D.Y., Alvarez, P.J., 2006. Comparative eco-toxicity of nanoscale TiO₂, SiO₂, and ZnO water suspensions. *Water Res.*, 40, 3527–3532.
- Allen, B.L., Kichambare, P.D., Gou, P., Vlasova, II, Kapralov, A.A., Konduru, N., Kagan, V.E., Star, A., 2008. Biodegradation of single-walled carbon nanotubes through enzymatic catalysis. *Nano Lett.*, 8, 3899–3903.
- Anastasio, C., Martin, S.T., 2001. Atmospheric nanoparticles, in: Banfield, J.F., Navrotsky, A. (Eds.), Nanoparticles and the Environment, pp. 293–349.
- Aruoja, V., Dubourguiera, H.C., Kasemetsa, K., Kahrua, A., 2009. Toxicity of nanoparticles of CuO, ZnO and TiO₂ to microalgae *Pseudokirchneriella subcapitata*. *Sci. Total Environ.*, 407, 1461–1468.
- Asharani, P.V., Serina, N.G.B., Nurmawati, M.H., Wu, Y.L., Gong, Z., Valiyaveettil, S., 2008a. Impact of multi-walled carbon nanotubes on aquatic species. *J. Nanosci. Nanotechnol.*, 8, 3603–3609.
- Asharani, P.V., Wu, Y.L., Gong, Z.Y., Valiyaveettil, S., 2008b. Toxicity of silver nanoparticles in zebrafish models. *Nanotechnology*, 19, 255102.
- Baalousha, M., Manciulea, A., Cumberland, S., Kendall, K., Lead, J.R., 2008. Aggregation and surface properties of iron oxide nanoparticles: Influence of pH and natural organic matter. *Environ. Toxicol. Chem.*, 27, 1875–1882.

- Baun, A., Hartmann, N.B., Grieger, K., Kusk, K.O., 2008. Ecotoxicity of engineered nanoparticles to aquatic invertebrates: a brief review and recommendations for future toxicity testing. *Ecotoxicology*, 17, 387–395.
- Benn, T.M., Westerhoff, P., 2008. Nanoparticle silver released into water from commercially available sock fabrics. *Environ. Sci. Technol.*, 42, 4133–4139.
- Birkefeld, A., Schulin, R., Nowack, B., 2007. In situ transformations of fine lead oxide particles in different soils. *Environ. Pollut.*, 145, 554–561.
- Blaser, S.A., Scheringer, M., MacLeod, M., Hungerbuhler, K., 2008. Estimation of cumulative aquatic exposure and risk due to silver: Contribution of nano-functionalized plastics and textiles. *Sci. Total Environ.*, 390, 396–409.
- Boxall, A.B.A., Chaudhry, Q., Sinclair, C., Jones, A.D., Aitken, R., Jefferson, B., Watts, C., 2007. Current and future predicted environmental exposure to engineered nanoparticles. Central Science Laboratory, Sand Hutton, UK.
- Brayner, R., Ferrari-Illiou, R., Brivois, N., Djediat, S., Benedetti, M.F., Fiévet, F., 2006. Toxicological impact studies based on Escherichia coli bacteria in ultrafine ZnO nanoparticles colloidal medium. *Nano Lett.*, 6, 866–870.
- Buffle, J., Leppard, G.G., 1995. Characterization of aquatic colloids and macromolecules. 1. Structure and behavior of colloidal material. *Environ. Sci. Technol.*, 29, 2169–2175.
- Buffle, J., Wilkinson, K.J., Stoll, S., Filella, M., Zhang, J.W., 1998. A generalized description of aquatic colloidal interactions: The three-colloidal component approach. *Environ. Sci. Technol.*, 32, 2887–2899.
- Burtscher, H., Zürcher, M., Kasper, A., Brunner, M., 2002. Efficiency of flue gas cleaning in waste incineration for submicron particles, in: Mayer, A. (Ed.), Proceedings of International ETH Conference on Nanoparticle Measurement, BUWAL.
- Buseck, P.R., Adachi, K., 2008. Nanoparticles in the atmosphere. *Elements*, 4, 389–394.
- Chang, M.R., Lee, D.J., Lai, J.Y., 2006. Coagulation and filtration of nanoparticles in wastewater from Hsinchu Science-based Industrial Park (HSIP). *Sep. Sci. Technol.*, 41, 1303–1311.
- Chang, M.R., Lee, D.J., Lai, J.Y., 2007. Nanoparticles in wastewater from a science-based industrial park – Coagulation using polyaluminum chloride. *J. Environ. Manage.*, 85, 1009–1014.

- Chin, C.J.M., Chen, P.W., Wang, L.J., 2006. Removal of nanoparticles from CMP wastewater by magnetic seeding aggregation. *Chemosphere*, 63, 1809–1813.
- Choy, C.C., Wazne, M., Meng, X.G., 2008. Application of an empirical transport model to simulate retention of nanocrystalline titanium dioxide in sand columns. *Chemosphere*, 71, 1794–1801.
- Den, W., Huang, C.P., 2006. Electrocoagulation of silica nanoparticles in wafer polishing wastewater by a multichannel flow reactor: A kinetic study. *J. Environ. Eng.*, 132, 1651–1658.
- Domingos, R.F., Tufenkji, N., Wilkinson, K.J., 2009. Aggregation of titanium dioxide nanoparticles: Role of a fulvic acid. *Environ. Sci. Technol.*, 43, 1282–1286.
- Doshi, R., Braida, W., Christodoulatos, C., Wazne, M., O'Connor, G., 2008. Nano-aluminum: Transport through sand columns and environmental effects on plants and soil communities. *Environ. Res.*, 106, 296–303.
- Drobne, D., Jemec, A., Tkalec, Z.P., 2009. In vivo screening to determine hazards of nanoparticles: Nanosized TiO₂. *Environ. Pollut.*, 157, 1157–1164.
- Dubascoux, S., Von Der Kammer, F., Le Hecho, I., Gautier, M.P., Lespes, G., 2008. Optimisation of asymmetrical flow field flow fractionation for environmental nanoparticles separation. *J. Chromatogr. A*, 1206, 160–165.
- Dunphy Guzman, K.A., Finnegan, D.L., Banfield, J.F., 2006. Influence of surface potential on aggregation and transport of titania nanoparticles. *Environ. Sci. Technol.*, 40, 7688–7693.
- ECB, 2003. *Technical Guidance Document on Risk Assessment*, European Chemicals Bureau.
- Espinasse, B., Hotze, E.M., Wiesner, M.R., 2007. Transport and retention of colloidal aggregates of C-60 in porous media: Effects of organic macromolecules, ionic composition, and preparation method. *Environ. Sci. Technol.*, 41, 7396–7402.
- Fang, J., Shan, X.Q., Wen, B., Lin, J.M., Owens, G., 2009. Stability of titania nanoparticles in soil suspensions and transport in saturated homogeneous soil columns. *Environ. Pollut.*, 157, 1101–1109.
- Farre, M., Gajda-Schrantz, K., Kantiani, L., Barcelo, D., 2009. Ecotoxicity and analysis of nanomaterials in the aquatic environment. *Anal. Bioanal. Chem.*, 393, 81–95.
- Fortner, J.D., Kim, D.I., Boyd, A.M., Falkner, J.C., Moran, S., Colvin, V.L., Hughes, J.B., Kim, J.H., 2007. Reaction of water-stable C-60 aggregates with ozone. *Environ. Sci. Technol.*, 41, 7497–7502.

- Franklin, N.M., Rogers, N.J., Apte, S.C., Batley, G.E., Gadd, G.E., Casey, P.S., 2007. Comparative toxicity of nanoparticulate ZnO, bulk ZnO, and ZnCl₂ to a freshwater microalga (*Pseudokirchneriella subcapitata*): The importance of particle solubility. *Environ. Sci. Technol.*, 41, 8484–8490.
- French, R.A., Jacobson, A.R., Kim, B., Isley, S.L., Penn, R.L., Baveye, P.C., 2009. Influence of ionic strength, pH, and cation valence on aggregation kinetics of titanium dioxide nanoparticles. *Environ. Sci. Technol.*, 43, 1354–1359.
- Fukushi, K., Sato, T., 2005. Using a surface complexation model to predict the nature and stability of nanoparticles. *Environ. Sci. Technol.*, 39, 1250–1256.
- Gagne, F., Auclair, J., Turcotte, P., Fournier, M., Gagnon, C., Sauve, S., Blaise, C., 2008. Ecotoxicity of CdTe quantum dots to freshwater mussels: Impacts on immune system, oxidative stress and genotoxicity. *Aquat. Toxicol.*, 86, 333–340.
- Gao, J., Youn, S., Hovsepyan, A., Llaneza, V.L., Wang, Y., Bitton, G., Bonzongo, J.C.J., 2009. Dispersion and toxicity of selected manufactured nanomaterials in natural river water samples: Effects of water chemical composition. *Environ. Sci. Technol.*, 43, 3322–3328.
- Gottschalk, F., Sonderer, T., Scholz, R.W., Nowack, B., 2010. Possibilities and limitations of modeling environmental exposure to engineered nanomaterials by probabilistic material flow analysis. *Environ. Toxicol. Chem.*, 29, 1036–1048.
- Gottschalk, F., Sonderer, T., Scholz, R.W., Nowack, B., 2009. Modeled environmental concentrations of engineered nanomaterials (TiO₂, ZnO, Ag, CNT, fullerenes) for different regions. *Environ. Sci. Technol.*, 43, 9216–9222.
- Griffitt, R.J., Luo, J., Gao, J., Bonzongo, J.C., Barber, D.S., 2008. Effects of particle composition and species on toxicity of metallic nanomaterials in aquatic organisms. *Environ. Toxicol. Chem.*, 27, 1972–1978.
- Griffitt, R.J., Weil, R., Hyndman, K.A., Denslow, N.D., Powers, K., Taylor, D., Barber, D.S., 2007. Exposure to copper nanoparticles causes gill injury and acute lethality in zebrafish (*Danio rerio*). *Environ. Sci. Technol.*, 41, 8178–8186.
- Grolimund, D., Elimelech, M., Borkovec, M., Barmettler, K., Kretzschmar, R., Sticher, H., 1998. Transport of in situ mobilized colloidal particles in packed soil columns. *Environ. Sci. Technol.*, 32, 3562–3569.
- Guzman, K.A.D., Taylor, M.R., Banfield, J.F., 2006. Environmental risks of nanotechnology: National nanotechnology initiative funding, 2000–2004. *Environ. Sci. Technol.*, 40, 1401–1407.

- Handy, R.D., Henry, T.B., Scown, T.M., Johnston, B.D., Tyler, C.R., 2008a. Manufactured nanoparticles: Their uptake and effects on fish – a mechanistic analysis. *Ecotoxicology*, 17, 396–409.
- Handy, R.D., van der Kammer, F., Lead, J.R., Hassellov, M., Owen, R., Crane, M., 2008b. The ecotoxicology and chemistry of manufactured nanoparticles. *Ecotoxicology*, 17, 287–314.
- Hasselov, M., Readman, J.W., Ranville, J.F., Tiede, K., 2008. Nanoparticle analysis and characterization methodologies in environmental risk assessment of engineered nanoparticles. *Ecotoxicology*, 17, 344–361.
- Hasselov, M., von der Kammer, F., 2008. Iron oxides as geochemical nanovectors for metal transport in soil-river systems. *Elements*, 4, 401–406.
- Heinlaan, M., Ivask, A., Blinova, I., Dubourguier, H.C., Kahru, A., 2008. Toxicity of nanosized and bulk ZnO, CuO and TiO₂ to bacteria *Vibrio fischeri* and crustaceans *Daphnia magna* and *Thamnocephalus platyurus*. *Chemosphere*, 71, 1308–1316.
- Holland, A., Wick, P., Koehler, A., Schmid, K., Som, C., 2007. Reviewing the environmental and human health knowledge base of carbon nanotubes. *Environ. Health Perspect.*, 115, 1125–1131.
- Hou, W.C., Jafvert, C.T., 2009. Photochemical transformation of aqueous C-60 clusters in sunlight. *Environ. Sci. Technol.*, 43, 362–367.
- Hsu, L.Y., Chein, H.M., 2007. Evaluation of nanoparticle emission for TiO₂ nanopowder coating materials. *J. Nanopart. Res.*, 9, 157–163.
- Huang, C., Jiang, W., Chen, C., 2004. Nano silica removal from IC wastewater by pre-coagulation and microfiltration. *Water Sci. Technol.*, 50, 133–138.
- Huang, Z.B., Zheng, X., Yan, D.H., Yin, G.F., Liao, X.M., Kang, Y.Q., Yao, Y.D., Huang, D., Hao, B.Q., 2008. Toxicological effect of ZnO nanoparticles based on bacteria. *Langmuir*, 24, 4140–4144.
- Hull, M.S., Kennedy, A.J., Steevens, J.A., Bednar, A.J., Weiss, C.A., Vikesland, P.J., 2009. Release of metal impurities from carbon nanomaterials influences aquatic toxicity. *Environ. Sci. Technol.*, 43, 4169–4174.
- Hund-Rinke, K., Simon, M., 2006. Ecotoxic effect of photocatalytic active nanoparticles TiO₂ on algae and daphnids. *Environ. Sci. Pollut. Res.*, 13, 225–232.
- Hydutsky, B.W., Mack, E.J., Beckerman, B.B., Skluzacek, J.M., Mallouk, T.E., 2007. Optimization of nano- and microiron transport through sand columns using polyelectrolyte mixtures. *Environ. Sci. Technol.*, 41, 6418–6424.

- Hyung, H., Fortner, J.D., Hughes, J.B., Kim, J.H., 2007. Natural organic matter stabilizes carbon nanotubes in the aqueous phase. *Environ. Sci. Technol.*, 41, 179–184.
- Hyung, H., Kim, J.H., 2008. Natural organic matter (NOM) adsorption to multi-walled carbon nanotubes: Effect of NOM characteristics and water quality parameters. *Environ. Sci. Technol.*, 42, 4416–4421.
- Impellitteri, C.A., Tolaymat, T.M., Scheckel, K.G., 2009. The speciation of silver nanoparticles in antimicrobial fabric before and after exposure to a hypochlorite/detergent solution. *J. Environ. Qual.*, 38, 1528–1530.
- Jaisi, D.P., Saleh, N.B., Blake, R.E., Elimelech, M., 2008. Transport of single-walled carbon nanotubes in porous media: Filtration mechanisms and reversibility. *Environ. Sci. Technol.*, 42, 8317–8323.
- Ju-Nam, Y., Lead, J.R., 2008. Manufactured nanoparticles: An overview of their chemistry, interactions and potential environmental implications. *Sci. Total Environ.*, 400, 396–414.
- Kaegi, R., Ulrich, A., Sinnet, B., Vonbank, R., Wichser, A., Zuleeg, S., Simmler, H., Brunner, S., Vommont, H., Burkhardt, M., Boller, M., 2008a. Synthetic TiO₂ nanoparticle emission from exterior facades into the aquatic environment. *Environ. Pollut.*, 156, 233–239.
- Kaegi, R., Wagner, T., Hetzer, B., Sinnet, B., Tzuetkov, G., Boller, M., 2008b. Size, number and chemical composition of nanosized particles in drinking water determined by analytical microscopy and LIBD. *Water Res.*, 42, 2778–2786.
- Kallay, N., Zalac, S., 2001. Introduction of the surface complexation model into the theory of colloid stability. *Croat. Chem. Acta*, 74, 479–497.
- Kallay, N., Zalac, S., 2002. Stability of nanodispersions: A model for kinetics of aggregation of nanoparticles. *J. Colloid Interface Sci.*, 253, 70–76.
- Kanel, S.R., Goswami, R.R., Clement, T.P., Barnett, M.O., Zhao, D., 2008. Two dimensional transport characteristics of surface stabilized zero-valent iron nanoparticles in porous media. *Environ. Sci. Technol.*, 42, 896–900.
- Kanel, S.R., Kang, S., Jung, H., Choi, H., 2005. Transport characteristics of surfactant stabilized iron nano particle in unsaturated porous media. *Abst. Pap. Amer. Chem. Soc.*, 54, 683–687.
- Kanel, S.R., Nepal, D., Manning, B., Choi, H., 2007. Transport of surface-modified iron nanoparticle in porous media and application to arsenic(III) remediation. *J. Nanopart. Res.*, 9, 725–735.
- Kennedy, A.J., Hull, M.S., Steevens, J.A., Dontsova, K.M., Chappell, M.A., Gunter, J.C., Weiss, C.A., 2008. Factors influencing the partitioning and toxicity

- of nanotubes in the aquatic environment. *Environ. Toxicol. Chem.*, 27, 1932–1941.
- Kim, H.-J., Phenrat, T., Tilton, R.D., Lowry, G.V., 2009. Fe0 nanoparticles remain mobile in porous media after aging due to slow desorption of polymeric surface modifiers. *Environ. Sci. Technol.*, 43, 3824–3830.
- King-Heiden, T.C., Wiecinski, P.N., Mangham, A.N., Metz, K.M., Nesbit, D., Pedersen, J.A., Hamers, R.J., Heideman, W., Peterson, R.E., 2009. Quantum dot nanotoxicity assessment using the zebrafish embryo. *Environ. Sci. Technol.*, 43, 1605–1611.
- Kiser, M.A., Westerhoff, P., Benn, T., Wang, Y., Perez-Rivera, J., Hristovski, K., 2009. Titanium nanomaterial removal and release from wastewater treatment plants. *Environ. Sci. Technol.*, 43, 6757–6763.
- Klaine, S.J., Alvarez, P.J.J., Batley, G.E., Fernandes, T.F., Handy, R.D., Lyon, D.Y., Mahendra, S., McLaughlin, M.J., Lead, J.R., 2008. Nanomaterials in the environment: Behavior, fate, bioavailability, and effects. *Environ. Toxicol. Chem.*, 27, 1825–1851.
- Klaper, R., Crago, J., Barr, J., Arndt, D., Setyowati, K., Chen, J., 2009. Toxicity biomarker expression in daphnids exposed to manufactured nanoparticles: Changes in toxicity with functionalization. *Environ. Pollut.*, 157, 1152–1156.
- Koelmans, A.A., Nowack, B., Wiesner, M.R., 2009. Comparison of manufactured and black carbon nanoparticle concentrations in aquatic sediments. *Environ. Pollut.*, 157, 1110–1116.
- Lead, J.R., Wilkinson, K.J., 2006. Aquatic colloids and nanoparticles: Current knowledge and future trends. *Environ. Chem.*, 3, 159–171.
- Lecoanet, H.F., Bottero, J.Y., Wiesner, M.R., 2004. Laboratory assessment of the mobility of nanomaterials in porous media. *Environ. Sci. Technol.*, 38, 5164–5169.
- Lecoanet, H.F., Wiesner, M.R., 2004. Velocity effects on fullerene and oxide nanoparticle deposition in porous media. *Environ. Sci. Technol.*, 38, 4377–4382.
- Li, Q.L., Xie, B., Hwang, Y.S., Xu, Y.J., 2009. Kinetics of C-60 fullerene dispersion in water enhanced by natural organic matter and sunlight. *Environ. Sci. Technol.*, 43, 3574–3579.
- Li, Y.S., Wang, Y.G., Pennell, K.D., Abriola, L.M., 2008. Investigation of the transport and deposition of fullerene (C60) nanoparticles in quartz sands under varying flow conditions. *Environ. Sci. Technol.*, 42, 7174–7180.
- Limbach, L.K., Bereiter, R., Müller, E., Krebs, R., Galli, R., Stark, W.J., 2008. Removal of oxide nanoparticles in a model wastewater treatment

- plant: Influence of agglomeration and surfactants on clearing efficiency. *Environ. Sci. Technol.*, 42, 5828–5833.
- Liu, Y., Gao, L., Zheng, S., Wang, Y., Sun, J., Kajiura, H., Li, Y., Noda, K., 2007. Debundling of single-walled carbon nanotubes by using natural polyelectrolytes. *Nanotechnology*, 18, 365702.
- Lovern, S.B., Klaper, R., 2006. Daphnia magna mortality when exposed to titanium dioxide and fullerene (C₆₀) nanoparticles. *Environ. Toxicol. Chem.*, 25, 1132–1137.
- Lovern, S.B., Strickler, J.R., Klaper, R., 2007. Behavioral and physiological changes in Daphnia magna when exposed to nanoparticle suspensions (titanium dioxide, nano-C₆₀ and C₆₀HxC₇₀Hx). *Environ. Sci. Technol.*, 41, 4465–4470.
- Luoma, S.N., 2008. Old problems or new challenges? Silver nanotechnologies and the environment. Project on Emerging Nanotechnologies, Woodrow Wilson International Center for Scholars, Washington, DC.
- Mahendra, S., Zhu, H.G., Colvin, V.L., Alvarez, P.J., 2008. Quantum dot weathering results in microbial toxicity. *Environ. Sci. Technol.*, 42, 9424–9430.
- McGechan, M.B., Lewis, D.R., 2002. Transport of particulate and colloid-sorbed contaminants through soil, part 1: General principles. *Biosys. Eng.*, 83, 255–273.
- Metz, K.M., Mangham, A.N., Bierman, M.J., Jin, S., Hamers, R.J., Pedersen, J.A., 2009. Engineered nanomaterial transformation under oxidative environmental conditions: Development of an in vitro biomimetic assay. *Environ. Sci. Technol.*, 43, 1598–1604.
- Morones, J.R., Elechiguerra, J.L., Camacho, A., Holt, K., Kouri, J.B., Ramirez, J.T., Yacaman, M.J., 2005. The bactericidal effect of silver nanoparticles. *Nanotechnology*, 16, 2346–2353.
- Mueller, N.C., Nowack, B., 2008. Exposure modeling of engineered nanoparticles in the environment. *Environ. Sci. Technol.*, 42, 4447–4453.
- Navarro, E., Baun, A., Behra, R., Hartmann, N.B., Filsinger, J., Miao, A.J., Quigg, A., Santschi, P.H., Sigg, L., 2008a. Environmental behavior and ecotoxicity of engineered nanoparticles to algae, plants, and fungi. *Ecotoxicology*, 17, 372–386.
- Navarro, E., Piccapietra, F., Wagner, B., Marconi, F., Kaegi, R., Odzak, N., Sigg, L., Behra, R., 2008b. Toxicity of silver nanoparticles to Chlamydomonas reinhardtii. *Environ. Sci. Technol.*, 42, 8959–8964.
- Nowack, B., 2008. Pollution prevention and treatment using nanotechnology, in: Krug, H.F. (Ed.), *Nanotechnology*, Vol. 2, Environmental aspects, Springer, pp. 1–15.

- Nowack, B., Bucheli, T.D., 2007. Occurrence, behavior and effects of nanoparticles in the environment. *Environ. Pollut.*, 150, 5–22.
- Oberdörster, E., McClellan-Green, P., Haasch, M.L., 2006. Ecotoxicity of engineered nanomaterials, in: Kumar, C. (Ed.), Nanomaterials – Toxicity, health and environmental issues. Wiley-VCH, Weinheim.
- Pal, S., Tak, Y.K., Song, J.M., 2007. Does the antibacterial activity of silver nanoparticles depend on the shape of the nanoparticle? A study of the gram-negative bacterium *Escherichia coli*. *Appl. Environ. Microbiol.*, 73, 1712–1720.
- Panessa-Warren, B.J., Maye, M.M., Warren, J.B., Crosson, K.M., 2009. Single walled carbon nanotube reactivity and cytotoxicity following extended aqueous exposure. *Environ. Pollut.*, 157, 1140–1151.
- Park, B., Donaldson, K., Duffin, R., Tran, L., Kelly, F., Mudway, I., Morin, J.P., Guest, R., Jenkinson, P., Samaras, Z., Giannouli, M., Kouridis, H., Martin, P., 2008. Hazard and risk assessment of a nanoparticulate cerium oxide-based diesel fuel additive – A case study. *Inhalation Toxicol.*, 20, 547–566.
- Peters, T.M., Elzey, S., Johnson, R., Park, H., Grassian, V.H., Maher, T., O'Shaughnessy, P., 2009. Airborne monitoring to distinguish engineered nanomaterials from incidental particles for environmental health and safety. *J. Occup. Environ. Hyg.*, 6, 73–81.
- Phenrat, T., Long, T.C., Lowry, G.V., Veronesi, B., 2009. Partial Oxidation ("Aging") and surface modification decrease the toxicity of nanosized zerovalent iron. *Environ. Sci. Technol.*, 43, 195–200.
- Ratte, H.T., 1999. Bioaccumulation and toxicity of silver compounds: A review. *Environ. Toxicol. Chem.*, 18, 89–108.
- Renault, S., Baudrimont, M., Mesmer-Dudons, N., Gonzalez, P., Mornet, S., Brisson, A., 2008. Impacts of gold nanoparticle exposure on two freshwater species: A phytoplanktonic alga (*Scenedesmus subspicatus*) and a benthic bivalve (*Corbicula fluminea*). *Gold Bull.*, 41, 116–126.
- Roberts, A.P., Mount, A.S., Seda, B., Souther, J., Qiao, R., Lin, S., Ke, P.C., Rao, A.M., Klaine, S.J., 2007. *In vivo* biomodification of lipid-coated carbon nanotubes by *Daphnia magna*. *Environ. Sci. Technol.*, 41, 3025–3029.
- Saleh, N.B., Pfefferle, L.D., Elimelech, M., 2008. Aggregation kinetics of multiwalled carbon nanotubes in aquatic systems: Measurements and environmental implications. *Environ. Sci. Technol.*, 42, 7963–7969.
- Scott-Fordsmann, J.J., Krogh, P.H., Schaefer, M., Johansen, A., 2008. The toxicity testing of double-walled nanotubes-contaminated food to *Eisenia veneta* earthworms. *Ecotoxicol. Environ. Saf.*, 71, 616–619.

- Seijo, M., Ulrich, S., Filella, M., Buffle, J., Stoll, S., 2006. Effects of surface site distribution and dielectric discontinuity on the charging behavior of nanoparticles. A grand canonical Monte Carlo study. *Phys. Chem. Chem. Phys.*, 8, 5679–5688.
- Sen, T.K., Khilar, K.C., 2006. Review on subsurface colloids and colloid-associated contaminant transport in saturated porous media. *Adv. Colloid Interface Sci.*, 119, 71–96.
- Simonet, B.M., Valcarcel, M., 2009. Monitoring nanoparticles in the environment. *Anal. Bioanal. Chem.*, 393, 17–21.
- Sobek, A., Bucheli, T.D., 2009. Testing the resistance of single- and multi-walled carbon nanotubes to chemothermal oxidation used to isolate soots from environmental samples. *Environ. Pollut.*, 157, 1065–1071.
- Terashima, M., Nagao, S., 2007. Solubilization of [60]fullerene in water by aquatic humic substances. *Chem. Lett.*, 36, 302–303.
- Theng, B.K.G., Yuan, G.D., 2008. Nanoparticles in the soil environment. *Elements*, 4, 395–399.
- Tiede, K., Boxall, A.B.A., Tear, S.P., Lewis, J., David, H., Hassellov, M., 2008. Detection and characterization of engineered nanoparticles in food and the environment. *Food Addit. Contam.*, 25, 795–821.
- Tiede, K., Boxall, A.B.A., Tiede, D., Tear, S.P., Davide, H., Lewis, J., 2009. A robust size-characterisation methodology for studying nanoparticle behaviour in “real” environmental samples, using hydrodynamic chromatography coupled to ICP-MS. *J. Anal. At. Spectrom.*, 24, 964–972.
- Tong, Z., Bischoff, M., Nies, L., Applegate, B., Turco, R.F., 2007. Impact of fullerene (C60) on a soil microbial community. *Environ. Sci. Technol.*, 41, 2985–2991.
- Ulrich, S., Laguerre, A., Stoll, S., 2004. Complex formation between a nanoparticle and a weak polyelectrolyte chain: Monte Carlo simulations. *J. Nanopart. Res.*, 6, 595–603.
- Ulrich, S., Seijo, M., Laguerre, A., Stoll, S., 2006. Nanoparticle adsorption on a weak polyelectrolyte. Stiffness, pH, charge mobility, and ionic concentration effects investigated by Monte Carlo Simulations. *J. Phys. Chem. B*, 110, 20954–20964.
- Vorbau, M., Hillemann, L., Stintz, M., 2009. Method for the characterization of the abrasion induced nanoparticle release into air from surface coatings. *Aerosol Sci.*, 40: 209–217.
- Wang, Y.G., Li, Y.S., Fortner, J.D., Hughes, J.B., Abriola, L.M., Pennell, K.D., 2008a. Transport and retention of nanoscale C-60 aggregates in water-saturated porous media. *Environ. Sci. Technol.*, 42, 3588–3594.

- Wang, Y.G., Li, Y.S., Pennell, K.D., 2008b. Influence of electrolyte species and concentration on the aggregation and transport of fullerene nanoparticles in quartz sands. *Environ. Toxicol. Chem.*, 27, 1860–1867.
- Waychunas, G.A., Kim, C.S., Banfield, J.F., 2005. Nanoparticulate iron oxide minerals in soils and sediments: Unique properties and contaminant scavenging mechanisms. *J. Nanopart. Res.*, 7, 409–433.
- Waychunas, G.A., Zhang, H.Z., 2008. Structure, chemistry, and properties of mineral nanoparticles. *Elements*, 4, 381–387.
- Wigginton, N.S., Haus, K.L., Hochella, M.F., 2007. Aquatic environmental nanoparticles. *J. Environ. Monit.*, 9, 1306–1316.
- Xia, X., Xie, C., Cai, S., Yang, Z., Yang, X., 2006. Corrosion characteristics of copper microparticles and copper nanoparticles in distilled water. *Corros. Sci.*, 48, 3924–3932.
- Yang, G.C.C., Tu, H.C., Hung, C.H., 2007. Stability of nanoiron slurries and their transport in the subsurface environment. *Sep. Purif. Technol.*, 58, 166–172.
- Zhan, J.J., Zheng, T.H., Piringer, G., Day, C., McPherson, G.L., Lu, Y.F., Papadopoulos, K., John, V.T., 2008. Transport characteristics of nanoscale functional zerovalent iron/silica composites for *in situ* remediation of trichloroethylene. *Environ. Sci. Technol.*, 42, 8871–8876.
- Zhang, Y., Chen, Y., Westerhoff, P., Hristovski, K., Crittenden, J.C., 2008a. Stability of commercial metal oxide nanoparticles in water. *Water Res.*, 42, 2204–2212.
- Zhang, Y., Chen, Y.S., Westerhoff, P., Crittenden, J.C., 2008b. Stability and removal of water soluble CdTe quantum dots in water. *Environ. Sci. Technol.*, 42, 321–325.
- Zhu, X.S., Zhu, L., Duan, Z.H., Qi, R.Q., Li, Y., Lang, Y.P., 2008. Comparative toxicity of several metal oxide nanoparticle aqueous suspensions to Zebrafish (*Danio rerio*) early developmental stage. *J. Environ. Sci. Health Part A Toxic/Hazard. Subst. Environ. Eng.*, 43, 278–284.

This page intentionally left blank

Nanoparticles and nano-sized materials created by nanotechnology (NT) have been considered unique and sole solution to overcome the limitations of other technologies and widen their applications. Although these materials have been widely used in environmental technology (ET), most of environmental applications of nanoparticles were limited to the fabrication of nano-sensors for the detection of volatile organic compounds (VOC) and as nano-sized catalysts for air purification systems. So, the use of nanoparticles for the direct removal of pollutants from contaminated soil and wastewater has been seldom reported. However, environmental processes for soil remediation, wastewater treatment, and air purification strongly need innovative new materials to highly improve their performance and efficiency. The demand for materials created by NT in ET is, therefore, stronger than ever.

This book presents the possible applications of nano-sized materials in all environmental processes, providing the most reliable guideline so far for the selection of nanomaterials to improve the efficiency of environmental processes. It focuses on designing specific nanomaterials for environmental processes and pollutants. It presents the impact and influence of nanomaterials on the environment and discusses how to avoid causing secondary contamination by the use of nanomaterials. The book provides proper information about nanomaterials for potential users who will use and apply nanomaterials in ET.



Juyoung Kim completed his PhD on the synthesis of amphiphilic polymeric networks and their applications in 1996 under the supervision of Prof. Kyungdo Suh at Hanyang University, South Korea. He undertook a postdoctoral fellowship with Prof. Claude Cohen at Cornell University from 1996 to 1998. He then began an academic career as Assistant Professor of Advanced Materials Department at Samcheok National University, South Korea, and was promoted in 2010 to Full Professor with tenure. He has published 70 peer-reviewed journal publications and 7 patents. Currently, his research focuses on the synthesis of core-crosslinked amphiphilic polymer nanoparticles using various amphiphilic reactive oligomers and bridged organosilica precursor containing amphiphilic polymer chains and their applications for target drug delivery, *in vivo* oxygen-sensing nanoparticles, and antimicrobial nanocarriers.



PAN STANFORD PUBLISHING

www.panstanford.com

V031

ISBN-978-981-4241-55-7

90000



9 789814 241557